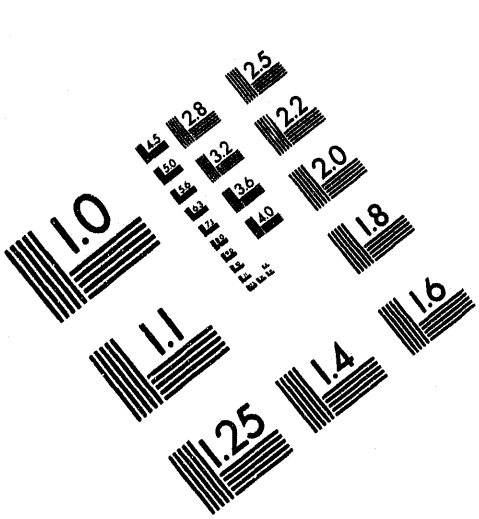

Association for Information and Image Management
1100 Wayne Avenue, Suite 1100
Silver Spring, Maryland 20910
301/587-8202

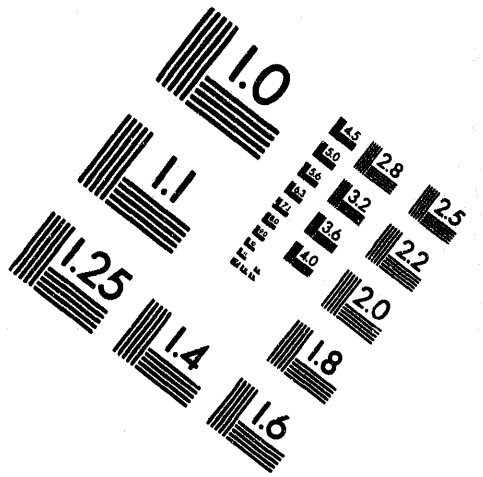

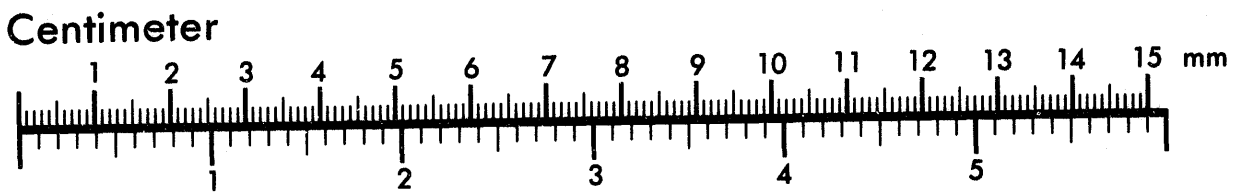

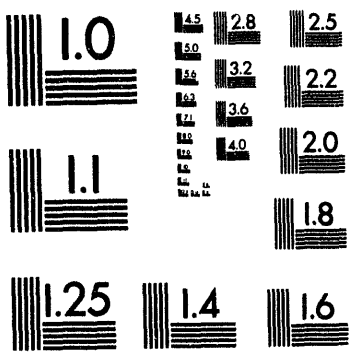

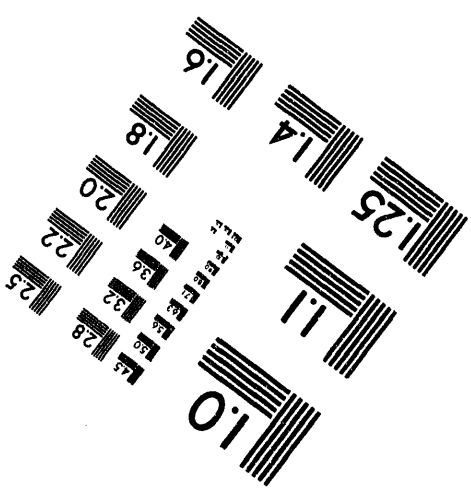

MANUFACTURED TO AIIM STANDARDS
BY APPLIED IMAGE, INC.

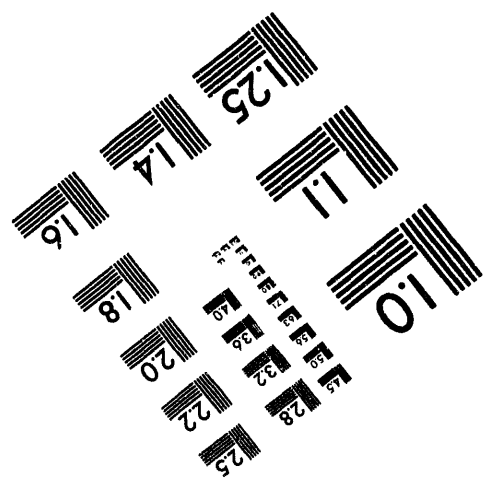

1 of 3

SAND93-7058
Unlimited Release
Printed March 1994

Distribution
Category UC-721
940

Hydrostatic and Shear Consolidation Tests With Permeability Measurements on Waste Isolation Pilot Plant Crushed Salt*

N.S. Brodsky
RE/SPEC Inc.
P.O. Box 725
Rapid City, SD 57709

ABSTRACT

Crushed natural rock salt is a primary candidate for use as backfill and barrier material at the Waste Isolation Pilot Plant (WIPP) and therefore Sandia National Laboratories (SNL) has been pursuing a laboratory program designed to quantify its consolidation properties and permeability. Variables that influence consolidation rate that have been examined include stress state and moisture content. The experimental results presented in this report complement existing studies and work in progress conducted by SNL. The experiments described in this report were designed to 1) measure permeabilities of consolidated specimens of crushed salt, 2) determine the influence of brine saturation on consolidation under hydrostatic loads, and 3) measure the effects of small applied shear stresses on consolidation properties. The laboratory effort consisted of 18 individual tests: three permeability tests conducted on specimens that had been consolidated at Sandia, six hydrostatic consolidation and permeability tests conducted on specimens of brine-saturated crushed WIPP salt, and nine shear consolidation and permeability tests performed on crushed WIPP salt specimens containing 3 percent brine by weight. For hydrostatic consolidation tests, pressures ranged from 1.72 MPa to 6.90 MPa. For the shear consolidation tests, confining pressures were between 3.45 MPa and 6.90 MPa and applied axial stress differences were between 0.69 and 4.14 MPa. All tests were run under drained conditions at 25°C.

Results of the hydrostatic consolidation tests on brine-saturated specimens show, not surprisingly, that consolidation rate increases with pressure. These data alone cannot be used to infer a difference in consolidation rate between damp and saturated specimens subjected to hydrostatic load, although that result has been observed in previous studies by SNL. Shear consolidation tests show that for small axial stress differences there is no systematic correlation between the magnitude of the stress difference and the consolidation rate.

Permeabilities decrease as specimen density increases. Fits to the permeability-versus-density data show that permeability decreases approximately two orders of magnitude as fractional density increases from 0.9 to nearly 1.0. Values of permeability over this range of fractional density were between 6×10^{-18} m^2 and 3×10^{-22} m^2.

* This report was prepared by RE/SPEC Inc. for Sandia National Laboratories under Contract No. 69-1725.

CONTENTS

CONTENTS (Continued)

CONTENTS (Continued)

Tables

Figures

1.0 INTRODUCTION

1.1 Background

The U.S. Department of Energy (DOE) is planning to dispose of transuranic (TRU) wastes at the Waste Isolation Pilot Plant (WIPP) near Carlsbad, New Mexico. The WIPP is expected to be a repository for both contact-handled (CH) and remotely handled (RH) TRU wastes and comprises both surface and underground facilities. The current mission of the WIPP is to provide a research and development facility to demonstrate the safe management, storage, and disposal of radioactive TRU waste resulting from defense programs of the U.S. Government.

The WIPP underground facility is located in the bedded salt of the Salado Formation at a depth of about 655 m. Ultimately, this facility will include eight storage panels of seven rooms each in addition to the rooms currently used for research activities and access rooms and shafts. Disposal system activities will include studies of seal and barrier materials because before the facility is decommissioned, seals will be placed in shafts and other critical points within the repository to retard fluid flow.

Crushed salt is a primary candidate backfill and seal material for use at the WIPP. Crushed salt is an attractive material because it will be produced in large volumes during mining of the access and storage rooms and is geochemically compatible with the host rock, i.e., rock salt. It is expected that the crushed salt will consolidate into a cohesive mass with low permeability comparable to that of intact salt. Consolidation is expected because the rooms and shafts will close with time as a result of creep deformations in the surrounding intact salt. Therefore, the mechanics of crushed-salt consolidation and the effect of consolidation on permeability are important in order to predict the times required for various permeability reductions.

Sandia National Laboratories (SNL) is responsible for investigation of the mechanics of crushed salt consolidation (Holcomb and Hannum, 1982; Holcomb and Shields, 1987; Holcomb and Zeuch, 1988; Zeuch, 1989; Zeuch, 1990; Zeuch and Holcomb, 1991; Zeuch et al., 1991). The objective of these studies is to develop a constitutive model for crushed salt that can be used in structural analyses to assess the compliance of the WIPP with regulatory requirements (Zeuch et al., 1985; Sjaardema and Krieg, 1987; Zeuch, 1990). In addition, it is important to develop relationships between density and permeability. This report presents results of consolidation and permeability experiments performed on specimens of crushed WIPP salt. The 15-test

experimental matrix was designed by Dr. D. H. Zeuch (Geomechanics Department 6117, SNL), and complements data collected by SNL.

1.2 Scope

Three types of experiments were performed. The first type consisted of three permeability tests performed on crushed-salt specimens that had been prepared and consolidated by Sandia National Laboratories. One of these three tests was terminated prematurely when the Viton jacket that protected the specimen from silicone oil (used to apply the hydrostatic stress) ruptured. The rupture probably occurred prior to testing, but was not detected until the specimen was pressurized. No permeability measurements were attempted on this specimen. The second type of experiment consisted of hydrostatic consolidation and permeability tests conducted on brine-saturated crushed WIPP salt specimens prepared at RE/SPEC Inc. Consolidation pressures ranged from 1.72 to 6.90 MPa and consolidation proceeded until Sandia-specified values of fractional density were reached. Hydrostatic stress was then decreased to half of the test value and a permeability test was conducted. The last class of experiment consisted of nine shear consolidation and permeability tests conducted on crushed WIPP salt specimens prepared at RE/SPEC Inc. containing 3 percent brine by weight. The specimens were consolidated for 60 days at confining pressures ranging from 3.45 to 6.90 MPa and at axial stress differences between 0.69 and 4.14 MPa. After consolidation, a hydrostatic stress equal to half of the former mean stress was applied and a permeability test was performed. All permeabilities were measured using apparatus and procedures similar to those used by Stroup and Senseny (1987) and Pfeifle (1989). The second and third experiments will be referred to in this report as consolidation/permeability tests because both the consolidation and permeability stages were conducted by RE/SPEC Inc.

1.3 Report Organization

Including this introduction, this report contains seven chapters and nine appendices. Chapter 2.0 describes the specimens used in this study. Chapter 3.0 describes the testing apparatus and is followed by Chapter 4.0, which describes test procedures. Chapter 5.0 gives the test results and a discussion of results. The report is concluded by a summary chapter, Chapter 6.0, and a list of cited references given in Chapter 7.0. Appendix A contains a report authored by Twin City Testing and summarizes their chemical analyses of crushed WIPP salt. A memorandum written by Dr. C. L. Stein and addressed to Dr. Darrell E. Munson that discusses the mineralogy

of WIPP salt is given in Appendix B. Appendix C contains a summary of the transducer calibration and verification data. Appendix D contains plots of fractional density as a function of time for all consolidation and permeability tests. Appendix E contains model fitting results for hydrostatic consolidation tests and Appendix F contains brine flow data for permeability tests. Appendices G through I provide data showing the stability of environmental conditions during consolidation/permeability tests. Appendix G contains plots of axial stress-versus-time for all shear consolidation tests. Plots of confining pressure-versus-time are given for all tests in Appendix H, and temperature-versus-time data for all tests are given in Appendix I.

2.0 SPECIMENS

This chapter is divided into two sections: Section 2.1 describes Sandia-furnished specimens used for permeability tests, and Section 2.2 describes the characterization and assembly of specimens prepared by RE/SPEC and used for consolidation/permeability tests.

2.1 Sandia-Furnished Specimens

2.1.1 Specimen Acquisition

Three specimens of consolidated crushed salt were received in two separate shipments from Division 6117, Sandia National Laboratories. The shipments arrived at RE/SPEC Inc. on October 15, 1990 and January 25, 1991, respectively. The specimens were packed in boxes (in one case, wood, and in the other, cardboard) with thick foam padding for protection from damage during shipping. Specimen temperature was measured upon arrival for the latter shipment by placing a thermocouple alongside one specimen and resealing the container. There was no evidence of exposure to cold or moisture for either shipment. The specimens were logged into RE/SPEC's computerized core inventory system and then placed in an environmentally controlled storage area until they were tested. Specimen 20SEP89 arrived in the first shipment and Specimens 19JUN90 and 20JUN90 arrived in the latter shipment. The specimen identifications were provided by Sandia and correspond to the date on which Sandia initiated testing.

2.1.2 Specimen Dimensions

The specimens used in this study had been consolidated previously in a testing program conducted by SNL, and therefore, arrived assembled in metal endcaps and protective sleeves (i.e., jackets). The specimen assembly used for 20SEP89 is shown in Figure 2-1. Sandia later improved the specimen assembly by changing the location of the porous felt metal and the new configuration shown in Figure 2-2 was used for 19JUN90 and for tests on RE/SPEC Inc.-furnished specimens. In calculating permeability from laboratory flow measurements, specimen length and diameter are required. Specimen dimensions could not be obtained directly without causing appreciable damage to the specimen (as a result of removing endcaps and jacketing materials). Therefore, dimensions were determined indirectly by making measurements of the

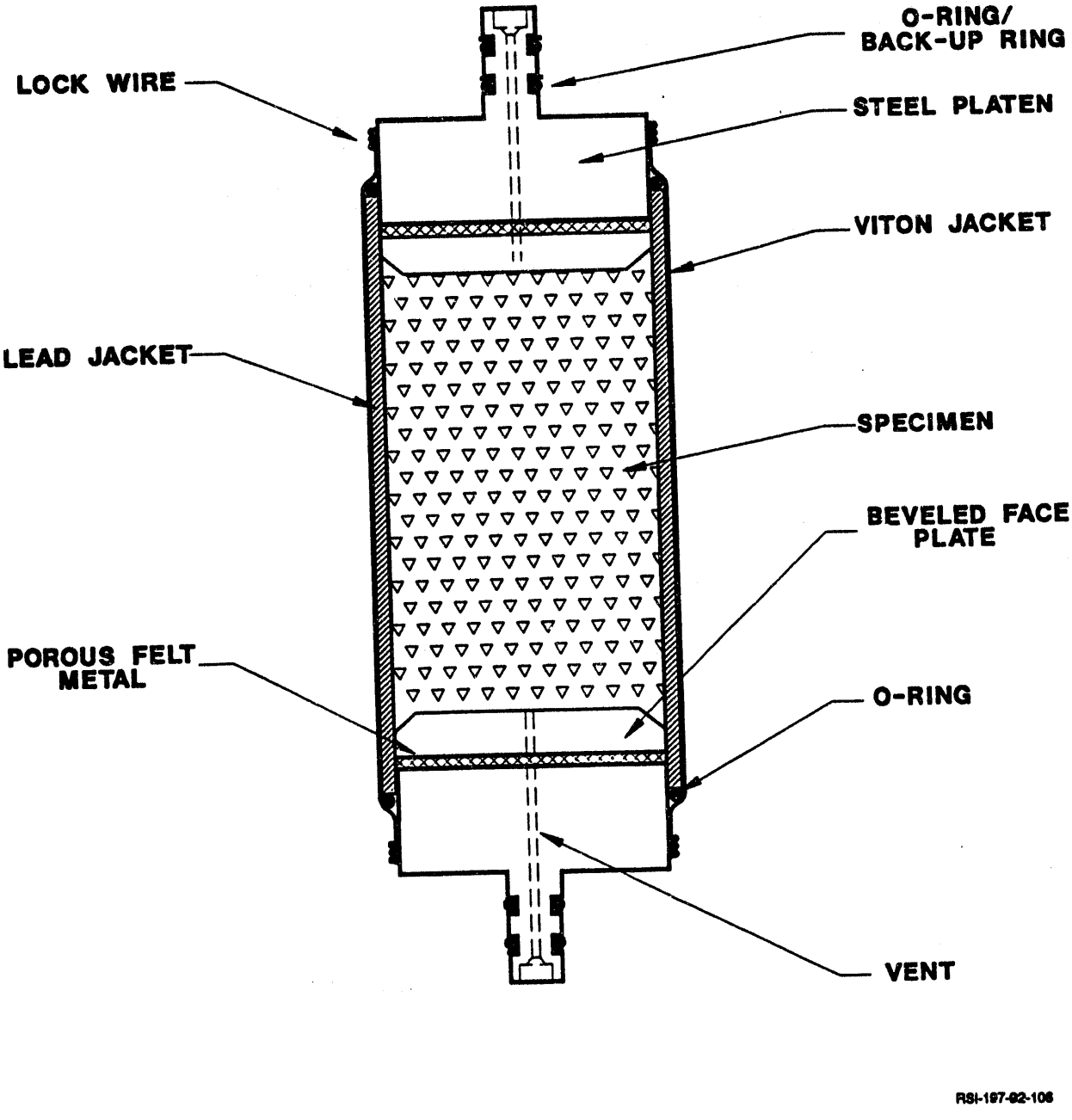

Figure 2-1. Specimen assembly for Sandia-furnished Specimen 20SEP89.

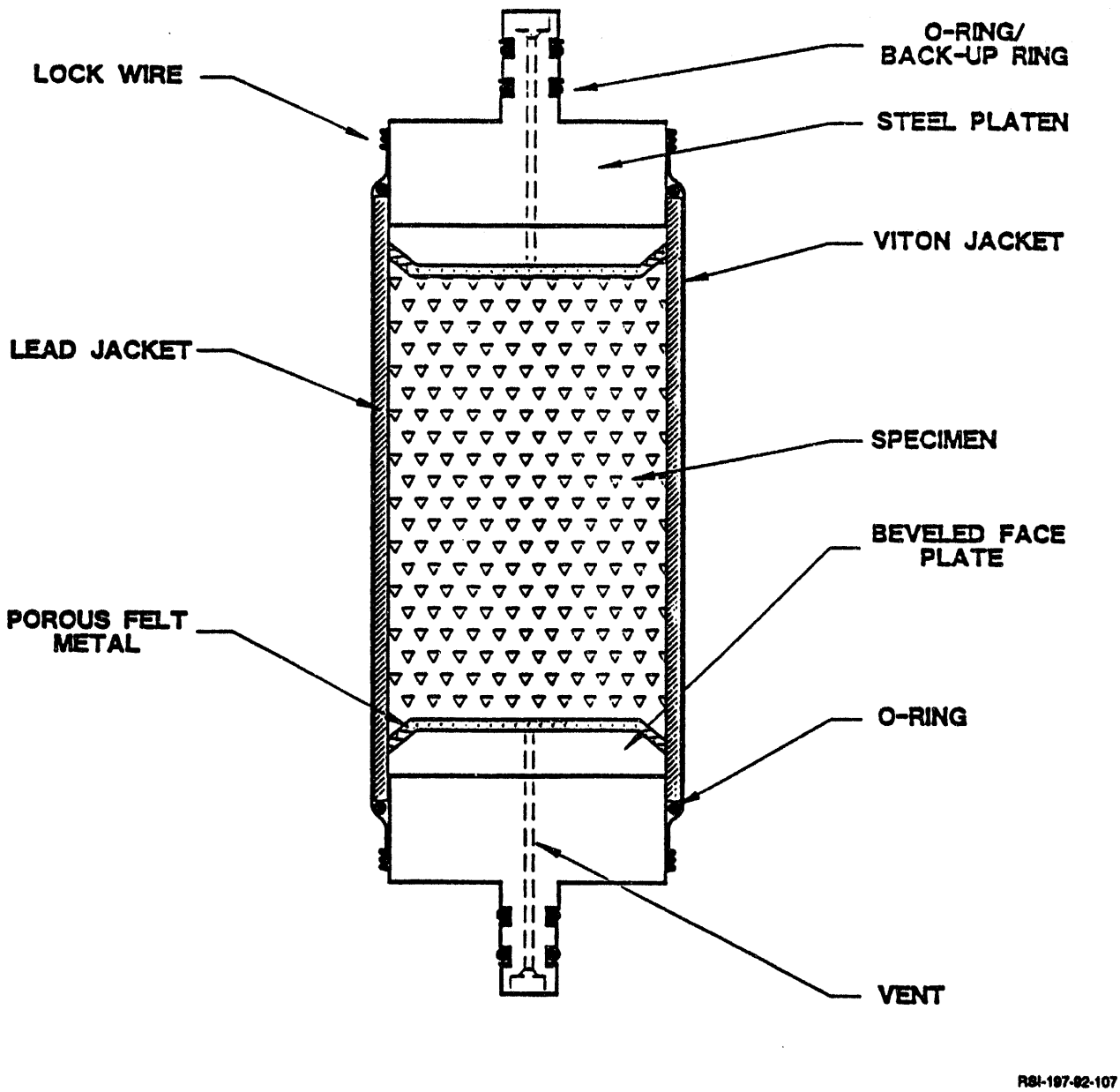

Figure 2-2. Specimen assembly used for Sandia-furnished Specimen 19JUN90 and for all hydrostatic and shear consolidation/permeability tests.

fully assembled specimen and correcting these measurements for non-specimen components. Measurements were made after each specimen was placed under a vacuum of approximately 630 mm of mercury for 2 hours. This method was used so that air trapped between the jacketing materials and the specimen and at other component interfaces within the assembly could be removed. The dimensions of the specimens are summarized in Table 2-1. The volume of Specimen 20SEP89 and fractional densities of Specimens 20SEP89 and 19JUN90 were measured by Sandia after the consolidation stage was completed. Their data, given in Table 2-2, shows very good agreement with the volume calculated from the length and diameter data given in Table 2-1. This implies that the indirect specimen measurements given in Table 2-1 are reasonably accurate and that very little or no relaxation occurred during the time interval between completion of the consolidation stage at Sandia and initiation of the permeability stage at RE/SPEC Inc.

Table 2-1. Summary of Specimen Dimensions

Specimen I.D.	Pre-Test[a] Specimen Dimensions		Post-Test[a] Specimen Dimensions	
	Length (mm)	Diameter (mm)	Length (mm)	Diameter (mm)
20SEP89	125.06	91.32	124.01	90.72
19JUN90	119.57	89.14	118.55	87.82
20JUN90	129.94	90.47	(b)	(b)

(a) Data were corrected for non-specimen component dimensions of L=189.91 mm and D=6.73 mm.
(b) No data due to jacket rupture.

Length measurements of the assembly included the specimen, the beveled faceplates, the porous felt metal, and the metal endcaps (platens), but not the endcap nipples. Measurements of the diameter included the specimen and the two jacketing materials. The dimensions of these materials were obtained from the Sandia Rock Mechanics Laboratory and were subtracted from the direct measurements. Direct length and diameter measurements were performed in six locations on each specimen. The dimensions shown in Table 2-1 represent the averages of multiple measurements made at the selected locations. Specimen identification numbers were provided by Sandia and are also shown in the table.

Table 2-2. Volume Measurements for Specimen 20SEP89

Specimen ID	Volume		Fractional Density
	Calculated[a] (m^3)	Measured (m^3)	
20SEP89	.000819	.000799	0.96
19JUN90	.000746	.000746	0.98

(a) Calculated from the length and diameter data in Table 2-1 assuming specimen is a right circular cylinder.

2.1.3 Post-Test Disposition

After the testing was completed, the Sandia-furnished specimens were returned to Division 6117, Sandia National Laboratories. The specimens were shipped to Sandia on October 22, 1991.

2.2 Consolidation/Permeability Specimens

2.2.1 Acquisition

Specimens consisted of crushed salt and brine. The crushed salt was provided by Sandia National Laboratories and was produced by a continuous miner during development of the WIPP test facility. The mine-run salt contains particles that range in size up to several centimeters. Specimens were manufactured from these raw materials at RE/SPEC Inc.

2.2.2 Particle Size Distribution

Because the test specimens have a nominal diameter of 102 mm, the mine-run salt was sieved to remove particles larger than 9.5 mm to produce a specimen-diameter-to-maximum-particle-size ratio of about 10. This produced two sample fractions: a smaller particle size

fraction containing all particles that passed though the 9.5-mm sieve and a larger particle size fraction. The particle size distribution of the smaller fraction was determined first. Using a sample splitter, a 3-kg sample was obtained and dried and then split into three 1-kg samples (the drying procedure and results are given in Section 2.2.3). Each 1-kg sample was sieved through a stack of stainless steel sieves mounted in a mechanical sieve shaker. The sieve sizes were 0.6 mm, 1.0 mm, 1.4 mm, 2.0 mm, 2.36 mm, 2.8 mm, 3.35 mm, 4.0 mm, 6.3 mm, 8.0 mm, and 9.5 mm. The particle size distribution, determined by measuring the mass of material remaining on each sieve, is shown in Figure 2-3 and labeled "Original Small Fraction."

The larger particle size fraction was crushed until all particles passed through the 9.5 mm sieve. A proportional amount of this crushed material was then mixed with the original small fraction. (The amount of coarse material was proportionately reduced to compensate for the 3-kg that had been removed from the finer sample.) The reason for this remixing was to preserve the in situ composition and impurity content of the salt. This mixed sample was split to obtain a 5-kg sample which was further split into a 2-kg and a 3-kg sample. The 2-kg sample was saved for chemical analyses (see Section 2.2.5) and the 3-kg sample was dried. (Drying results are given in Section 2.2.3.) The 3-kg sample was then divided into three equal parts and sieved to obtain the particle size distributions shown in Figure 2-3 and labeled "Final Mixed Sample." The data show good reproducibility and there appears to be no significant difference between the particle size distributions measured before and after adding the crushed larger particle size fraction. Holcomb and Shields (1987) sieved several batches of crushed WIPP salt and the envelope that contains their data is also shown in Figure 2-3. The current data fall within the window expected based on the work of Holcomb and Shields.

2.2.3 Moisture Content

Moisture contents of the smaller particle size fraction and of the mixed particle size fraction were determined using the same method. A 3-kg sample of each material was placed in a drying oven and dried at a temperature of 110°C until it reached a constant mass for a minimum of 2 days. The mass was determined using a Sartorius balance having a resolution of 0.01 g. The moisture contents based on dry weight were 0.1813 percent and 0.1523 percent for the smaller and mixed particle size fractions, respectively.

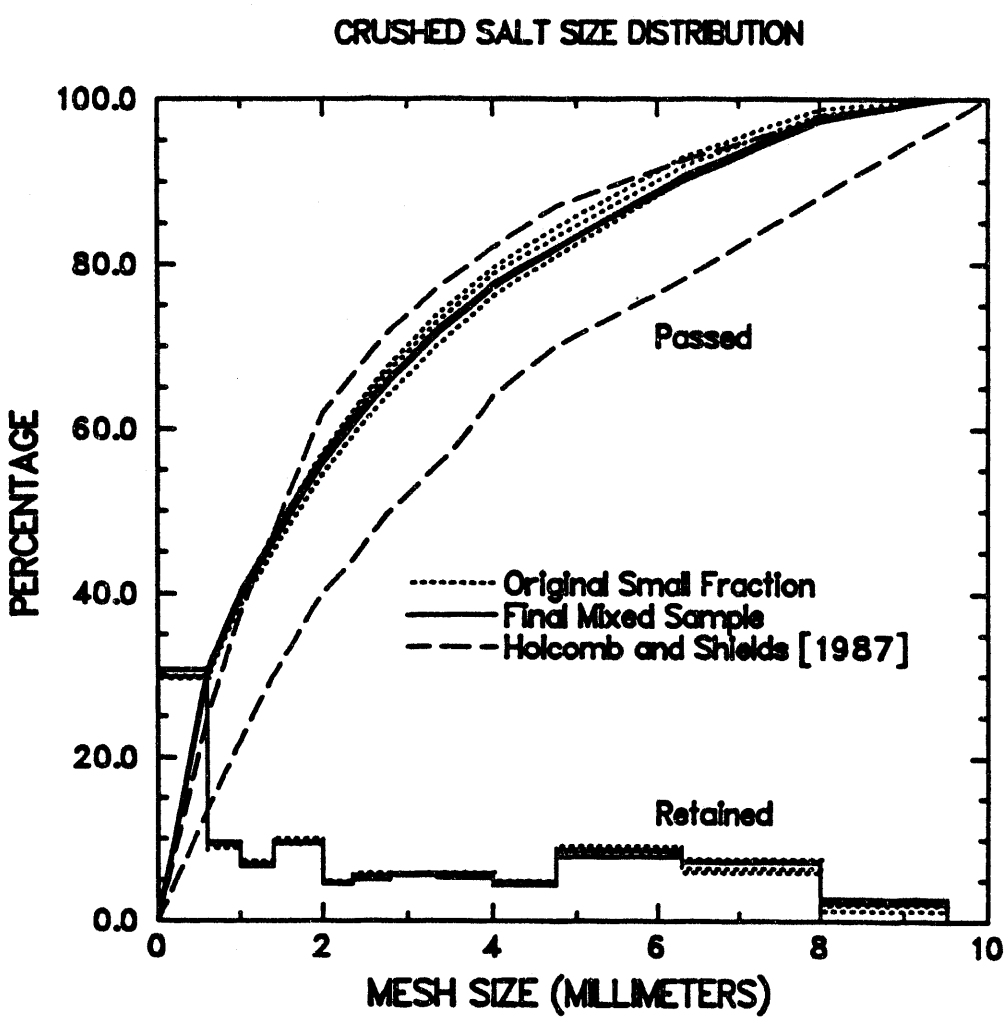

Figure 2-3. Particle size distribution measured for crushed WIPP salt.

2.2.4 Manufacture of Brine

Brine was manufactured from the final mixed sample. A sample of salt sufficient to manufacture 20 gallons of saturated brine was obtained using the sample splitter. This material was ground to a fine powder using a flour mill and was then mixed with distilled water until it precipitated out of solution. The density and moisture content of the brine were then measured. A 100-ml graduated cylinder was filled with brine and allowed to rest for several hours while all air bubbles were dislodged from the cylinder sides. The volume and mass of the brine were then measured. This measurement was repeated nine times and a value of brine density of 1,208 ± .001 kg · m^{-3} was determined. Approximately 500 ml of brine were then placed in a drying oven for 10 days until the mass stabilized. The brine was found to be 26.53 percent solids by weight. A fully saturated solution of salt and water at 20°C contains 26.43 percent solids by weight and has a density of 1,199 kg · m^{-3}. These two measurements are both consistent with using a value of 1,200 kg · m^{-3} for the density of brine.

2.2.5 Impurity Content

RE/SPEC Inc. does not have the facilities for performing quantitative chemical analyses, and so this work was subcontracted to Twin City Testing of Rapid City, South Dakota. Three nominally identical samples of the mixed fraction of WIPP salt were given to the testing laboratory. They determined the weight percent of calcium, chloride, magnesium, potassium, sodium, strontium, and sulfate in the soluble fraction of the salt. They also determined the weight percent of insolubles and the weight percent of insoluble materials that are also insoluble in ethylene diaminetetracetric acid (EDTA). The complete report from Twin City Testing is given in Appendix A and their results are summarized in Table 2-3. The weight percent of EDTA insolubles is listed twice, once under total insolubles and once under EDTA insolubles. The results are somewhat disappointing in that the components do not sum to 100 percent.

The average of the three trials was used in processing the data, and the data were scaled so that the weight percents summed to 100 percent (see Table 2-3). For the water soluble species, the weight percent was then divided by the atomic or molecular weight to obtain the number of moles of each species present in a representative gram of material.

The mineralogy expected in crushed WIPP salt was taken from a Sandia National Laboratories memorandum which is reproduced in Appendix B. The solubles were assumed to contain halite and some polyhalite. Anhydrite, gypsum, and magnesite are insoluble in water but

Table 2-3. Chemical Analyses of Crushed WIPP Salt

	Trial 1 Weight (%)	Trial 2 Weight (%)	Trial 3 Weight (%)	Average Weight (%)	Scaled Weight (%)	Molecular Weight (g/mole)	Moles[a]
Solubles							
Calcium	0.15	0.26	0.24	0.2167	0.23	40.08	5.74E-05
Chloride	58.0	58.0	56.0	57.3333	60.871	35.45	0.017171
Magnesium	0.062	0.074	0.084	0.0733	0.0779	24.31	3.2E-05
Potassium	0.151	0.174	0.232	0.1857	0.1971	39.09	5.04E-05
Sodium	35.0	34.2	34.1	34.4333	36.558	22.99	0.015902
Strontium	0.005	0.006	0.007	0.006	6.37E-03	87.62	7.27E-07
Sulfate	0.62	0.96	0.98	0.8533	0.906	96.06	9.43E-05
Insolubles (Total)	0.91	0.83	1.52	1.0867	1.1537		
EDTA Insolubles	0.32	0.51	1.01	0.6133	0.6512		
Total	94.898	94.504	93.163	94.1883	100		

(a) In a representative gram of material.

soluble in EDTA. Stein found anhydrite and magnesite to be the most abundant of these and so the difference between the weights of insolubles and EDTA insolubles was attributed to anhydrite and magnesite. The remaining insolubles (EDTA insolubles) were assumed to be quartz and clay (primarily montmorillonite) in accord with Stein's findings.

The mineralogy is given for each solubility classification in Table 2-4. The number of moles of each soluble mineral (halite or polyhalite) was calculated from the number of moles of the most limiting species. For halite, there were fewer moles of sodium than chloride, and so the abundance of sodium limited the calculated amount of halite. For polyhalite, sulfate was the most limiting species. Once the number of moles of each mineral was determined, it was multiplied by the molecular weight of the mineral to determine the mass of each mineral. The number of moles of each species that remained unused is also given in Table 2-4. For the insolubles, the number of moles of each mineral was not calculated. The mass of EDTA insolubles was evenly divided between clay and quartz, and the mass of total insolubles minus EDTA insolubles was evenly divided between anhydrite and magnesite.

Table 2-4. Analyses of Chemical Data

	Moles[a]	Molecular Weight (g/mole)	Mass[a] (g)	Weight[b] Percent (%)	Specific Gravity ($g \cdot cm^{-3}$)	Volume[a] (cm^3)
Solubles						
Halite	0.015902	58.44	0.929294	97.3035	2165.	0.429235
Polyhalite	2.36E-05	602.89	0.014215	1.4884	2780.	0.005113
Subtotal			0.943509	98.792		0.434349
Remaining Solubles						
Chloride	0.001269					
Potassium	3.27E-06					
Calcium	1.02E-05					
Magnesium	8.45E-06					
EDTA Insolubles						
Clay (montmorillonite)			0.003256	0.3409	2.5	0.001302
Quartz			0.003256	0.3409	2.65	0.001229
Insolubles Minus EDTA Insolubles						
Anhydrite			0.002513	0.2631	2.61	0.000963
Magnesite			0.002513	0.2631	3.1	0.000811
Total			0.955047	100		0.438653

(a) In a representative gram of material.
(b) Scaled so that components (minus remaining solubles) sum to 100 percent.

Once the mass of each mineral was determined, the weight percent of each mineral was calculated. The crushed salt is 98.8 percent soluble. It contains 97.3 percent halite and 1.5 percent polyhalite by weight. The insolubles are 1.2 percent of the crushed salt by weight. The EDTA insolubles (clay and quartz) are 0.68 percent of the sample by weight and the remaining insolubles (anhydrite and magnesite) are 0.53 percent by weight. The density of the crushed salt mixture was calculated from the mass and volume of each mineral component using specific gravity to convert masses to volumes. The density of the water soluble solids was 2.17 $g \cdot cm^{-3}$ and the density of all solids was 2.18 $g \cdot cm^{-3}$.

The final weight percent values for each mineral and the density values for the crushed salt mixture must be viewed with extreme caution because the input data needed to be scaled by 5 percent in order for the components to sum to 100 percent, because quantities of soluble species

remained after the calculations were completed, and because assumptions concerning mineralogy went into the data processing.

2.2.6 Specimen Manufacture and Density Determination

Specimens were manufactured following the procedure outlined by Holcomb and Shields (1987). An excess quantity of crushed salt was poured onto a clean flat surface to form a conical pile. The pile was divided into eight equal wedges and the mass of each wedge was determined using a Sartorius balance with a resolution of 0.01 g. Saturated brine was sprayed onto each wedge until the added brine comprised 3 percent of the sample mass. A small amount of damp salt was removed from each wedge for moisture content measurements and the remaining salt was poured into a cylindrical tube-shaped jacket. This process was repeated for each wedge until the appropriate specimen volume was reached. The mass of material used for moisture content measurements and the amounts remaining after pouring each wedge were recorded. These values were subtracted from the total mass of the damp wedges to obtain specimen mass.

The completed specimen assembly is shown in Figure 2-2. The same specimen configuration was used for these tests as for Specimen 19JUN90. It contains a two-component jacket and vented steel endcaps. All vents were 3.175 mm (0.125 in) in diameter. The jacket is fabricated using a 1.6-mm-thick lead inner jacket and a Viton outer jacket to seal the specimen from the silicone oil used as the confining pressure medium. The lead jacket protects the outer jacket from rupturing by preventing the Viton from intruding into the pores of the specimen during pressurization. Tapered aluminum faceplates were used to provide a smooth transition between the rigid steel endcaps and the highly deformable crushed salt. These faceplates prevented the jacket from conforming to sharp changes in dimension (i.e., diameter) at the endcap/specimen interface, and thus, reduced the chance for jacket rupture during specimen deformation. Shaped porous felt metal disks conformed to the faceplates and were used to provide a permeable pathway for the transport of brine and also to prevent salt from plugging the vents in the platens. Nominal specimen dimensions were 101.6 mm (4 in) in diameter and 184.2 mm (7.25 in) in length between the flat portions of the porous felt metal.

Density determinations were made after initial specimen manufacture, after preconsolidation, and after each test stage. Specimen mass was determined during specimen preparation. Volumes were determined after specimen assembly using two techniques: (1) fluid (water) displacement, and (2) indirect contact dimensional measurements. Both types of measurements were made after the specimen had been subjected to a vacuum of approximately 630 mm of mercury for 2 hours.

The vacuum served to remove air trapped between the layers of jacketing materials and between interfaces in the specimen assembly.

In the fluid displacement technique, the volume of the jacketed specimen was determined by submerging the specimen assembly in a water-filled container equipped with an overflow spout. The weight of the displaced water was measured and converted to a volume measurement using the specific gravity of the fluid. The volumes of the non-specimen components were determined from their masses and specific gravities and were subtracted from the total volume to obtain specimen volume.

The indirect contact measurement technique was discussed in Section 2.1.2. Specimen volume was determined from the length and diameter of the specimen assuming a right-circular cylindrical geometry. The diameter of the specimen was determined by first measuring the diameter of the jacketed specimen at six locations using a micrometer and then reducing these measurements by twice the lead and Viton jacket thicknesses. Similarly, the length of the specimen was determined by measuring the height of the jacketed specimen in four locations using a gage head and transfer standard and then subtracting the lengths of the endcaps, porous felt metal, and faceplates from this measured height. Specimen dimensions were required for processing the permeability data; however, this measurement also served as a check on the value calculated using the fluid displacement technique.

Tables 2-5 and 2-6 summarize volume measurements made using these two techniques for hydrostatic and shear consolidation tests, respectively. Measurements made using the two techniques differ by 1.59 ± 1.38 percent and 1.66 ± 2.56 percent for hydrostatic and shear consolidation tests, respectively. The two measurements can differ either because irregularities in the specimen geometry cause the direct contact measurements to be inaccurate, or because evaporation of displaced fluid causes errors in the immersion measurement.

The volume from the fluid displacement technique was almost always the basis for density determinations because this method does not rely on point measurements and makes no assumptions about specimen geometry. The indirect contact measurements were used only if the values obtained using the two techniques differed by more than 5 percent and if the immersion value did not appear reasonable (i.e., the value showed the specimen to have substantially expanded during a compression stage). The volumes given in bold font in Tables 2-5 and 2-6 were used for calculations. The indirect contact measurements were only used for final volume measurements for two tests, HC5A and SC4A.

Table 2-5. Summary of Specimen Volume Measurements for Hydrostatic Consolidation Tests

Test	Measurement Technique	Specimen Volume (m^3)[a]			
		Initial Measurement	After Conditioning	After Stage 1	After Stage 2
HC1	Immersion	**.00149143**	**.00141529**	**.00113533**	**.00112786**
	Indirect Contact	.00145903	.00139893	.00110582	.00108831
	Difference (%)	2.17	1.16	2.60	3.46
HC2	Immersion	**.00152182**	**.00138378**	**.00104277**	**.00104315**
	Indirect Contact	.00151451	.00139039	.00107498	.00103960
	Difference (%)	0.48	0.48	3.09	.034
HC3	Immersion	**.00148941**	**.00135480**	**.00105617**	**.00106979**
	Indirect Contact	.00146306	.00135371	.00105339	.00103963
	Difference (%)	1.77	0.08	0.26	2.82
HC4	Immersion	**.00148253**	**.00131283**	**.00100729**	**.00104323**
	Indirect Contact	.00147027	.00131996	.00103628	.00102406
	Difference (%)	0.83	0.54	2.88	1.84
HC5	Immersion	**.00145204**	**.00128273**	**.00102299**	.00107873
	Indirect Contact	.00142079	.00128549	.00103415	**.00101581**
	Difference (%)	2.15	0.21	1.09	5.83
HC6	Immersion	**.00155874**	**.00129399**	**.00102317**	**.00101131**
	Indirect Contact	.00152825	.00128240	.00102348	.00102356
	Difference (%)	1.96	0.90	0.03	1.21

(a) Values printed in bold were used in calculations.

Table 2-6. Summary of Specimen Volume Measurements for Shear Consolidation Tests

Test	Measurement Technique	Specimen Volume (m^3)[a]			
		Initial Measurement	After Conditioning	After Stage 1	After Stage 2
SC1	Immersion	**.0014852**	**.0013435**	**.0010774**	**.0010433**
	Indirect Contact	.0014477	.0013238	.0010603	.0010399
	Difference (%)	2.52	1.46	1.58	0.33
SC2	Immersion	**.0013919**	**.0013005**	**0.0010192**	**.0009737**
	Indirect Contact	.0014131	.0013080	0.001038	.0011113
	Difference (%)	1.53	0.57	1.84	14.13
SC3	Immersion	**.0015078**	**.0013604**	**.0010974**	**.0010522**
	Indirect Contact	.0015013	.0013546	.0010648	.0010523
	Difference (%)	0.43	0.43	2.97	0.01
SC4	Immersion	**.0014765**	**.0013245**	**.0010505**	.0011260
	Indirect Contact	.0014702	.0013146	.0010296	**.0010353**
	Difference (%)	0.42	.075	1.98	8.05
SC5	Immersion	**.0015148**	**.0013244**	**.0010781**	**.0010621**
	Indirect Contact	.0014903	.0013164	.0010662	.0010620
	Difference (%)	1.61	0.60	1.11	0.01
SC6	Immersion	**.0015159**	**.0012630**	**.0010111**	**.0009974**
	Indirect Contact	.0014901	.0012634	.0010343	.0010277
	Difference (%)	1.70	0.03	2.30	3.03
SC7	Immersion	**.0015275**	**.0013410**	**.0010646**	**.0010615**
	Indirect Contact	.0015218	.0013448	.0010789	.0010583
	Difference (%)	0.38	.028	1.34	0.30
SC8	Immersion	**.0014826**	**.0012702**	**.0009997**	**.0010145**
	Indirect Contact	.0014623	.0012664	.0010162	.0010072
	Difference (%)	1.37	0.29	1.64	0.72
SC9	Immersion	**.0015309**	**.0012921**	**.0010434**	**.0010227**
	Indirect Contact	.0015169	.0013014	.0010516	.0010387
	Difference (%)	0.91	0.73	0.79	1.56

(a) Values given in bold were used in calculations.

3.0 TEST APPARATUS

3.1 Consolidation

3.1.1 Load Frame

Figure 3-1 presents a cross section of a typical consolidation load frame with prominent components labeled for reference. The frames are nearly identical to those used by Division 6117, Sandia National Laboratories, and accommodated the assembled Sandia-furnished specimens without modification. The frames use single-ended, triaxial pressure vessels. A linear actuator (hydraulic cylinder) bolted to the base of the load frame drives the loading piston, which in turn applies axial compressive force to the specimen. Confining pressure is applied to the jacketed specimens by pressurizing the sealed vessel chamber with silicone oil. A dilatometer system maintains constant confining pressure and provides the volumetric measurement.

The testing machines can apply compressive axial loads up to 1.5 MN and confining pressures up to 70 MPa. The heating system, including seals on the pressure vessel, can maintain specimen temperatures up to 200°C.

A control panel houses the accumulators, hydraulic pumps, pressure intensifiers, transducer signal conditioners, temperature controllers, and confining pressure controllers for two adjacent test frames. The panels contain digital meters that display the output of the transducers. The temperature controller gives a digital output of the temperature. Mechanical pressure gages mounted in the panel give readings of oil pressure in the hydraulic cylinder.

3.1.2 Instrumentation

Axial force is measured by a load cell in the load train outside the pressure vessel, while confining pressure is measured by a pressure transducer in the line between the intensifier and the pressure vessel. Temperature is measured by a thermocouple in the wall of the pressure vessel. The relationship between specimen temperature and that recorded by this thermocouple has been determined by calibration runs at several temperatures spanning the operating range. Two Linear Variable Differential Transformers (LVDTs) mounted outside the pressure vessel monitor displacement of the loading piston relative to the bottom of the pressure vessel.

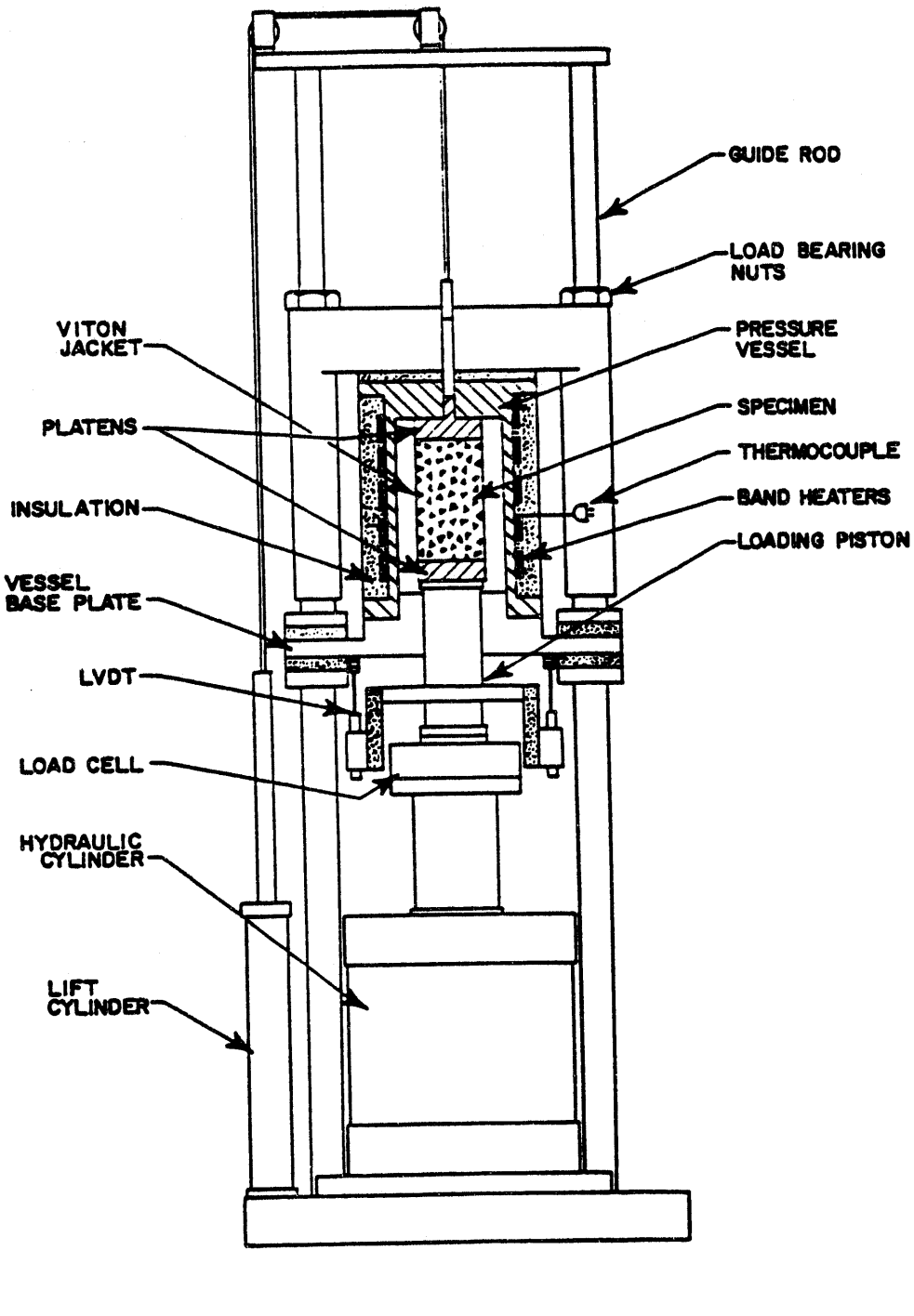

Figure 3-1. Consolidation machine load frame.

Volumetric deformation is measured using a dilatometer. With this technique, volumetric deformation is determined at fixed pressure by first measuring the volume of oil that the dilatometer supplies to the pressure vessel, and then compensating for the axial deformation measured by the LVDTs. A rotary potentiometer or stroke transducer is mounted on the dilatometer shaft to provide a signal proportional to the volume of oil supplied to the pressure vessel.

3.1.3 Control

Temperature is maintained with a manual set-point controller that regulates power to the band heaters on the vessel. The thermocouple in the pressure vessel wall supplies the feedback signal. Hydrostatic stress during the hydrostatic consolidation tests and confining pressure during the shear consolidation tests are controlled by inputting the pressure transducer signal to a unit that contains two manual set points. These set points are adjusted to maintain the hydrostatic stress or confining pressure constant within 20 kPa. The controller signals the intensifier to advance or retreat, depending upon whether the lower or upper set point has been reached. During shear consolidation, axial load is controlled by a Digital Equipment Corporation PDP-11/23 microcomputer. The computer determines the current cross-sectional area of the specimen from the outputs of the deformation transducers and then adjusts the load to maintain constant stress. The deadband on load under computer control is 0.4 kN. A standby diesel generator provides electrical power to the test system during periods of commercial electrical power outages.

3.1.4 Permeability System

Two systems were used for permeability measurements. The first, shown in Figure 3-2, was used to measure permeability of Sandia-furnished specimens. In this system, an accumulator was connected hydraulically to a manifold that supplied brine permeant under pressure to three load frames. The supply lines are 3.2-mm-inner-diameter (0.125-in.-i.d.) stainless steel tubes and extend from the manifold to the vent in the lower endcap of the specimen assembly. The accumulator is filled with brine and charged with nitrogen using a standard nitrogen bottle. The charge pressure (and, therefore, the pressure drop across each specimen) is regulated manually with a valve located on the nitrogen bottle and is measured using a diaphragm-type pressure transducer in the line between the accumulator and the manifold. The pressure drop in the lines between the pressure transducer and the specimen is negligible because flow rates through the specimen are very small. Brine flow through the specimen is captured and measured by a buret

attached to the upper endcap of the specimen assembly. Evaporation of water is controlled by placing a thin film of mineral oil on top of the brine column in the buret.

To ensure that this method of preventing evaporation was effective, a brine-filled buret capped with a thin film of mineral oil was placed in the laboratory approximately in the center of the testing machines used for this work. The brine level was monitored for 320 days and the data are shown in Figure 3-3. Over the first 15 days of testing, the brine level dropped due to the release of air bubbles entrapped against the walls of the buret. (This drop appears as a step function due to the resolution of the calibration marks of the buret.) There was no further decrease in buret level over the duration of the test, signifying that this method of preventing evaporation was effective.

The temperature of the brine entering the pressure vessel was assumed to be the ambient temperature of the laboratory (20 ± 1°C). To verify this assumption, a thermocouple was installed inside one of the brine accumulators and monitored regularly. The temperature as measured in the brine between Feb. 5, 1992 and Dec. 1, 1992 is given in Figure 3-4. The brine temperature, calculated as the average of the readings obtained, is 20.00 ± 1.06°C. Occasional peaks in the data are due to malfunctions of the heat pump that controls laboratory temperature.

The system used to measure permeability in the consolidation/permeability tests is shown in Figure 3-5. This system differs from the first only in that a separate accumulator is used for each test system.

3.1.5 Calibration

3.1.5.1 TRANSDUCER CALIBRATIONS AND VERIFICATIONS

The transducers used to collect force, pressure, deformation, and temperature data were calibrated using standards traceable to the National Institute of Standards and Technology and documented procedures. Each transducer is calibrated in its normal operating position on the test system so that the signal conditioners, filters, and analog-to-digital converters are included within the end-to-end calibration. Calibration constants are determined for each transducer from a linear, least-squares regression of indicated reading versus standard input. Readings are collected at 20 standard inputs equally spaced over the range of the transducer. These constants are verified immediately before a test begins by comparing the predicted response of the transducer

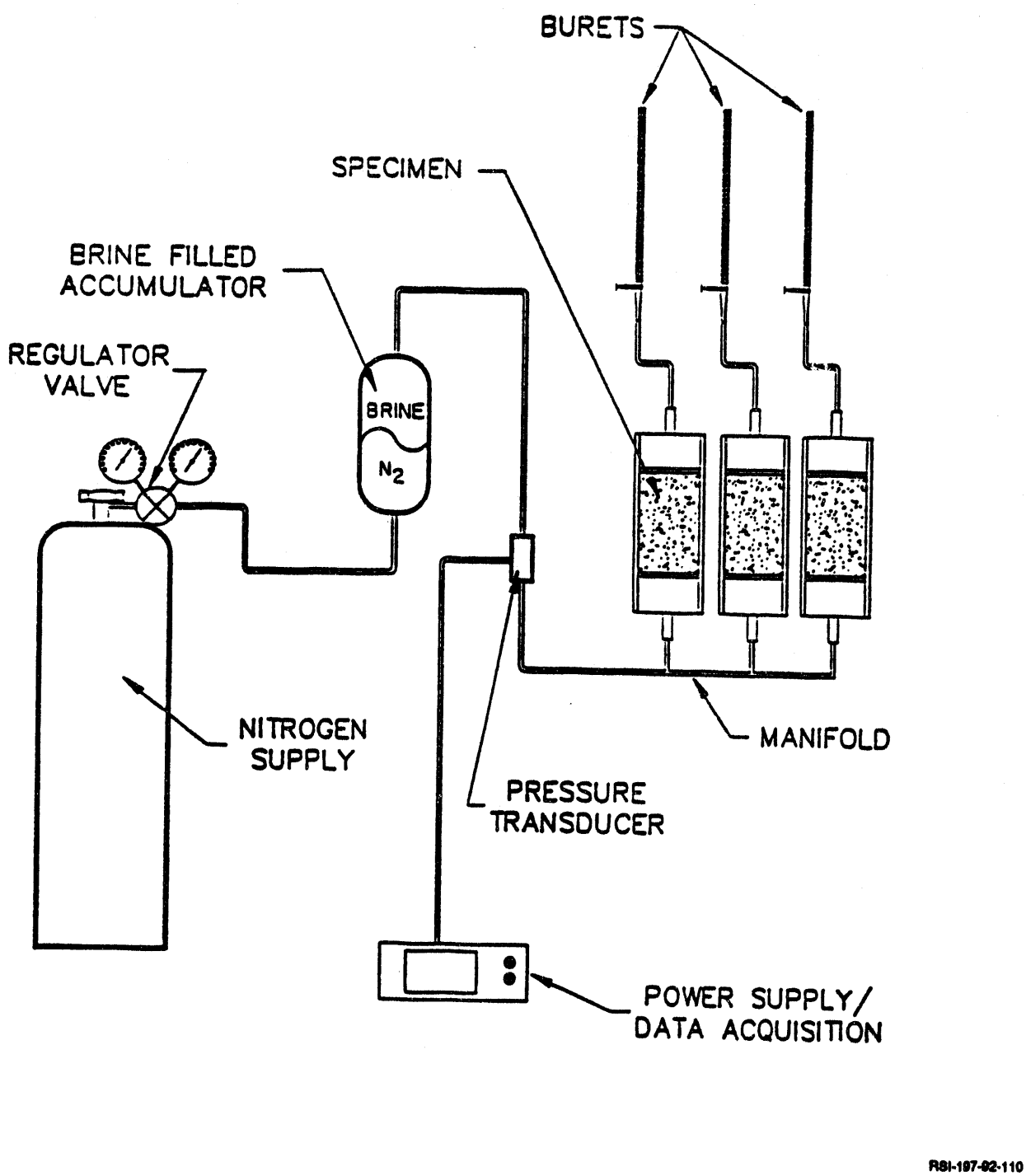

Figure 3-2. Schematic of brine permeability test apparatus used for Sandia-furnished specimens.

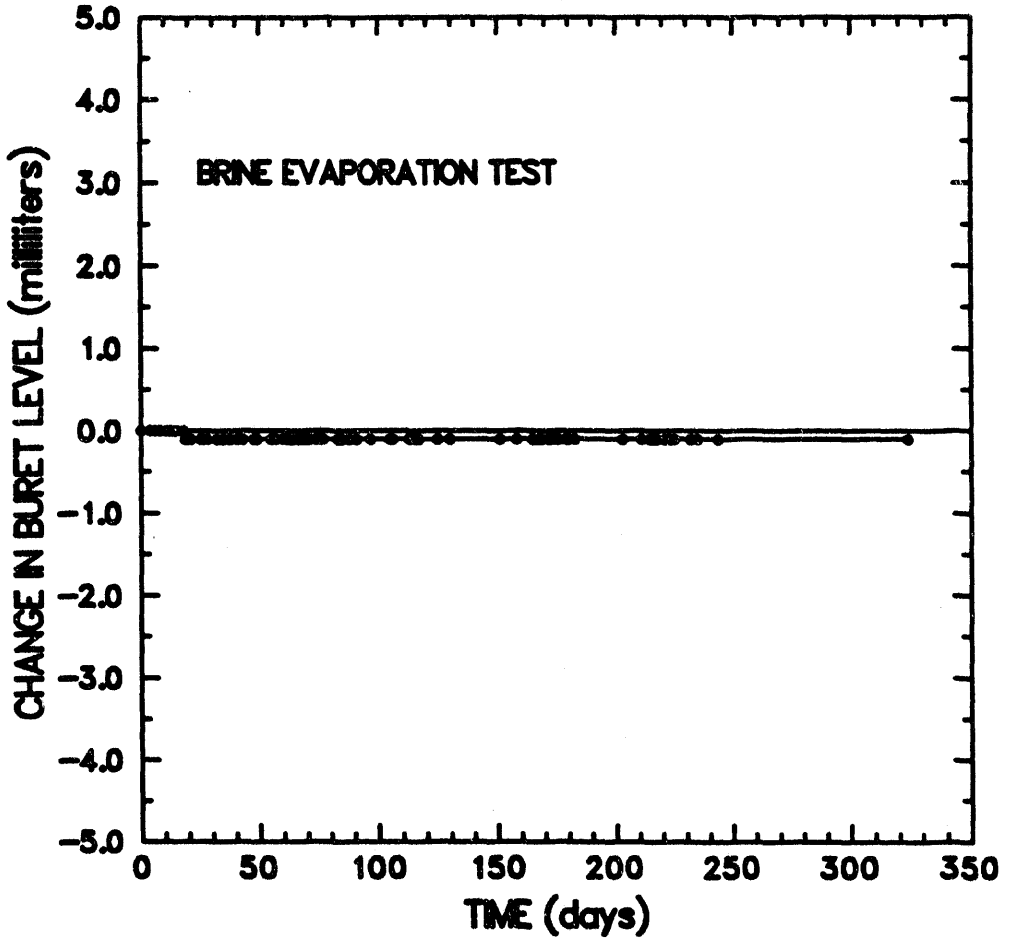

Figure 3-3. Change in brine volume as a function of time during brine evaporation test.

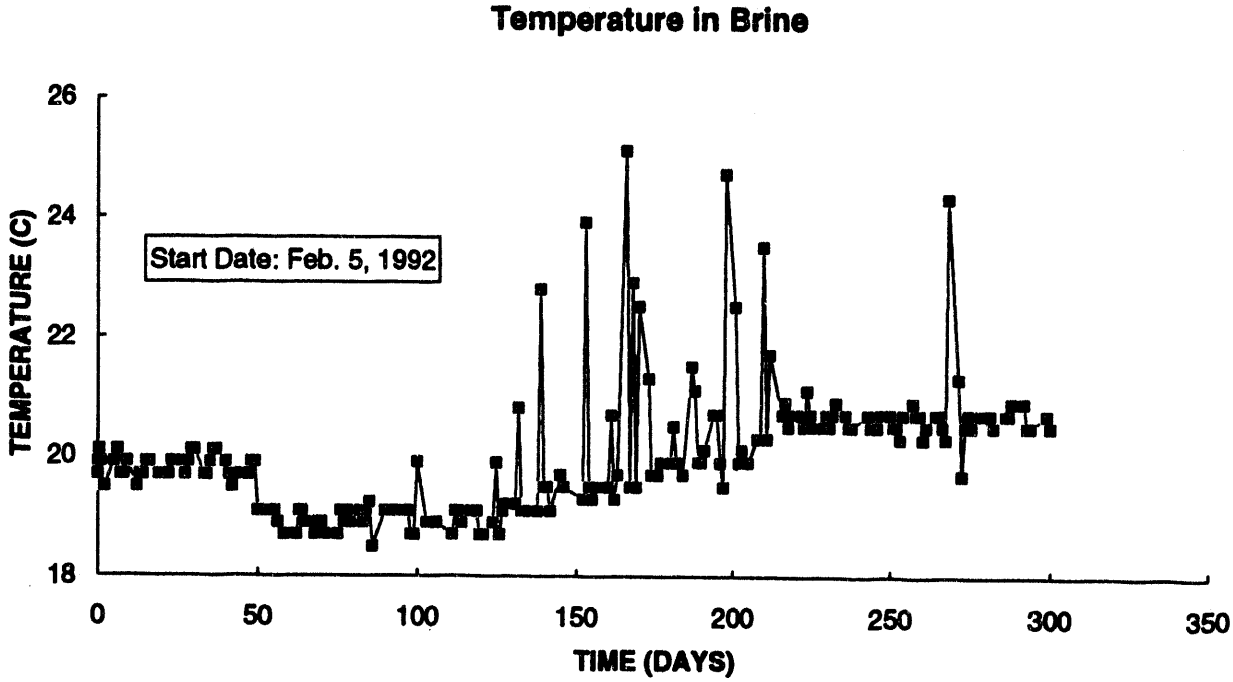

Figure 3-4. Temperature in brine as measured during permeability testing by thermocouple located inside upstream brine reservoir.

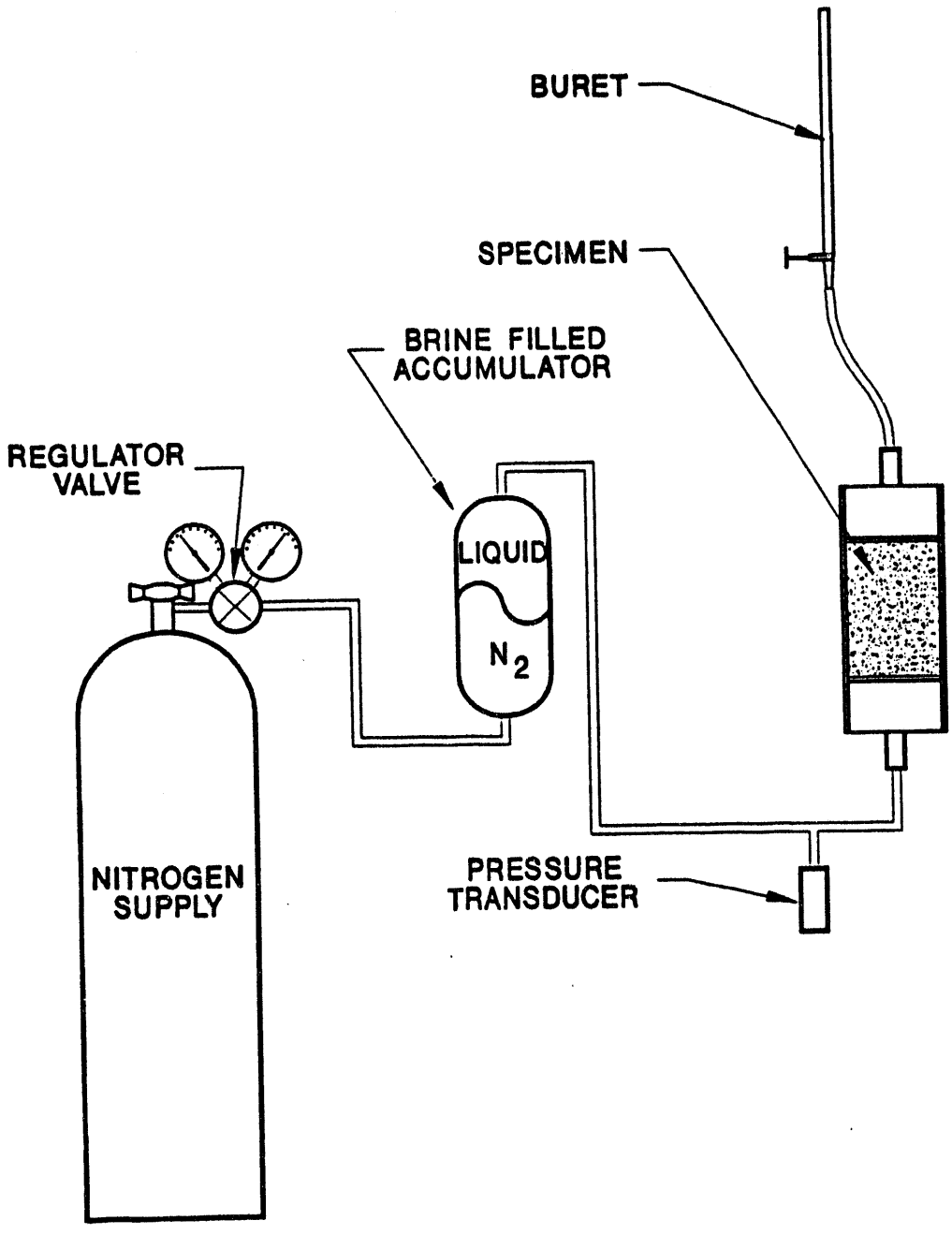

RSH-187-82-113

SCALE: NONE

Figure 3-5. Schematic of brine permeability test apparatus used for hydrostatic and shear consolidation tests.

using these constants with the standard input applied in ten equally spaced steps over the calibrated range. This verification procedure is also performed at the end of each test so that drift or malfunctions of the transducers can be identified. Table 3-1 gives the range and resolution for these transducers. Prior to testing, the accuracy of force and pressure transducers was 1 percent of reading, that of deformation transducers was 2 percent of reading, and that of thermocouples was ±1°C. The accuracy specifications include both nonlinearity and repeatability. The burets used were Class A and are accurate to within 0.1 ml. A summary of the transducer reverification data obtained after completion of each test is given in Appendix C.

Table 3-1. Calibration Specifications

Measurement	Range	Resolution
CONSOLIDATION		
Axial Force (kN)[a]	0 to 250	0.03[b]
Confining Pressure (MPa)[a]	0 to 34.5	0.004[b]
Lateral Strain (%)[c]	0 to 8	0.001[b]
Axial Strain (%)[c]	0 to 12.5	0.002[b]
Temperature (°C)[d]	0 to 250	0.03[b]
PERMEABILITY		
Pressure (kPa)[e]	0 to 345	0.70[f]
Pressure (MPa)[g]	0 to 6.895	0.0008[b]

(a) Accuracy: 1 percent of reading including nonlinearity and repeatability.
(b) 14-bit analog-to-digital converter.
(c) Accuracy: 2 percent of reading including nonlinearity and repeatability.
(d) Accuracy: ± 1°C.
(e) System used for Sandia-furnished specimens.
(f) 4-1/2-digit panel meter. Accuracy during reverification was to within 1.5 percent of reading, including nonlinearity and repeatability.
(g) System used for consolidation/permeability specimens.

3.1.5.2 ADIABATIC TEMPERATURE CHANGE CALIBRATION TEST

All test specimens were subjected to pressurization and therefore to adiabatic heating of the confining fluid. Following the procedure of Holcomb and Shields (1987), a test was run on an aluminum specimen to determine the apparent volumetric strain that accumulates due to cooling of the confining fluid after pressurization. The test was initiated by placing an aluminum specimen in the pressure vessel, filling the vessel with oil, and allowing its temperature to stabilize for at least 2 hours. The pressure was then raised to a value that would later be used in crushed-salt consolidation tests. Apparent changes in volume of the aluminum specimen were measured by the dilatometer as the confining oil cooled. Pressure was held at the test value for at least 7 hours to determine the total apparent volume change associated with cooling and the length of time required for the system temperature to stabilize. This process was repeated for all confining pressures that would be used during testing.

The total apparent changes in volume that occurred at each test pressure due to cooling are shown in Figure 3-6. For pressures of 3.45 MPa and above, the cooling process was completed within 1.5 hours and the data show a consistent trend. The apparent volume change associated with cooling for these tests was 0.23 ml/MPa and this correction was applied to the data. This value compares reasonably well with the value of 0.4 ml/MPa reported by Holcomb and Shields, considering that these are not identical machines. One test at 1.72 MPa required dilatometric corrections for 7 hours, after which it stabilized. A nominally identical test at 1.72 MPa showed a lower apparent volumetric strain, but did not completely stabilize after 15 hours although the dilatometer rate continued to decrease throughout this time period. These low pressure data were therefore not included in the fit. It is assumed that at the lowest pressure, the seals in the pressure vessel creep in a time-dependent manner until they form a proper seal. The maximum apparent changes in volume are on the order of $2.5 \times 10^{-6} m^3$. The specimen volumes after preconsolidation are approximately .001300 m^3, and so if no corrections were made, the errors incurred in volumetric strain due to this apparent strain would be approximately 0.1 percent.

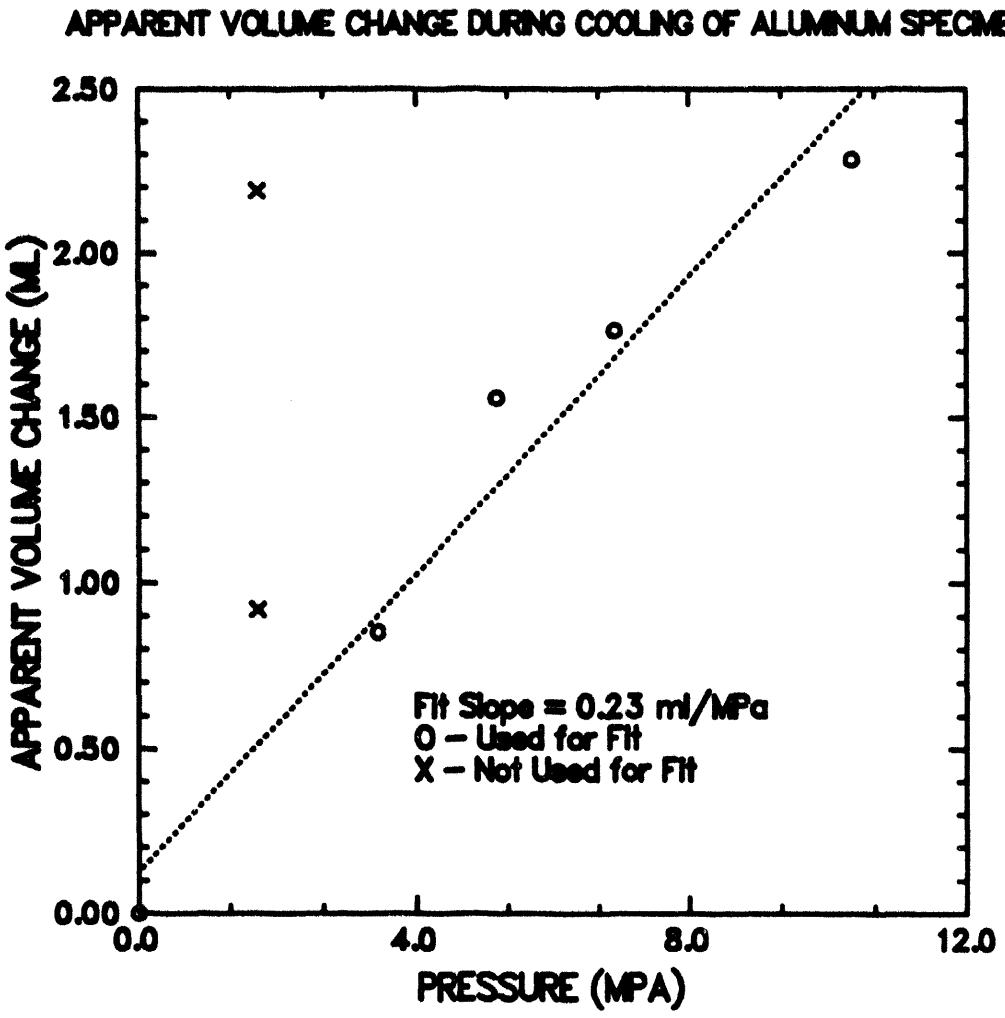

Figure 3-6. Apparent volume change measured during cooling of an aluminum specimen after adiabatic compression of confining oil.

4.0 TEST PROCEDURES

4.1 Preconditioning

The initial application of hydrostatic compressive stress produces large changes in density. These density changes cannot be accurately measured in the testing machine and so a preconditioning step is used before compressive load is applied. The preconditioning consists of placing the assembled specimen in the load frame, hydrostatically loading to the desired preconditioning pressure as quickly as possible, holding the specimen at pressure for one minute, and then unloading. The hydrostatic pressure is applied by pressurizing the confining oil using an air-driven pump. For hydrostatic consolidation tests, the preconditioning pressure was equal in magnitude to the pressure used in the first test stage; for shear consolidation tests, the mean stress of the first test stage was used. Density measurements were made before and after the preconditioning step using the methods described in Section 2.2.6. Preconditioning was not required for Sandia-furnished specimens because they were already consolidated. It was also not required before permeability stages because the specimens had already been compacted at higher compressive loads. Preconditioning was only carried out before the first stages of hydrostatic and shear consolidation tests.

4.2 Hydrostatic Consolidation and Testing

All Sandia-furnished specimens and six hydrostatic consolidation specimens were subjected to hydrostatic consolidation stages. Each of the Sandia-furnished specimens used for permeability measurements was first subjected to a stage of hydrostatic pressurization at 6.9 MPa and 25°C as shown in Table 4-1.

Six hydrostatic consolidation tests on specimens assembled at RE/SPEC Inc. were performed at 25°C and at the stress conditions shown in Table 4-2. Tests were labeled in a manner that corresponds to the test matrix given. The designation "HC" signifies hydrostatic consolidation. The first HC1 test to be pressurized was given the designation "A" and the test label became HC1A. If a test was repeated, the designation "B" would be added. Prior to testing, each specimen was preconditioned, its new density was determined, and then it was saturated with brine. Saturation was accomplished by removing the upper platen and faceplate and pouring a measured quantity of brine into the specimen assembly. The assembly was then covered to prevent evaporation. Quantities of brine were added until no further absorption occurred over a 12-hour period.

Table 4-1. Summary of Test Conditions for Sandia-Furnished Specimens

Specimen ID	Stage	Hydrostatic Stress (MPa)	Fluid Pressure (MPa)
19JUN90	1	6.90	0
	2	3.45	0.345
20SEP89	1	6.90	0
	2	3.45	0.345

Table 4-2. Summary of Hydrostatic Brine-Saturated Test Conditions

Test No.	Stage[a]	Hydrostatic Stress (MPa)	Fluid Pressure (MPa)	Termination Criteria
HC1A	1	1.72	0	Fractional density > 0.90
	2	0.86	0.05	60 days
HC2A	1	1.72	0	Fractional density > 0.90
	2	0.86	0.43	60 days
HC3A	1	3.45	0	Fractional density > 0.95
	2	1.72	0.86	60 days
HC4A	1	3.45	0	Fractional density > 0.95
	2	1.72	0.86	60 days
HC5A	1	6.90	0	Fractional density > 0.95
	2	3.45	1.73	60 days
HC6A	1	6.90	0	Fractional density > 0.95
	2	3.45	1.73	60 days

(a) Stage 1 = Consolidation Stage
Stage 2 = Permeability Stage

To initiate the pressurization stage, assembled specimens were placed in the load frame and the pressure vessel was lowered over the specimen. The pressure vessel was then filled with silicone oil and heated to 25°C. After temperature stabilization (~24 hours), pressure was applied in approximately 30 seconds by pressurizing the oil with an air-driven pump. Data acquisition began when the prescribed pressure was reached and control of the pressure was given to the automatic controller which signaled the dilatometer system to either inject or withdraw oil to maintain the pressure. The volume of oil either entering or exiting the vessel was measured and was used to calculate volumetric deformation.

During the pressurization stage, the lower platen vent was plugged; however, the upper vent was open and equipped with a flexible tube filled with brine leading to a buret. The brine-filled tube prevented evaporation of water from the specimen and allowed brine to exit or enter the specimen during stabilization and testing. A thin film of mineral oil was placed on top of the brine column to prevent evaporation.

For Sandia-furnished specimens, this stage was performed for a fixed period of time, as specified by Sandia, so that any transient pore pressures in the specimens could be relieved via drainage of brine out of the specimen. The stage lasted 12 days for Specimen 19JUN90 and 15 days for Specimen 20SEP89. The stages had slightly different lengths owing to a computer failure. Volumetric strains were recorded during the stage. For hydrostatic consolidation tests described in Table 4-2, stress conditions for Stage 1 were maintained until the fractional densities specified in the table were reached. Specimens were then removed from the pressure vessels and volumes were remeasured using both the fluid displacement and indirect contact dimensional measurement techniques.

4.3 Shear Consolidation Testing

Nine shear consolidation tests were conducted on specimens assembled at RE/SPEC Inc. at the conditions given in Table 4-3. The same test labeling convention applies to these tests as was described in the previous section for hydrostatic consolidation tests. The first attempts at tests SC1 and SC9 had mechanical failures and so these tests were repeated. Specimens were prepared and preconditioned as described above except they were not saturated.

The shear consolidation tests were set up and heated in the same manner as described for hydrostatic consolidation tests. Because they were not saturated, burets were not connected to the upper platen vent and instead a vapor barrier was used to prevent evaporation. To initiate a shear test, the specimen was first pressurized to a hydrostatic pressure equal to the required

Table 4-3. Summary of Shear Consolidation Test Conditions

Test No.	Stage[a]	Confining Pressure (MPa)	Axial Stress (MPa)	Axial Stress Difference (MPa)	Fluid Pressure (MPa)
SC1B	1	3.45	4.14	0.69	0
	2	1.84	1.84	0	0.92
SC2A	1	3.45	4.83	1.38	0
	2	1.95	1.95	0	0.98
	3	2.93	2.93	0	0.98
SC3A	1	3.45	5.52	2.07	0
	2	2.07	2.07	0	1.03
SC4A	1	6.90	7.59	0.69	0
	2	3.57	3.57	0	1.78
SC5A	1	6.90	8.97	2.07	0
	2	3.79	3.79	0	1.90
SC6A	1	6.90	10.34	3.44	0
	2	4.02	4.02	0	2.01
SC7A	1	5.17	6.55	1.38	0
	2	2.81	2.81	0	1.41
SC8A	1	5.17	7.93	2.76	0
	2	3.05	3.05	0	1.52
SC9B	1	5.17	9.31	4.14	0
	2	3.28	3.28	0	1.64

(a) Stage 1 = Consolidation Stage
Stage 2 = Permeability Stage
Stage 3 = Permeability Stage
(All Stages Except SC2A Stage 2 Ran a Minimum of 60 Days)

confining pressure. The axial piston was then advanced until the upper endcap contacted the top of the pressure vessel. The required stress difference was then applied quickly (in less than 30 seconds) using the axial actuator, and control of the test and data acquisition was turned over to

the DEC LSI-11/23 control software. Tests were continued for a period of at least 60 days. Specimens were then removed from the pressure vessels and volumes were remeasured using both the fluid displacement and indirect contact dimensional measurement techniques.

4.4 Permeability Testing

After the consolidation stage was completed, the pressure was decreased and a permeability test was performed on each specimen. RE/SPEC Inc.-furnished specimens were removed from the pressure vessel between the consolidation and permeability stages so that dimensions and volumes could be measured. Permeability was determined by measuring the steady-state flow rate of brine through the specimen and the pressure drop across the specimen. The pressure drop was controlled throughout the duration of the test and the flow rate was determined by monitoring the level of brine in the downstream reservoir (buret) over the test duration.

Permeability measurements were made at reduced hydrostatic stresses to minimize further consolidation. The actual hydrostatic stresses are given in Tables 4-1 through 4-3 for Sandia-furnished, hydrostatic, and shear consolidation tests, respectively. In general, for hydrostatic consolidation tests, the permeability stage was conducted at a hydrostatic pressure that was one half of the Stage 1 pressure; for shear consolidation tests, the hydrostatic pressure was half of the Stage 1 mean stress. The brine inflow pressures were 0.345 MPa for Sandia-furnished specimens and were half of the hydrostatic pressure for other tests. There were two exceptions to this general scheme. Very high initial brine flow rates were observed in Tests HC1A and SC2A. For Test HC1A, the brine inflow pressure was therefore reduced to 0.05 MPa, and for Test SC2A, a third stage was initiated at higher hydrostatic pressure. The higher pressure was applied to prevent brine from bypassing the specimen and traveling along the specimen/jacket interface.

Permeability stages were initiated by bringing the specimen to pressure and temperature and allowing it to stabilize for approximately 2 days before supplying pressure to the upstream brine reservoir. During stabilization, the downstream reservoir (buret) was filled with brine so that brine was free to enter the specimen and displace air. Recording of flow data was initiated when pressure was applied to the upstream reservoir.

After the permeability stage was completed, specimens were removed from the pressure vessel and for RE/SPEC Inc.-furnished specimens, densities were remeasured using both the fluid displacement technique and indirect contact dimension measurements. For most RE/SPEC Inc.-furnished specimens the porous felt metal disks, the platens, and the aluminum faceplates were

tested to be sure that they were free of obstructions and that brine freely flowed through these elements of the permeability system. Several tests were completed before this fluid-flow test was standardized.

4.5 Data Acquisition and Reduction

4.5.1 Data Acquisition

A DEC LSI-11/23 microprocessor was used to acquire data from all test systems. The computer scanned the data channels at 15-second intervals and logged data based on either time or axial displacement. Hydrostatic test data was logged every hour. Shear consolidation data was logged either every hour or for each 0.02 mm of axial displacement, whichever occurred first. During data logging, measurements of time, axial load, confining pressure, volumetric deformation, axial (piston) displacement, and temperature were written to disk on the microprocessor. These logged data were later transmitted to a separate computer for data reduction and analysis. Permeability data were logged manually at approximately 24-hour intervals. Permeability data included time, pressure drop across the specimen, and the brine level in the buret.

The volumetric deformations were corrected for the fluid displaced by the advancing piston using measurements of axial displacement and the cross-sectional area of the piston. Piston displacements measured during shear tests were corrected for machine softness to obtain specimen shortening. The axial and volumetric deformations were used to calculate axial and lateral strains. The axial stress was calculated from the axial force and the current specimen dimensions.

The data acquisition computer was also used for control of the axial force during shear consolidation tests. Based on current specimen geometry, the computer updated the axial force during the test so that the applied stress difference remained constant throughout the test. The computer also recorded the total axial and lateral deformation incurred during the application of the stress difference.

4.5.2 Reduction of Consolidation Data

The data acquired during consolidation were used to determine fractional density, D, as a function of time, where $D=\rho/\rho_{max}$. The intact density of the salt, ρ_{max}, was assumed to be 2,140 $kg \cdot m^{-3}$. The density during testing is calculated from

$$\rho=\frac{\rho_0}{(1-\varepsilon_v)} \tag{4-1}$$

where ρ_0 is the density of the salt matrix at the beginning of the consolidation stage and ε_v is the engineering volumetric strain measured during the test. The sign convention used here is that compression is positive, and so compressive volumetric strains lead to an increase in density.

Despite the use of a preconditioning cycle, some volumetric compaction occurs during loading to hydrostatic stress. This deformation is not directly measurable during testing and must be calculated based on the specimen volume measurements made after completion of the stage. The total volume change occurring during the stage was initially calculated based on the pre-stage specimen volume and the volumetric strain data obtained during testing. This total volume change was then compared with the total volume change obtained by subtracting the post-stage immersion volume from the pre-stage volume. The difference between the two volume change measurements was attributed to volumetric compaction occurring during hydrostatic loading. The pre-stage volume measurement was then modified accordingly, and the forward calculation was repeated.

4.5.3 Reduction of Permeability Data

Permeability was determined from Darcy's law, i.e.,

$$k=\frac{Q\mu L}{A\Delta P} \tag{4-2}$$

where

k	=	Permeability (having units of L^2)
Q	=	Measured flow rate of brine (having units of L^3t^{-1})
A	=	Current cross-sectional area (having units of L^2)
μ	=	Brine viscosity (having units of $ML^{-1}t^{-1}$)
L	=	Current length (having units of L)
ΔP	=	Pressure drop across specimen (having units of $ML^{-1}t^{-2}$)

The steady-state flow rate, Q, was measured during testing by fitting the flow volume-versus-time data with a linear model using least squares. Values of specimen length and diameter were obtained just prior to the permeability stage using indirect contact dimension measurements. A brine viscosity of 1.26cP (1.26×10^{-3} kg $\cdot$ $m^{-1} \cdot s^{-1}$) was used for data reduction. This viscosity corresponds to the viscosity of brine used by Stroup and Senseny (1987) and is similar to that used by Shor et al. (1981) in their permeability tests.

5.0 TEST RESULTS AND DISCUSSION

5.1 Sandia-Furnished Specimens

5.1.1 Pressurization Stage

During the pressurization stage, volumetric strains were recorded for each specimen. The volumetric strain-versus-time data for Specimens 19JUN90 and 20SEP89 are shown in Figure 5-1. The pressurization stages for Specimens 19JUN90 and 20SEP89 continued for 12 days and 15 days, respectively. Unfortunately, only data for the first 2 days of the stage were collected because the computer that both acquires data and controls the tests failed. Failure of the computer suspended data acquisition, but the stage was completed successfully because both the pressure and temperature are controlled by manual set-point controllers.

The volumetric strains at the end of 2 days were about 1 percent and 2 percent for Specimens 19JUN90 and 20SEP89, respectively. Although data were not collected beyond 2 days, the volumetric strain rates at the end of 2 days in both tests are significantly lower than the rates at the beginning of the tests, and little additional strain is likely to have occurred after 2 days.

No volumetric strain data were obtained for the specimen identified as 20JUN90. Immediately upon pressurizing this specimen, silicone oil began to leak rapidly from the upper permeability vent. The test was aborted and the specimen removed from the loading frame. A post-test inspection revealed a small circular hole in the jacket. The diameter of the hole was approximately the size of the diameter of the lockwire used to attach the jacket to the endcaps. Based on this evidence, it was assumed that the jacket was punctured by lockwire. The actual timing of the event was not determined, but it was surmised that the puncture occurred during shipping.

5.1.2 Permeability Stage; Consolidation Data

Volumetric strain data were also recorded during the permeability stages of each test. The data from both the permeability stages and the pressurization stages are shown in Figure 5-2. The results show that the volumetric strain rate for Specimen 19JUN90 is nearly zero while the

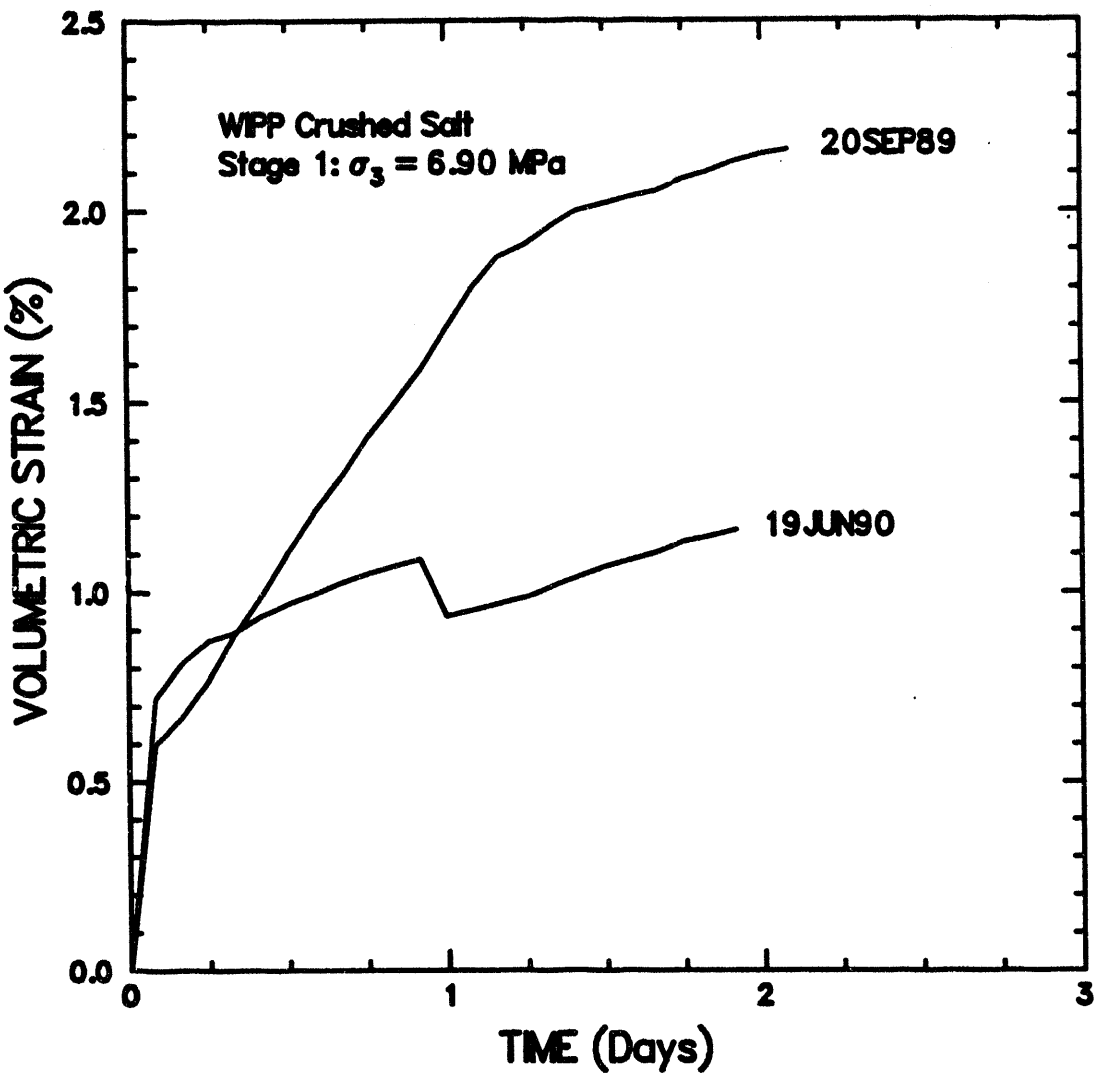

Figure 5-1. Volumetric strain-versus-time for Sandia-furnished Specimens 19JUN90 and 20SEP89 during pressurization stage.

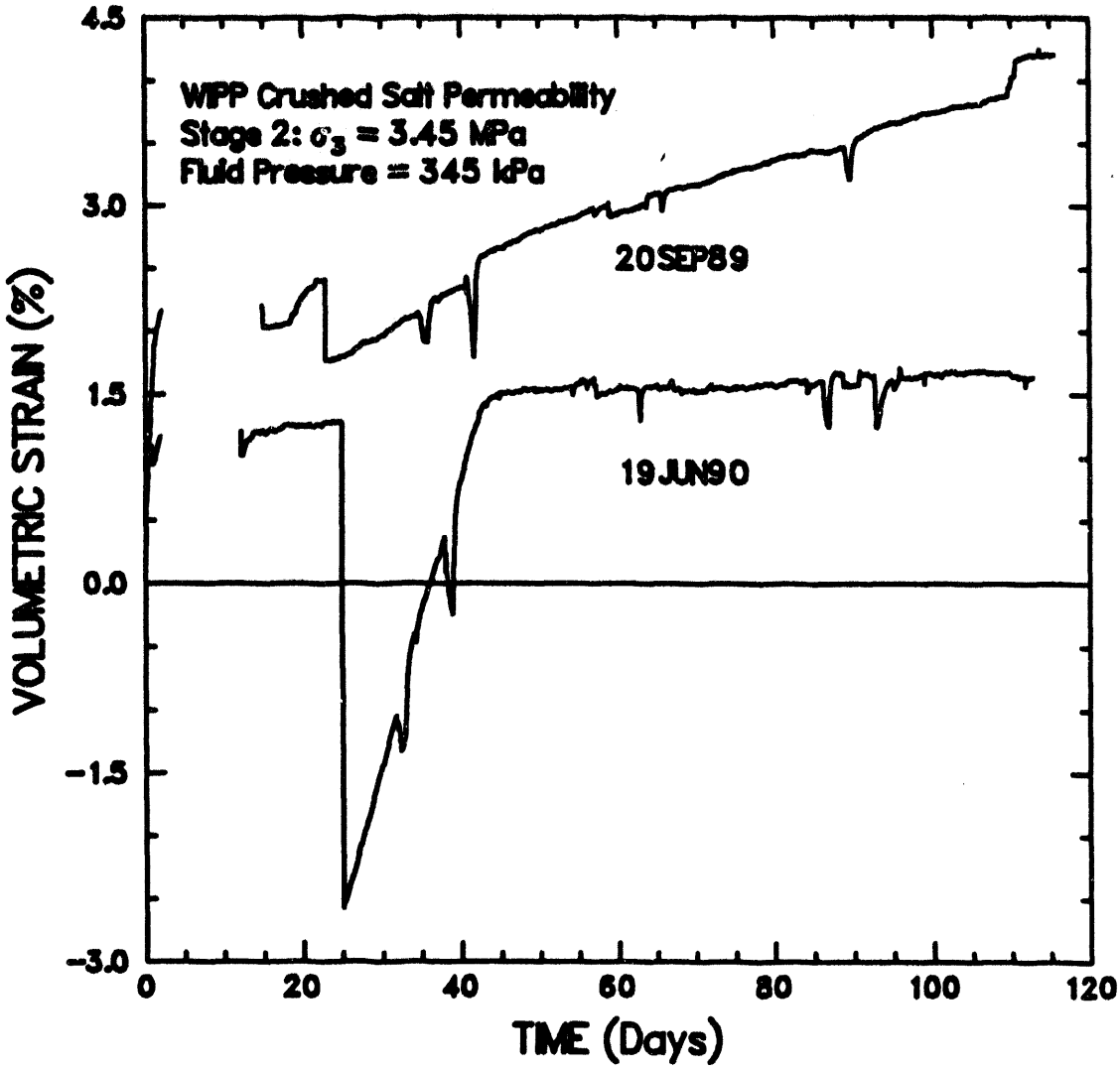

Figure 5-2. Volumetric strain-versus-time for Sandia-furnished Specimens 19JUN90 and 20SEP89 during pressurization and permeability stages.

strain rate for Specimen 20SEP89 is about $2\times10^{-9}s^{-1}$. Assuming that no additional strain occurred during the period when the computer failed as described earlier, the total volumetric strains for both stages were about 1.5 percent and 4.2 percent for Specimens 19JUN90 and 20SEP89, respectively. Using a sign convention of compression positive, the strains shown indicate a reduction in volume for both specimens. These strains differ from those indicated by the pre-test and post-test measurements (3.77 and 2.14 percent for Specimens 19JUN90 and 20SEP89, respectively). This discrepancy is attributed to the irregular shape of the test specimens and resulting inaccuracies in the direct measurements. It is possible that there was a small confining pressure leak on Specimen 20SEP89 that resulted in measurements of erroneous volumetric strains.

The fluctuations in the volumetric strain data occurring in the first 45 days of testing were caused by changes in the loading piston position. The original testing procedure specified that the piston be positioned at the bottom of the pressure vessel so that no corrections to fluid volume measurements would be needed. During testing, however, it was discovered that the piston had drifted up away from its original position. This movement of the piston was not accounted for in data reduction and produced the anomalous volumetric strain data shown in Figure 5-2. After the problem was identified, the loading piston was returned to its original position and this position was then maintained throughout the remainder of the stage.

5.1.3 Permeability Stage; Permeability Data

At the beginning of each permeability stage, the lower face of each specimen was subjected to a brine fluid pressure of 345 kPa, while the upper face was exposed to atmospheric pressure. The brine flow-versus-time data are shown in Figures 5-3 and 5-4 for Specimens 19JUN90 and 20SEP89, respectively. Flow is given as volume and refers to the cumulative change in fluid level in the downstream reservoir. Data are plotted so that negative values of flow indicate flow of brine from the downstream reservoir (buret) into the specimen, while positive values indicate flow out of or through the specimen. Surprisingly, the data for both specimens (at least at early times) indicate flow of brine into the specimen. This result implies that the specimens were not fully saturated upon receipt or that evaporation of water from the specimens occurred during handling and testing. During the last 50 days of testing, the flow data for Specimen 19JUN90 showed a reverse in trend indicating flow through the specimen. It is possible that the difference in flow characteristics between the two specimens is related to differences in specimen assemblies. The specimen assembly used for Specimen 20SEP89 shown in Figure 2-1 provides for less specimen drainage than the assembly used for later tests (Figure 2-2). The slope of the

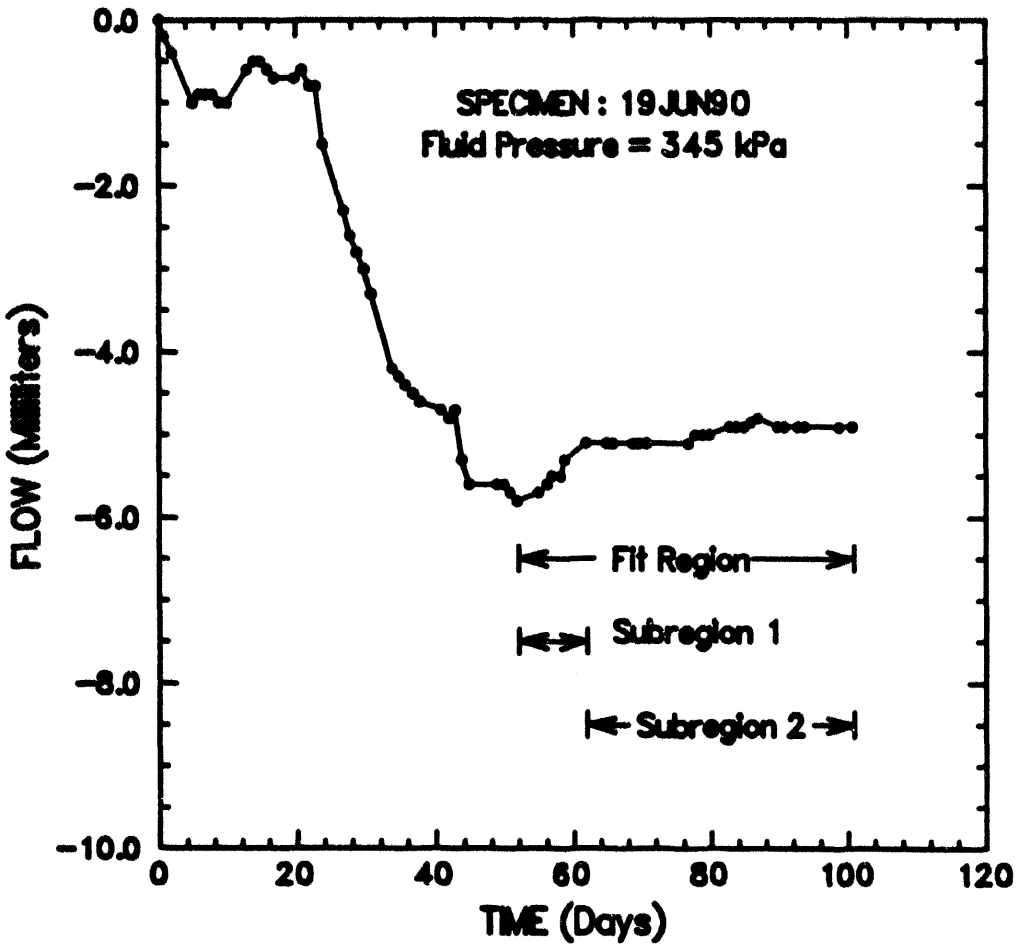

Figure 5-3. Brine volume-versus-time for Sandia-furnished Specimen 19JUN90.

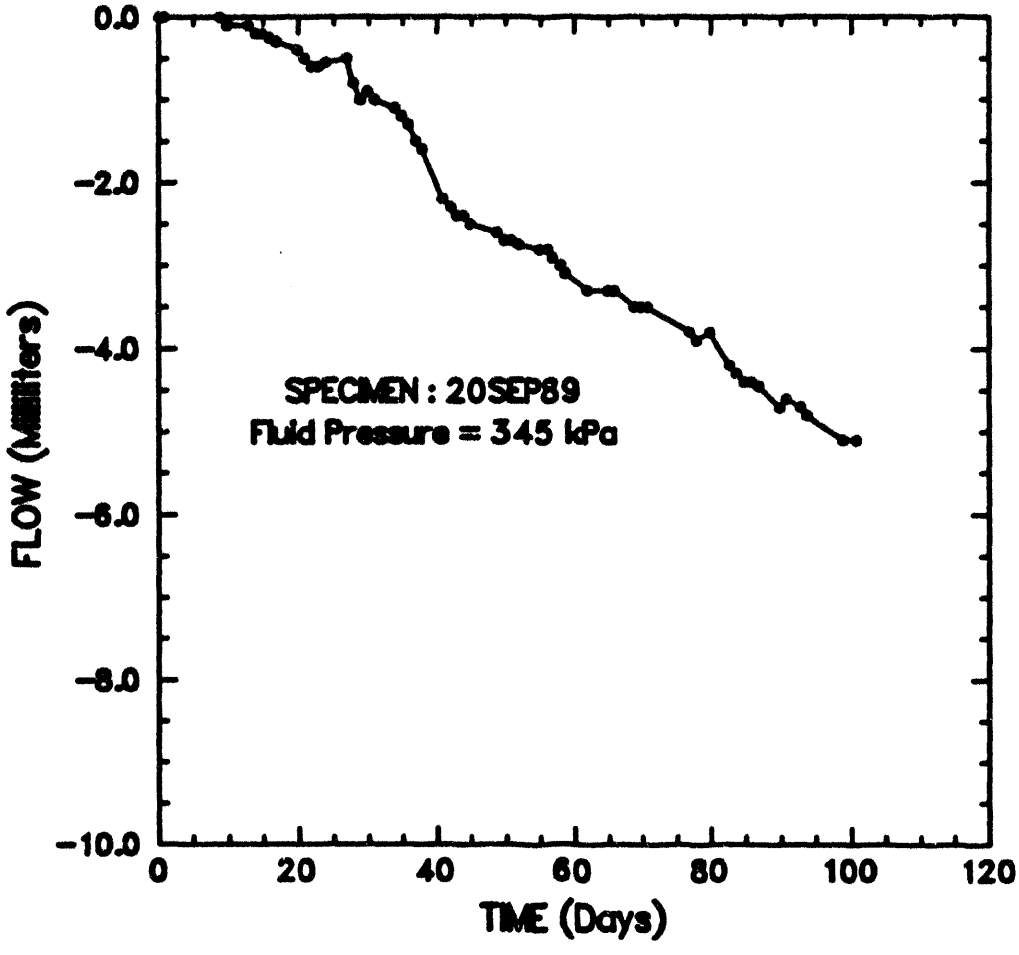

Figure 5-4. Brine volume-versus-time for Sandia-furnished Specimen 20SEP89.

flow-versus-time data is the flow rate. The data from the last 50 days of Specimen 19JUN90 were fitted using a linear model and least squares to obtain a flow rate of 0.0178 ml/day ($2.06\times10^{-13}m^3s^{-1}$). This time period is labeled "Fit Region" in Figure 5-3. Most of the fluid movement occurred within the first 10 days of this period and so the fit region was subdivided as shown in the figure. The flow rates obtained for Subregions 1 and 2 using linear least-squares fitting were 0.0712 ml/day ($8.24\times10^{-13}m^3s^{-1}$) and 0.00787 ml/day ($9.11\times10^{-14}m^3s^{-1}$), respectively.

Permeabilities were calculated for the three regions defined in Figure 5-3 and are summarized in Table 5-1. Because most deformation occurred early in the test, the post-test dimensions of the specimen (Table 2-1) were used to calculate permeability. The difference in permeabilities between the two subregions is nearly an order of magnitude. This is much larger than the measurement error of approximately 5 percent.

Table 5-1. Summary of Permeability Measurements

Specimen ID	Flow Rate[a] (m^3s^{-1})	Permeability[b] (m^2)
20SEP89	0	0
19JUN90	(a)	
Fit region	2.06×10^{-13}	1.44×10^{-20}
Subregion 1	8.24×10^{-13}	5.77×10^{-20}
Subregion 2	9.11×10^{-14}	6.37×10^{-21}
20JUN90	(c)	(c)

(a) Flow rates for Specimen 19JUN90 are determined for regions shown in Figure 5-3.
(b) Based on pressure drop across the specimen of 345 kPa and permeant viscosity of 1.26 cP.
(c) No data due to jacket rupture upon pressurization.

5.2 Hydrostatic Consolidation Tests; Consolidation Data

5.2.1 Test Results

Fractional density is plotted as a function of time for Stage 1 of all hydrostatic consolidation tests in Figure 5-5. Complete plots of fractional density-versus-time for both stages of each test are given in Appendix D. Fractional density data obtained during Stage 2 of Test HC6A show a dramatic increase from those obtained in Stage 1 even though the hydrostatic stress was lower in this stage. This increase was found to be an anomoly that resulted from a confining pressure fluid leak in the test system rather than an actual change in specimen density. Mass, moisture content and saturation level, and dry fractional density are given for hydrostatic consolidation tests in Tables 5-2, 5-3, and 5-4, respectively.

Table 5-2. Specimen Masses for Hydrostatic Consolidation Tests

Test	Specimen Mass			
	Initial Value		After Saturation	
	Wet Mass (kg)	Mass of Salt Matrix (kg)	Wet Mass (kg)	Mass of Salt Matrix (kg)
HC1A	2.2492	2.1812	2.6332	2.1812
HC2A	2.1829	2.1130	2.4895	2.1130
HC3A	2.2134	2.1565	2.5194	2.1565
HC4A	2.1549	2.0895	2.4273	2.0895
HC5A	2.2420	2.1731	2.4604	2.1731
HC6A	2.2364	2.1741	2.4530	2.1741

Figure 5-5 shows that for these saturated specimens, the greater the consolidation pressure, the faster the densification rate at a given fractional density. Previous work (Zeuch et al., 1991) has shown that for specimens that are already damp (i.e., containing 3 percent brine by weight), saturation has little effect on the consolidation rate; at worst, slightly retarding it. The data presented here show higher consolidation rates than comparable tests conducted by Zeuch et al., and show slightly higher rates than were obtained by Holcomb and Shields (1987) on unsaturated WIPP salt specimens. The specimen assembly used in those studies differed from that used here, so these discrepancies are not surprising. The earlier specimen assembly (shown in Figure 2-1) provides for less specimen drainage than the assembly used in later tests and shown in Figure 2-2. Further work is needed to fully evaluate the effect of saturation on consolidation rate.

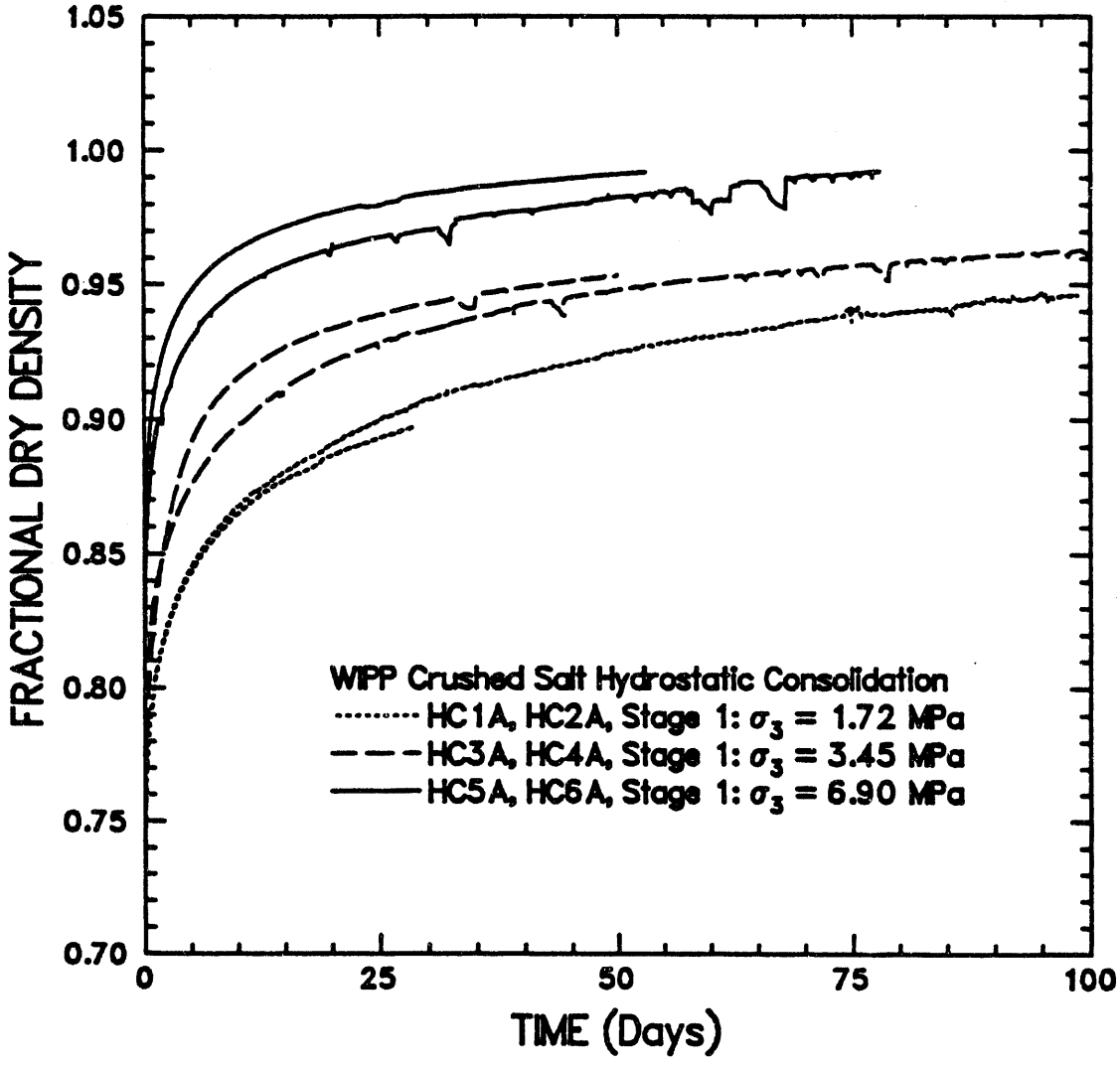

Figure 5-5. Fractional density-versus-time for Stage 1 of all hydrostatic consolidation tests.

Table 5-3. Moisture Contents and Saturation Levels for Hydrostatic Consolidation Tests

Test	Initial		After Preconditioning and Saturation		After Stage 1	
	Moisture[a] Content (%)	Saturation Level (%)	Moisture[a] Content (%)	Saturation Level (%)	Moisture[a] Content (%)	Saturation Level (%)
HC1A	2.27	12.0	14.43	95.10	3.99	100
HC2A	2.41	10.9	12.50	79.15	2.68	100
HC3A	1.92	9.8	11.83	87.12	0.26	100
HC4A	2.28	10.8	11.39	83.67	1.49	100
HC5A	2.31	13.2	9.38	89.58	2.17	100
HC6A	2.09	9.6	9.12	83.59	1.38	100

(a) Mass of water divided by dry mass.

Table 5-4. Dry Fractional Densities for Hydrostatic Consolidation Tests[a]

Test	Initial Value	After Conditioning	After Load Application	After Stage 1	After Stage 2
HC1A	0.6834	0.7202	0.7880	0.8978	0.9037
HC2A	0.6488	0.7135	0.7357	0.9469	0.9465
HC3A	0.6766	0.7438	0.7242	0.9541	0.9420
HC4A	0.6586	0.7437	0.7521	0.9693	0.9359
HC5A	0.6993	0.7916	0.8134	0.9926	1.0
HC6A	0.6518	0.7851	0.8043	0.9929	1.0

(a) Densities are based on volume measurements given in Table 2-5.

5.2.2 Model Fitting

Following the work of Holcomb and Shields (1987), the Stage 1 hydrostatic consolidation data were fit to the equation

$$\frac{\Delta V}{V_0} = \varepsilon_v = a \log_{10}(t) + b \qquad (5\text{-}1)$$

where

t = Time in seconds
a, b = Fitting parameters

This equation has a singularity at t=0 and provides a poor fit for data at early times and so a cutoff time of 3600 seconds was used. The fitting parameters are given in Table 5-5. The rate parameter, a, is consistent with values given by Holcomb and Shields (1987), however, values of b differ. Predicted and actual volumetric strains-versus-logarithm of time and volumetric strains-versus-time are given in Appendix E for all hydrostatic consolidation tests. Solid lines show actual data and dotted lines show predictions based on the model. The predicted data track the actual data reasonably well.

Table 5-5. Fitting Parameters Determined for Hydrostatic Consolidation of Saturated WIPP Salt

Test	a	b
HC1A	0.0581	-0.176
HC2A	0.0680	-0.248
HC3A	0.0604	-0.155
HC4A	0.05936	-0.188
HC5A	0.0409	-0.0891
HC6A	0.0445	-0.114

As discussed in Chapter 1, the Rock Mechanics Laboratory of Sandia National Laboratories is investigating crushed-salt consolidation in an effort to develop a constitutive model. Zeuch et al., (1985), Zeuch (1990), and Holcomb and Zeuch (1991) have developed a model for

hydrostatic consolidation of nominally dry salt which differs from that presented in Equation 5-1. That model is based on isostatic hot pressing and has been modified to include the micro-mechanisms appropriate to salt. The hydrostatic consolidation data presented here are for saturated rather than dry specimens, so that model is not applicable to these results. That model predicts densification rate as a function of time and fractional density. For reference, the time rate of change in fractional density is given as a function of fractional density for all hydrostatic consolidation tests in Figure 5-6.

5.3 Shear Consolidation Tests; Consolidation Data

Fractional density is given as a function of time in Figures 5-7, 5-8, and 5-9 for shear consolidation tests at confining pressures of 3.45 MPa, 5.17 MPa, and 6.90 MPa, respectively. Only Stage 1 data are shown. Each plot contains data for specimens containing 3 percent brine by weight obtained at three values of stress difference. Figures 5-7 and 5-9 also include data for saturated specimens consolidated hydrostatically. These data show no correlation between consolidation and applied axial stress difference. Mass, moisture content and saturation level, and dry fractional density are given for shear consolidation tests in Tables 5-6, 5-7, and 5-8, respectively. Complete plots of fractional density-versus-time for both stages of shear

Table 5-6. Specimen Masses for Shear Consolidation Tests

Test	Specimen Mass	
	Wet Mass (kg)	Mass of Salt Matrix
SC1B	2.2203	2.1512
SC2A	2.1219	2.0584
SC3A	2.2497	2.1835
SC4A	2.1740	2.1083
SC5A	2.3857	2.3058
SC6A	2.1476	2.0849
SC7A	2.2930	2.2220
SC8A	2.1761	2.1099
SC9B	2.2351	2.1658

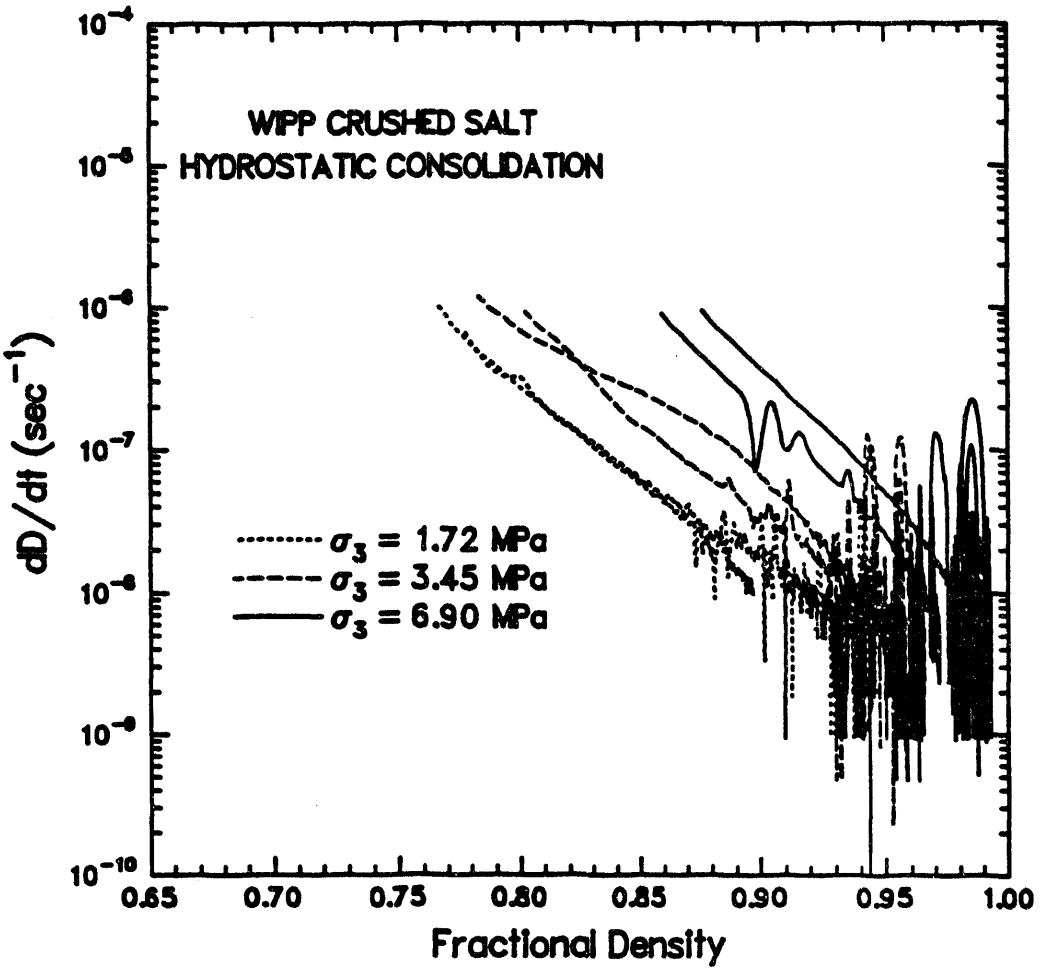

Figure 5-6. Rate change in fractional density-versus-fractional density for Stage 1 of all hydrostatic consolidation tests.

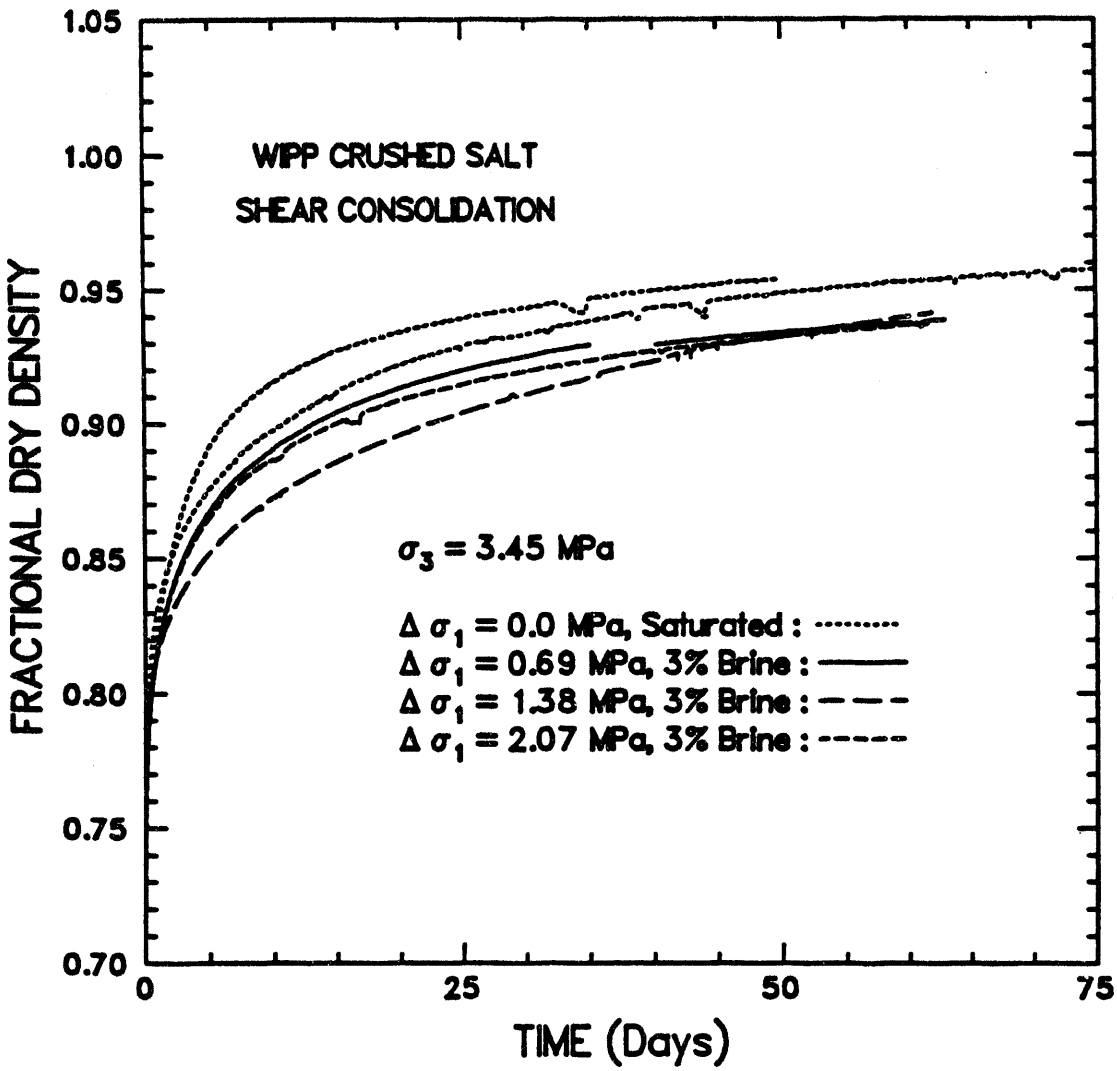

Figure 5-7. Fractional density-versus-time for consolidation tests at 3.45 MPa confining pressure. Damp shear consolidation tests and saturated hydrostatic consolidation tests are included.

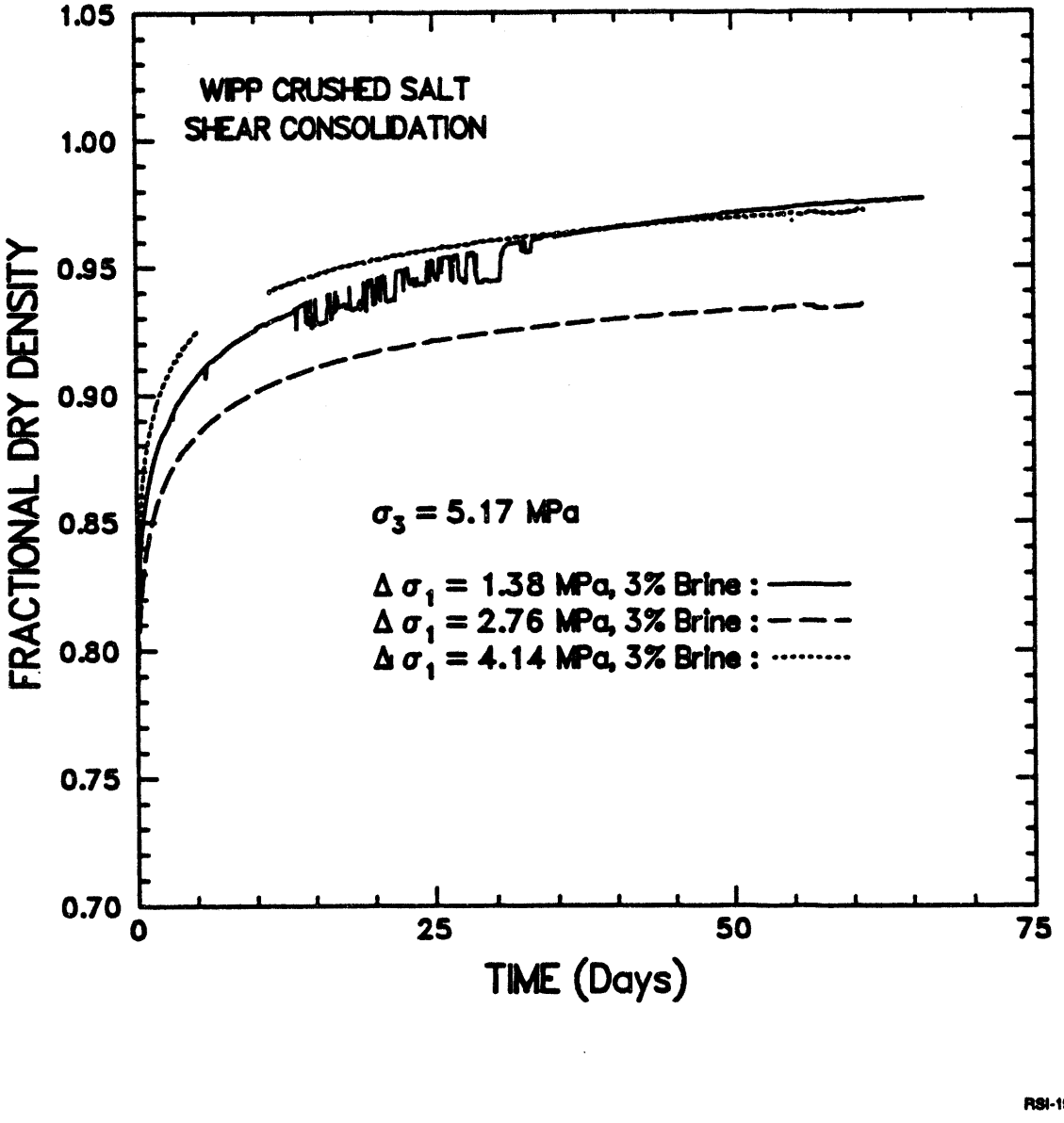

Figure 5-8. Fractional density-versus-time for damp shear consolidation tests at 5.17 MPa confining pressure.

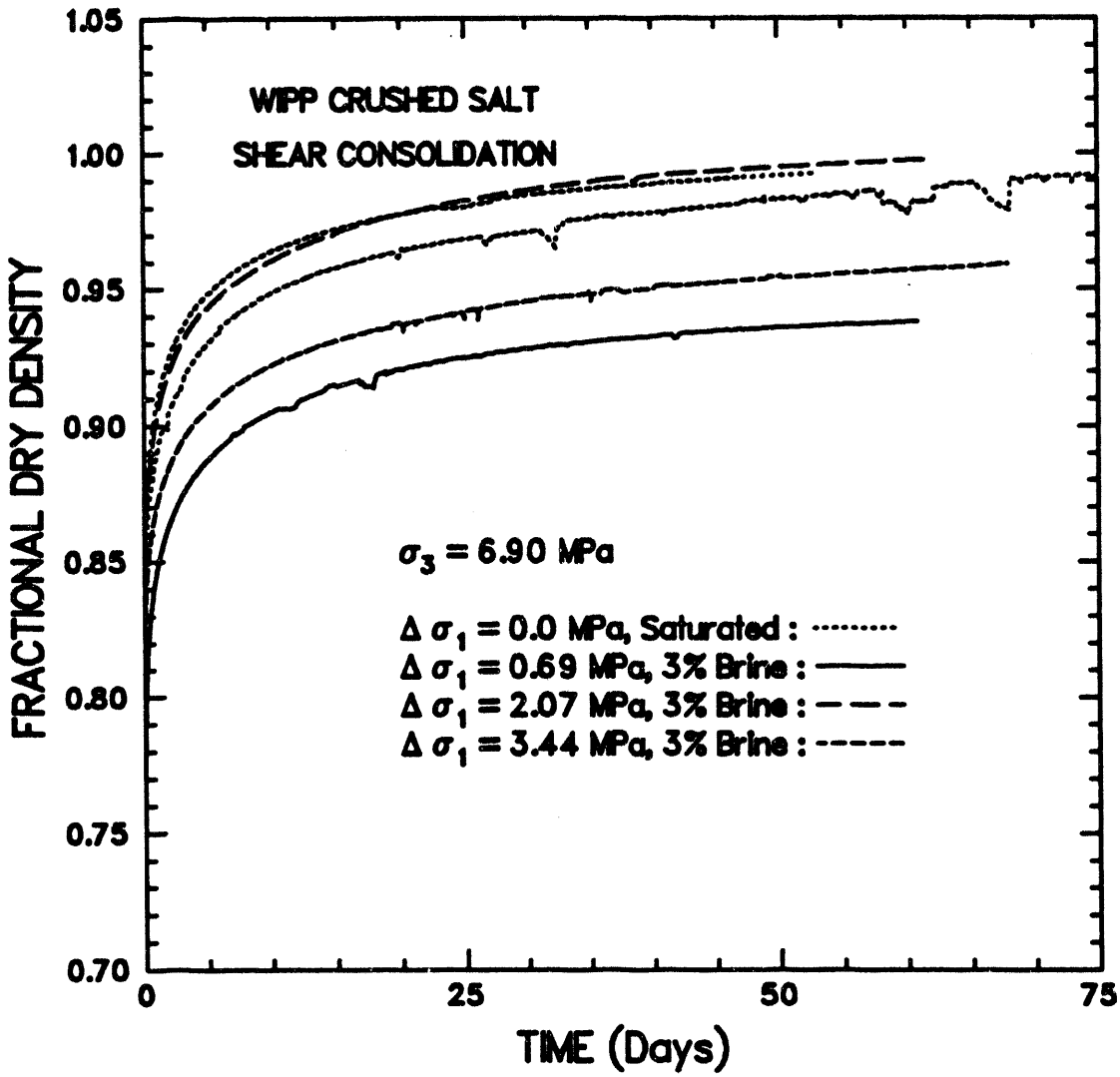

Figure 5-9. Fractional density-versus-time for consolidation tests at 6.90 MPa confining pressure. Damp shear consolidation tests and saturated hydrostatic consolidation tests are included.

Table 5-7. Moisture Contents and Saturation Levels for Shear Consolidation Tests

Test	Initial Value		After Stage 1	
	Moisture[a] Content (%)	Saturation Level (%)	Moisture[a] Content (%)	Saturation Level (%)
SC1B	2.34	12.0	2.34	79.84
SC2A	2.25	12.3	2.25	92.27
SC3A	2.21	11.3	2.21	71.54
SC4A	2.27	11.1	2.27	83.81
SC5A	2.52	15.2	0.09	100
SC6A	2.19	9.6	1.61	100
SC7A	2.33	12.1	1.11	100
SC8A	2.29	11.1	0.64	100
SC9B	2.33	11.1	1.34	100

(a) Mass of water divided by dry mass.

Table 5-8. Dry Fractional Densities for Shear Consolidation Tests[a]

Test	Initial Value	After Conditioning	After Load Application	After Stage 1	After Stage 2
SC1	0.6769	0.7482	0.7354	0.9331	0.9635
SC2	0.6911	0.7396	0.7515	0.9437	0.9879
SC3	0.6767	0.7500	0.7359	0.9297	0.9697
SC4	0.6673	0.7438	0.7508	0.9378	0.9516
SC5	0.7113	0.8136	0.8244	0.9994	1
SC6	0.6427	0.7714	0.7947	0.9636	0.9768
SC7	0.6797	0.7743	0.7778	0.9753	0.9782
SC8	0.6650	0.7763	0.7530	0.9862	0.9719
SC9	0.6611	0.7833	0.7863	0.9700	0.9896

(a) Densities are based on volume measurements given in Table 2-6.

consolidation tests are given in Appendix D. The fractional density data obtained during Stage 2 of Tests SC4A and SC6A show increases due to leaks in the test systems and are anomalies. A sudden increase in fractional density during Stage 2 of Test SC3A accompanies the intentional shut-down of pressure vessel heaters.

Rates of change in fractional density are plotted versus fractional density in Figures 5-10, 5-11, and 5-12 for Stage 1 of tests at each of the three confining pressures. These data also show no systematic correlation between densification rate and the magnitude of axial stress difference and are given for reference.

Axial strains are plotted as a function of time in Figures 5-13, 5-14, and 5-15 for shear consolidation tests at confining pressures of 3.45, 5.17, and 6.90 MPa, respectively. Each plot contains data obtained at three values of stress difference. Lateral strains are given in Figures 5-16, 5-17, and 5-18 for the three confining pressures. The strains accumulated during application of the stress difference are shown in these plots. These load-up strains were determined by matching the displacements measured with the LVDT and dilatometer to those determined using pre-stage and post-stage indirect contact measurements. Initial specimen densities are not uniform for these tests so that direct comparisons of axial and lateral strain data are questionable; however, the data generally show that at each pressure, tests with greater axial stress differences show greater axial strain and less lateral compaction.

It is evident from these data that for each of the three pressures shown, the magnitude of the stress difference has no systematic effect on consolidation rate. This conclusion is consistent with the results of Zeuch et al. (1991) who obtained conflicting results from two shear consolidation tests. Although a higher stress difference contributes to a higher mean stress, thus serving to increase the consolidation rate, the applied stress difference may also enhance the development of void volume within the specimen and thereby slow consolidation.

Comparison of hydrostatic and shear consolidation data show that at a confining pressure of 3.45 MPa, the brine-saturated specimens under hydrostatic load tend to consolidate more quickly than do damp specimens under shear load. The data obtained at 6.90 MPa show some overlap between consolidation rates obtained during hydrostatic tests on saturated specimens and during shear consolidation tests on damp specimens. Unfortunately, the effects of saturation and small applied shear loads on consolidation rate cannot be separated using this limited data set.

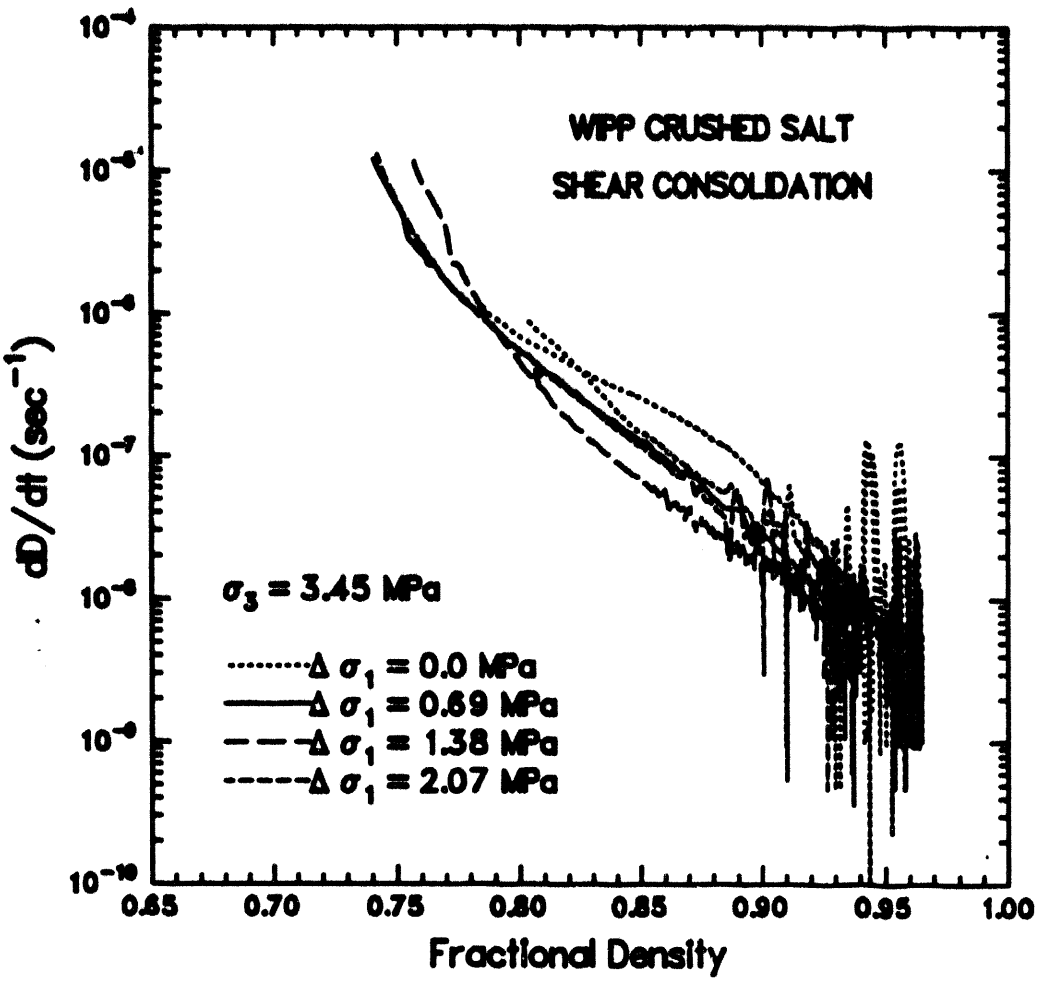

RSI-197-92-124

Figure 5-10. Rate change in fractional density-versus-fractional density for consolidation tests at 3.45 MPa confining pressure. Damp shear consolidation tests and saturated hydrostatic consolidation tests are included.

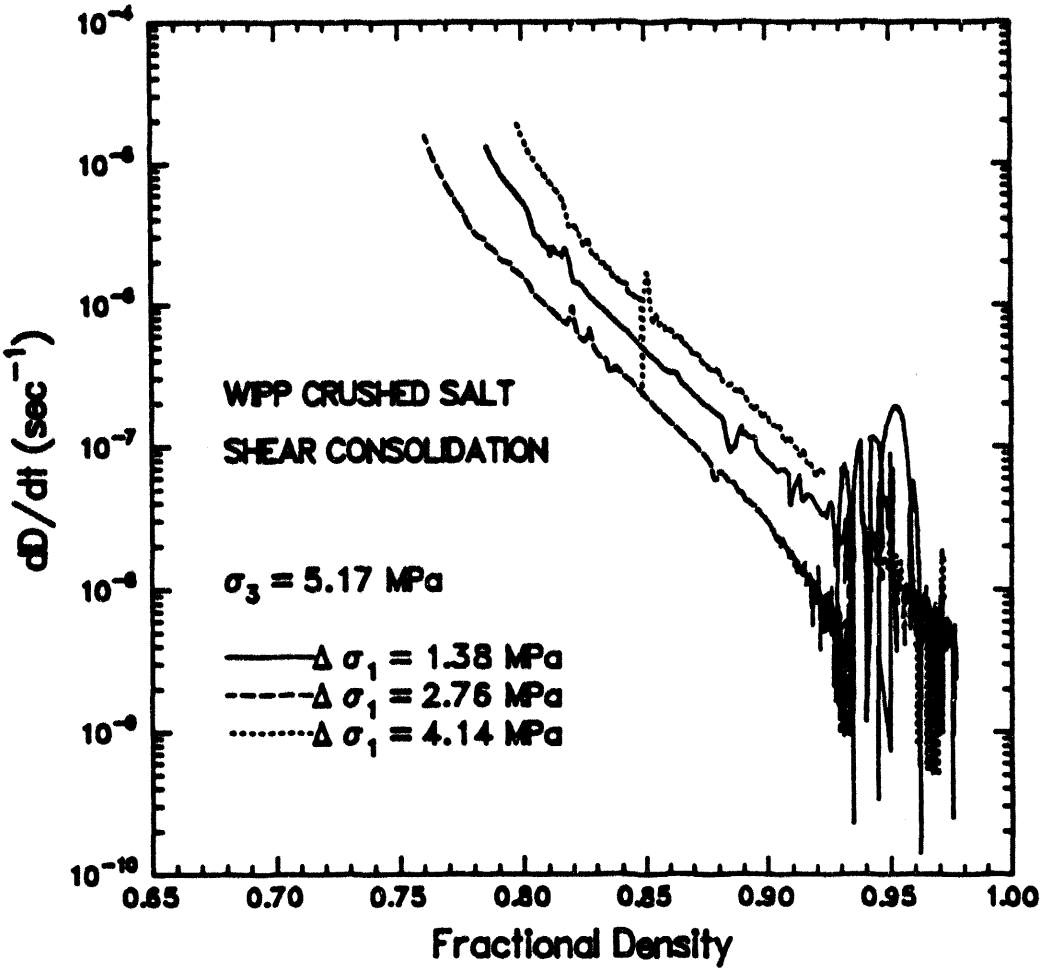

RSI-107-92-125

Figure 5-11. Rate change in fractional density-versus-fractional density for damp shear consolidation tests at 5.17 MPa confining pressure.

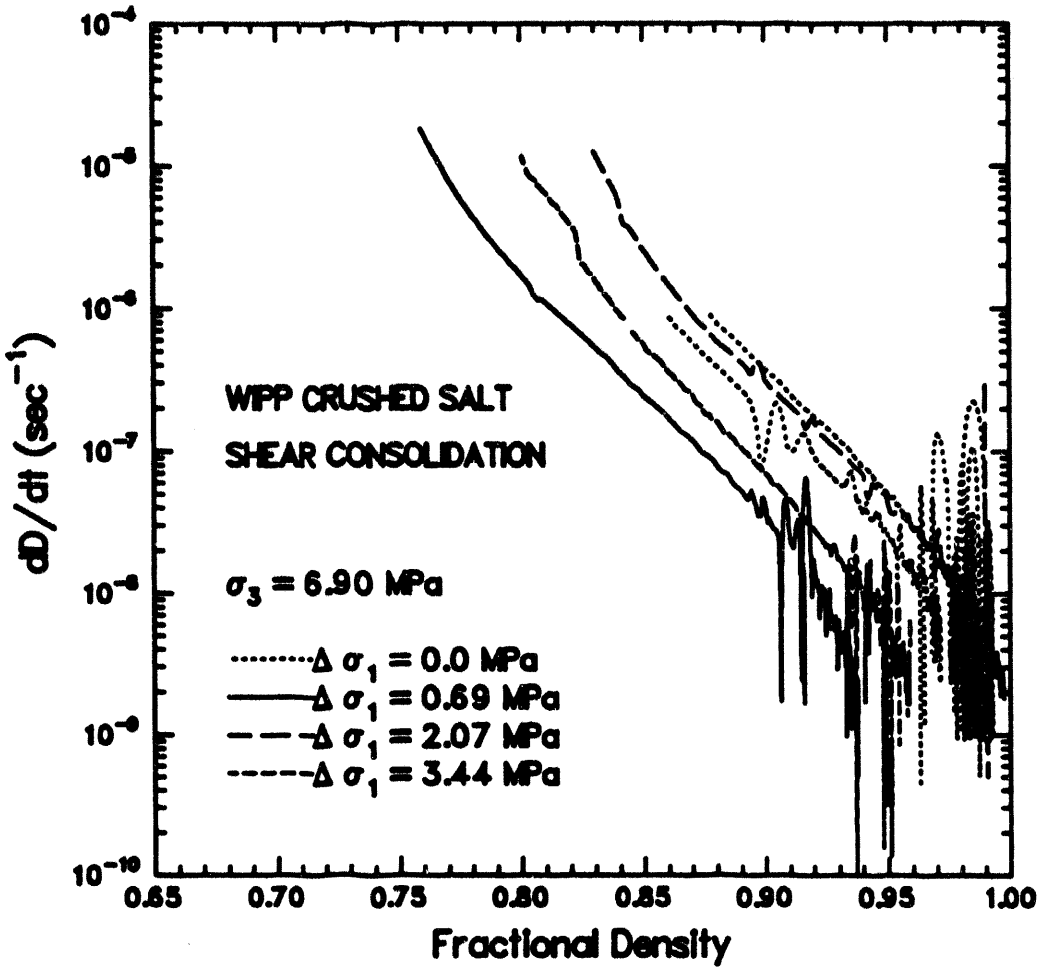

RSI-197-92-126

Figure 5-12. Rate change in fractional density-versus-fractional density for consolidation tests at 6.90 MPa confining pressure. Damp shear consolidation tests and saturated hydrostatic consolidation tests are included.

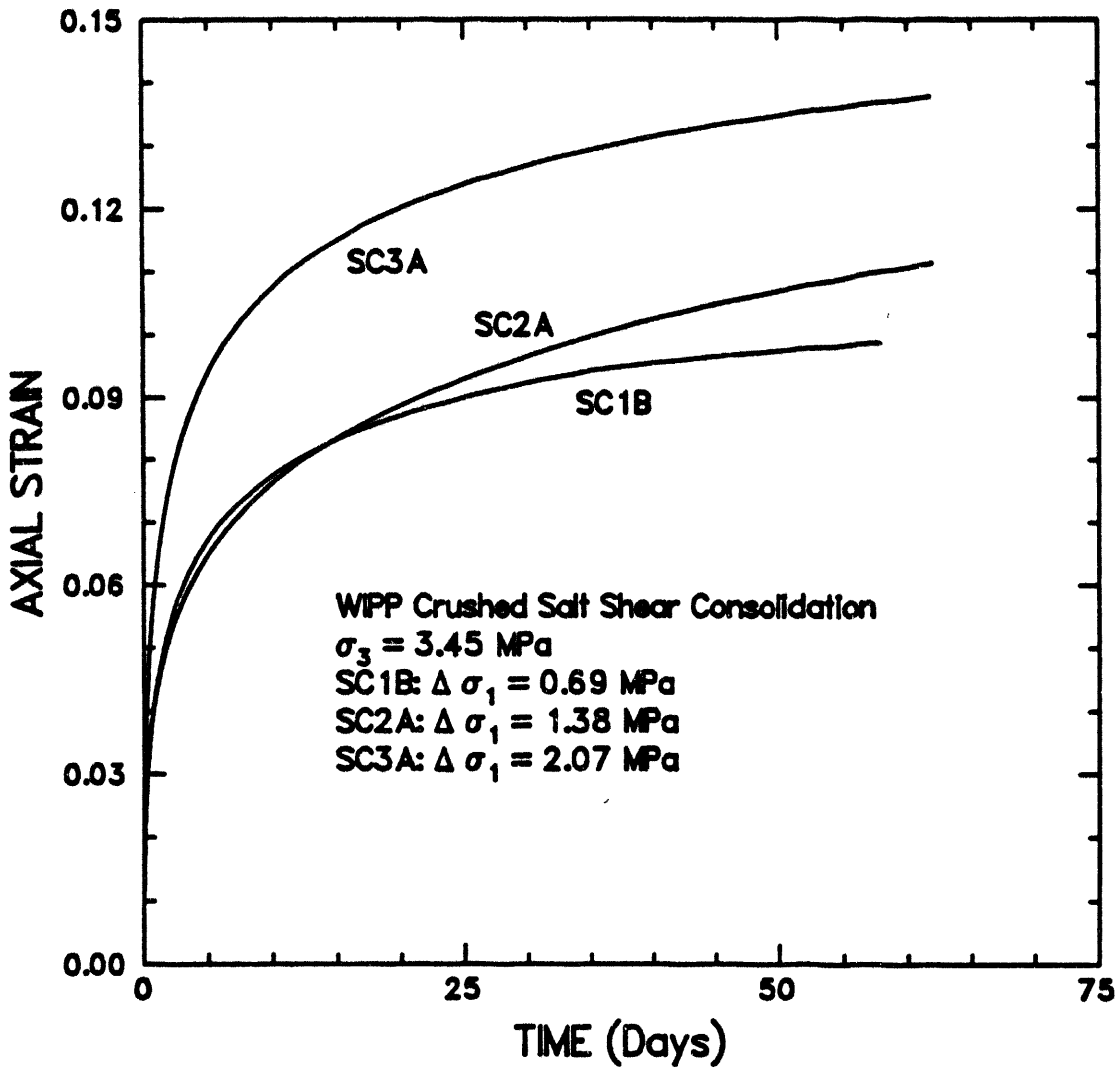

Figure 5-13. Axial strain-versus-time for Stage 1 of all shear consolidation tests at 3.45 MPa confining pressure.

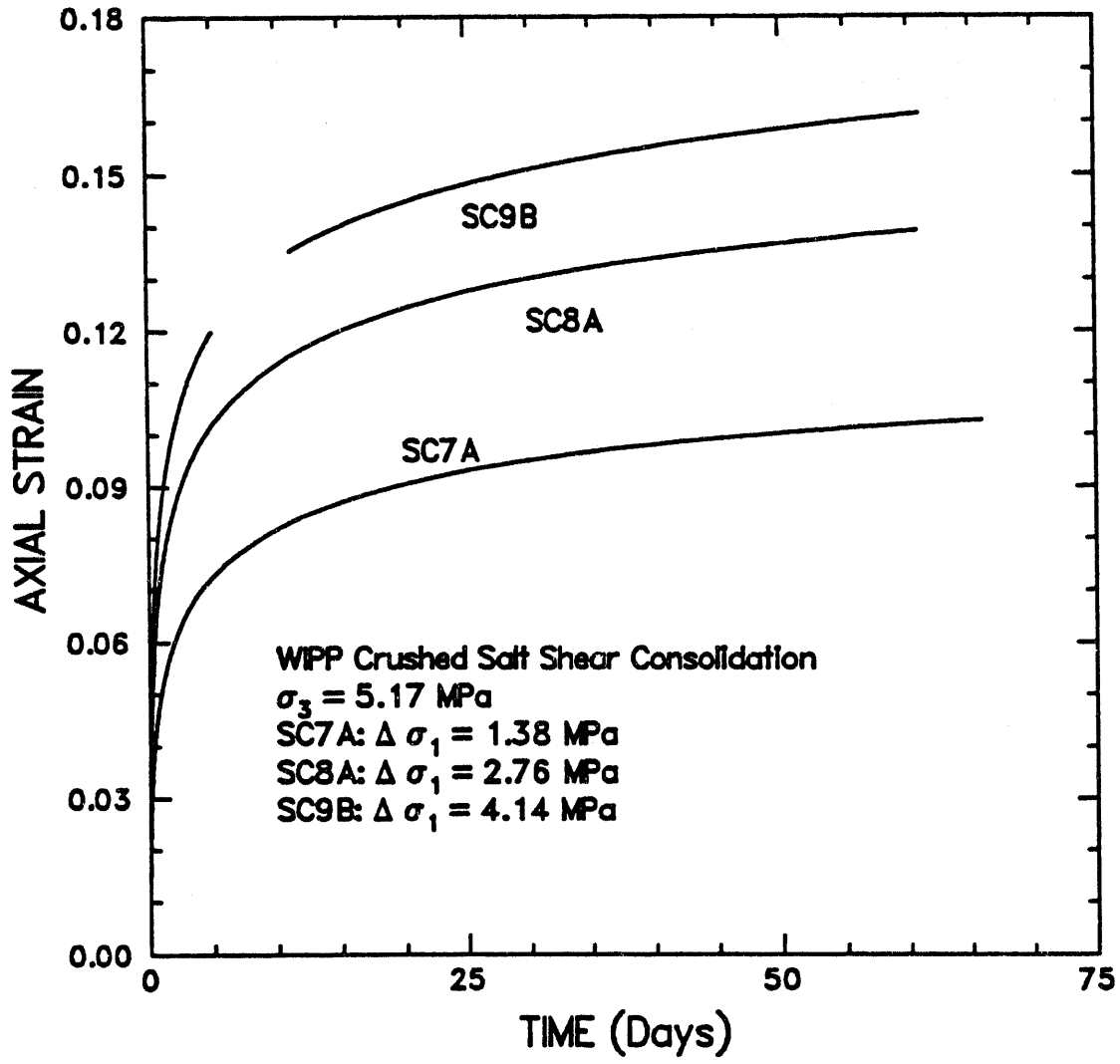

Figure 5-14. Axial strain-versus-time for Stage 1 of all shear consolidation tests at 5.17 MPa confining pressure.

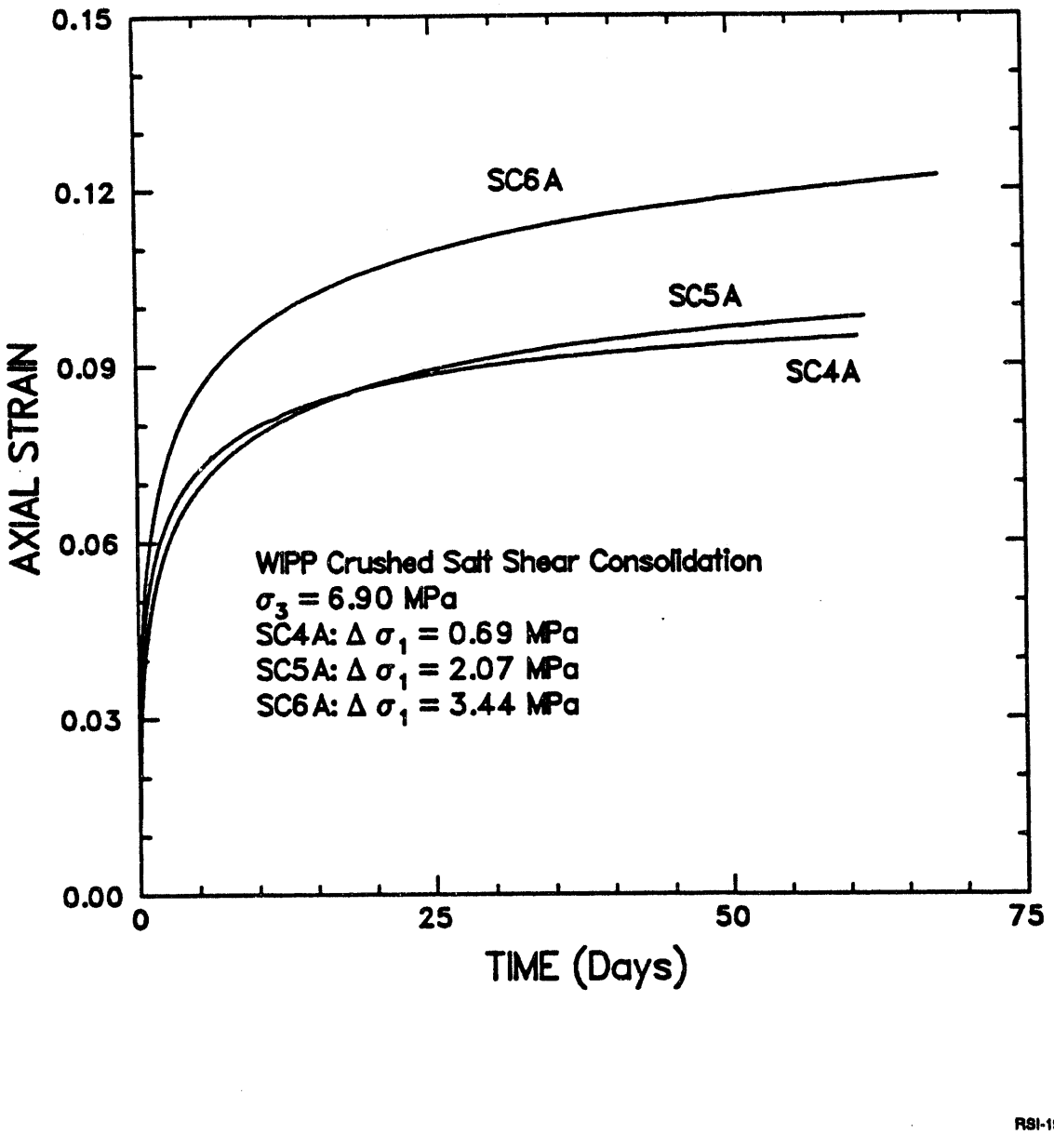

Figure 5-15. Axial strain-versus-time for Stage 1 of all shear consolidation tests at 6.90 MPa confining pressure.

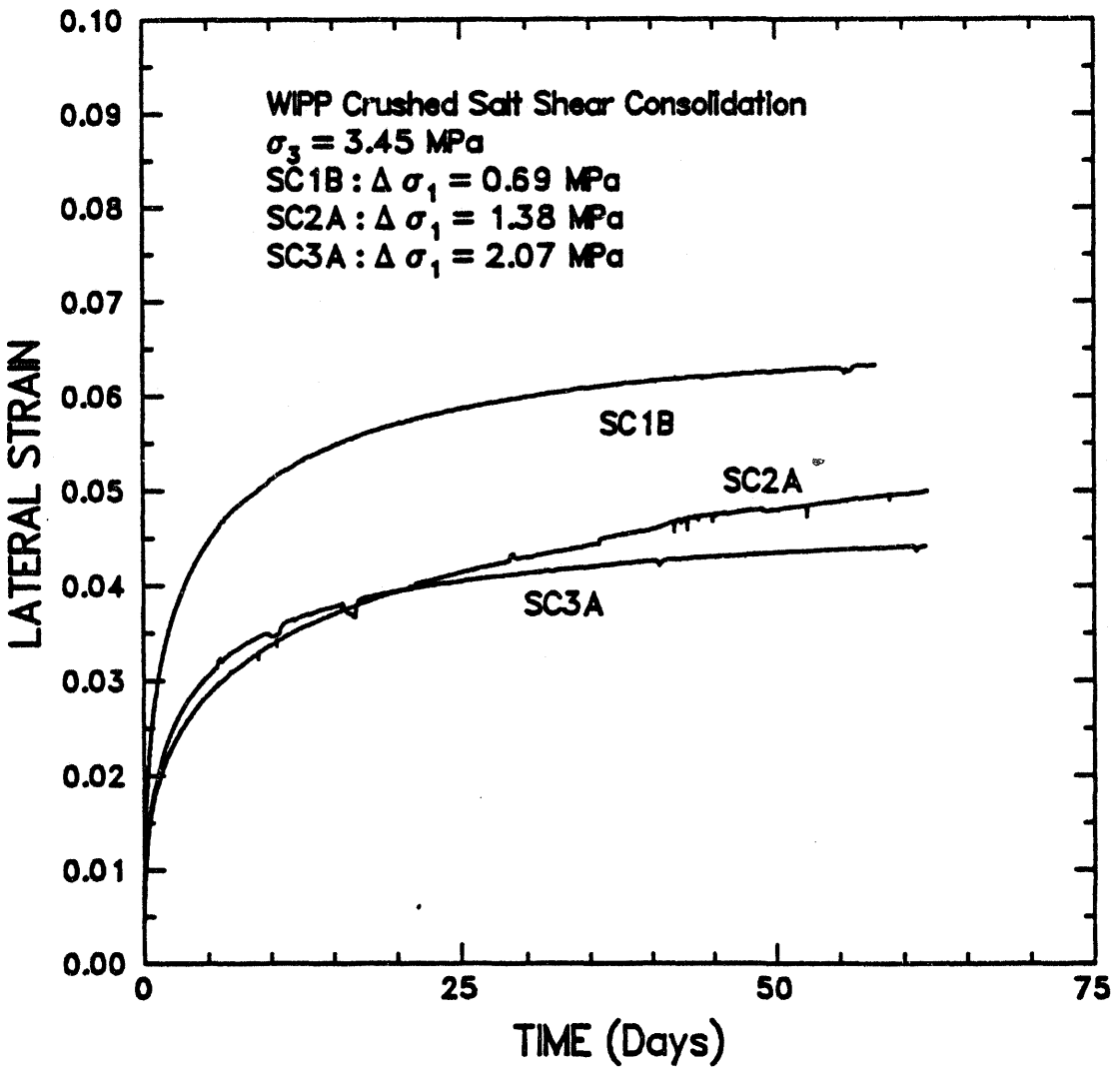

Figure 5-16. Lateral strain-versus-time for Stage 1 of all shear consolidation tests at 3.45 MPa confining pressure.

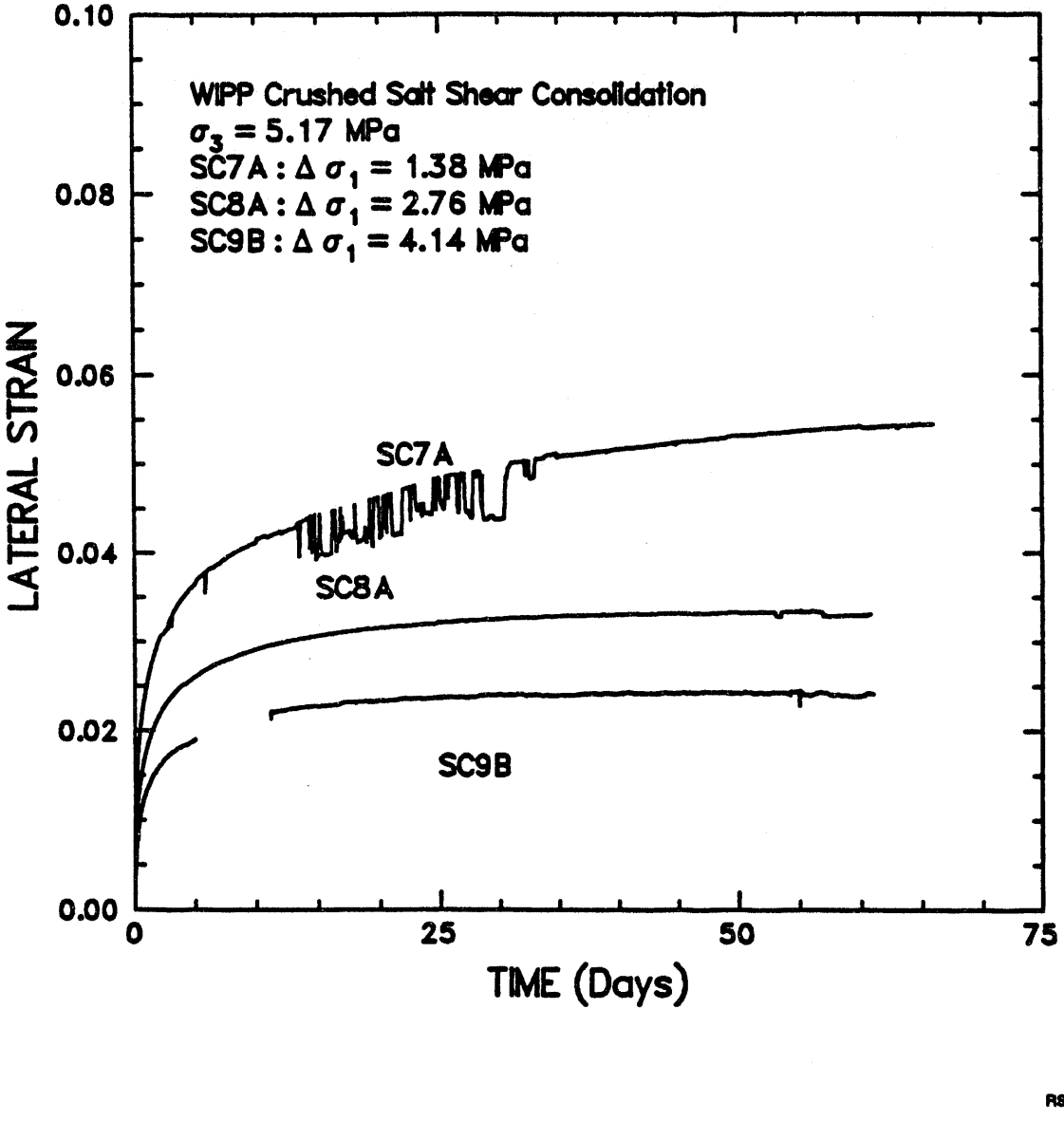

Figure 5-17. Lateral strain-versus-time for Stage 1 of all shear consolidation tests at 5.17 MPa confining pressure.

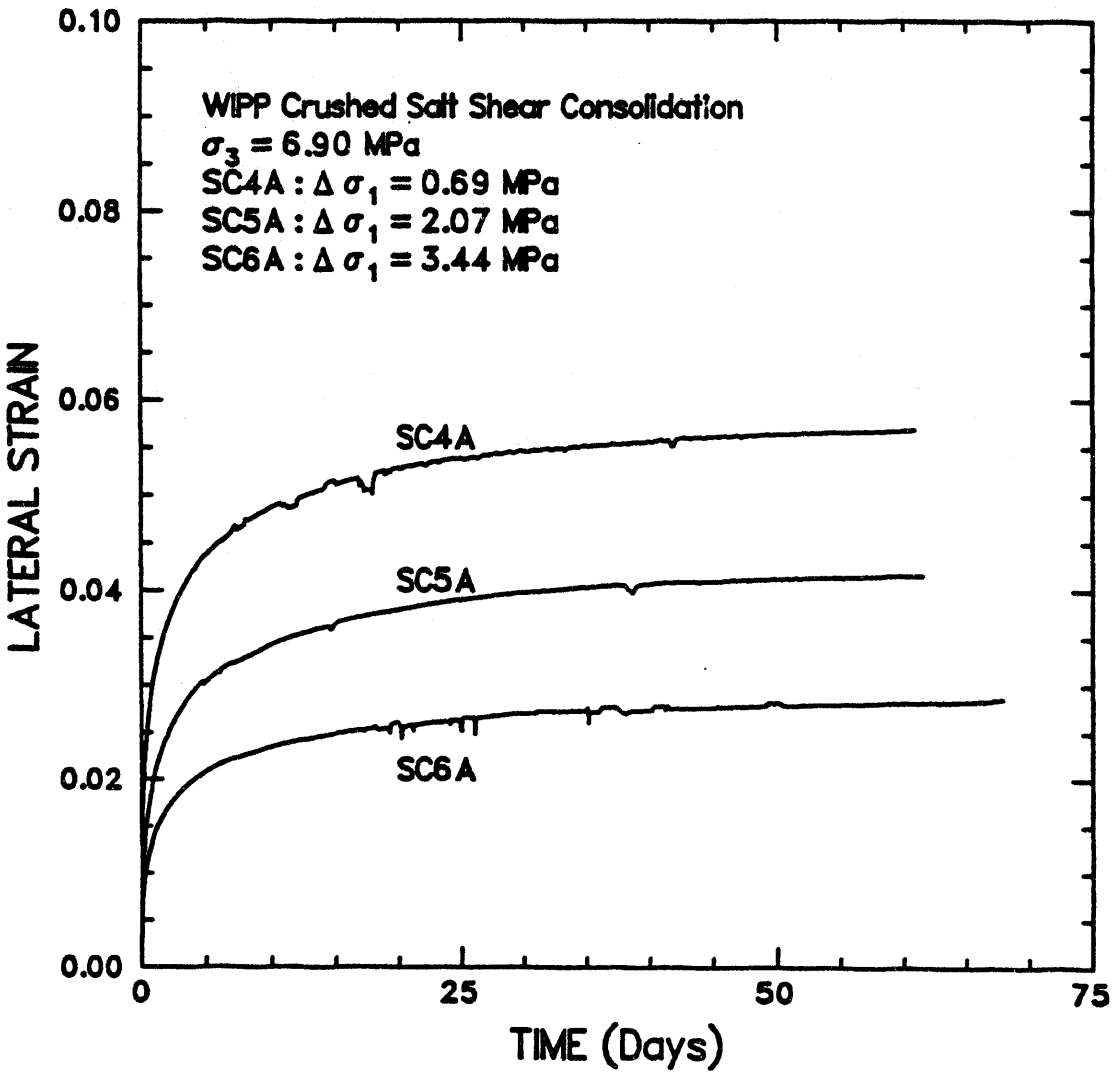

Figure 5-18. Lateral strain-versus-time for Stage 1 of all shear consolidation tests at 6.90 MPa confining pressure.

5.4 Permeability Data

Brine flow-versus-time data are presented in Appendix F for the RE/SPEC Inc.-furnished specimens. Flow is given as volume and refers to the cumulative change in fluid level in the downstream reservoir. As mentioned in Section 4.4, post-test fluid continuity checks were performed on specimen assembly components for most tests. The results of these checks are summarized in Table 5-9. The only test in which one component was completely blocked to fluid flow was SC7A. The results were inconclusive for several tests because removal of the specimen assembly components may have opened an otherwise blocked passageway.

The flow-versus-time curves for all tests except HC5 and SC7 show an overall positive slope, indicating the flow of brine from the high pressure to the low pressure reservoir. A negative slope indicates that the specimen was unsaturated and that brine flowed from the downstream reservoir back into the specimen, displacing air. When air bubbles were observed to emanate

Table 5-9. Results of Post-Test Fluid Continuity Checks of Platens, Faceplates, and Porous Felt Metal Disks for RE/SPEC Inc.-Furnished Specimens.

Test	Check Performed		Results		
	Yes	No	Pass	Fail	Inconclusive
HC1A		X			
HC2A	X				X
HC3A		X			
HC4A	X		X		
HC5A		X			
HC6A	X		X		
SC1B		X			
SC2A		X			
SC3A	X				X
SC4A	X		X		
SC5A	X				X
SC6A	X		X		
SC7A	X			X	
SC8A	X		X		
SC9B	X		X		

from a specimen, the fluid level in the downstream buret was recorded before and after the air bubble caused the fluid level to drop, and the data were subsequently corrected so that the drop would not be reflected in the processed data. This procedure was initiated when it was thought that the appearance of air bubbles were isolated incidents and would falsely lower the measured flow rates. Correcting the data provides maximum flow rates and highest permeabilities, and therefore the worst case scenario from the standpoint of repository performance. Many air bubbles apparently were undetected.

The levels of saturation at the start of the permeability stage are given for each specimen in Tables 5-3 and 5-7. These saturation levels were determined from specimen volumes measured after Stage 1 and from moisture content measurements (modified by saturation and by the extrusion of brine from the specimen during Stage 1 consolidation). Surprisingly, several specimens that were unsaturated at the start of the permeability stage (SC1B, SC2A, SC3A, and SC4A) showed flow rates with positive slopes, while several saturated specimens (HC5A, HC6A, SC5A, SC6A, SC7A, and SC9B) showed episodes of negative slope. It therefore appears possible that even in saturated specimens, localized areas may remain unsaturated, while in unsaturated specimens, a continuous saturated zone may connect the upper and lower specimen surfaces and provide a pathway for brine movement.

Flow rate decreases as a function of time for all tests. For tests in which flow rate changed substantially throughout the test, separate fits were made to the data over different regions of the flow-versus-time curve. Tables 5-10 and 5-11 give a summary of the permeability data for hydrostatic and shear consolidation tests, respectively, and list the intervals that were used for these separate fits. The tables give the flow rate for each interval, the calculated permeability, and dry fractional densities determined before and after the permeability stage.

All positive permeability values shown in Table 5-10 and 5-11, as well as all data for Specimen 19JUN90, are plotted in Figure 5-19 as a function of the final dry fractional density. The data (log permeability versus fractional dry density) were fit using linear regression to obtain a change in permeability of 1.9 orders of magnitude for a 0.1 change in fractional density. The coefficient of determination for this fit (r^2) is 0.25 and the standard deviation for any predicted permeability value is ± 0.85 orders of magnitude. The low coefficient of determination suggests that a linear model may not be appropriate for describing the relationship between permeability and fractional density. To obtain the highest permeabilities (and therefore the worst case scenario from the standpoint of repository performance), the data were replotted in Figure 5-20 using only the initial slopes for tests in which flow rates slowed substantially. All data marked with an asterisk in Table 5-9, as well as data for Specimen 19JUN90 fit within subregion 1, are included

Table 5-10. Summary of Permeability Data for Hydrostatic Consolidation Test Specimens

Test	Length (m)	Diameter (m)	Fluid Pressure (MPa)	Confining Pressure (MPa)	Initial Fractional Density	Final Fractional Density	Flow Rate ml/s	Permeability (m^2)
HC1A								
*Days 1-20	0.17	0.091	0.05	0.86	0.8978	0.9037	9.65E-06	6.34E-18
Day 20-64	0.17	0.091	0.05	0.86	0.8978	0.9037	1.08E-06	7.08E-19
HC2A								
*Days 1-19.5	0.167	0.091	0.43	0.86	0.947	0.9465	6.42E-05	4.88E-18
HC3A								
*Days 7-14	0.164	0.090	0.86	1.72	0.9541	0.942	5.75E-06	2.14E-19
Days 7-35	0.164	0.090	0.86	1.72	0.9541	0.942	3.81E-06	1.42E-19
Days 36-63	0.164	0.090	0.86	1.72	0.9541	0.942	1.26E-06	4.70E-20
Whole Test	0.164	0.090	0.86	1.72	0.9541	0.942	2.64E-06	9.86E-20
HC4A								
*Whole Test	0.163	0.09	0.86	1.72	0.9693	0.9359	3.67E-06	1.37E-19
HC5A								
*Whole Test	0.159	0.091	1.73	3.45	0.9926	1	1.93E-08	3.42E-22
HC6A								
*Whole Test	0.164	0.089	1.73	3.45	0.9929	1	5.26E-07	1E-20

within this plot. The data in this figure were also fitted using a linear regression to obtain a change of 2.1 orders of magnitude in permeability for a 0.1 change in dry fractional density. The coefficient of determination for this fit (r^2) is 0.32, and the standard deviation for any predicted permeability value is ± 0.89 orders of magnitude. Again, a linear relationship between permeability and fractional density may not be appropriate. The scatter in permeability values obtained at a given value of fractional density is much larger than the measurement error of approximately 5 percent. The permeability values determined here are higher than those obtained by Holcomb and Shields (1987) using argon gas as the permeant.

The decrease in flow rate as a function of time for each test was unexpected. It was hypothesized that the change in brine temperature from 25°C in the pressure vessel to 20°C at the downstream reservoir might have caused salt precipitation at the exit. To test this hypothesis the pressure vessel heaters were turned off after 62 days of permeability testing for test SC3A. The data, shown in Figure 5-21, indicate that turning off the heaters had no measurable effect on flow rate. One speculative idea for the decrease in flow rate is that some amount of

Table 5-11. Summary of Permeability Data for Shear Consolidation Test Specimens

Test	Length (m)	Diameter (m)	Fluid Pressure (MPa)	Confining Pressure (MPa)	Initial Fractional Density	Final Fractional Density	Flow Rate ml/s	Permeability (m^2)
SC1B								
*Days 0-3	0.16	0.092	0.92	1.84	0.9331	0.9635	1.08E-05	3.54E-19
Days 3-62	0.16	0.092	0.92	1.84	0.9331	0.9635	9.88E-07	3.25E-20
Days 56-62	0.16	0.092	0.92	1.84	0.9331	0.9635	1.93E-07	6.25E-21
Whole Test	0.16	0.092	0.92	1.84	0.9331	0.9635	1.29E-06	4.23E-20
SC2A								
*Days 29-32	0.151	0.093	0.98	2.93	0.9437	0.9879	4.34E-05	1.23E-18
Days 36-56	0.151	0.093	0.98	2.93	0.9437	0.9879	2.78E-06	7.89E-20
SC3A								
*Days 0-18	0.156	0.093	1.03	2.07	0.9297	0.9697	1.16E-05	3.22E-19
Days 85-95	0.156	0.093	1.03	2.07	0.9297	0.9697	2.97E-06	8.26E-20
Days 95-125	0.156	0.093	1.03	2.07	0.9297	0.9697	3.40E-07	9.45E-21
Whole Test	0.156	0.093	1.03	2.07	0.9297	0.9697	2.96E-06	8.24E-20
SC4A								
*Days 0-17	0.158	0.091	1.78	3.57	0.9378	0.9516	3.00E-05	5.18E-19
Days 17-64	0.158	0.091	1.78	3.57	0.9378	0.9516	-2.19E-07	-3.78E-21
Whole Test	0.158	0.091	1.78	3.57	0.9378	0.9516	4.76E-06	8.22E-20
SC5A								
*Days 0-1	0.16	0.092	1.9	3.79	0.9994	1.0145	4.32E-05	6.90E-19
Whole Test	0.16	0.092	1.9	3.79	0.9994	1.0145	3.74E-07	5.97E-21
SC6A								
*Days 0-13	0.153	0.093	2.01	4.02	0.9636	0.9768	1.80E-06	2.56E-20
Test to Date	0.153	0.093	2.01	4.02	0.9636	0.9768	6.68E-08	9.53E-22
SC7A								
*Days 0-2	0.16	0.093	1.41	2.81	0.9753	0.9782	4.37E-06	9.24E-20
Test to Date	0.16	0.093	1.41	2.81	0.9753	0.9782	-3.38E-07	-7.15E-21
SC8A								
*Days 0-6	0.151	0.093	1.52	3.05	0.9862	0.9719	6.99E-06	1.29E-19
Days 30-36	0.151	0.093	1.52	3.05	0.9862	0.9719	1.61E-05	2.99E-19
Whole Test	0.151	0.093	1.52	3.05	0.9862	0.9719	3.45E-06	6.39E-20
SC9B								
*Days 107	0.151	0.094	1.64	3.28	0.9701	0.9896	1.99E-06	3.31E-20

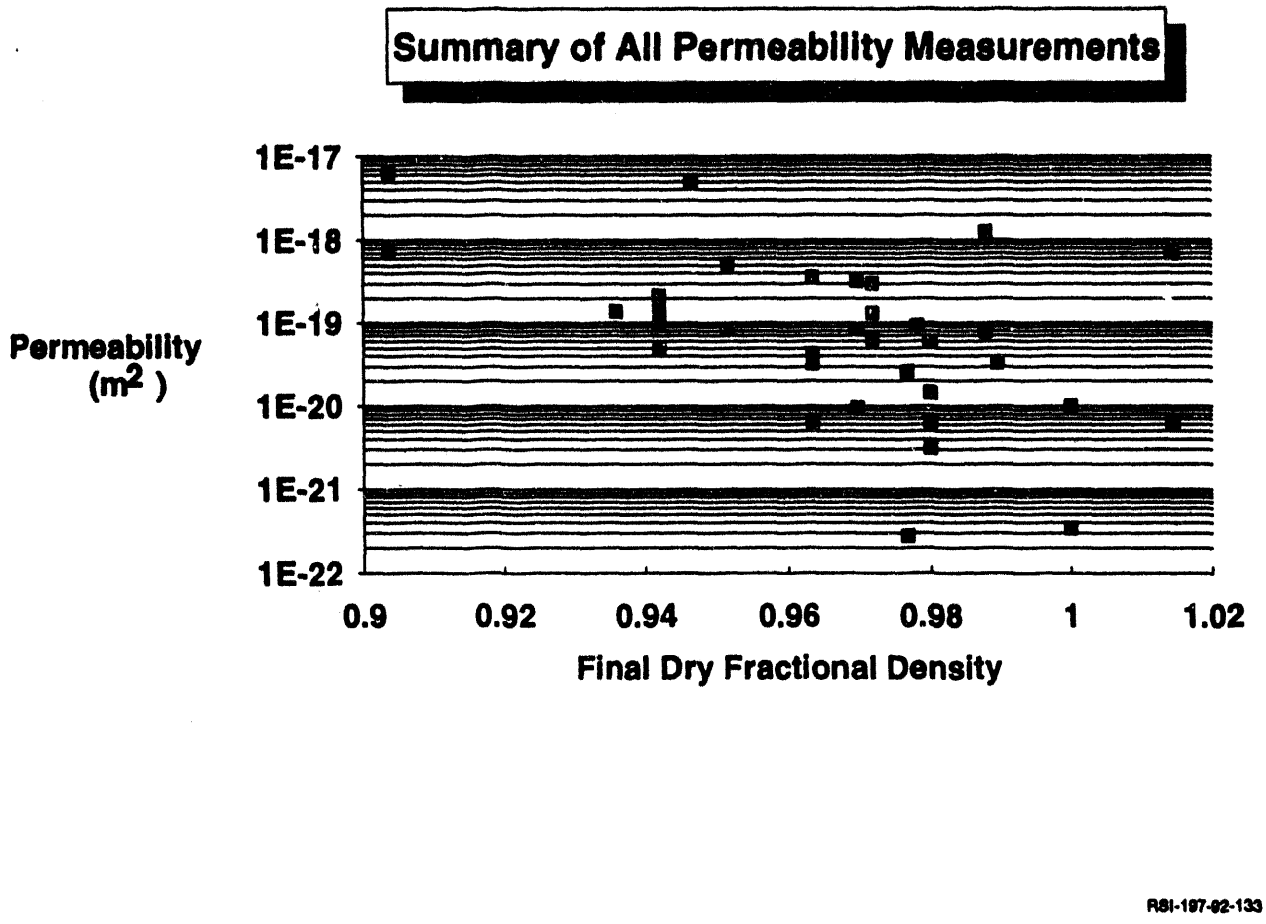

Figure 5-19. Permeability-versus-fractional density. All fits to the data given in Tables 5-10 and 5-11 are shown.

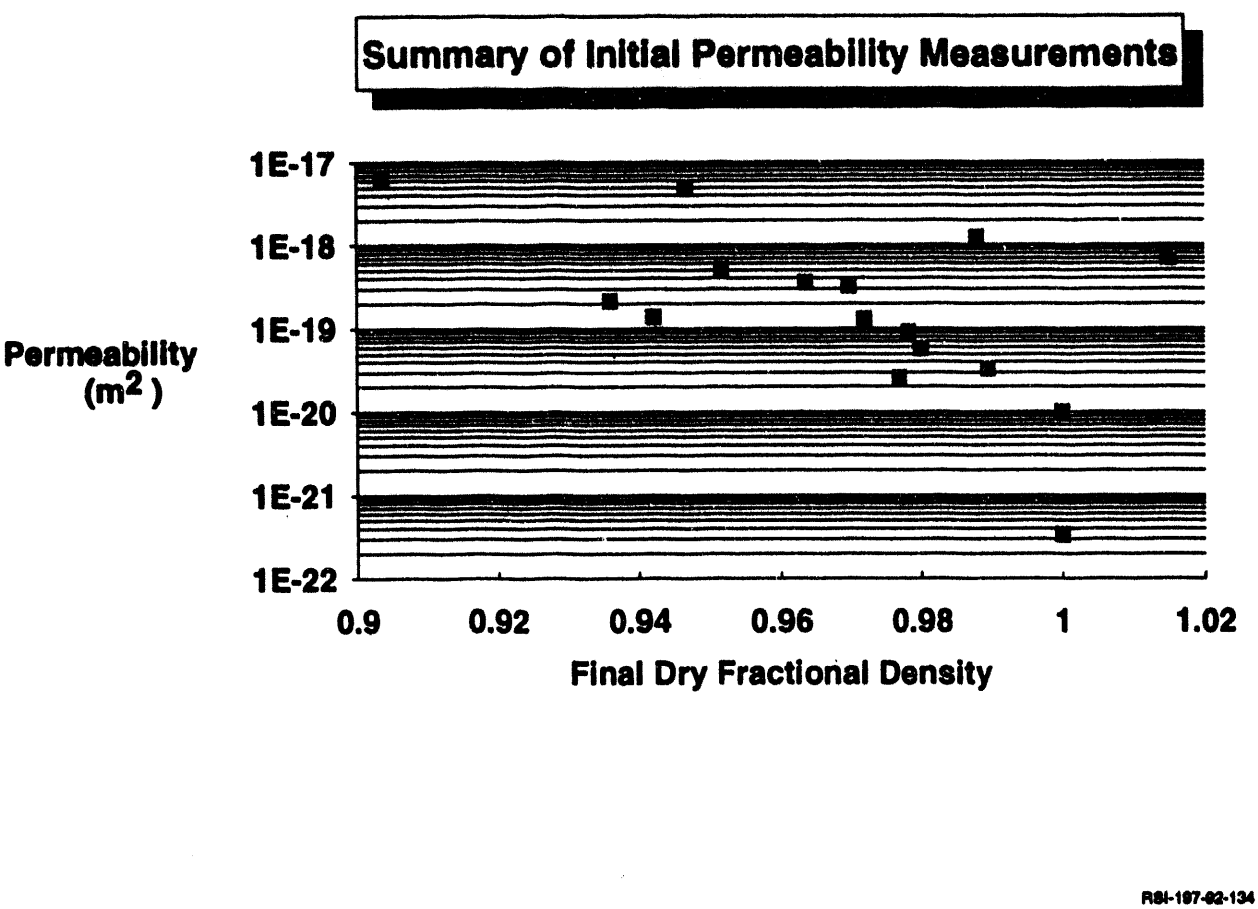

Figure 5-20. Permeability-versus-fractional density. Only values marked by an asterisk in Tables 5-10 and 5-11 are shown.

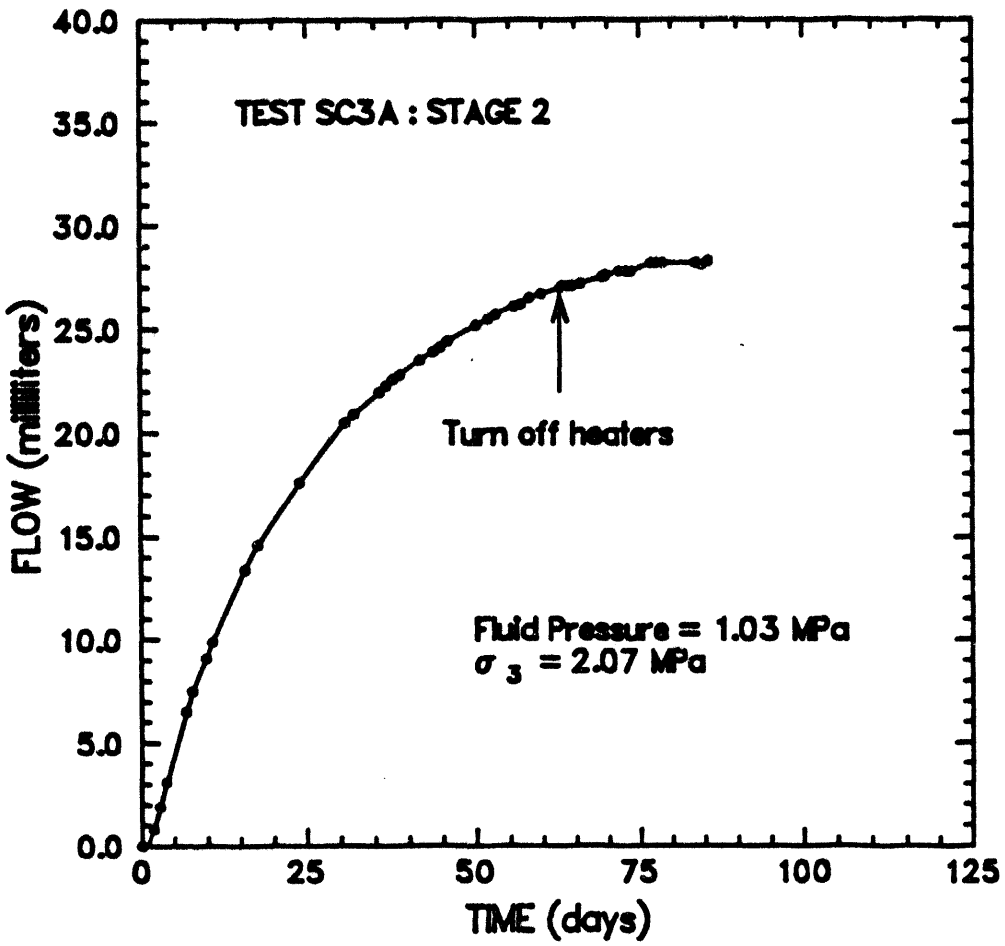

RSI-197-92-132

Figure 5-21. Brine volume-versus-time for Test SC3.

dissolution and precipitation occurs as the brine moves through the specimen. It is possible that precipitation causes the narrowing of some passageways, and so causes the flow rate to decrease.

5.5 Test Control

Stresses and temperatures were held at constant values by feedback mechanisms in the test systems. Appendices G, H, and I contain test data illustrating the conditions maintained during each test. Appendix G contains plots of axial stress-versus-time for Stage 1 of all shear consolidation tests, and Appendix H contains plots of confining pressure-versus-time for both stages of all tests on RE/SPEC Inc.-furnished specimens. Appendix I provides records of temperature-versus-time for these tests as measured by a thermocouple located in the pressure vessel wall. A temperature of 299.5 K (26.5°C) at the pressure vessel wall corresponds to a specimen temperature of 298 K (25°C).

The data acquisition and control computer underwent three malfunctions during the testing sequence causing lapses in data acquisition that can be seen in several tests. The test conditions were maintained through manual control during these outages.

Several tests show short duration increases in temperature due to malfunctions in the heat pump that controlled laboratory temperature. These temperature excursions are measurable at the pressure vessel wall but are substantially damped at the specimen. Sharp drops in temperature, down to 290-291 K, reflect a malfunction such as a loose electrical connection in the temperature readout device. This was seen in Test SC4A; however, the error was only in the computer readout of temperature. The temperature used by the temperature-control feedback loop was unaffected.

6.0 SUMMARY

Fifteen consolidation tests and eighteen permeability tests were performed on WIPP crushed salt to determine the effects of brine saturation and small applied stress differences on consolidation properties and the relation between brine permeability and crushed salt density. Three of the test specimens were consolidated by Division 6117, Sandia National Laboratories and then furnished to RE/SPEC Inc. for permeability testing. The remaining specimens were prepared, assembled, and tested at RE/SPEC Inc.

The Sandia-furnished specimens were subjected to a hydrostatic stress of 6.90 MPa for a period of greater than 10 days to allow pore fluid pressures to stabilize. In the second stage, the hydrostatic stress was dropped to 3.45 MPa and a brine fluid pressure was applied at one end of the specimen to produce a fluid pressure drop across the specimen of 345 kPa. The duration of the second stage was 100 days during which time flow measurements were made at specified time intervals. During both stages, volumetric strains were measured and the test temperature was held constant at 25°C. Two Sandia-furnished specimens, 20SEP89 and 19JUN90, were tested successfully, while the test on Specimen 20JUN90 was aborted during the first stage because of a rupture in the jacket protecting the specimen from the pressurizing oil. No volumetric strain or permeability measurements were made for the aborted test. In the two successful tests, the brine flow measurements made during the second stage of each test were used to calculate permeability. For Specimen 20SEP89, steady-state flow could not be established in 100 days of testing. In fact, flow measurements indicated that the specimen was not saturated. Similar results were obtained for the first 50 days of testing on Specimen 19JUN90; however, over the last 50 days of testing, a positive but very low flow rate was achieved.

Six brine-saturated crushed-salt specimens were placed under hydrostatic stress for up to 111 days while changes in volume were measured. Nine damp specimens containing 3 percent brine by weight were placed under triaxial creep conditions at small shear stresses for 60 days. After densities above 90 percent of the intact salt density were reached, stresses were decreased to stop further consolidation and permeability tests were performed using the steady-state flow method. Confining pressure used for consolidation stages ranged from 1.72 to 6.90 MPa, and axial stress differences were between 0.69 and 4.14 MPa.

Results of the hydrostatic consolidation tests show that consolidation rate increases with increasing confining pressure. Previous work (Zeuch et al., 1991) indicates that saturation has

little effect, or perhaps only a slight retardation effect, on consolidation rates for specimens that are already damp. Because of differences in specimen assemblies, the data presented here cannot be directly compared with previously published data. These data, therefore, offer no further clarification of this issue at this time.

The shear consolidation tests show that for the small axial stress differences used in this study, there is no systematic correlation between the magnitude of the applied shear stress and the consolidation rate. This is consistent with results obtained by Zeuch et al., 1991.

Permeability tests show that permeabilities for consolidated crushed salt decrease as dry fractional density increases. Permeability also decreased as a function of time for each test. The initial permeabilities provide the "worst case scenario" from the perspective of repository performance and so the initial data were used to determine a relationship between permeability and dry fractional density. It was found that permeability decreased approximately 2.1 orders of magnitude as fractional density increased from 0.90 to 1.0. Values of permeability ranged from 6×10^{-18} m^2 for a fractional density of 0.90 to 3×10^{-22} m^2 for a fractional density of 1.0. Permeability changes in crushed-salt seal components are likely to decrease over an even greater range of values, however. The reference seal system design (Nowak et al., 1990) calls for emplacement at a fractional density of 0.80, though recent design considerations suggest the desirability of emplacement at a slightly higher value (Van Sambeek et al., 1993); the permeabilities reported here correspond to fractional densities of about 0.90 and greater.

7.0 REFERENCES

Holcomb, D.J., and D.H. Zeuch. 1990. "Modeling the Consolidation of a Porous Aggregate of Salt as Isostatic Hot-Pressing," J. Geophys. Res., Vol. 95, 15,611-15,622.

Holcomb, D.J., and D.H. Zeuch. 1988. *Consolidation of Crushed Salt, Part I: Experimental Results for Dry Salt Analyzed Using a Hot-Pressing Model.* SAND88-1469. Albuquerque, NM: Sandia National Laboratories.

Holcomb, D.J., and M.E. Shields. 1987. *Hydrostatic Creep of Crushed Salt With Added Water.* SAND87-1990. Albuquerque, NM: Sandia National Laboratories.

Holcomb, D.J., and D.W. Hannum. 1982. *Consolidation of Crushed Salt Backfill Under Conditions Appropriate to the WIPP Facility.* SAND82-0630. Albuquerque, NM: Sandia National Laboratories.

Nowak, E.J., J.R. Tillerson, and T.M. Torres. 1990. *Initial Reference Seal System Design: Waste Isolation Pilot Plant.* SAND90-0355. Albuquerque, NM: Sandia National Laboratories.

Pfeifle, T.W. 1989. *Consolidation, Permeability and Strength of Crushed Salt/Bentonite Mixtures With Application to the WIPP.* SAND90-7009. Rapid City, SD: RE/SPEC Inc., for Sandia National Laboratories, Albuquerque, NM.

Shor, A.J., C.F. Baes, Jr., and C.M. Canonico. 1981. *Consolidation and Permeability of Salt in Brine.* ORNL-5774. Oak Ridge, TN: Oak Ridge National Laboratory.

Sjaardema, G.D., and R.D. Krieg. 1987. *A Constitutive Model for the Consolidation of WIPP Crushed Salt and Its Use in Analyses of Backfilled Shaft and Drift Configurations.* SAND87-1977. Albuquerque, NM: Sandia National Laboratories.

Stroup, D.E., and P.E. Senseny. 1987. *Influence of Bentonite Content on Consolidation and Permeability of Crushed Salt From the WIPP.* RSI-309. Rapid City, SD: RE/SPEC Inc., for Sandia National Laboratories, Albuquerque, NM.

Van Sambeek, L.L., D.D. Luo, M.S. Lin, W. Ostrowski, and D. Oyenuga. 1993. *Seal Design Alternatives Study.* SAND92-7340. Rapid City, SD: RE/SPEC Inc.; and San Francisci, CA: Parsons Brinckerhoff Quade & Douglas, Inc., for Sandia National Laboratories, Albuquerque, NM.

Zeuch, D.H., and D.J. Holcomb. 1991. *Experimental and Modeling Results for Reconsolidation of Crushed Natural Rock Salt Under Varying Physical Conditions.* SAND90-2509. Albuquerque, NM: Sandia National Laboratories.

Zeuch, D.H., D.J. Zimmerer, and M.E. Shields. 1991. *Interim Report on the Effects of Brine-Saturation and Shear Stress on Consolidation of Crushed, Natural Rock Salt from the Waste Isolation Pilot Plant (WIPP).* SAND91-0105. Albuquerque, NM: Sandia National Laboratories.

Zeuch, D.H. 1990. "Isostatic Hot-Pressing Mechanism Maps for Pure and Natural Sodium Chloride-Applications to Nuclear Waste Isolation in Bedded and Domal Salt Formations," *International Journal of Rock Mechanics and Mining Sciences and Geomechanics Abstracts.* Vol. 27, No. 3, 505-524.

Zeuch, D.H. 1989. *Isostatic Hot-Pressing Mechanism Maps for Pure and Natural Sodium Chloride: Applications to Nuclear Waste Isolation in Bedded and Domal Salt Formations.* SAND88-2207. Albuquerque NM: Sandia National Laboratories.

Zeuch, D.H., D.J. Holcomb, and H.S. Lauson. 1985. *Analysis of Consolidation of Granulated Rocksalt Using a Plastic Flow Model for Isostatic Hot-Pressing.* SAND84-1106 Albuquerque, NM: Sandia National Laboratories.

APPENDIX A. REPORT CONTAINING RESULTS OF CHEMICAL ANALYSES OF WIPP SALT, SUBMITTED TO RE/SPEC INC. BY TWIN CITY TESTING CORP., RAPID CITY, SOUTH DAKOTA

twin city testing
corporation

781 INDUSTRIAL AVENUE
RAPID CITY, SD 57702
PHONE 605/348-5850

640 WEST MAIN
LEAD, SD 57754
PHONE 605/584-2007

CHEMISTRY LABORATORY
1854 LOMBARDY DRIVE
RAPID CITY, SD 57701
PHONE 605/341-7284

February 7, 1992

RE/SPEC INC.
P.O. Box 725
Rapid City, S.D. 57709
394-6400

Job Number: 6110-92- 266 PO#: 5737
Sample Description: WIPP/CS-A

Lab Number: 3601

PARAMETER	RESULT, %	DATE/ANALYST
Calcium	0.15	2/6/92 BC
Chloride	58.0	2/7/92 JQ
Magnesium	0.062	2/6/92 BC
Potassium	0.151	2/6/92 BC
Sodium	35.0	2/6/92 BC
Strontium	0.005	2/6/92 BC
Sulfate	0.62	2/7/92 KC
Total Dissolved Solids	4850	2/7/92 JQ
% Insolubles	0.91	2/5/92 JQ
% EDTA Insolubles	0.32	2/7/92 JQ

Date Received: 1/31/92

Reviewed By: K. Cooper

twin city testing corporation

781 INDUSTRIAL AVENUE
RAPID CITY, SD 57702
PHONE 605/348-5850

640 WEST MAIN
LEAD, SD 57754
PHONE 605/584-2007

CHEMISTRY LABORATORY
1854 LOMBARDY DRIVE
RAPID CITY, SD 57701
PHONE 605/341-7284

February 7, 1992

RE/SPEC INC.
P.O. Box 725
Rapid City, S.D. 57709
394-6400

Job Number: 6110-92- 266 PO#: 5737
Sample Description: WIPP/CS-B

Lab Number: 3602

PARAMETER	RESULT, %	DATE/ANALYST
Calcium	0.26	2/6/92 BC
Chloride	58.0	2/7/92 JQ
Magnesium	0.074	2/6/92 BC
Potassium	0.174	2/6/92 BC
Sodium	34.2	2/6/92 BC
Strontium	0.006	2/6/92 BC
Sulfate	0.96	2/7/92 KC
Total Dissolved Solids	4800	2/7/92 JQ
% Insolubles	0.83	2/5/92 JQ
% EDTA Insolubles	0.51	2/7/92 JQ

Date Received: 1/31/92

Reviewed By: K. Cooper

twin city testing corporation

781 INDUSTRIAL AVENUE
RAPID CITY, SD 57702
PHONE 605/348-5850

640 WEST MAIN
LEAD, SD 57754
PHONE 605/584-2007

CHEMISTRY LABORATORY
1854 LOMBARDY DRIVE
RAPID CITY, SD 57701
PHONE 605/341-7284

February 7, 1992

RE/SPEC INC.
P.O. Box 725
Rapid City, S.D. 57709
394-6400

Job Number: 6110-92- 266 PO#: 5737
Sample Description: WIPP/CS-C

Lab Number: 3603

PARAMETER	RESULT, %	DATE/ANALYST
Calcium	0.24	2/6/92 BC
Chloride	56.0	2/7/92 JQ
Magnesium	0.084	2/6/92 BC
Potassium	0.232	2/6/92 BC
Sodium	34.1	2/6/92 BC
Strontium	0.007	2/6/92 BC
Sulfate	0.98	2/7/92 KC
Total Dissolved Solids	4750	2/7/92 JQ
% Insolubles	1.52	2/5/92 JQ
% EDTA Insolubles	1.01	2/7/92 JQ

Date Received: 1/31/92

Reviewed By: K. Cooper

APPENDIX B. MEMORANDUM SUMMARIZING RESULTS OF MINERALOGICAL ANALYSES OF WASTE ISOLATION PILOT PLANT SALT, SUBMITTED TO DR. DARRELL E. MUNSON BY C. L. STEIN

WP07352

Sandia National Laboratories

Albuquerque, New Mexico 87185

date. August 10, 1983

to: D. E. Munson - 6332

Carol

from: C. L. Stein - 6331

subject. Results of Mineralogical Analyses

The results of 28 analyses for mineral residue content of WIPP-SPDV halites are presented here. These samples, ranging generally in amounts of approximately 100-500 g, were first weighed out accurately, then stirred and dissolved overnight in distilled water; the water-insoluble residues were filtered onto preweighed Whatman filter paper discs, dried, reweighed, and the weight percent of water-insoluble mineral residue thus calculated (Table 1). Splits of this material were removed for x-ray diffraction analyses and the remainder used in the EDTA treatment as follows. The remainders of the water-insoluble residues were weighed out, boiled for 4 hours in 0.25 M di-sodium EDTA, filtered onto preweighed Whatman filter paper discs, dried, reweighed, and the EDTA-insoluble weight percents calculated as before (Table 1). Note that the EDTA weight percents are calculated from the sample weights which are water-insoluble residues, not the total sample weights. In a few cases, there was simply not enough of the water-insoluble residue left to treat with EDTA. In a few other cases, the amounts were so small that, while I did manage to obtain EDTA-insoluble weight percentages, I am not completely confident of their accuracy. As a check of the reproducibility of the EDTA numbers, I repeated the procedure on splits of 4 samples where sufficient material was available. The EDTA-insoluble weight percentages I obtained were reproducible to within ±2%.

The x-ray diffraction results from the water-insoluble residues (Table 2) showed the major components to be quartz, anhydrite, gypsum, magnesite, polyhalite, and a clay (probably montmorillonite). Based on visual inspection of the XRD peaks and knowledge of the relative diffraction efficiencies of these minerals, their relative abundances are qualitatively reported here as presence in major (M), minor (m), and trace (tr) amounts. Note that this is not a quantitative technique, and these results must not be interpreted in such a way.

After treatment with EDTA, the samples contained only quartz and clay; it is of interest to see that, following the removal of the EDTA-insoluble minerals (anhydrite, gypsum, magnesite, and polyhalite), the clay fraction is seen to contain kaolinite and a 10Å clay (presumably Illite) in addition to montmorillonite (Table 3). Owing to the tremendous contrast in diffraction efficiences between the quartz, which was essentially ubiquitous, and these clays, it was felt that even a qualitative estimate

e340 SWCF MIN

SP 12-16-91

of relative mineral abundances would be misleading. Hence I report here only the presence or absence of these phases. However, since the water-insoluble XRD patterns did pick up the montmorillonite (but not the 10Å or 7Å reflections), it may be safely assumed that it is the most abundant of the clay species present. I have requested additional XRD work (involving standard techniques for heat and ethylene glycol treatment) for more specific clay identification; I expect those results within a week or two.

This work is to be continued; I am awaiting completion of about a dozen thin sections of DO-52 and DO-53. I requested them primarily for the purpose of examining them for clay distribution and the authigenic quartz that I have reported on previously. Plans are presently underway for an experimental attempt at using radiography and/or gamma-beam densitometry (all facilities available at Sandia) to examine core for non-NaCl constituents. Until one of these techniques proves feasible, selected samples may be analyzed by the dissolution method described here although the time scale is, at present, somewhat uncertain. A request has been made to UNM to find a replacement for Richard Haaker, the student who performed these XRD analyses, and every effort is being made to coordinate with UNM so that this portion of the project will be running smoothly by September 1st.

CLS:6331:cds(3621)

TABLE 1

WIPP-SPDV Samples:Insoluble Residues

	Sample Number	Water-Insoluble			EDTA-Insoluble		
		Sample Weight	Residue Weight	Weight Percent	Sample Weight	Residue Weight	Weight Percent
1.	DO-52-49.2-49.9 12u	394.46	3.99	1.01	3.13	2.70	86.26
2.	DO-52-48.7-49.2 12u	315.06	16.59	5.27	5.31	4.33	81.54
3.	DO-52-42.6-43.5 11u	543.62	17.97	3.31	5.13	4.58	89.28
4.	DO-52-39.4-40.0 10u	336.10	0.11	0.03			
5.	DO-52-33.8-34.7 9u	538.73	20.28	3.76	5.05	3.98	78.81
	DO-52-27.1-27.9 8u	479.19	10.54	2.20	4.62	2.54	54.98
7.	DO-52-24.1-24.7 7u	300.20	0.11	0.04			
8.	DO-52-20.4-21.0 6u	362.35	2.49	0.69	1.50	0.71	47.33
9.	DO-52-14.3-15.0 5u	415.57	2.15	0.52	1.61	0.72	44.72
10.	DO-52-10.8-11.7 4u	554.81	4.84	0.87	3.28	1.64	50.00
11.	DO-52-9.0-9.7 3u	451.09	0.03	0.01			
12.	DO-52-2.0-2.75 2u	436.67	2.16	0.49	1.32	0.91	68.94
13.	DO-52-0.5-1.0 1u	354.33	0.73	0.21	0.45	0.39	86.67*
14.	DO-53-2.35-2.6- 1D	106.42	0.60	0.56	0.22	0.12	54.55*
	DO-53-4.0-4.3 1D	206.53	1.28	0.62	0.80	0.28	35.00*
16.	DO-53-core frags. 2D	236.37	8.27	3.50	3.37	2.58	76.56
17.	DO-53-14.1-14.5 3D	251.72	0.40	0.16	0.36	0.14	38.89*
18.	DO-53-17.15-17.80 3D	464.01	5.47	1.18	3.03	1.77	58.42
19.	DO-53-23.7-24.1 4D	155.36	1.26	0.81	0.96	0.59	61.46
20.	DO-53-24.1-24.65 4D	326.42	7.93	2.43	5.09	1.71	33.60
21.	DO-53-27.1-27.8 5D	526.10	4.63	0.88	3.19	1.68	52.66
22.	DO-53-31.0-31.5 6D	342.93	0.21	0.06			
	DO-53-36.1-36.7 7D	364.13	1.89	0.52	1.47	1.17	79.59
24.	DO-53-43.2-43.6 8D	243.82	0.50	0.21	0.22	0.22	100.00*
25.	DO-53-43.6-44.0 8D	248.19	0.35	0.14	0.25	0.12	48.00*
26.	DO-53-47.7-48.05 9D	231.51	3.89	1.68	2.87	1.53	53.31
27.	DO-53-48.05-48.25 9D	112.96	1.48	1.31	1.18	0.77	62.25
28.	2065	290.20	2.28	0.79			

*Very little material to work with; these values may be inaccurate.

CLS:6331(3621)
May 27, 1983

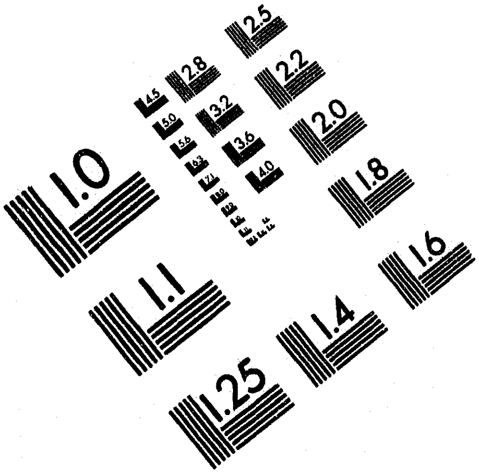
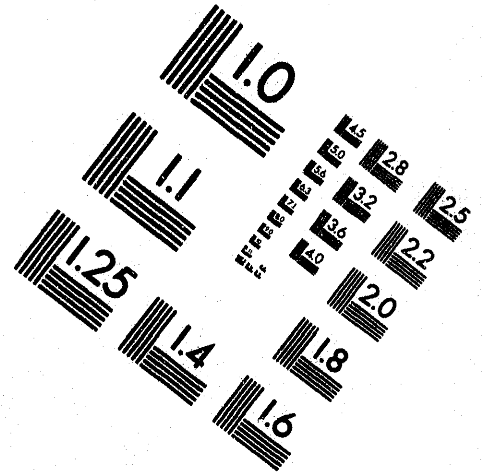

AIIM

Association for Information and Image Management

1100 Wayne Avenue, Suite 1100
Silver Spring, Maryland 20910

301/587-8202

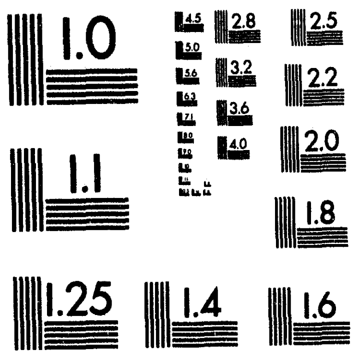
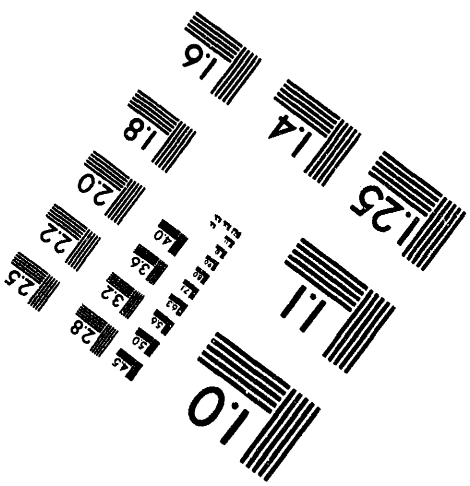
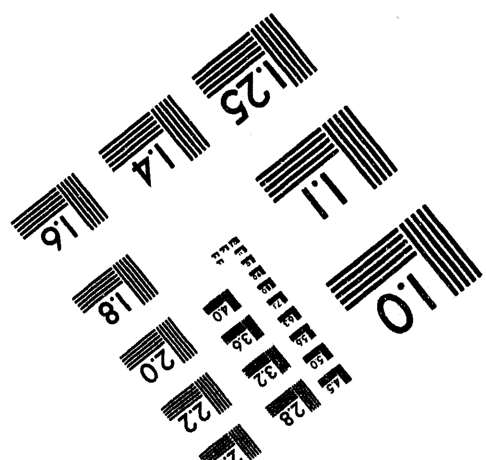

MANUFACTURED TO AIIM STANDARDS
BY APPLIED IMAGE, INC.

2 of 3

TABLE 2

X-RAY DIFFRACTION ANALYSES OF WATER-INSOLUBLE RESIDUES

Sample No.	Quartz	Anhydrite	Gypsum	Magnesite	Polyhalite	Clay Montmoril-lonite
DO-52-49.2-49.9	M	m		m		m
DO-52-48.7-49.2	M			m		tr
DO-52-42.6-43.5 11u	M	m			tr	
DO-52-33.8-34.7	M			m		tr
DO-52-27.1-27.9	M			M		tr
DO-52-20.4-21.0 6u		M	m	M	M	
DO-52-14.3-15.0		M	M			
DO-52-10.8-11.7	m	M	M	M	M	
DO-52-2.0-2.75 2U	M	M	m	M		tr
DO-52-0.5-1.0 1u	M			M		tr
2065*	M	M		m		
DO-53-2.35-2.60 1D	m	M	M	m	m	
DO-53-4.0-4.3 1D	M	m	M	m	m	tr
DO-53-Core fragments			M		M	
DO-53-14.1-14.5 3D	m	M	M		m	
DO-53-17.15-17.80	M		m	M		tr
DO-53-23.7-24.1	M	tr	M		tr	tr
DO-53-24.1-24.65 4D	M	M	m	M	M	m
DO-53-27.1-27.8 5D	M	tr		M		tr
DO-53-31.0-31.5				M		
DO-53-36.1-36.7 7D	m			M		tr
DO-53-43.2-43.6 8D	M			M		tr
DO-53-43.6-44.0 8D	M	M		M		m
DO-53-47.7-48.05	m			M		tr
DO-53-48.05-48.25	m			M		tr

*Further work on this sample was dropped when it was learned that its location was unknown.

TABLE 3

X-RAY DIFFRACTION ANALYSES OF EDTA-INSOLUBLE RESIDUES

Sample No.	Quartz	Montmorillonite 14Å	Illite (10Å)	Kaolinite (7Å)
DO-52-49.2-49.9	X	X	X	X
DO-52-48.7-49.2				
DO-52-42.6-43.5 11u	X			
DO-52-33.8-34.7	X	X	X	X
DO-52-27.1-27.9	X	X	X	
DO-52-20.4-21.0 6u	X	X	X	X
DO-52-14.3-15.0				
DO-52-10.8-11.7	X	X	X	
DO-52-2.0-2.75 2u	X	X	X	X
DO-52-0.5-1.0 1u	X			
DO-53-2.35-2.60 1D				
DO-53-4.0-4.3 1D	X		X	X
DO-53-Core fragments			X	
DO-53-14.1-14.5 3D				
DO-53-17.15-17.80	X	X	X	X
DO-53-23.7-24.1	X	X		X
DO-53-24.1-24.65 4D				
DO-53-27.1-27.8 5D	X	X	X	X
DO-53-31.0-31.5				
DO-53-36.1-36.7 7D	X	X		
DO-53-43.2-43.6 8D				
DO-53-43.6-44.0 8D				
DO-53-47.7-48.05	X	X	X	X
DO-53-48.05-48.25	X	X	X	X
H-2a-646 (base of Culebra)	X	X	X	X

Copy to:
J. Treadwell - DOE/WPO
A. Hunt ------ DOE/WPO
D. Shukla ---- TSC (D'Appolonia)
D. Stevenson - TSC (D'Appolonia)
J. Smrha ----- Bechtel-AL
H. Taylor ---- Bechtel (S.F.)
D. L. Wu ----- Bechtel (S.F.)
Ching Wu ----- Bechtel (S.F.)
D. Roberts --- Bechtel (S.F.)
R. McKinney -- D'Appolonia (Carlsbad)
1521 R. D. Krieg
1521 H. S. Morgan
1521 C. M. Stone
1521 D. W. Webb
1542 B. M. Butcher
1542 W. Wawersik
6330 W. D. Weart
6331 A. R. Lappin
6331 D. J. Borns
6331 S. J. Lambert
6331 K. L. Robinson
6331 S-E. Shaffer
6332 T. O. Hunter
6332 R. V. Matalucci
6332 T. M. Torres
6332 WPO File
6331 C. L. Stein

APPENDIX C. SUMMARY OF TRANSDUCER REVERIFICATION DATA FOR ALL HYDROSTATIC AND SHEAR CONSOLIDATION TESTS

Tables

Table C-1. Reverification Data for Test HC1A

Test and Stage	Transducer	Test Condition	Transducer Reverification Status at Test Condition or Nearest Calibration Point[a]
HC1A Stage 1	Axial Load Cell	10.7 kN	1.68 percent high
	Confining Pressure	1.72 MPa	5.64 percent low
	Pore Pressure	N/A	N/A
	LVDT	0 - 25.4 mm	Reverified
	Dilatometer	0 - 100,000 mm^3	Reverified
	Temperature	25°C	Reverified
HC1A Stage 2	Axial Load Cell	5.3 kN	1.68 percent high
	Confining Pressure	0.86 MPa	5.64 percent low
	Pore Pressure	0.05 - 0.42 MPa	Reverified
	LVDT	0 - 25.4 mm	Reverified
	Dilatometer	0 - 100,000 mm^3	Reverified
	Temperature	25°C	Reverified

(a) Errors are given as a percent of reading. Successful reverification requires load and pressure transducers accurate to within 1 percent of reading, deformation transducers accurate to within 2 percent of reading, temperature accurate to within ±1°C.

Table C-2. Reverification Data for Test HC2A

Test and Stage	Transducer	Test Condition	Transducer Reverification Status at Test Condition or Nearest Calibration Point[a]
HC2A Stage 1	Axial Load Cell	10.7 kN	2.40 percent high
	Confining Pressure	1.72 MPa	Reverified
	Pore Pressure	N/A	N/A
	LVDT	0 - 25.4 mm	Reverified
	Dilatometer	0 - 100,000 mm^3	Reverified
	Temperature	25°C	Reverified
HC2A Stage 2	Axial Load Cell	5.3 kN	3.02 percent low
	Confining Pressure	0.86 MPa	Reverified
	Pore Pressure	0.43 MPa	Reverified
	LVDT	0 - 25.4 mm	Reverified
	Dilatometer	0 - 100,000 mm^3	Reverified
	Temperature	25°C	Reverified

(a) Errors are given as a percent of reading. Successful reverification requires load and pressure transducers accurate to within 1 percent of reading, deformation transducers accurate to within 2 percent of reading, temperature accurate to within ±1°C.

Table C-3. Reverification Data for Test HC3A

Test and Stage	Transducer	Test Condition	Transducer Reverification Status at Test Condition or Nearest Calibration Point[a]
HC3A Stage 1	Axial Load Cell	21.4 kN	1.04 percent low
	Confining Pressure	3.45 MPa	Reverified
	Pore Pressure	N/A	N/A
	LVDT	0 - 25.4 mm	Reverified
	Dilatometer	0 - 100,000 mm^3	Reverified
	Temperature	25°C	3.3°C high
HC3A Stage 2	Axial Load Cell	10.7 kN	1.04 percent low
	Confining Pressure	1.72 MPa	Reverified
	Pore Pressure	0.86 MPa	2.04 percent high
	LVDT	0 - 25.4 mm	Reverified
	Dilatometer	0 - 100,000 mm^3	Reverified
	Temperature	25°C	3.3°C high

(a) Errors are given as a percent of reading. Successful reverification requires load and pressure transducers accurate to within 1 percent of reading, deformation transducers accurate to within 2 percent of reading, temperature accurate to within ±1°C.

Table C-4. Reverification Data for Test HC4A

Test and Stage	Transducer	Test Condition	Transducer Reverification Status at Test Condition or Nearest Calibration Point[a]
HC4A Stage 1	Axial Load Cell	21.4 kN	Reverified
	Confining Pressure	3.45 MPa	2.40 percent low
	Pore Pressure	N/A	N/A
	LVDT	0 - 25.4 mm	Reverified
	Dilatometer	0 - 100,000 mm^3	Reverified
	Temperature	25°C	Reverified
HC4A Stage 2	Axial Load Cell	10.7 kN	Reverified
	Confining Pressure	1.72 MPa	2.40 percent low
	Pore Pressure	0.86 MPa	1.58 percent low
	LVDT	0 - 25.4 mm	Reverified
	Dilatometer	0 - 100,000 mm^3	Reverified
	Temperature	25°C	Reverified

(a) Errors are given as a percent of reading. Successful reverification requires load and pressure transducers accurate to within 1 percent of reading, deformation transducers accurate to within 2 percent of reading, temperature accurate to within ±1°C.

Table C-5. Reverification Data for Test HC5A

Test and Stage	Transducer	Test Condition	Transducer Reverification Status at Test Condition or Nearest Calibration Point[a]
HC5A Stage 1	Axial Load Cell	42.8 kN	Reverified
	Confining Pressure	6.90 MPa	2.91 percent low
	Pore Pressure	N/A	N/A
	LVDT	0 - 25.4 mm	Reverified
	Dilatometer	0 - 100,000 mm^3	Reverified
	Temperature	25°C	Reverified
HC5A Stage 2	Axial Load Cell	21.4 kN	Reverified
	Confining Pressure	3.45 MPa	5.77 percent low
	Pore Pressure	1.72 MPa	Reverified
	LVDT	0 - 25.4 mm	Reverified
	Dilatometer	0 - 100,000 mm^3	Reverified
	Temperature	25°C	Reverified

(a) Errors are given as a percent of reading. Successful reverification requires load and pressure transducers accurate to within 1 percent of reading, deformation transducers accurate to within 2 percent of reading, temperature accurate to within ±1°C.

Table C-6. Reverification Data for Test HC6A

Test and Stage	Transducer	Test Condition	Transducer Reverification Status at Test Condition or Nearest Calibration Point[a]
HC6A Stage 1	Axial Load Cell	42.8 kN	2.43 percent low
	Confining Pressure	6.90 MPa	Reverified
	Pore Pressure	N/A	N/A
	LVDT	0 - 25.4 mm	Reverified
	Dilatometer	0 - 100,000 mm^3	Reverified
	Temperature	25°C	Reverified
HC6A Stage 2	Axial Load Cell	21.4 kN	4.39 percent low
	Confining Pressure	3.45 MPa	Reverified
	Pore Pressure	1.72 MPa	Reverified
	LVDT	0 - 25.4 mm	Reverified
	Dilatometer	0 - 100,000 mm^3	Reverified
	Temperature	25°C	Reverified

(a) Errors are given as a percent of reading. Successful reverification requires load and pressure transducers accurate to within 1 percent of reading, deformation transducers accurate to within 2 percent of reading, temperature accurate to within ±1°C.

Table C-7. Reverification Data for Test SC1B

Test and Stage	Transducer	Test Condition	Transducer Reverification Status at Test Condition or Nearest Calibration Point[a]
SC1B Stage 1	Axial Load Cell	26.6 kN	2.32 percent high
	Confining Pressure	3.45 MPa	1.24 percent high
	Pore Pressure	N/A	N/A
	LVDT	0 - 25.4 mm	Reverified
	Dilatometer	0 - 100,000 mm^3	Reverified
	Temperature	25°C	Reverified
SC1B Stage 2	Axial Load Cell	11.4 KN	2.32 percent high
	Confining Pressure	1.84 MPa	1.24 percent high
	Pore Pressure	0.92 MPa	5.7 percent low
	LVDT	0 - 25.4 mm	Reverified
	Dilatometer	0 - 100,000 mm^3	Reverified
	Temperature	25°C	Reverified

(a) Errors are given as a percent of reading. Successful reverification requires load and pressure transducers accurate to within 1 percent of reading, deformation transducers accurate to within 2 percent of reading, temperature accurate to within ±1°C.

Table C-8. Reverification Data for Test SC2A

Test and Stage	Transducer	Test Condition	Transducer Reverification Status at Test Condition or Nearest Calibration Point[a]
SC2A Stage 1	Axial Load Cell	31.9 kN	Reverified
	Confining Pressure	3.45 MPa	3.03 percent low
	Pore Pressure	N/A	N/A
	LVDT	0 - 25.4 mm	3.97 percent low
	Dilatometer	0 - 100,000 mm^3	Reverified
	Temperature	25°C	Reverified
SC2A Stage 2	Axial Load Cell	11.4 kN	Reverified
	Confining Pressure	1.95 MPa	3.03 percent low
	Pore Pressure	0.98 MPa	Reverified
	LVDT	0 - 25.4 mm	3.97 percent low
	Dilatometer	0 - 100,000 mm^3	Reverified
	Temperature	25°C	Reverified
SC2A Stage 3	Axial Load Cell	11.4 kN	Reverified
	Confining Pressure	2.93 MPa	3.03 percent low
	Pore Pressure	0.98 MPa	Reverified
	LVDT	0 - 25.4 mm	3.97 percent low
	Dilatometer	0 - 100,000 mm^3	Reverified
	Temperature	25°C	Reverified

(a) Errors are given as a percent of reading. Successful reverification requires load and pressure transducers accurate to within 1 percent of reading, deformation transducers accurate to within 2 percent of reading, temperature accurate to within ±1°C.

Table C-9. Reverification Data for Test SC3A

Test and Stage	Transducer	Test Condition	Transducer Reverification Status at Test Condition or Nearest Calibration Point[a]
SC3A Stage 1	Axial Load Cell	36.9 kN	Reverified
	Confining Pressure	3.45 MPa	1.31 percent low
	Pore Pressure	N/A	N/A
	LVDT	0 - 25.4 mm	Reverified
	Dilatometer	0 - 100,000 mm^3	Reverified
	Temperature	25°C	Reverified
SC3A Stage 2	Axial Load Cell	12.8 kN	Reverified
	Confining Pressure	2.07 MPa	1.31 percent low
	Pore Pressure	1.03 MPa	Reverified
	LVDT	0 - 25.4 mm	Reverified
	Dilatometer	0 - 100,000 mm^3	Reverified
	Temperature	25°C	Reverified

(a) Errors are given as a percent of reading. Successful reverification requires load and pressure transducers accurate to within 1 percent of reading, deformation transducers accurate to within 2 percent of reading, temperature accurate to within ±1°C.

Table C-10. Reverification Data for Test SC4A

Test and Stage	Transducer	Test Condition	Transducer Reverification Status at Test Condition or Nearest Calibration Point[(a)]
SC4A Stage 1	Axial Load Cell	47.9 kN	Reverified
	Confining Pressure	6.90 MPa	Reverified
	Pore Pressure	N/A	N/A
	LVDT	0 - 25.4 mm	Reverified
	Dilatometer	0 - 100,000 mm^3	Reverified
	Temperature	25°C	Reverified
SC4A Stage 2	Axial Load Cell	22.1 kN	Reverified
	Confining Pressure	3.57 MPa	Reverified
	Pore Pressure	1.78 MPa	Reverified
	LVDT	0 - 25.4 mm	Reverified
	Dilatometer	0 - 100,000 mm^3	Reverified
	Temperature	25°C	Reverified

(a) Errors are given as a percent of reading. Successful reverification requires load and pressure transducers accurate to within 1 percent of reading, deformation transducers accurate to within 2 percent of reading, temperature accurate to within ±1°C.

Table C-11. Reverification Data for Test SC5A

Test and Stage	Transducer	Test Condition	Transducer Reverification Status at Test Condition or Nearest Calibration Point[a]
SC5A Stage 1	Axial Load Cell	58.3 kN	1.27 percent high
	Confining Pressure	6.90 MPa	1.71 percent high
	Pore Pressure	N/A	N/A
	LVDT	0 - 25.4 mm	Reverified
	Dilatometer	0 - 100,000 mm^3	Reverified
	Temperature	25°C	1.2°C low
SC5A Stage 2	Axial Load Cell	23.5 kN	3.30 percent high
	Confining Pressure	3.79 MPa	3.40 percent high
	Pore Pressure	1.90 MPa	Reverified
	LVDT	0 - 25.4 mm	Reverified
	Dilatometer	0 - 100,000 mm^3	Reverified
	Temperature	25°C	1.2°C low

(a) Errors are given as a percent of reading. Successful reverification requires load and pressure transducers accurate to within 1 percent of reading, deformation transducers accurate to within 2 percent of reading, temperature accurate to within ±1°C.

Table C-12. Reverification Data for Test SC6A

Test and Stage	Transducer	Test Condition	Transducer Reverification Status at Test Condition or Nearest Calibration Point[a]
SC6A Stage 1	Axial Load Cell	67.5 kN	3.78 percent high
	Confining Pressure	6.90 MPa	Reverified
	Pore Pressure	N/A	N/A
	LVDT	0 - 25.4 mm	Reverified
	Dilatometer	0 - 100,000 mm^3	Reverified
	Temperature	25°C	Reverified
SC6A Stage 2	Axial Load Cell	25.0 kN	2.51 percent low
	Confining Pressure	4.02 MPa	1.60 percent low
	Pore Pressure	2.01 MPa	Reverified
	LVDT	0 - 25.4 mm	Reverified
	Dilatometer	0 - 100,000 mm^3	Reverified
	Temperature	25°C	Reverified

(a) Errors are given as a percent of reading. Successful reverification requires load and pressure transducers accurate to within 1 percent of reading, deformation transducers accurate to within 2 percent of reading, temperature accurate to within ±1°C.

Table C-13. Reverification Data for Test SC7A

Test and Stage	Transducer	Test Condition	Transducer Reverification Status at Test Condition or Nearest Calibration Point[a]
SC7A Stage 1	Axial Load Cell	42.5 kN	Reverified
	Confining Pressure	5.17 MPa	Reverified
	Pore Pressure	N/A	N/A
	LVDT	0 - 25.4 mm	Reverified
	Dilatometer	0 - 100,000 mm^3	Reverified
	Temperature	25°C	Reverified
SC7A Stage 2	Axial Load Cell	17.4 kN	Reverified
	Confining Pressure	2.81 MPa	Reverified
	Pore Pressure	1.41 MPa	Reverified
	LVDT	0 - 25.4 mm	Reverified
	Dilatometer	0 - 100,000 mm^3	Reverified
	Temperature	25°C	Reverified

(a) Errors are given as a percent of reading. Successful reverification requires load and pressure transducers accurate to within 1 percent of reading, deformation transducers accurate to within 2 percent of reading, temperature accurate to within ±1°C.

Table C-14. Reverification Data for Test SC8A

Test and Stage	Transducer	Test Condition	Transducer Reverification Status at Test Condition or Nearest Calibration Point[a]
SC8A Stage 1	Axial Load Cell	52.0 kN	3.17 percent low
	Confining Pressure	5.17 MPa	Reverified
	Pore Pressure	N/A	N/A
	LVDT	0 - 25.4 mm	Reverified
	Dilatometer	0 - 100,000 mm^3	Reverified
	Temperature	25°C	Reverified
SC8A Stage 2	Axial Load Cell	18.9 kN	6.73 percent low
	Confining Pressure	3.05 MPa	Reverified
	Pore Pressure	1.52 MPa	Reverified
	LVDT	0 - 25.4 mm	Reverified
	Dilatometer	0 - 100,000 mm^3	Reverified
	Temperature	25°C	Reverified

(a) Errors are given as a percent of reading. Successful reverification requires load and pressure transducers accurate to within 1 percent of reading, deformation transducers accurate to within 2 percent of reading, temperature accurate to within ±1°C.

Table C-15. Reverification Data for Test SC9B

Test and Stage	Transducer	Test Condition	Transducer Reverification Status at Test Condition or Nearest Calibration Point[a]
SC9B Stage 1	Axial Load Cell	59.6 kN	4.25 percent low
	Confining Pressure	5.17 MPa	Reverified
	Pore Pressure	N/A	N/A
	LVDT	0 - 25.4 mm	Reverified
	Dilatometer	0 - 100,000 mm^3	Reverified
	Temperature	25°C	Reverified
SC9B Stage 2	Axial Load Cell	20.4 kN	6.85 percent low
	Confining Pressure	3.28 MPa	Reverified
	Pore Pressure	1.64 MPa	Reverified
	LVDT	0 - 25.4 mm	Reverified
	Dilatometer	0 - 100,000 mm^3	Reverified
	Temperature	25°C	Reverified

(a) Errors are given as a percent of reading. Successful reverification requires load and pressure transducers accurate to within 1 percent of reading, deformation transducers accurate to within 2 percent of reading, temperature accurate to within ±1°C.

APPENDIX D. FRACTIONAL DENSITY-VERSUS-TIME FOR ALL HYDROSTATIC AND SHEAR CONSOLIDATION TESTS

Figures

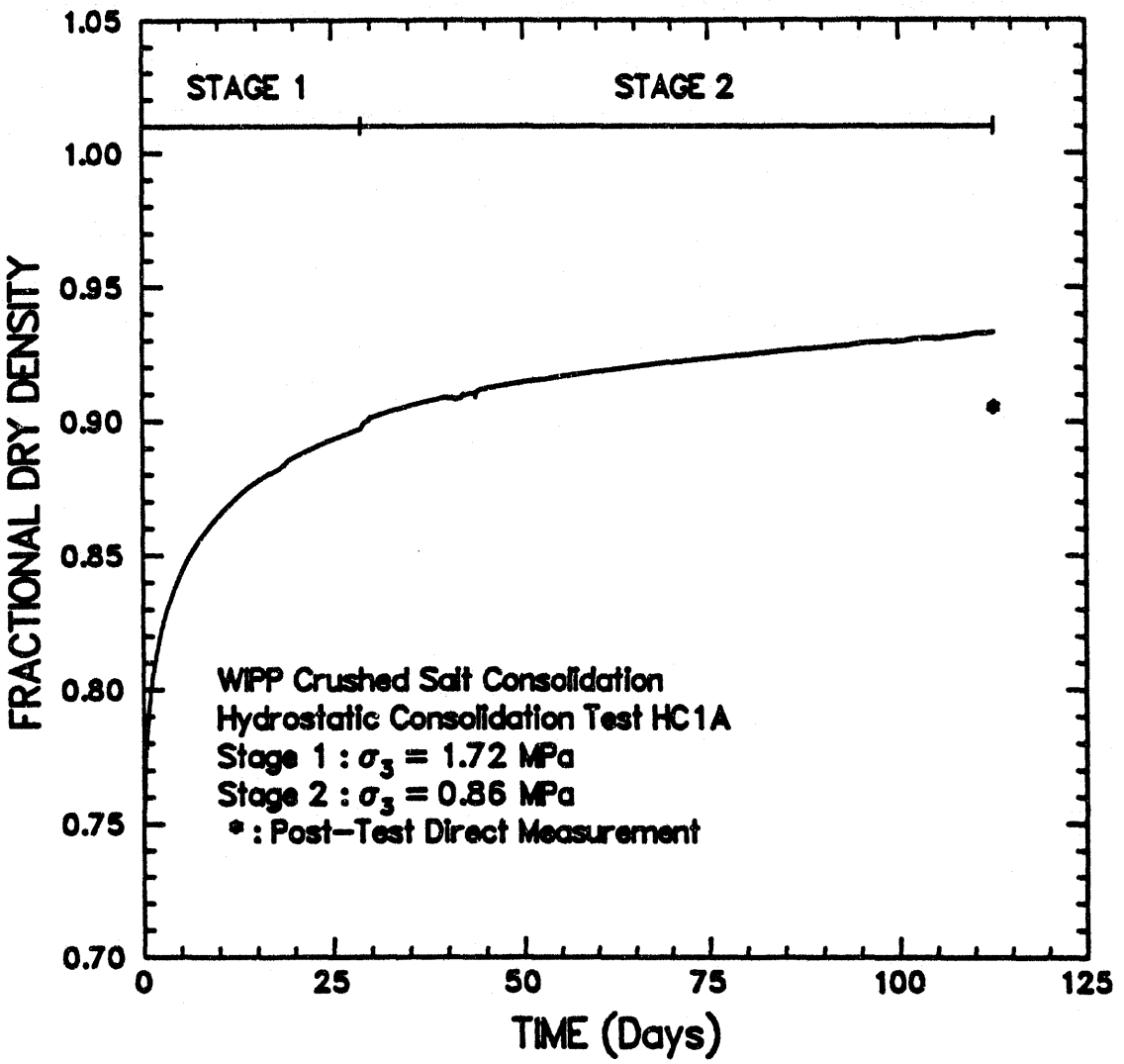

Figure D-1. Fractional density-versus-time for Test HC1A.

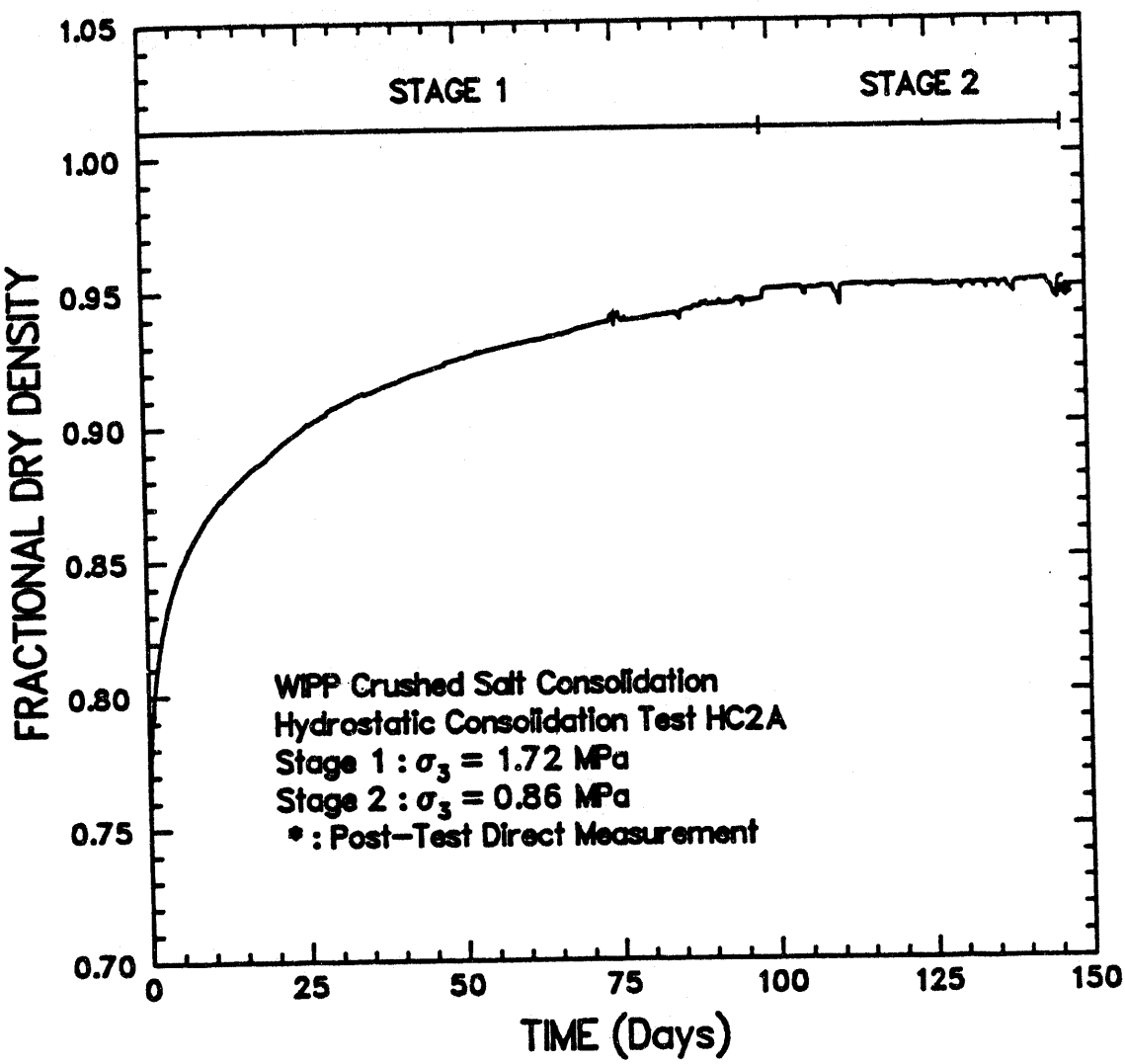

Figure D-2. Fractional density-versus-time for Test HC2A.

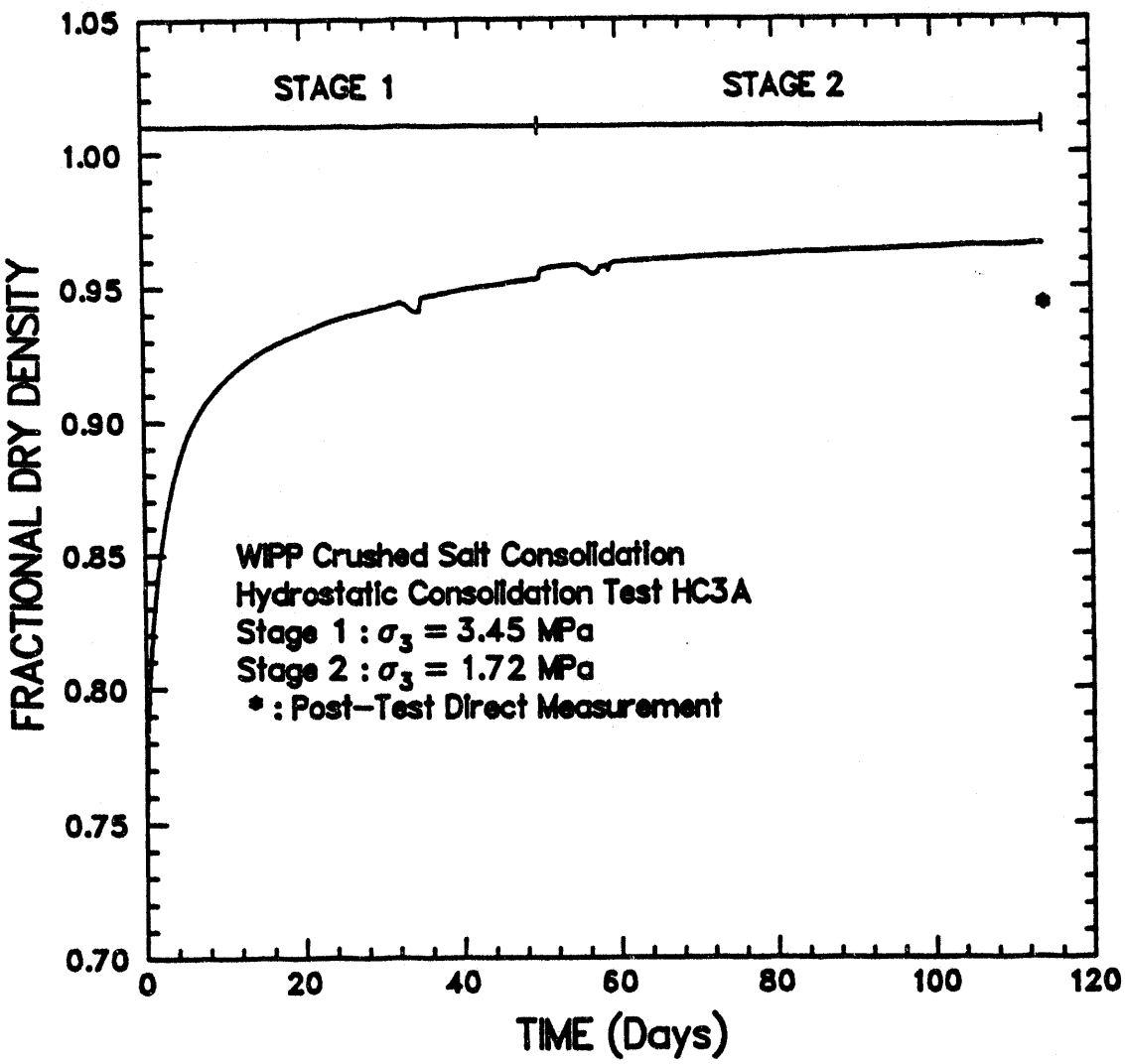

Figure D-3. Fractional density-versus-time for Test HC3A.

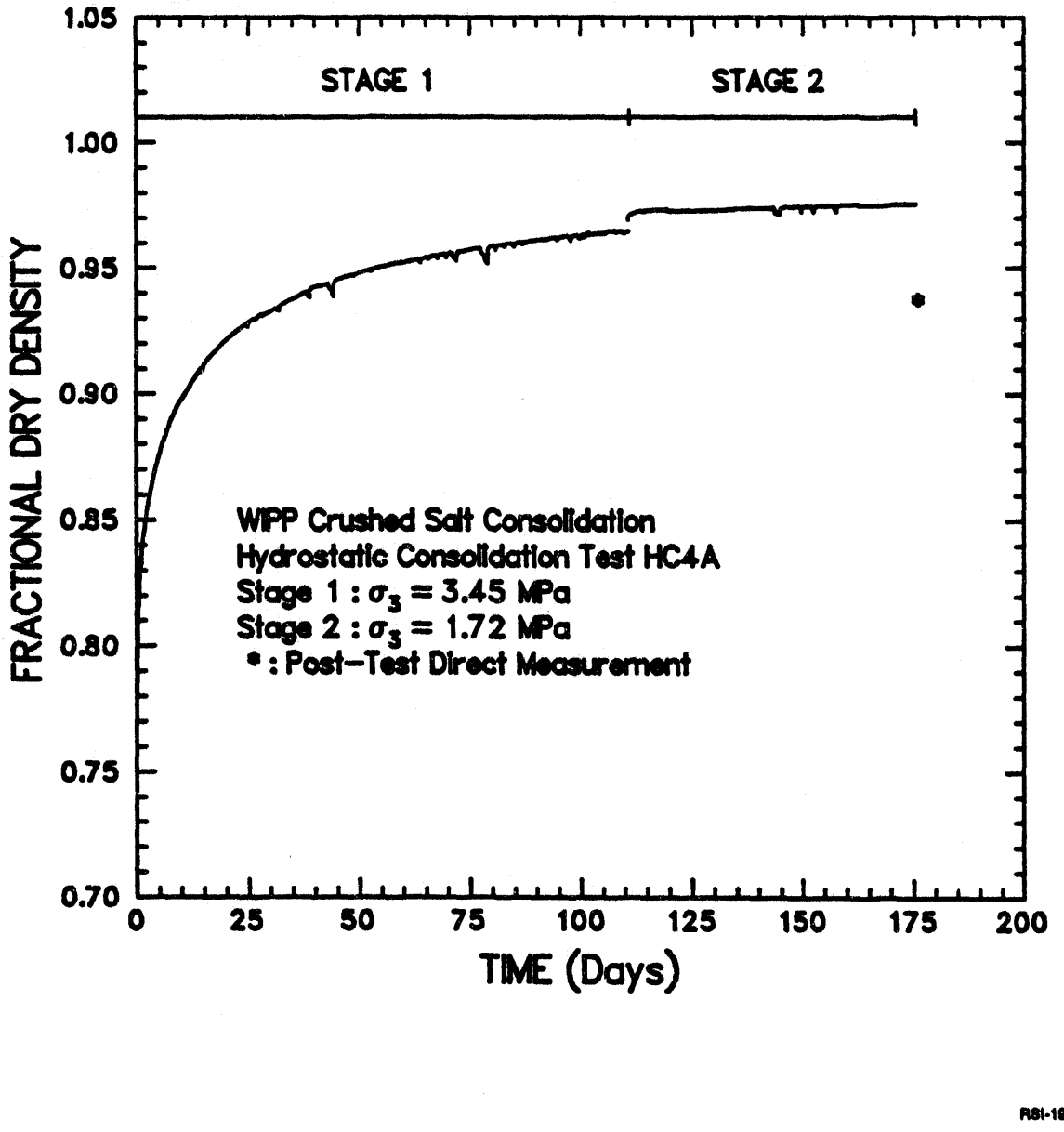

Figure D-4. Fractional density-versus-time for Test HC4A.

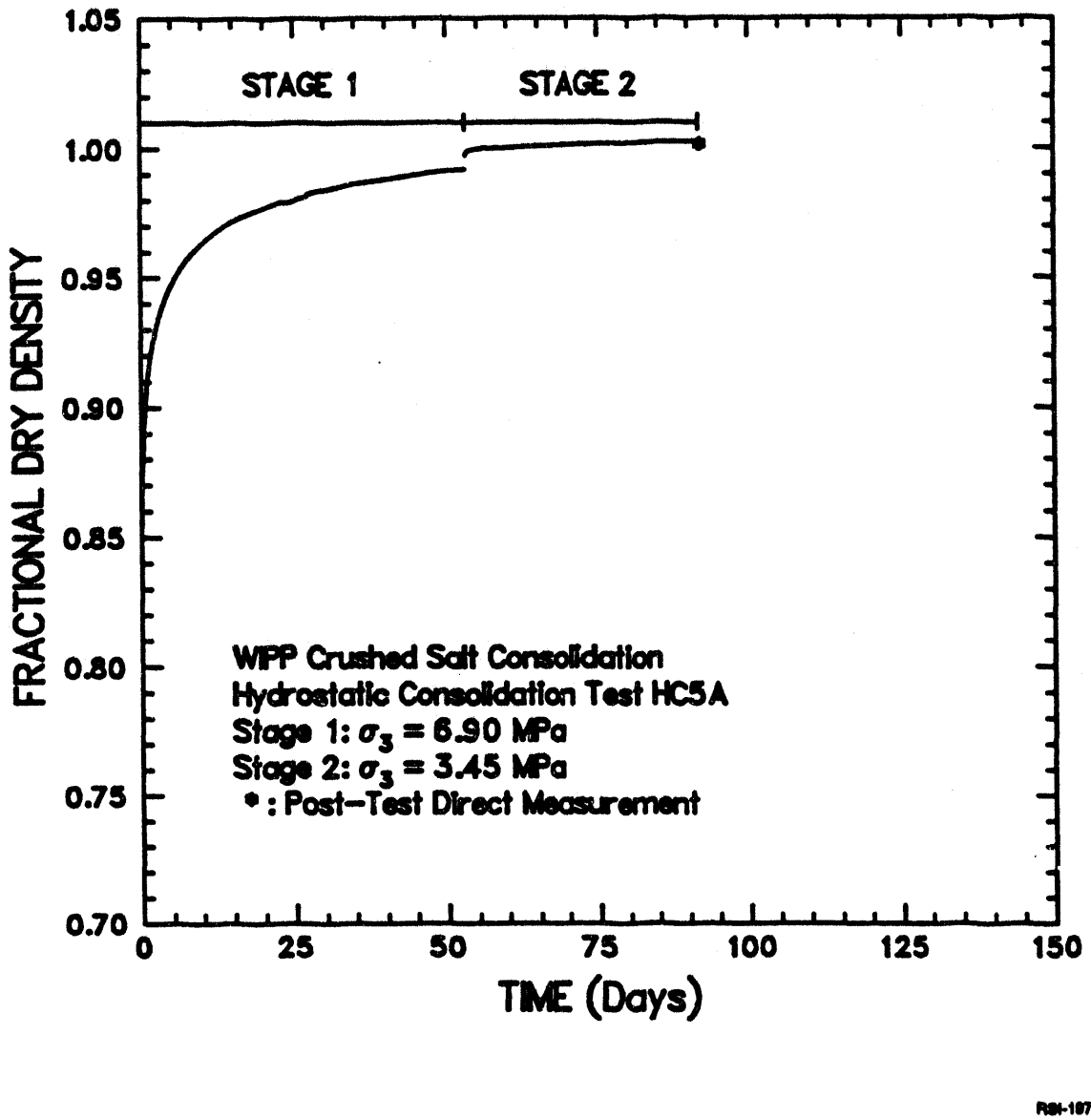

Figure D-5. Fractional density-versus-time for Test HC5A.

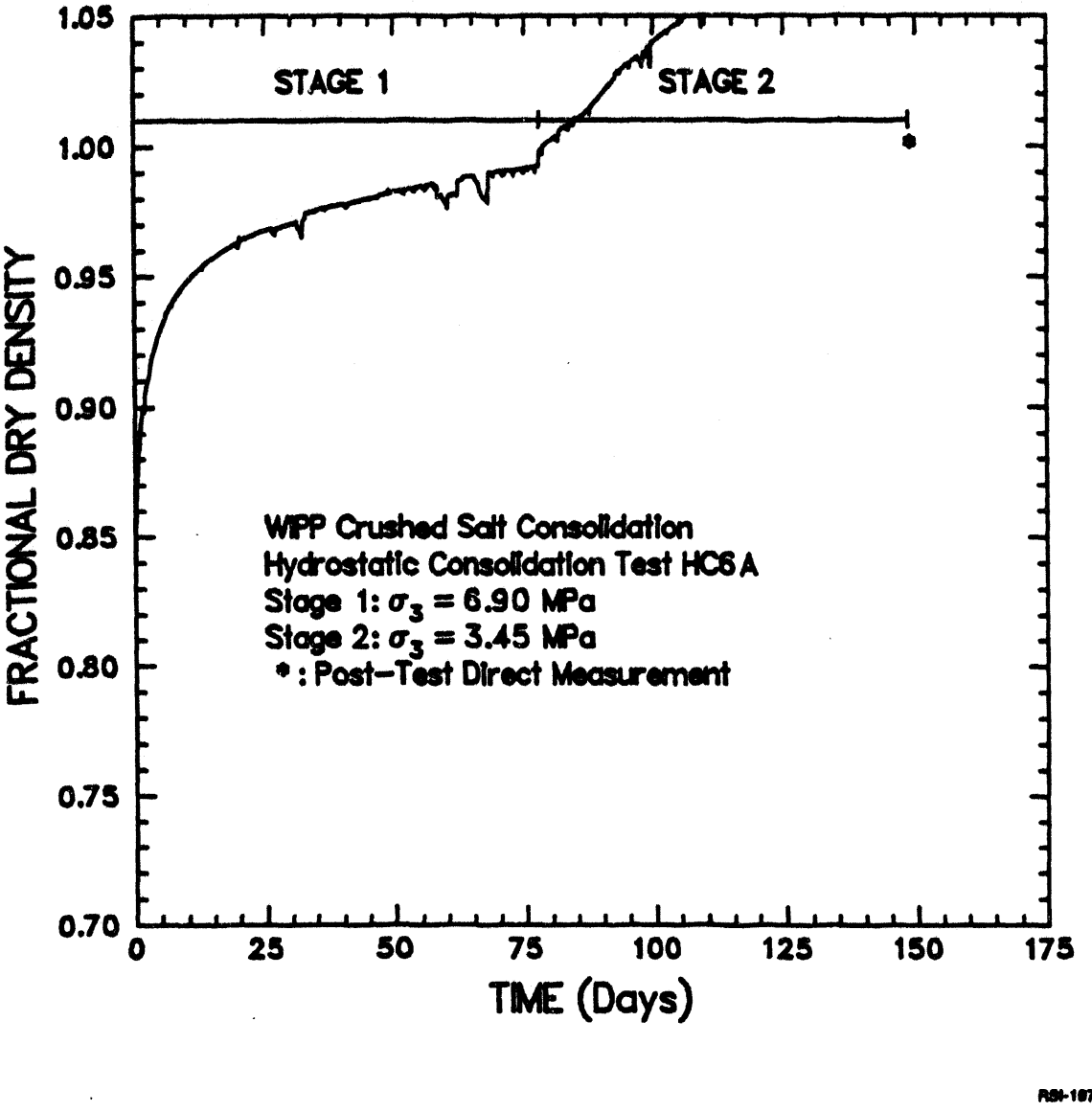

Figure D-6. Fractional density-versus-time for Test HC6A.

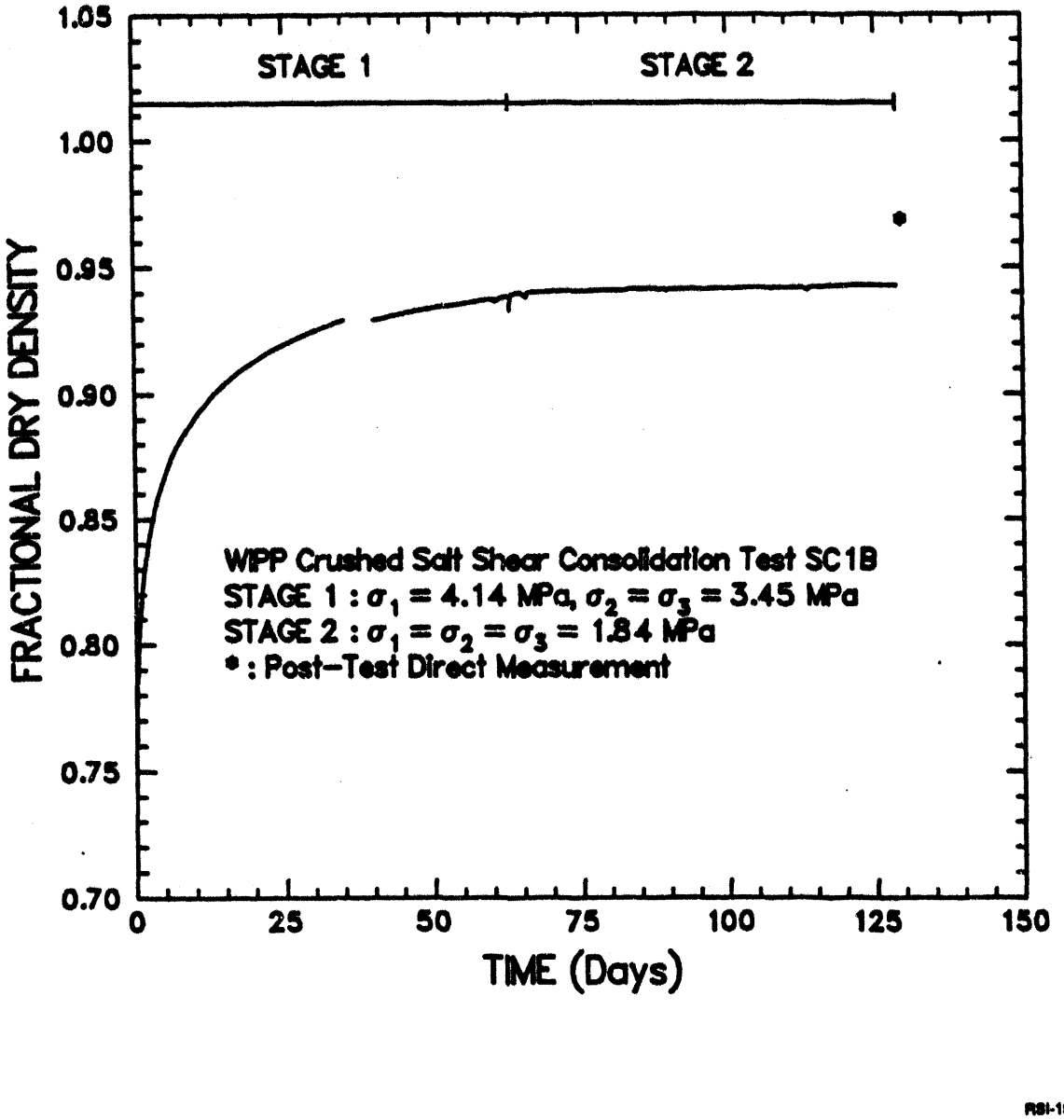

Figure D-7. Fractional density-versus-time for Test SC1B.

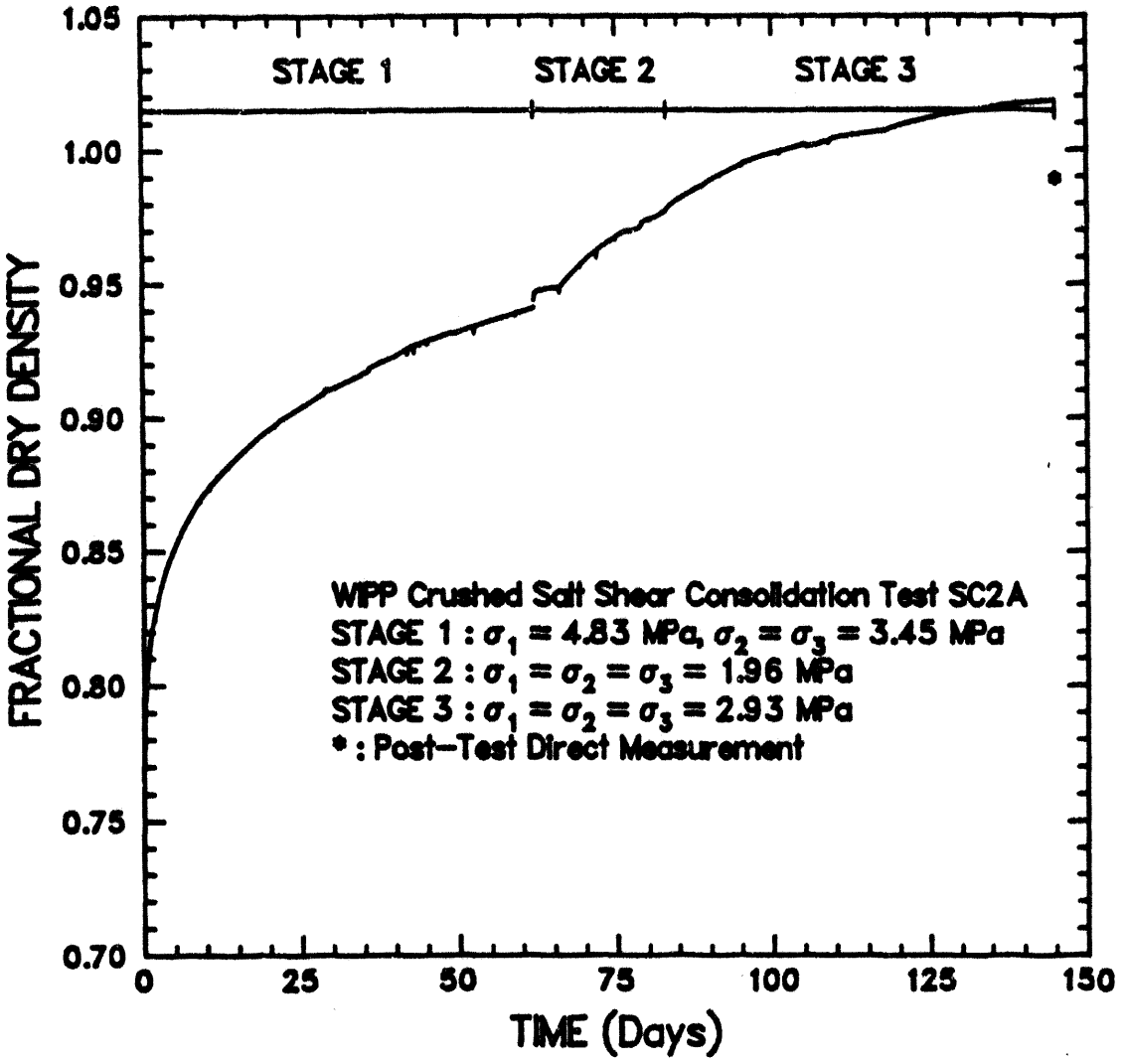

RSI-197-92-142

Figure D-8. Fractional density-versus-time for Test SC2A.

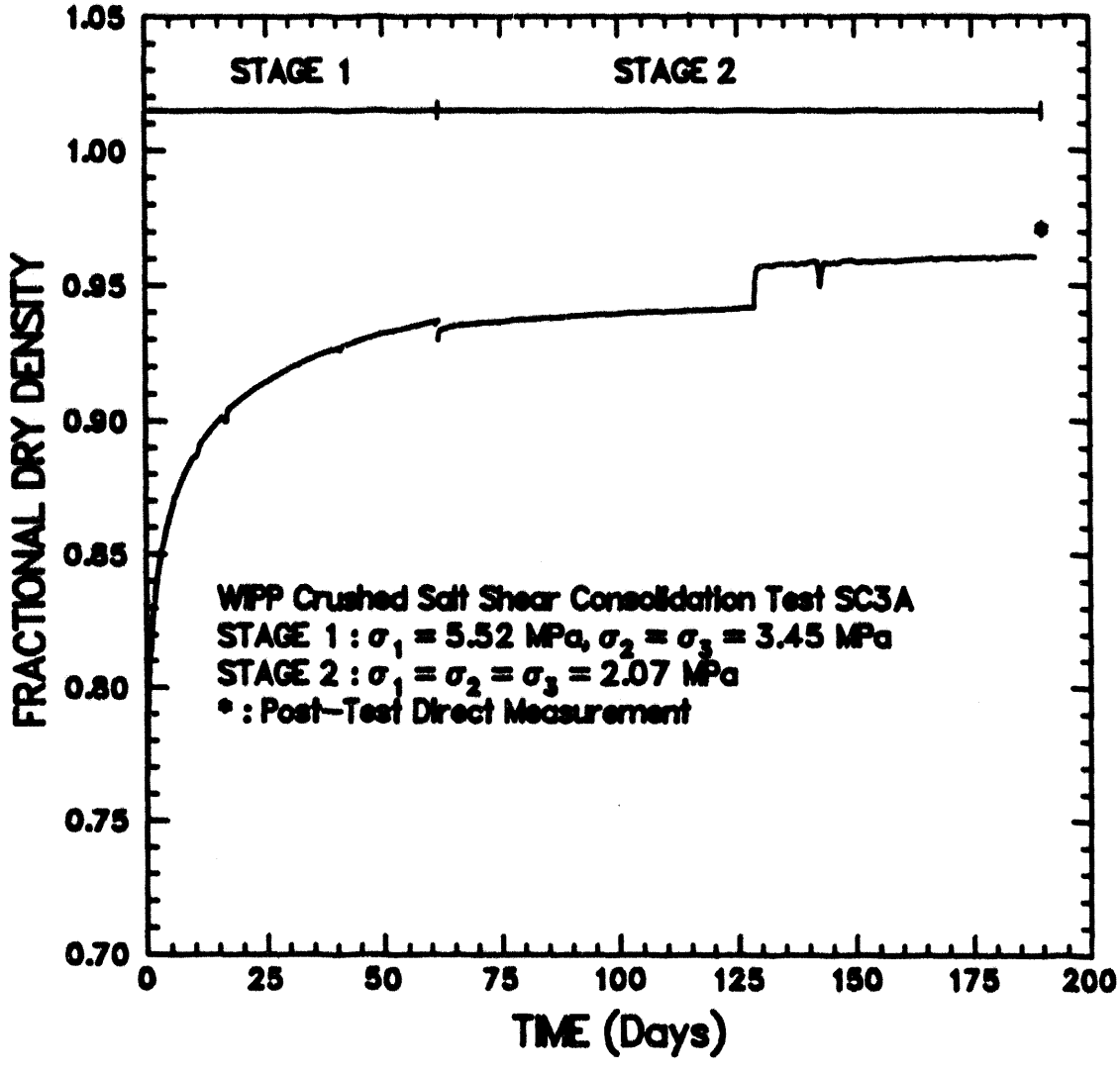

Figure D-9. Fractional density-versus-time for Test SC3A. The increase in fractional density at 126 days is due to turning off the pressure vessel heaters.

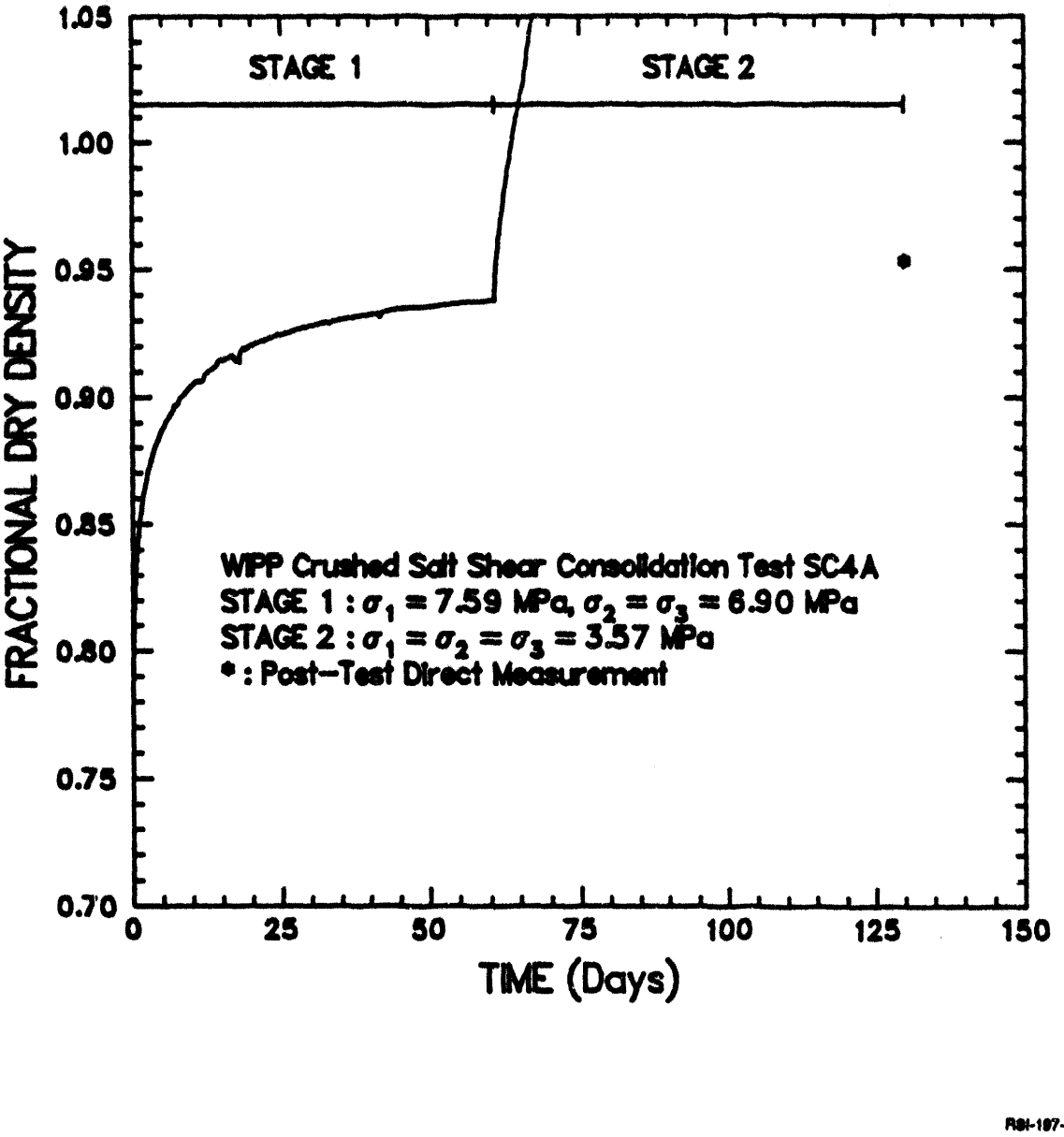

Figure D-10. Fractional density-versus-time for Test SC4A.

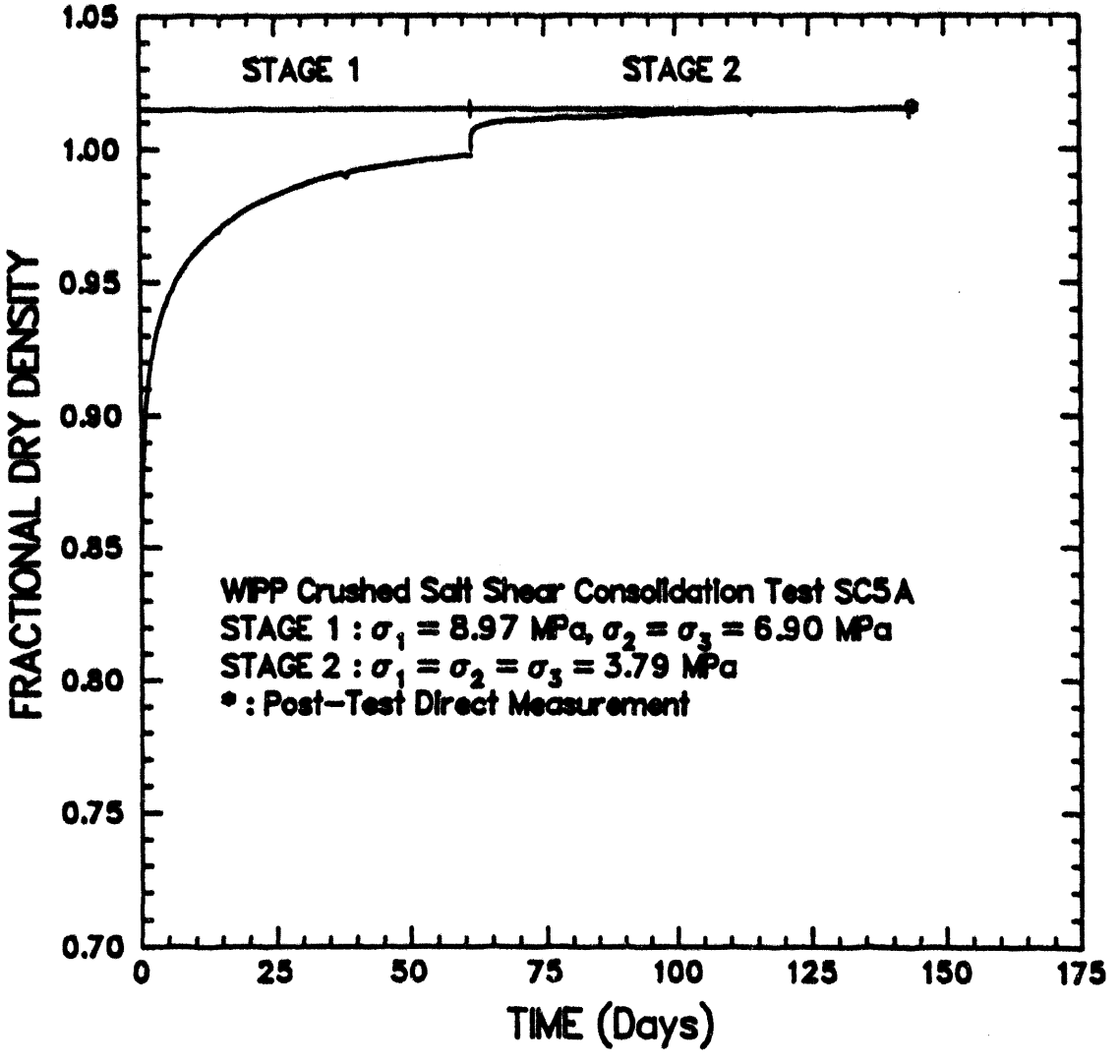

Figure D-11. Fractional density-versus-time for Test SC5A.

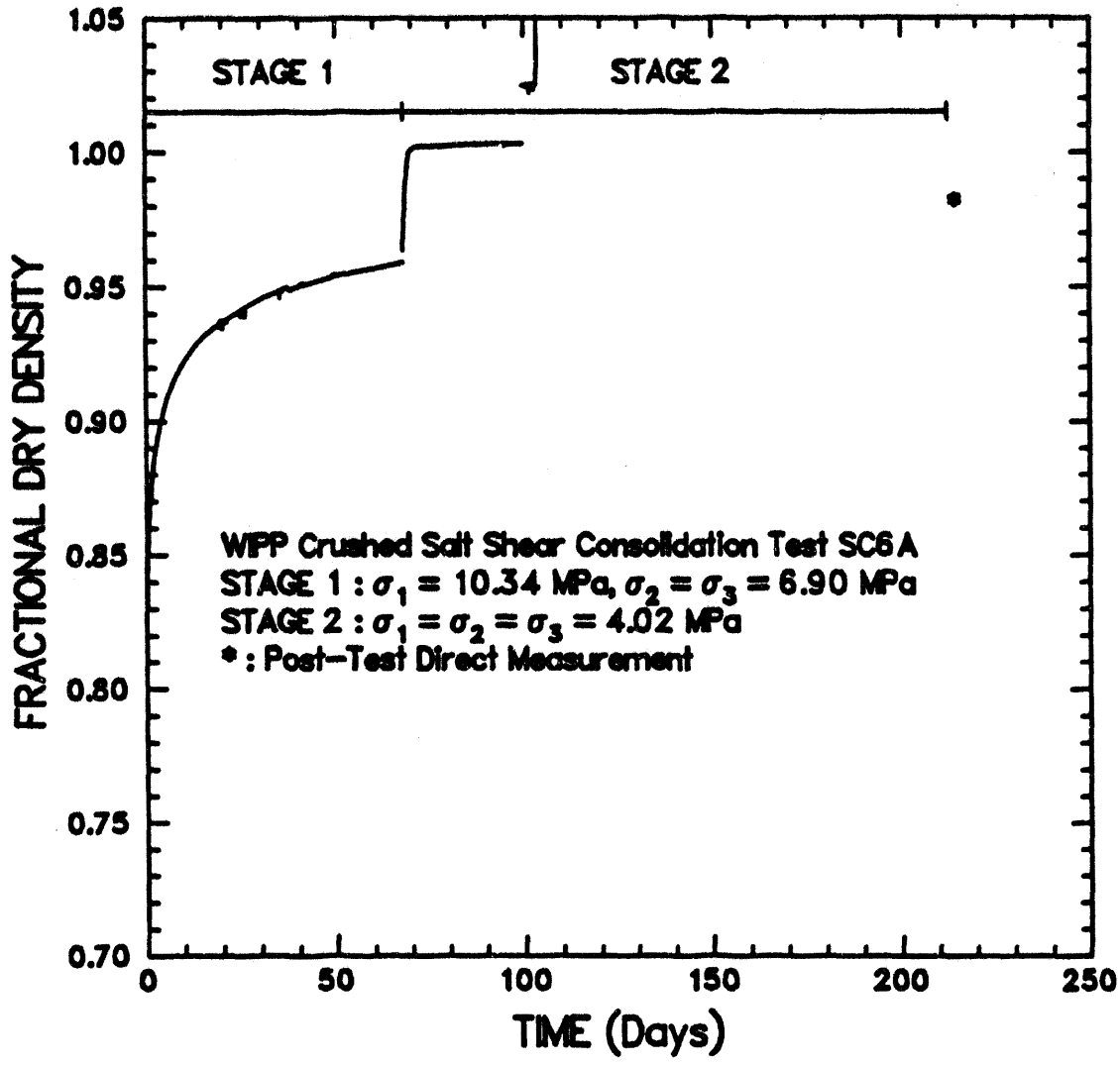

RSI-197-93-146

Figure D-12. Fractional density-versus-time for Test SC6A.

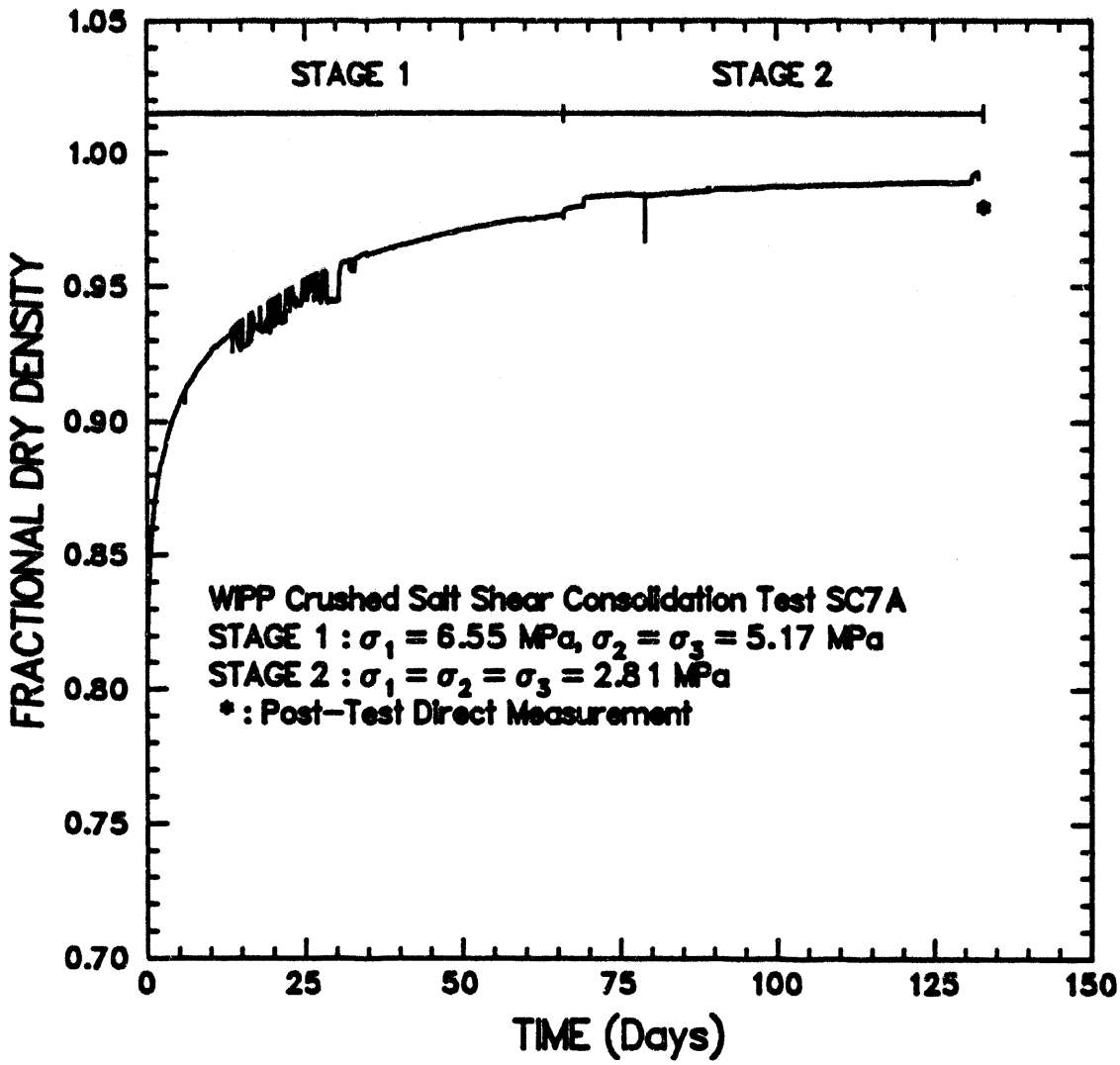

Figure D-13. Fractional density-versus-time for Test SC7A.

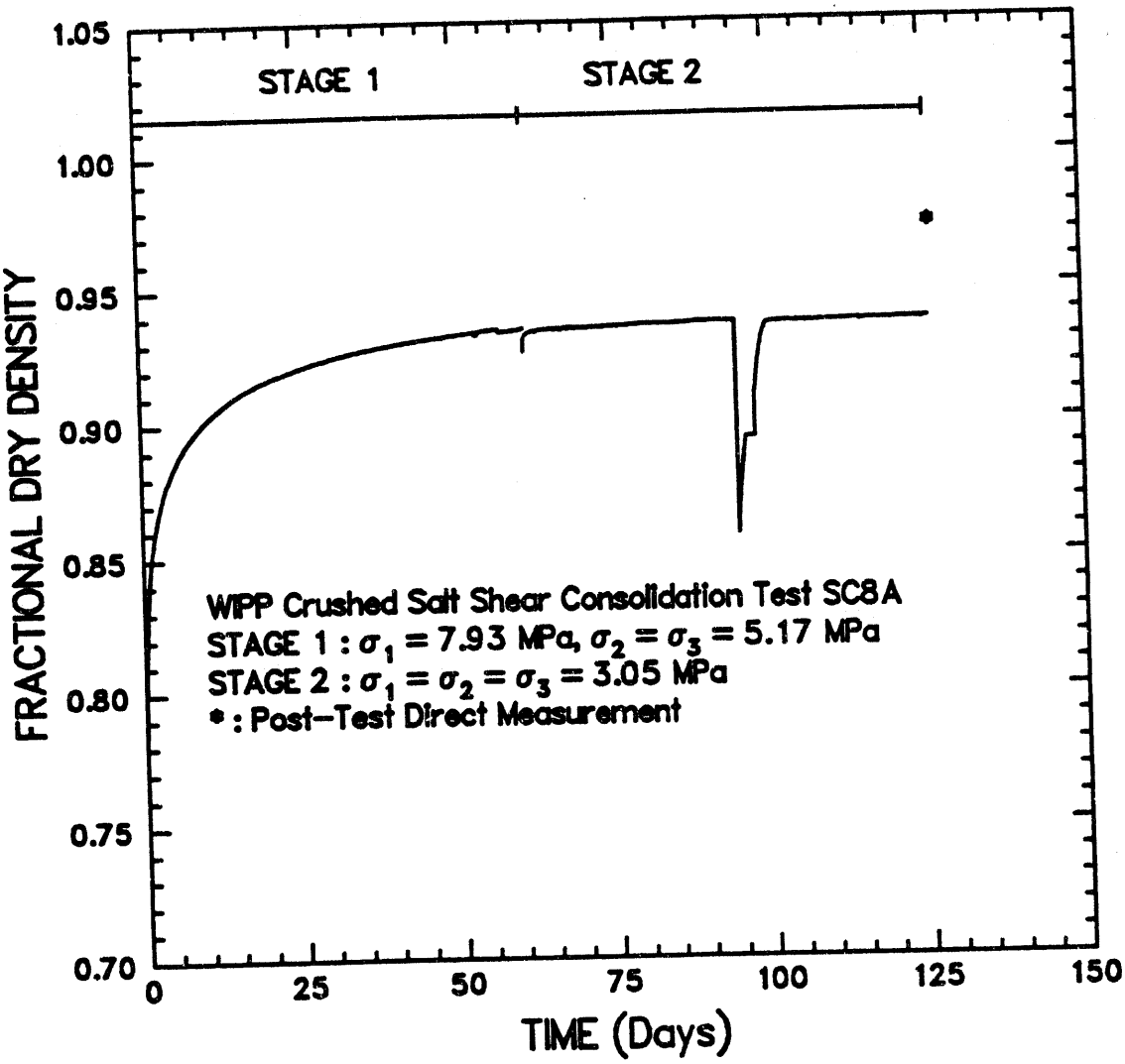

Figure D-14. Fractional density-versus-time for Test SC8A.

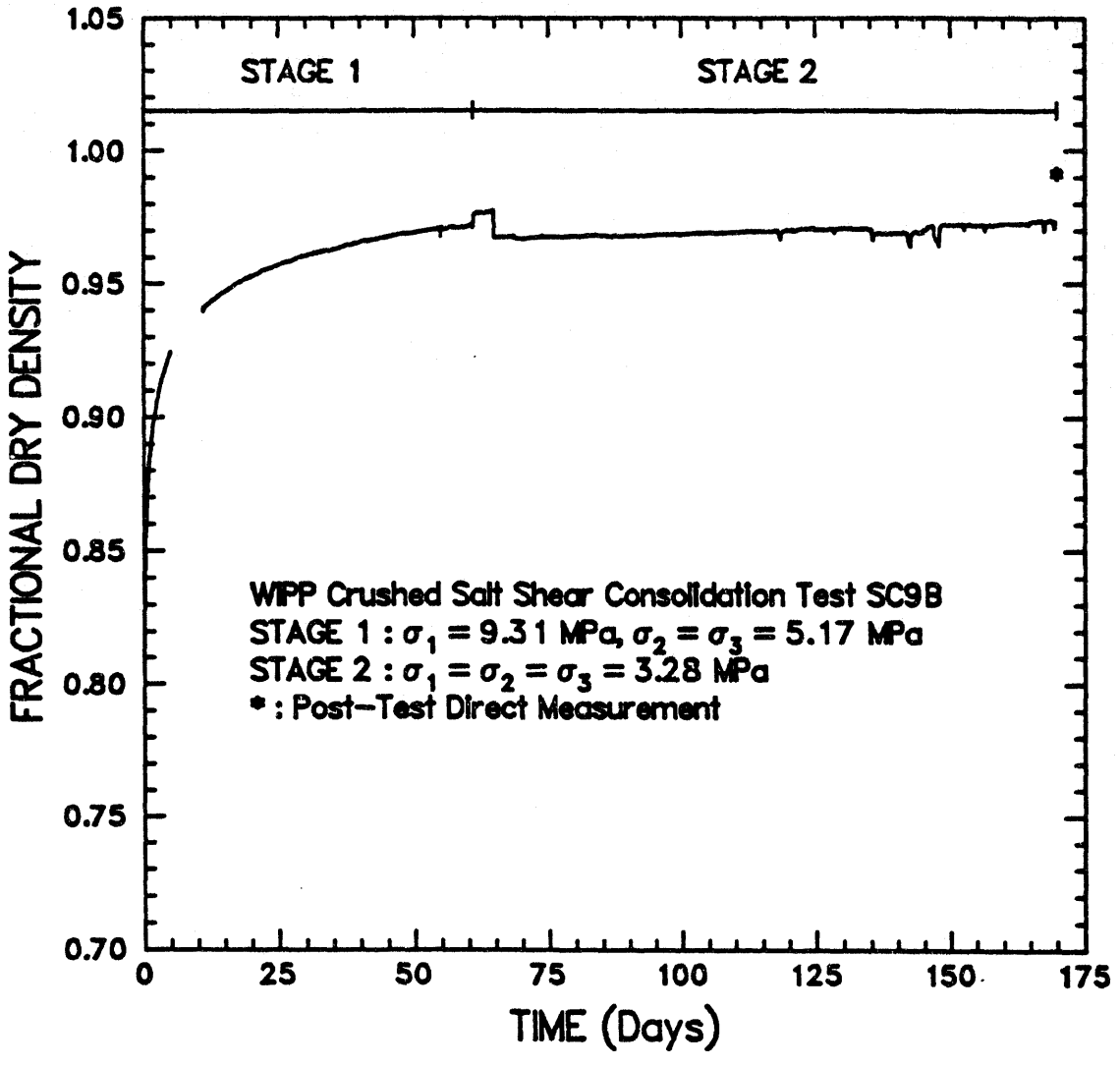

Figure D-15. Fractional density-versus-time for Test SC9B.

APPENDIX E. ACTUAL AND FITTED VOLUMETRIC STRAIN DATA FOR STAGE 1 OF HYDROSTATIC CONSOLIDATION TESTS

Figures

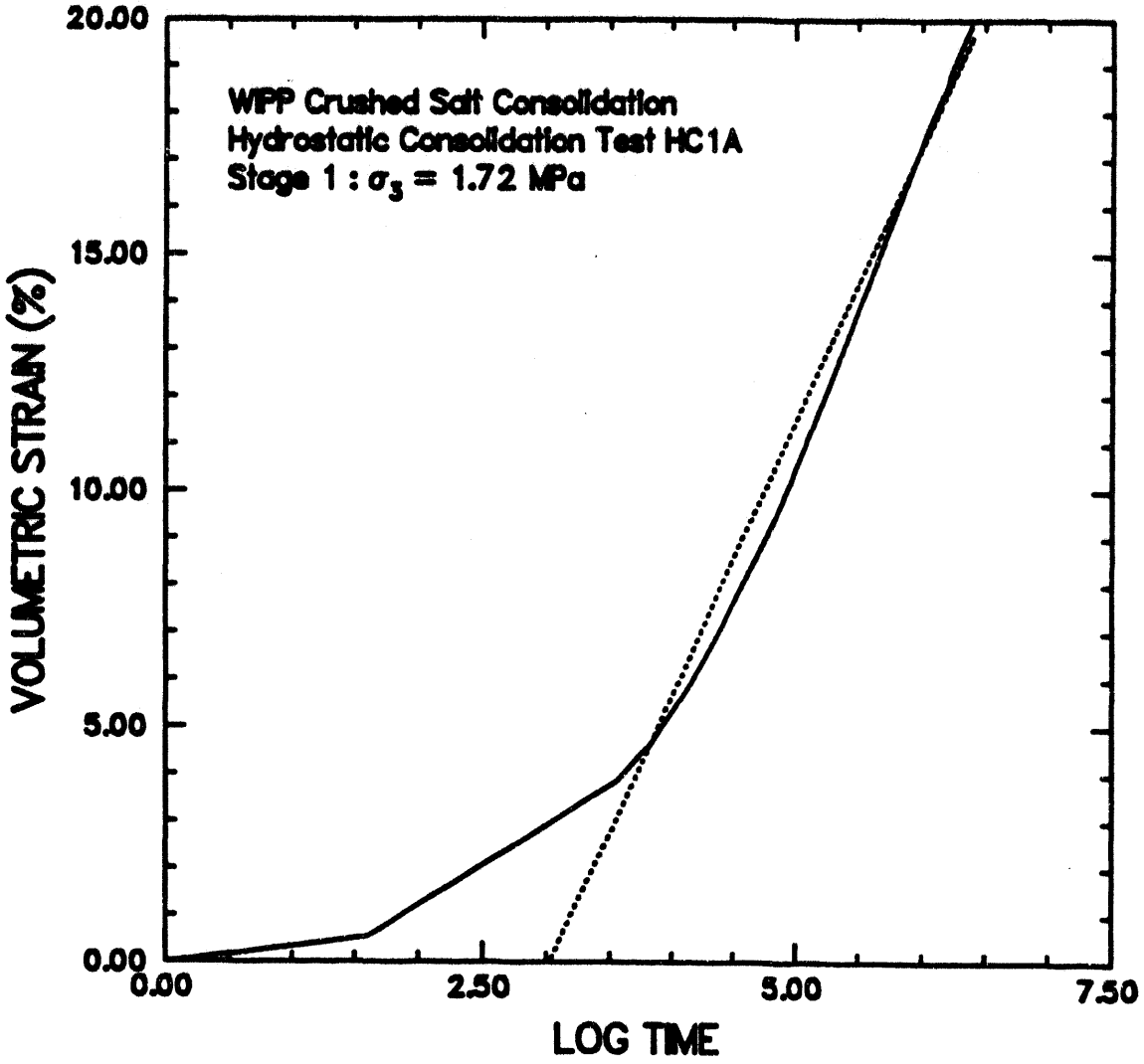

Figure E-1. Volumetric strain-versus-logarithm of time for Test HC1A. Solid lines are actual data and dotted lines show fits to data.

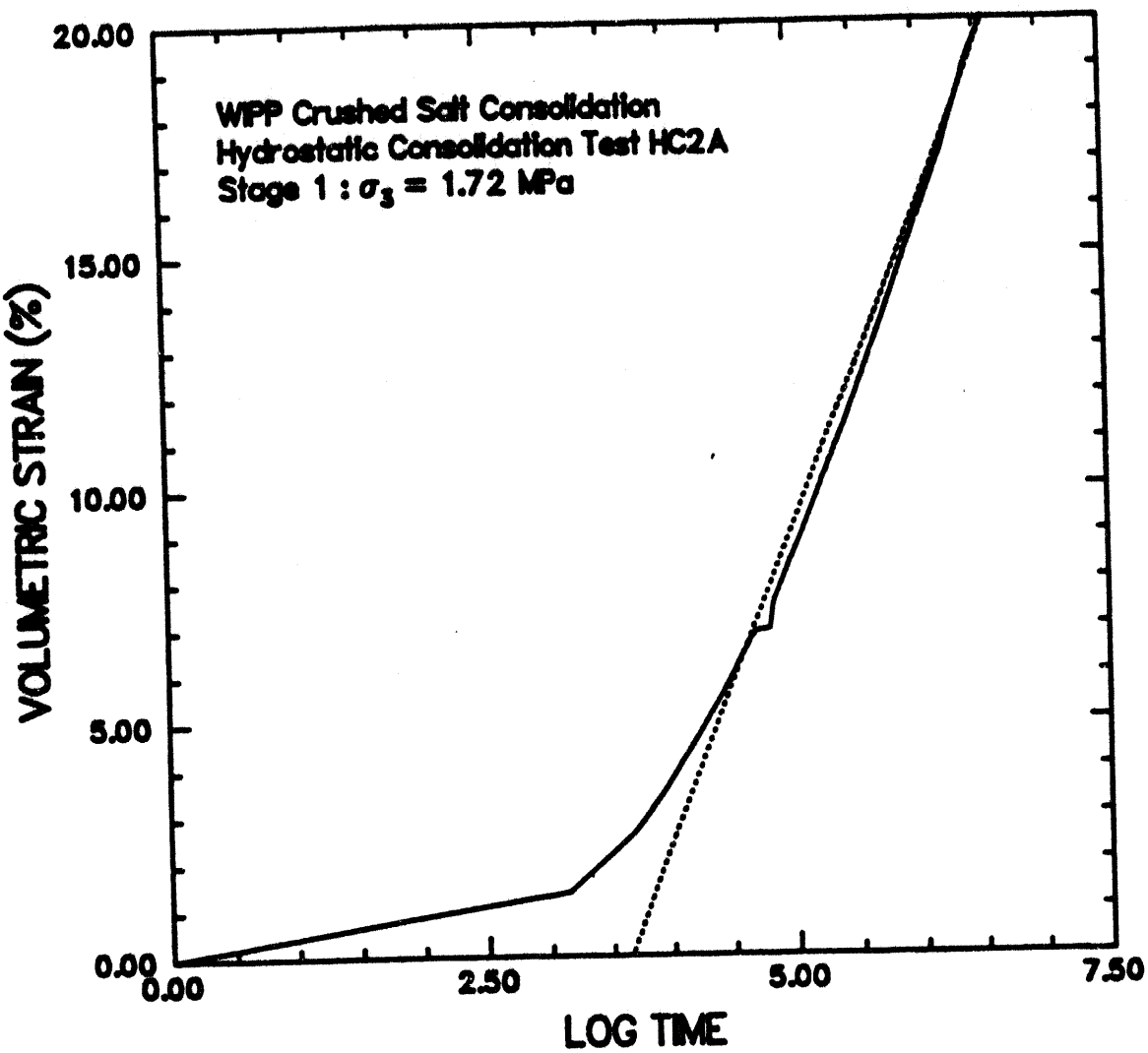

Figure E-2. Volumetric strain-versus-logarithm of time for Test HC2A. Solid lines are actual data and dotted lines show fits to data.

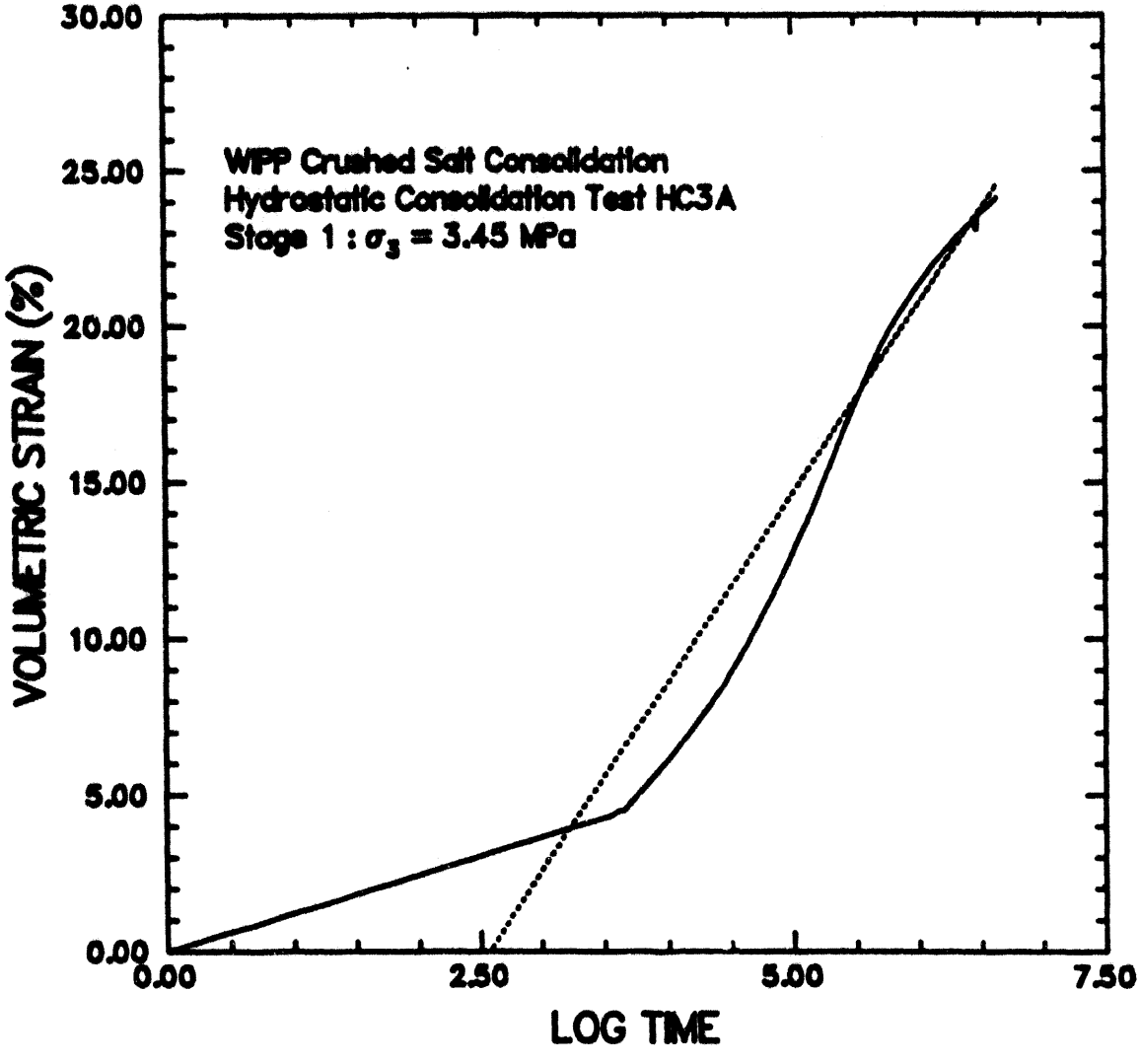

RSI-107-02-152

Figure E-3. Volumetric strain-versus-logarithm of time for Test HC3A. Solid lines are actual data and dotted lines show fits to data.

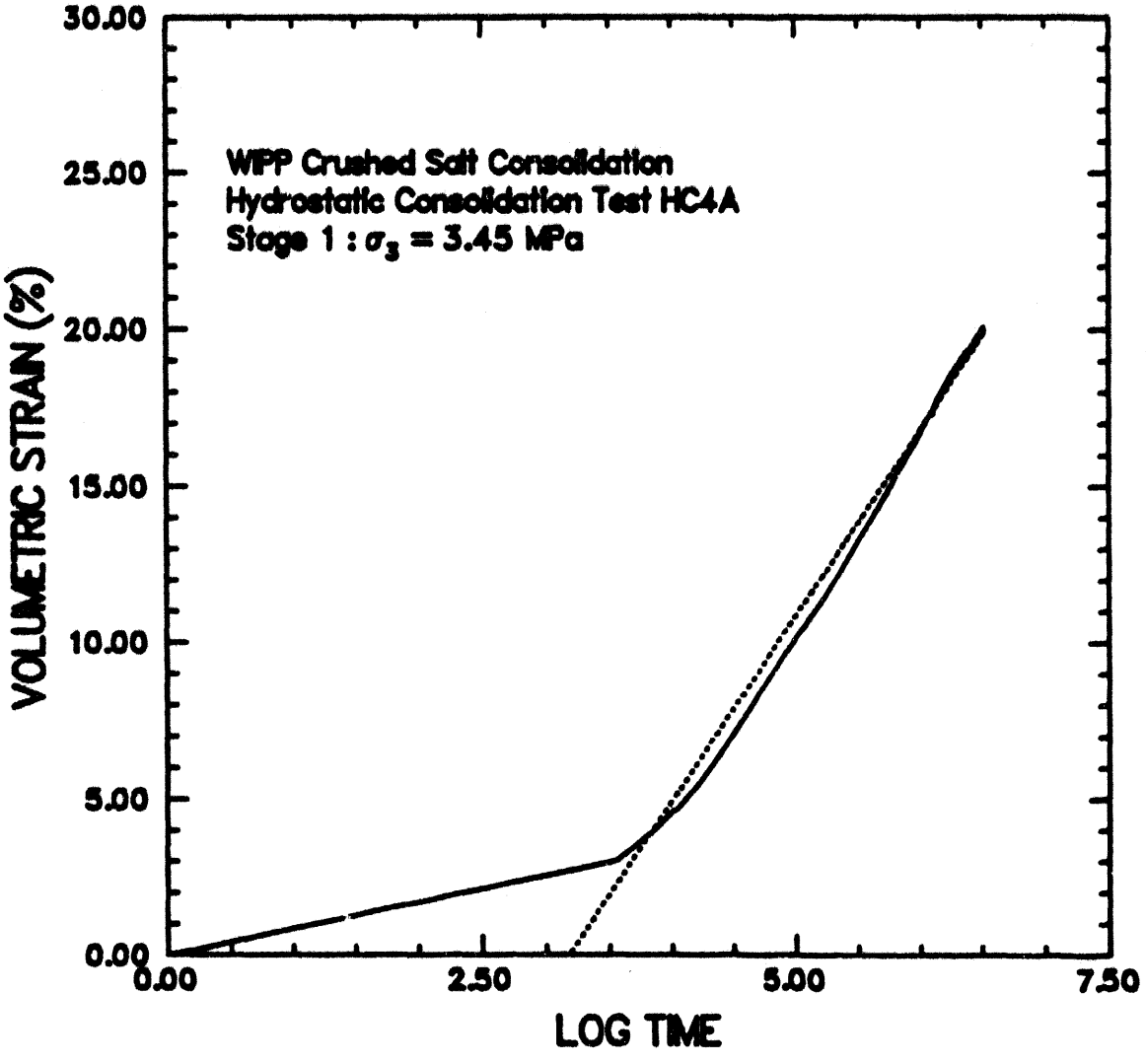

RSN-197-92-153

Figure E-4. Volumetric strain-versus-logarithm of time for Test HC4A. Solid lines are actual data and dotted lines show fits to data.

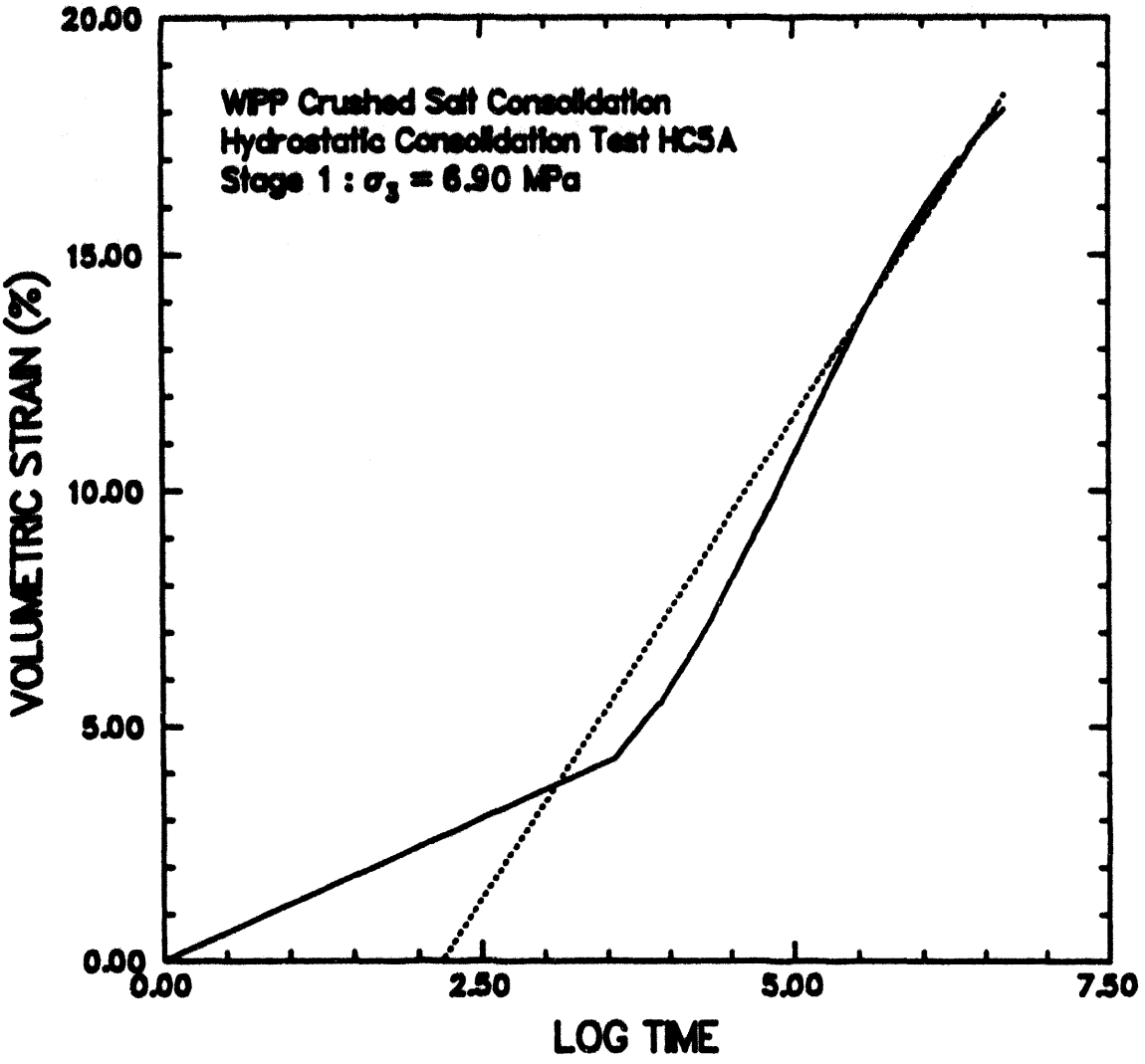

RSI-197-62-154

Figure E-5. Volumetric strain-versus-logarithm of time for Test HC5A. Solid lines are actual data and dotted lines show fits to data.

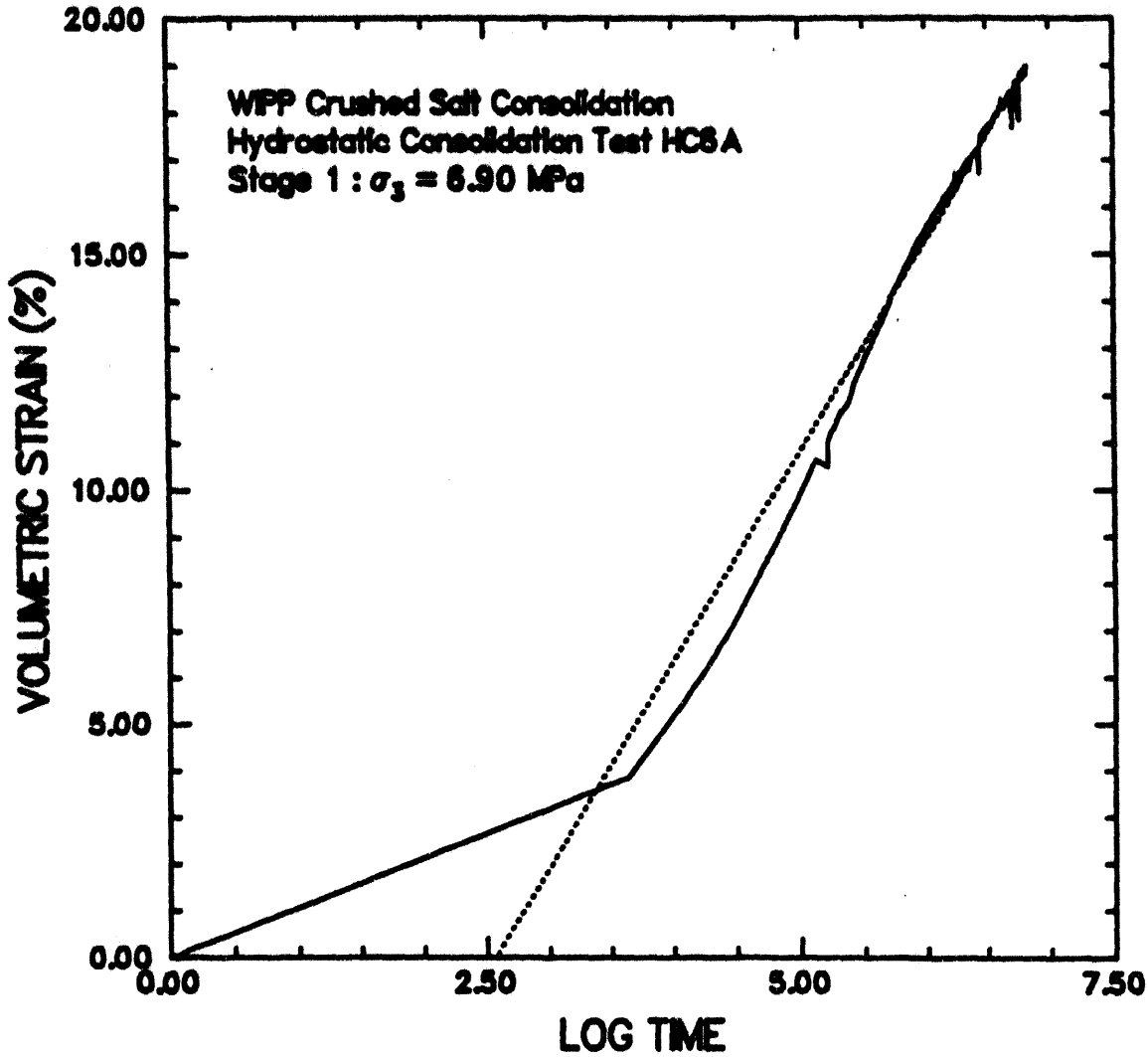

Figure E-6. Volumetric strain-versus-logarithm of time for Test HC6A. Solid lines are actual data and dotted lines show fits to data.

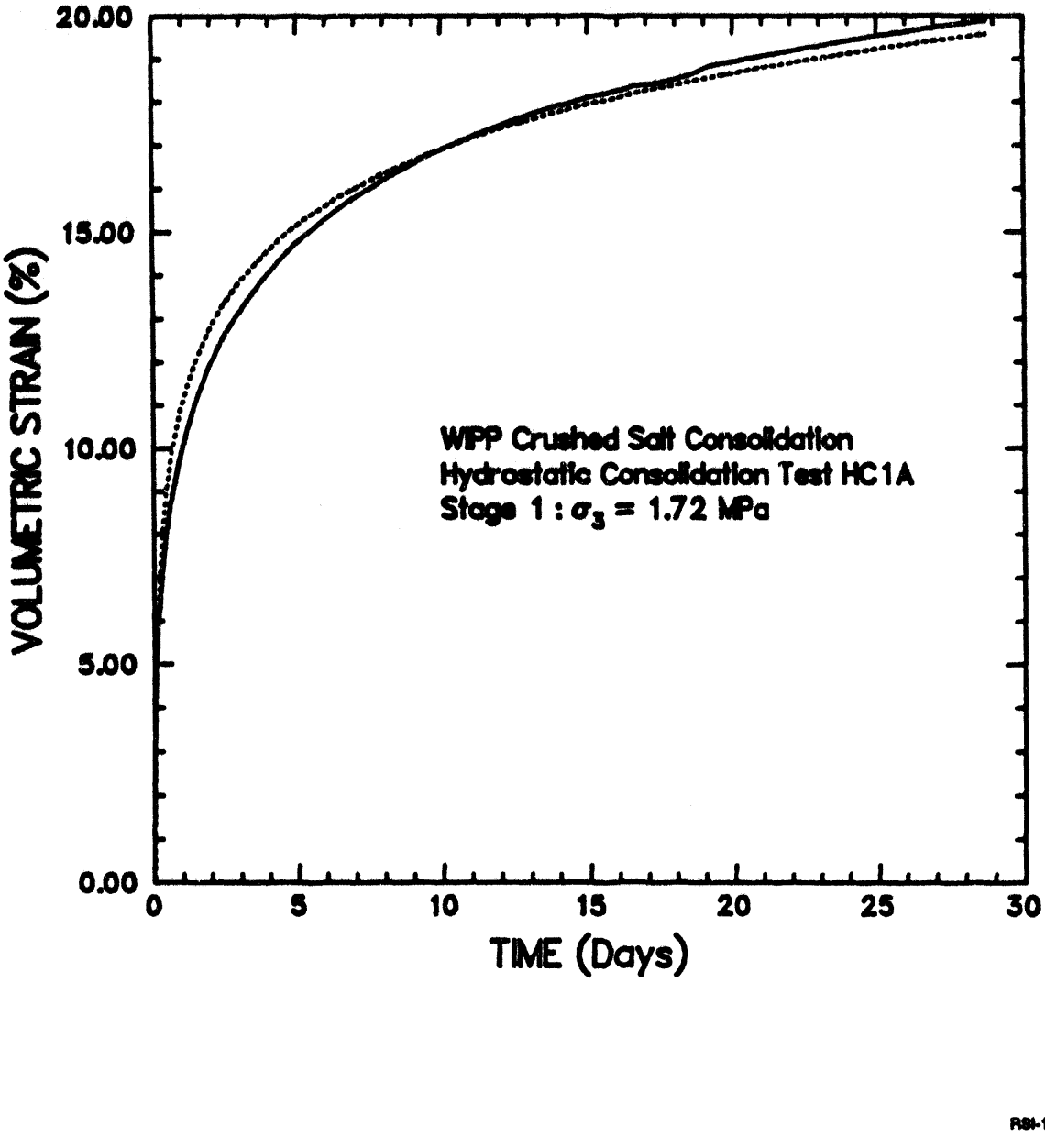

Figure E-7. Volumetric strain-versus-time for Test HC1A. Solid lines are actual data and dotted lines show fits to data.

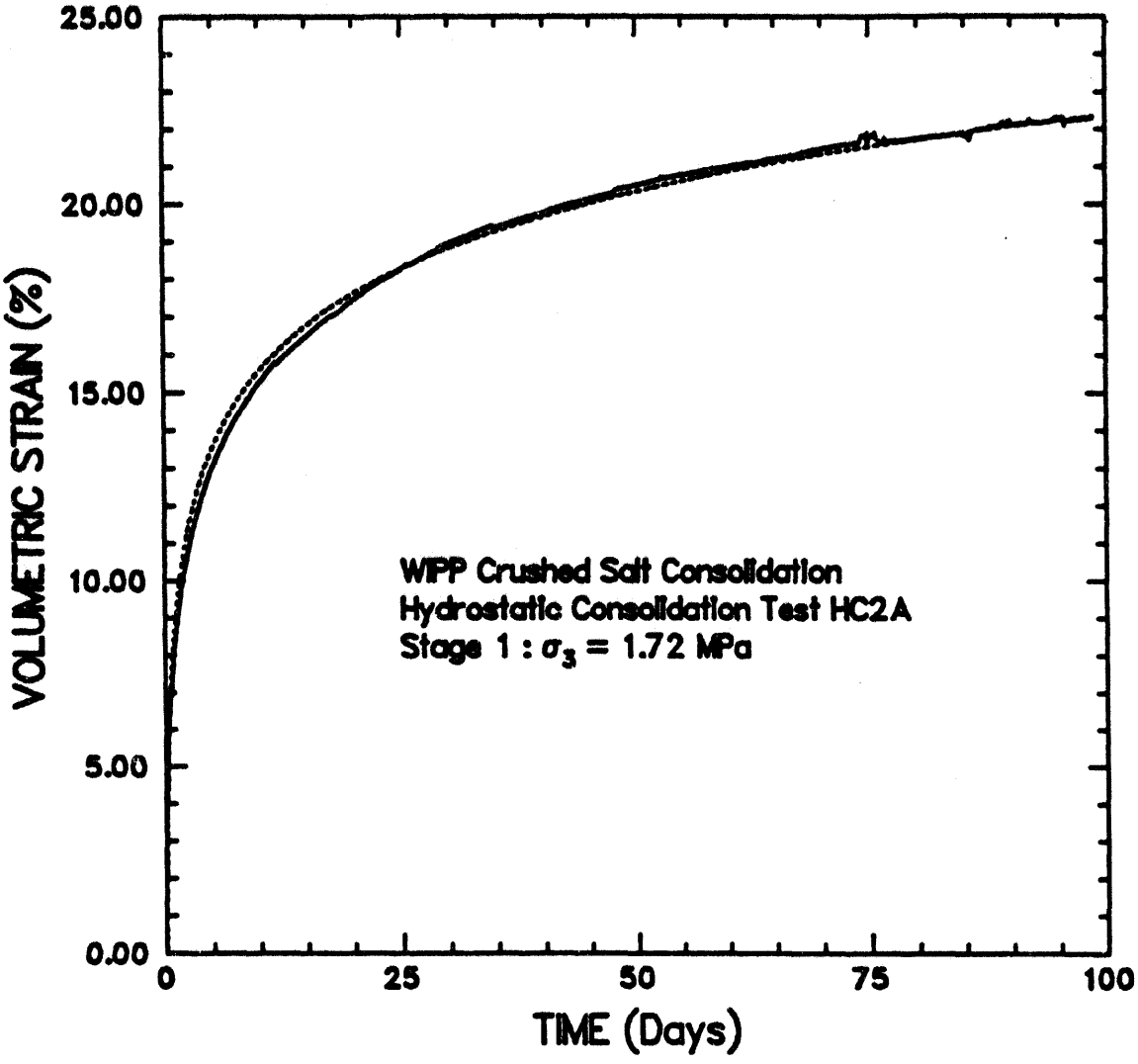

Figure E-8. Volumetric strain-versus-time for Test HC2A. Solid lines are actual data and dotted lines show fits to data.

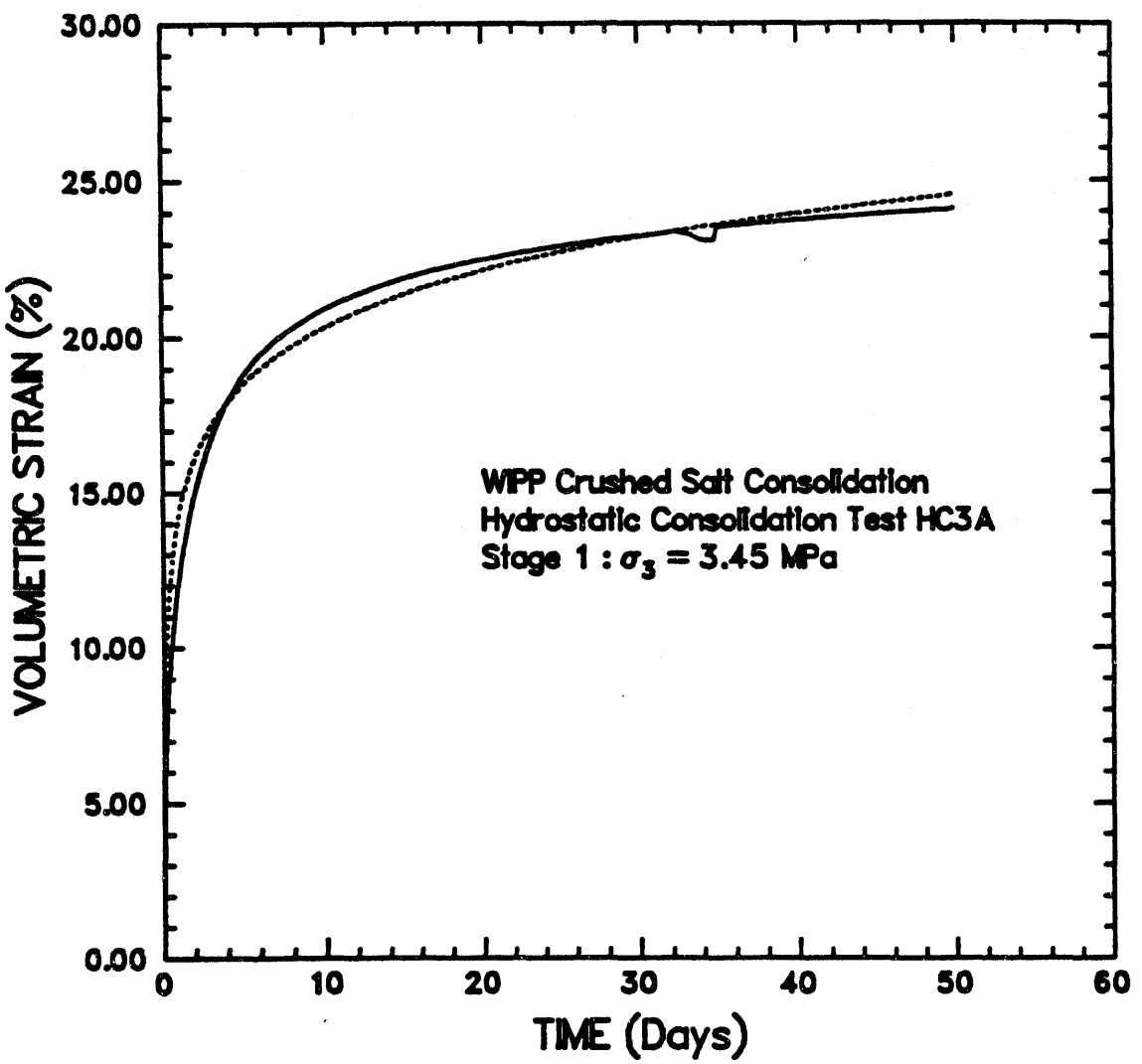

Figure E-9. Volumetric strain-versus-time for Test HC3A. Solid lines are actual data and dotted lines show fits to data.

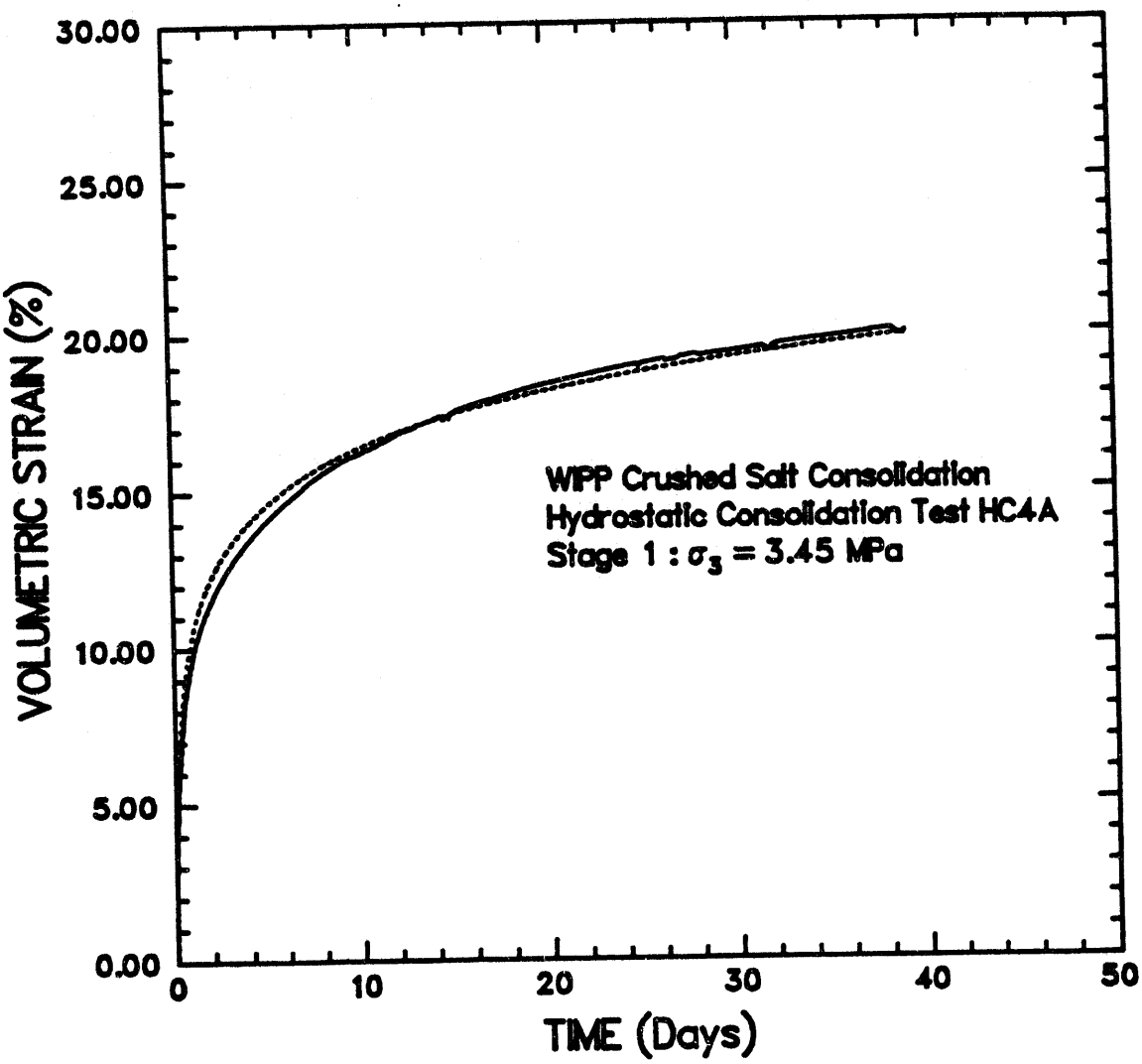

Figure E-10. Volumetric strain-versus-time for Test HC4A. Solid lines are actual data and dotted lines show fits to data.

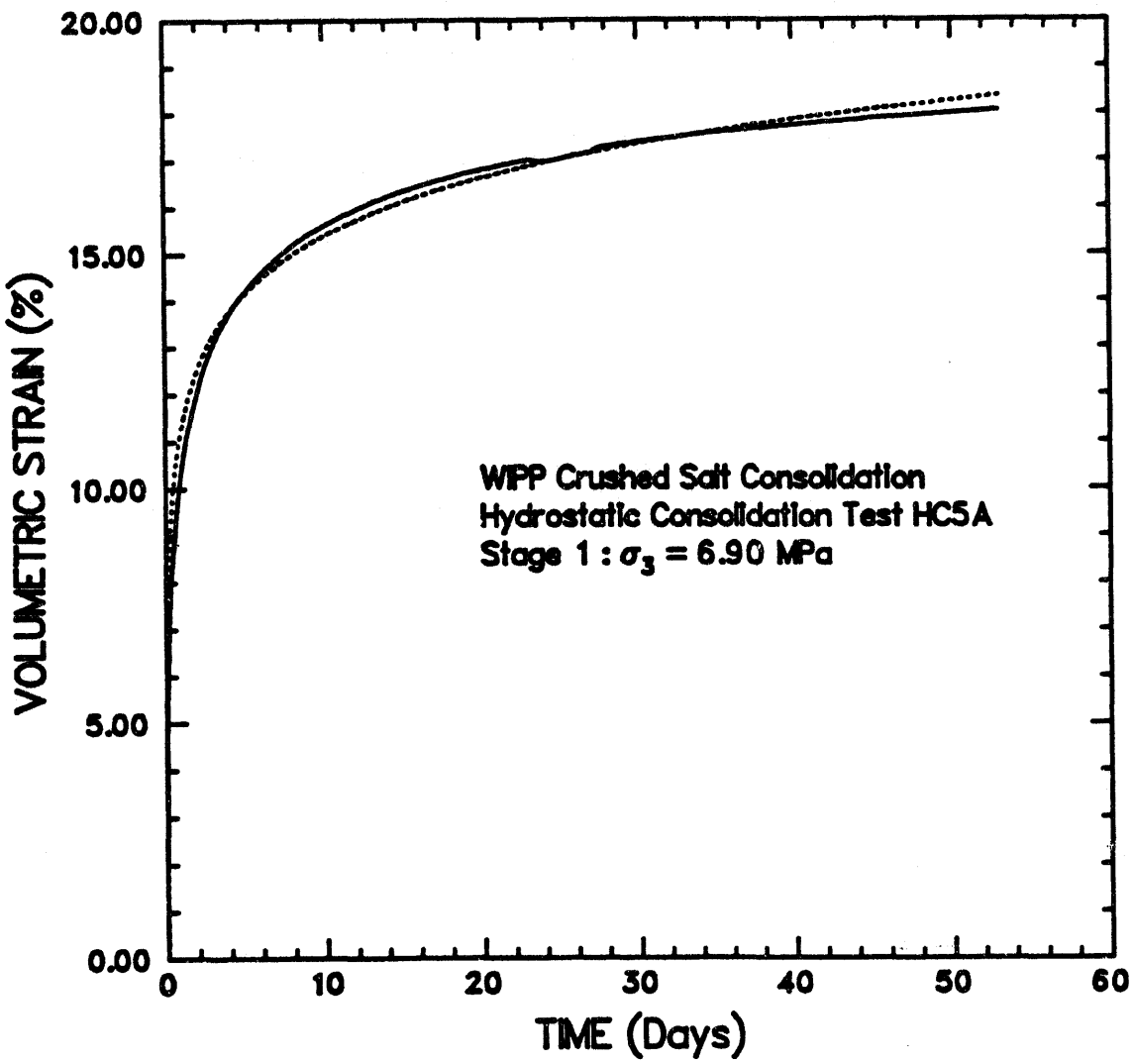

Figure E-11. Volumetric strain-versus-time for Test HC5A. Solid lines are actual data and dotted lines show fits to data.

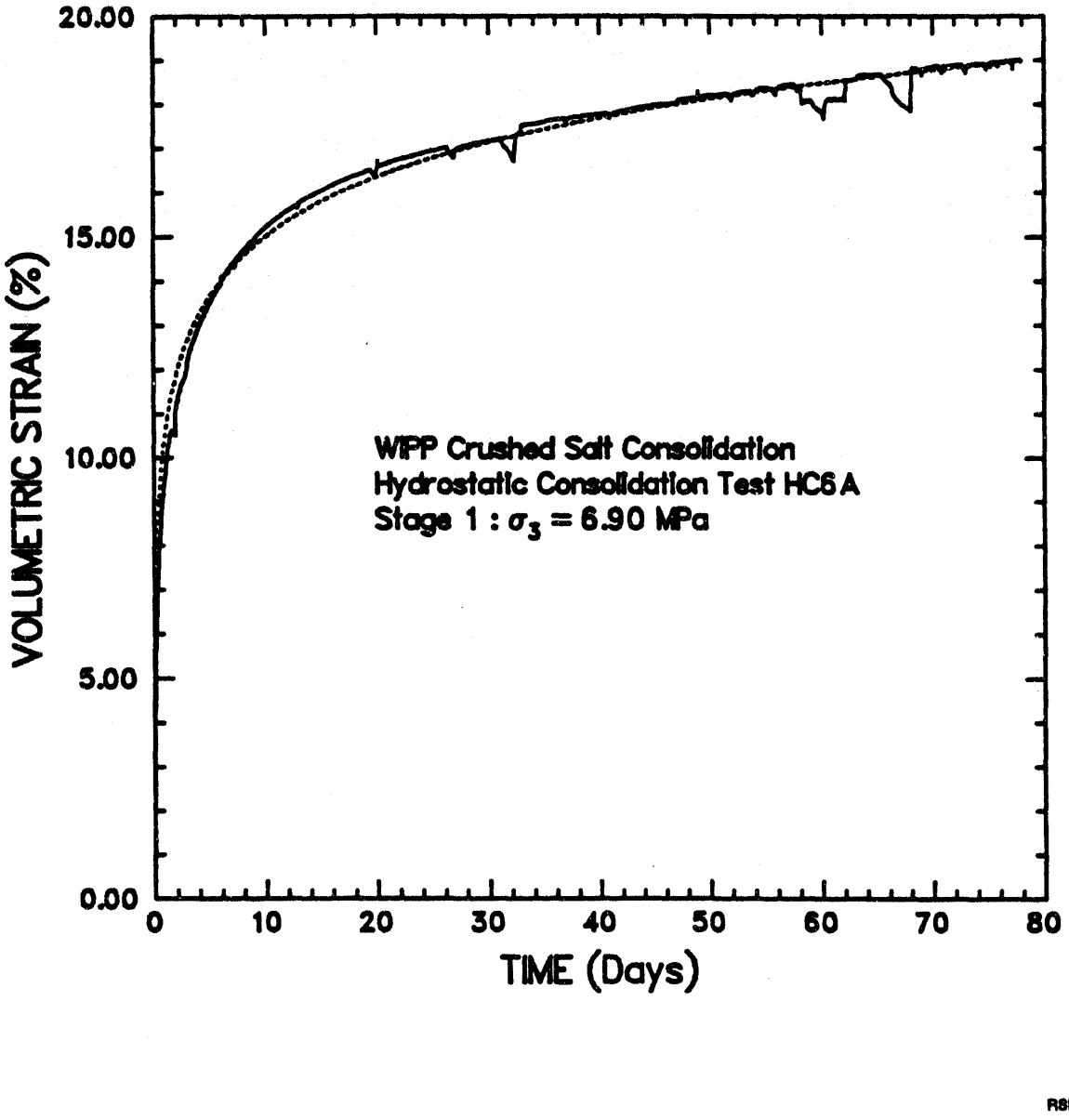

Figure E-12. Volumetric strain-versus-time for Test HC6A. Solid lines are actual data and dotted lines show fits to data.

APPENDIX F. BRINE FLOW DATA OBTAINED DURING PERMEABILITY MEASUREMENTS

Figures

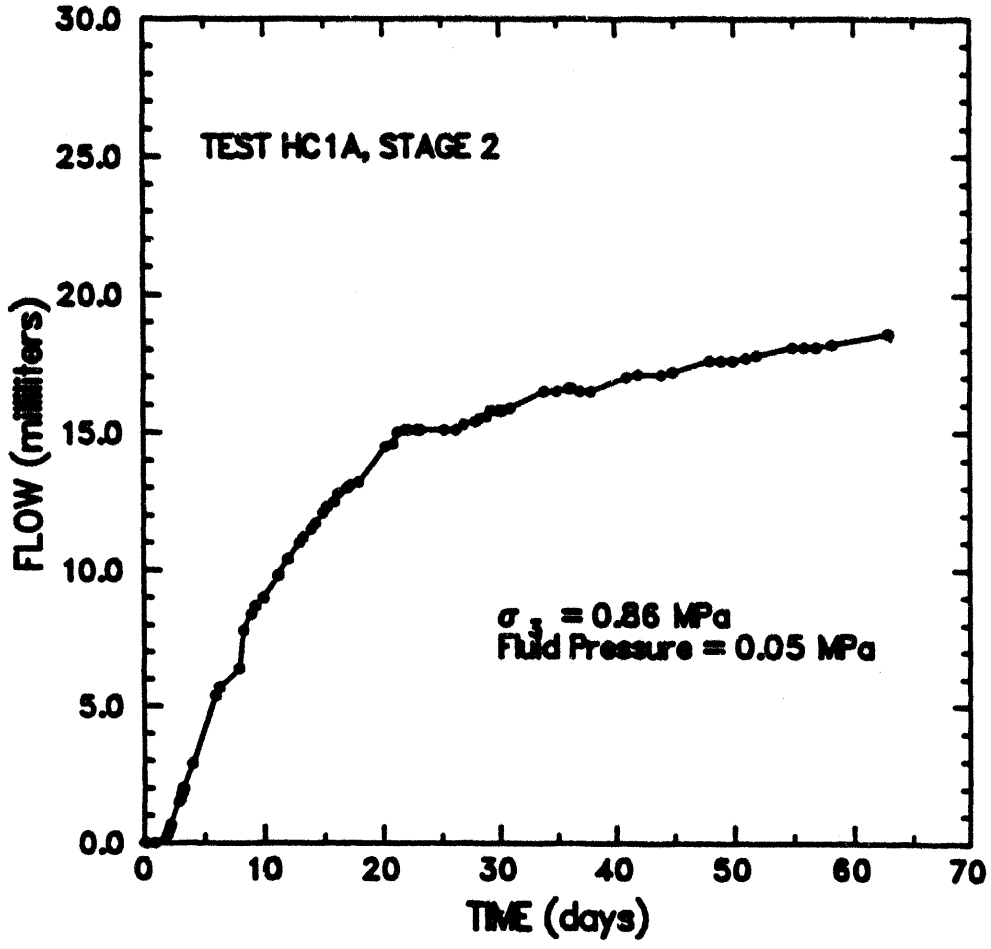

RSI-197-92-162

Figure F-1. Change in brine volume in downstream reservoir as a function of time during permeability stage for Test HC1A.

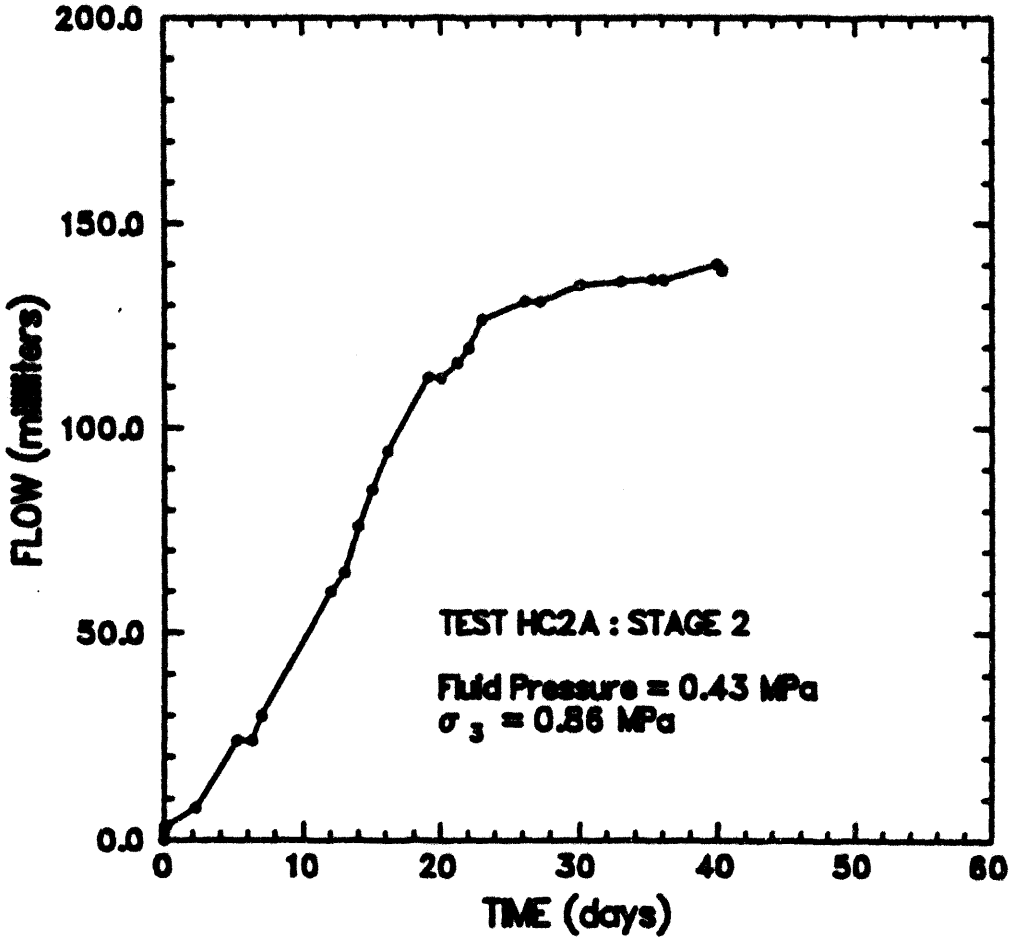

Figure F-2. Change in brine volume in downstream reservoir as a function of time during permeability stage for Test HC2A.

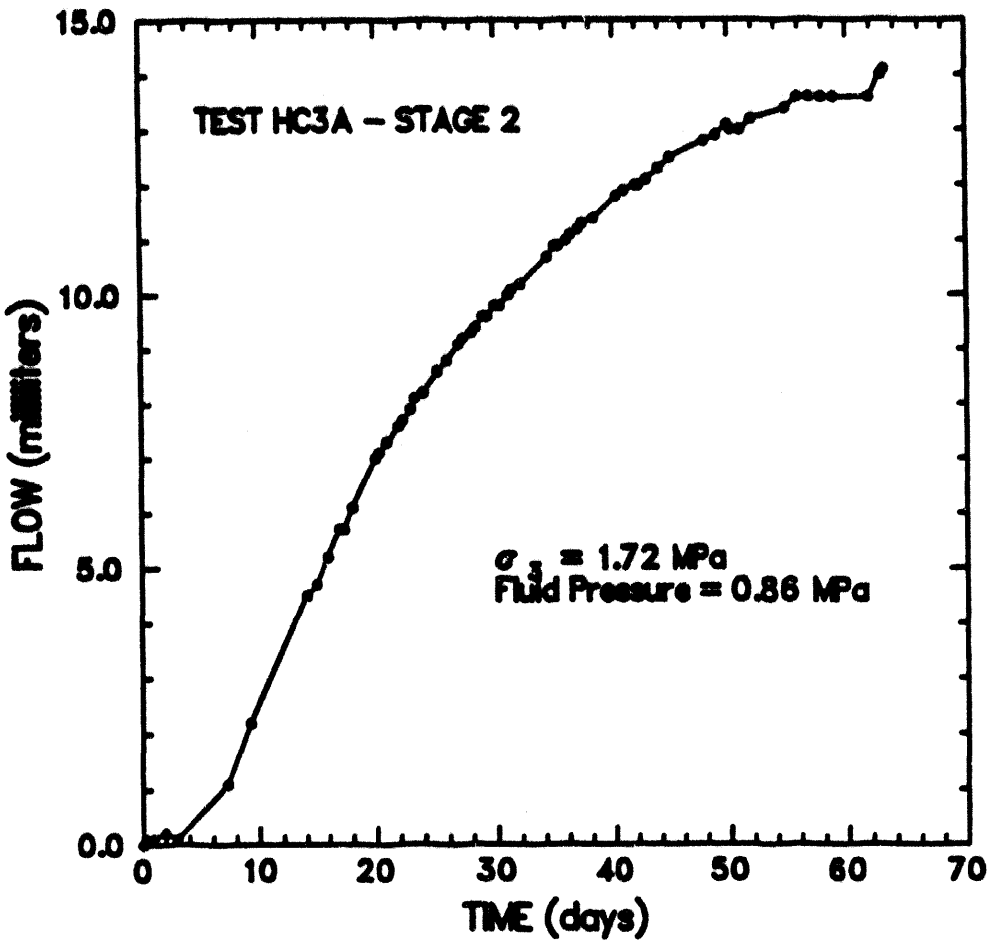

RSI-197-92-164

Figure F-3. Change in brine volume in downstream reservoir as a function of time during permeability stage for Test HC3A.

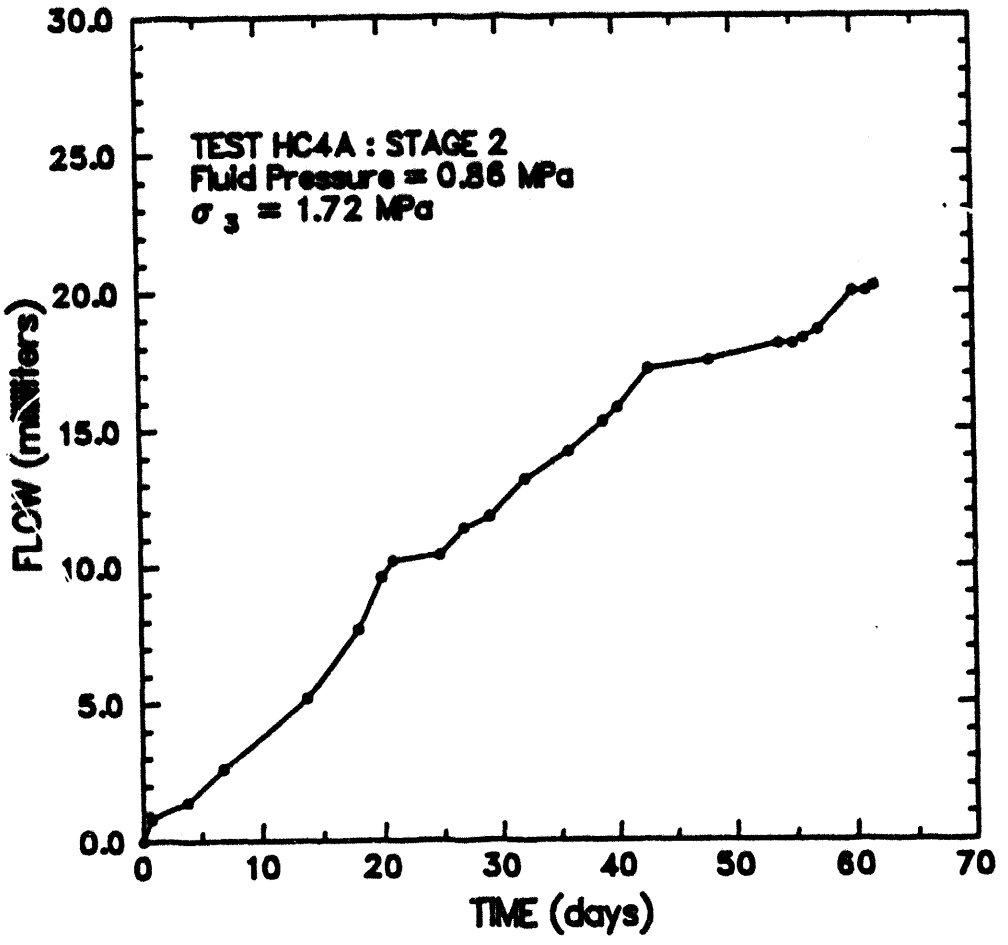

RSI-197-92-165

Figure F-4. Change in brine volume in downstream reservoir as a function of time during permeability stage for Test HC4A.

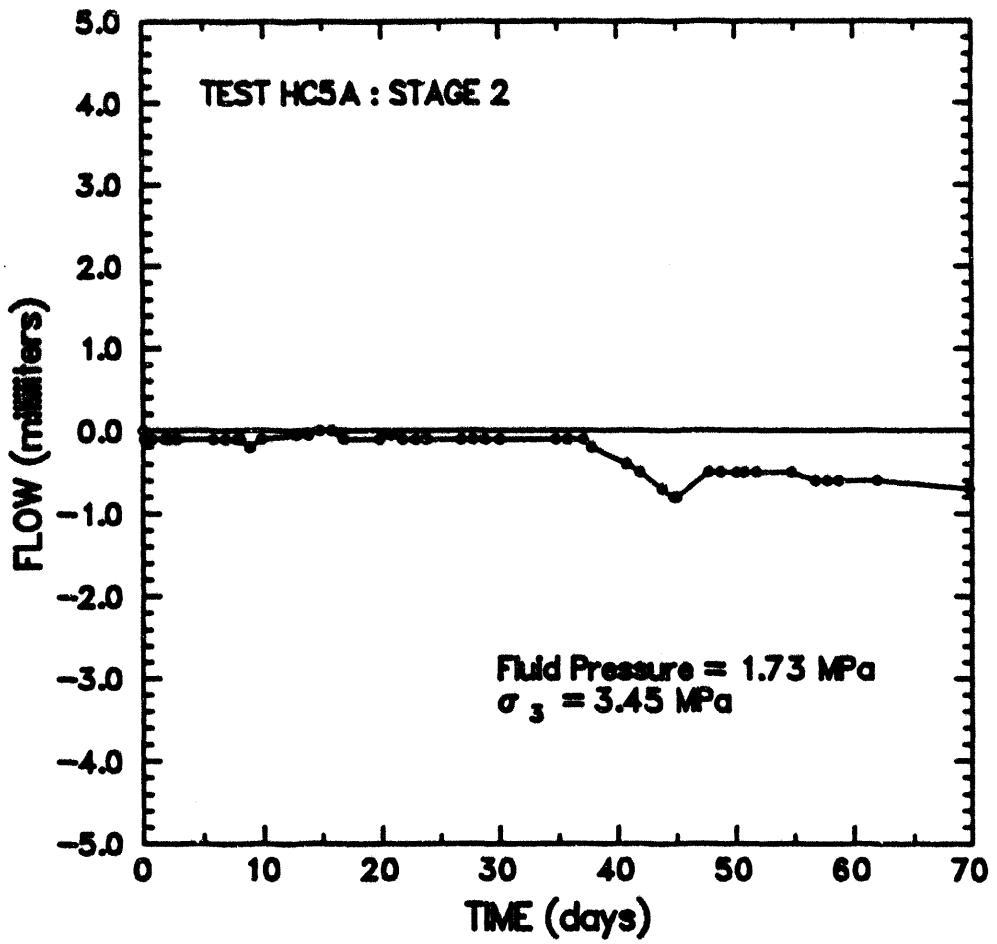

RSI-197-92-166

Figure F-5. Change in brine volume in downstream reservoir as a function of time during permeability stage for Test HC5A.

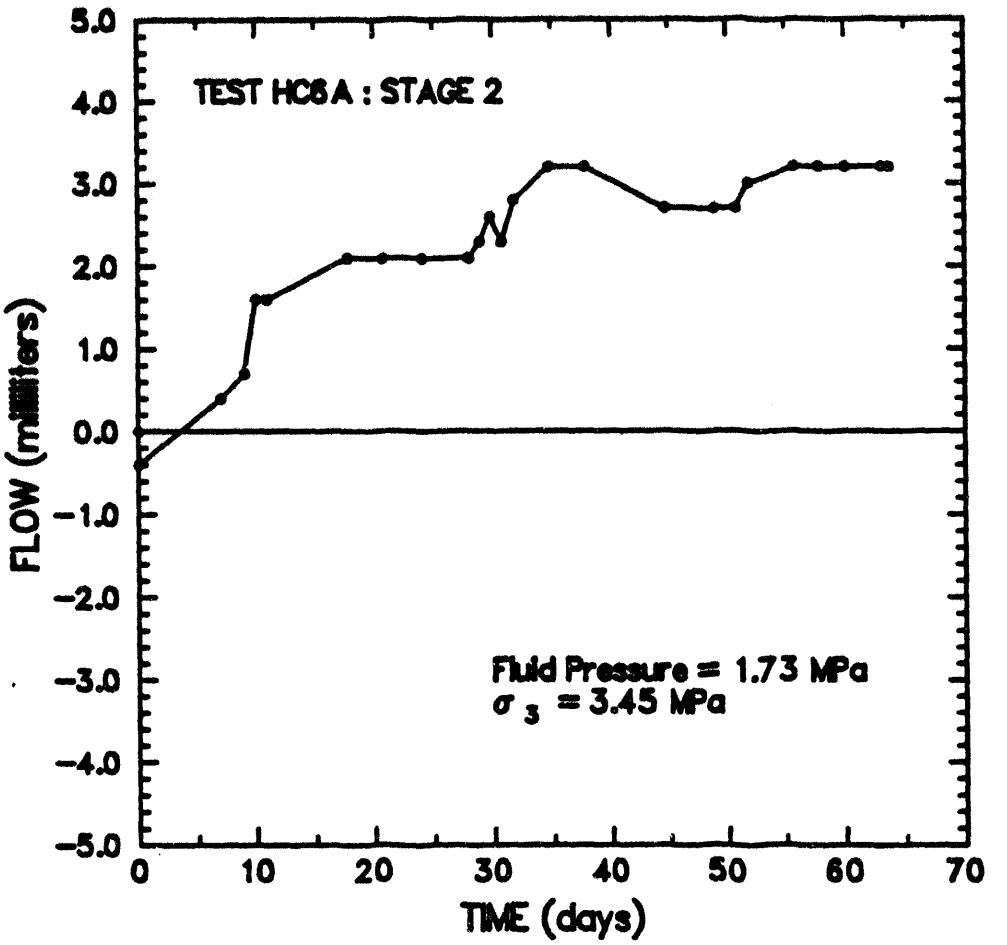

RSI-197-92-167

Figure F-6. Change in brine volume in downstream reservoir as a function of time during permeability stage for Test HC6A.

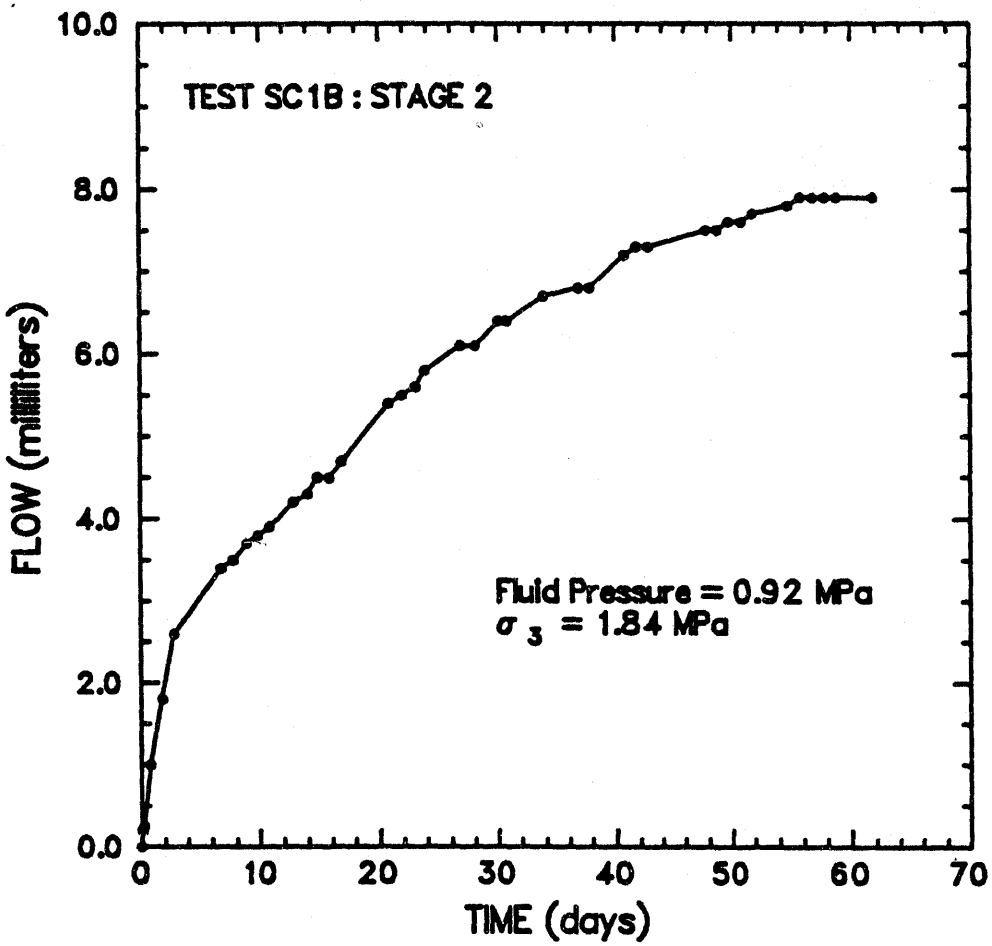

RSI-197-92-168

Figure F-7. Change in brine volume in downstream reservoir as a function of time during permeability stage for Test SC1B.

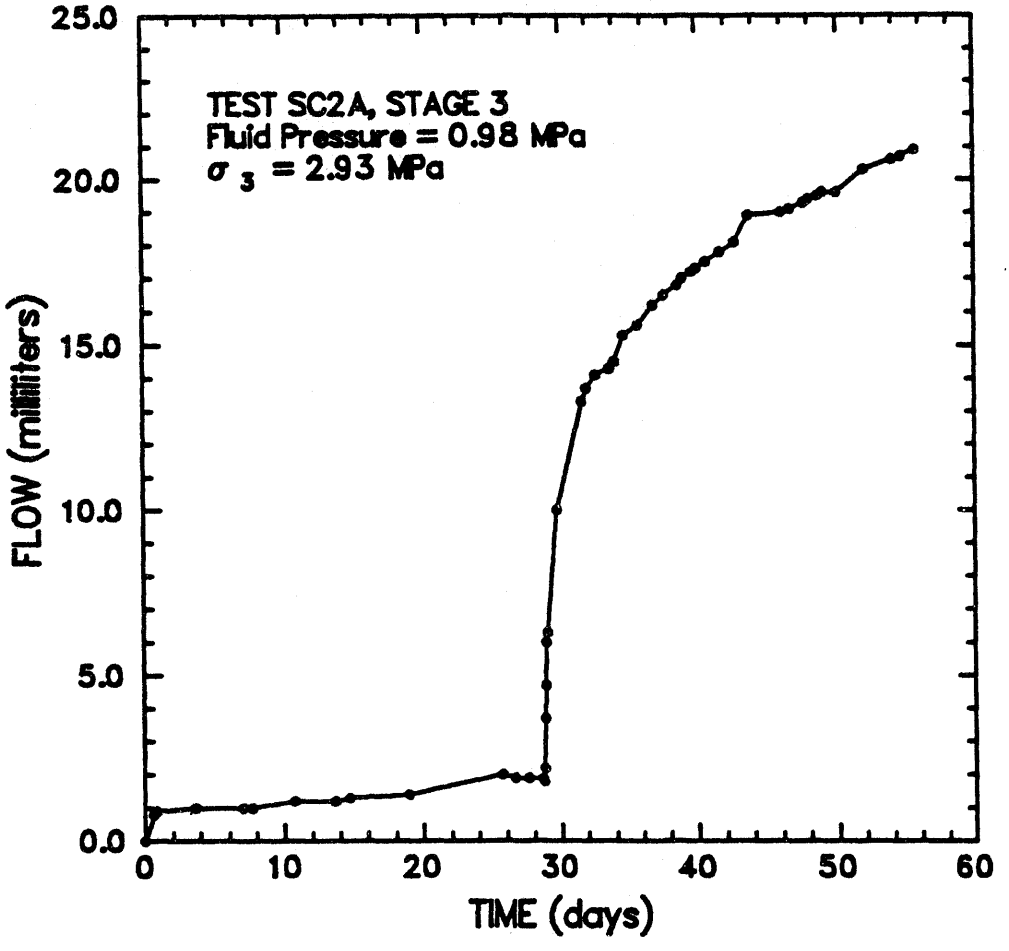

Figure F-8. Change in brine volume in downstream reservoir as a function of time during permeability stage for Test SC2A. The sudden increase in flow rate at 29 days is due to the release of an obstruction of salt precipitate.

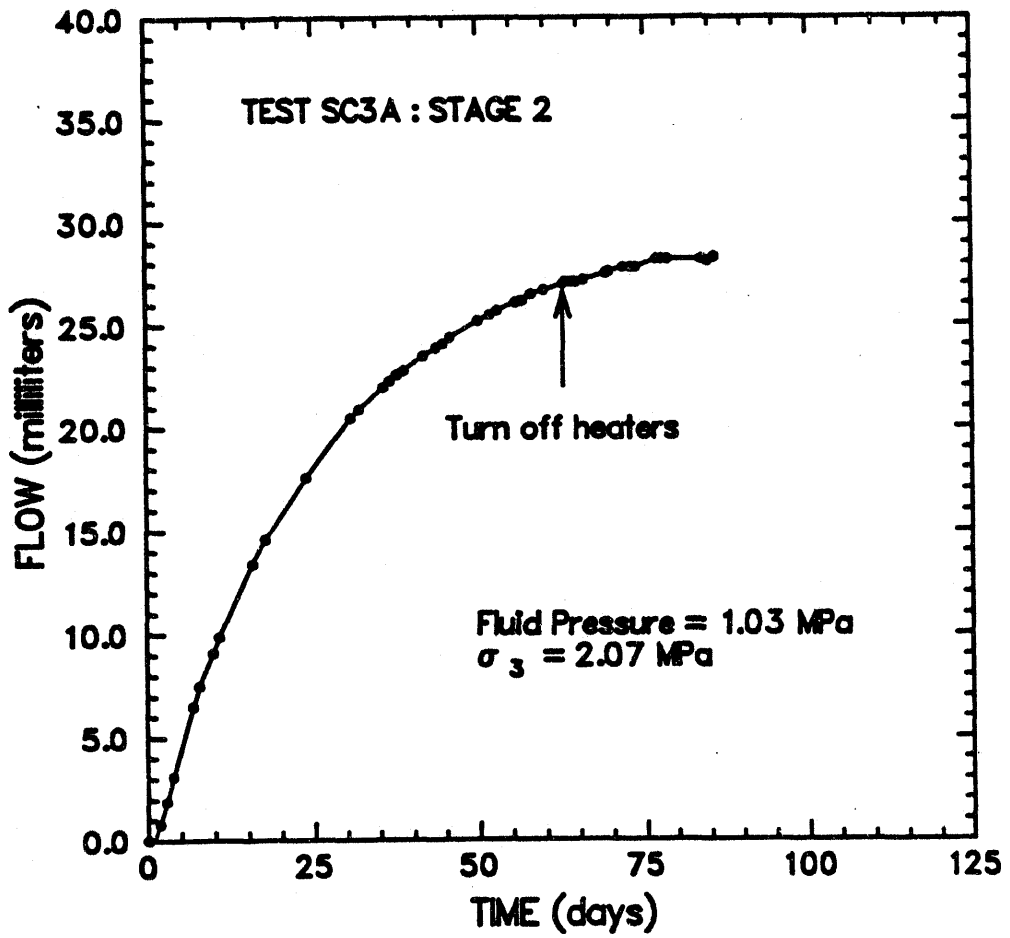

Figure F-9. Change in brine volume in downstream reservoir as a function of time during permeability stage for Test SC3A.

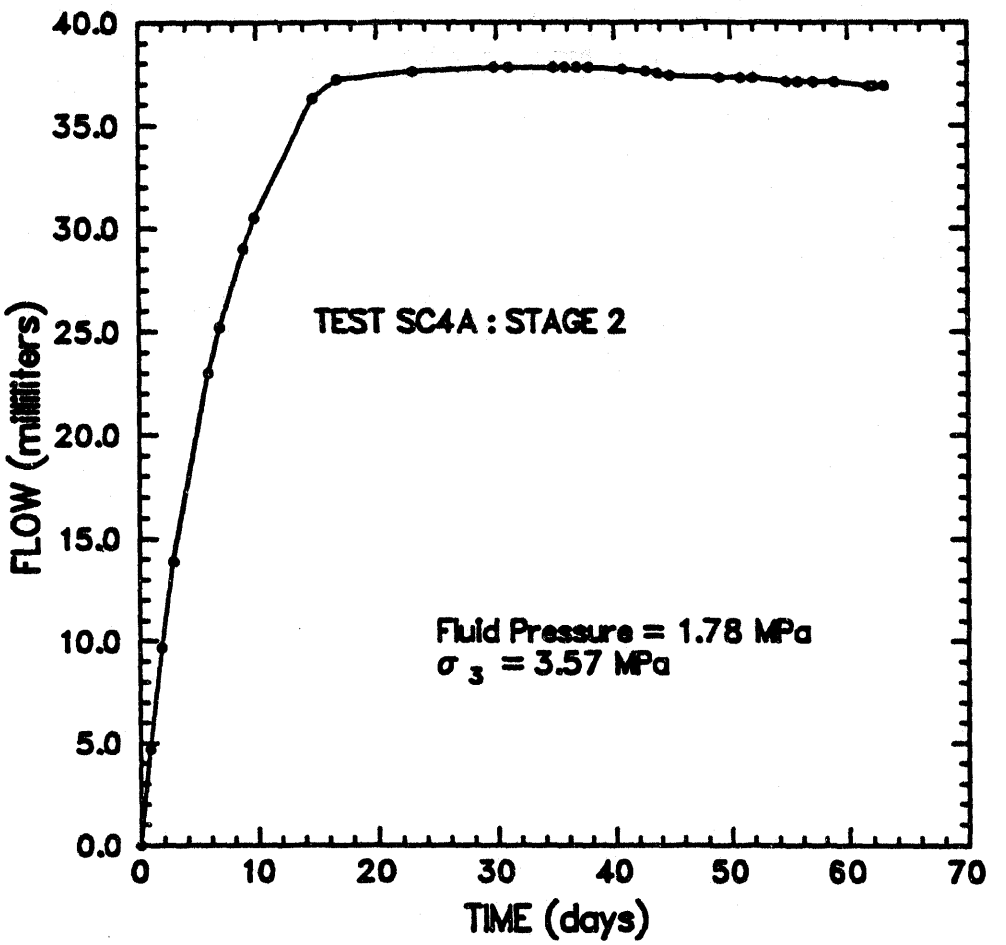

RSI-197-92-171

Figure F-10. Change in brine volume in downstream reservoir as a function of time during permeability stage for Test SC4A.

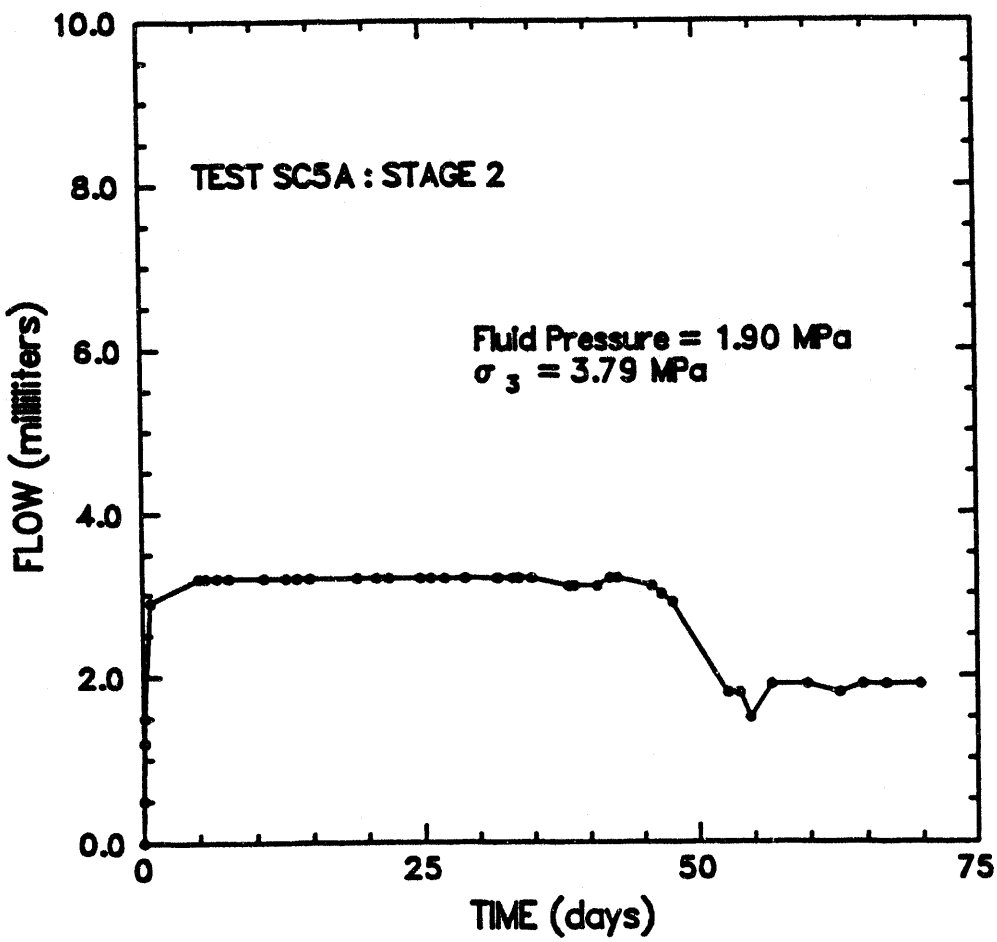

Figure F-11. Change in brine volume in downstream reservoir as a function of time during permeability stage for Test SC5A.

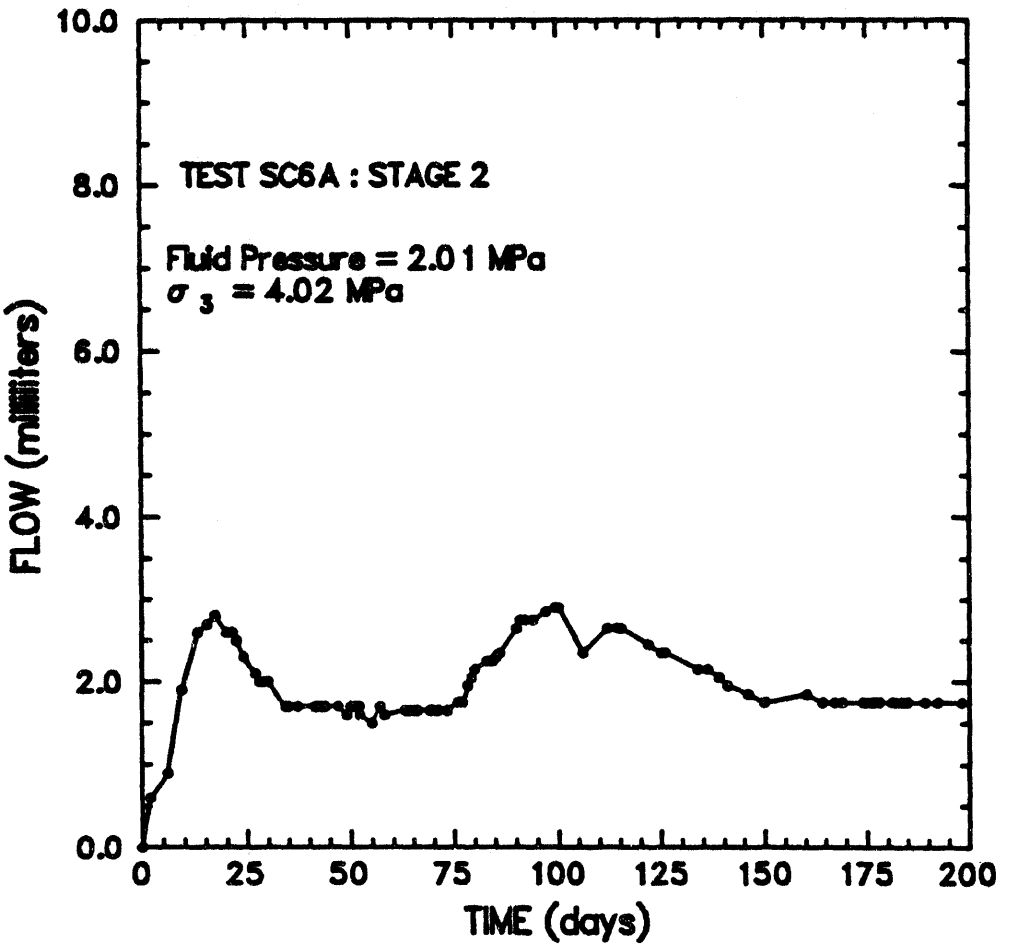

Figure F-12. Change in brine volume in downstream reservoir as a function of time during permeability stage for Test SC6A.

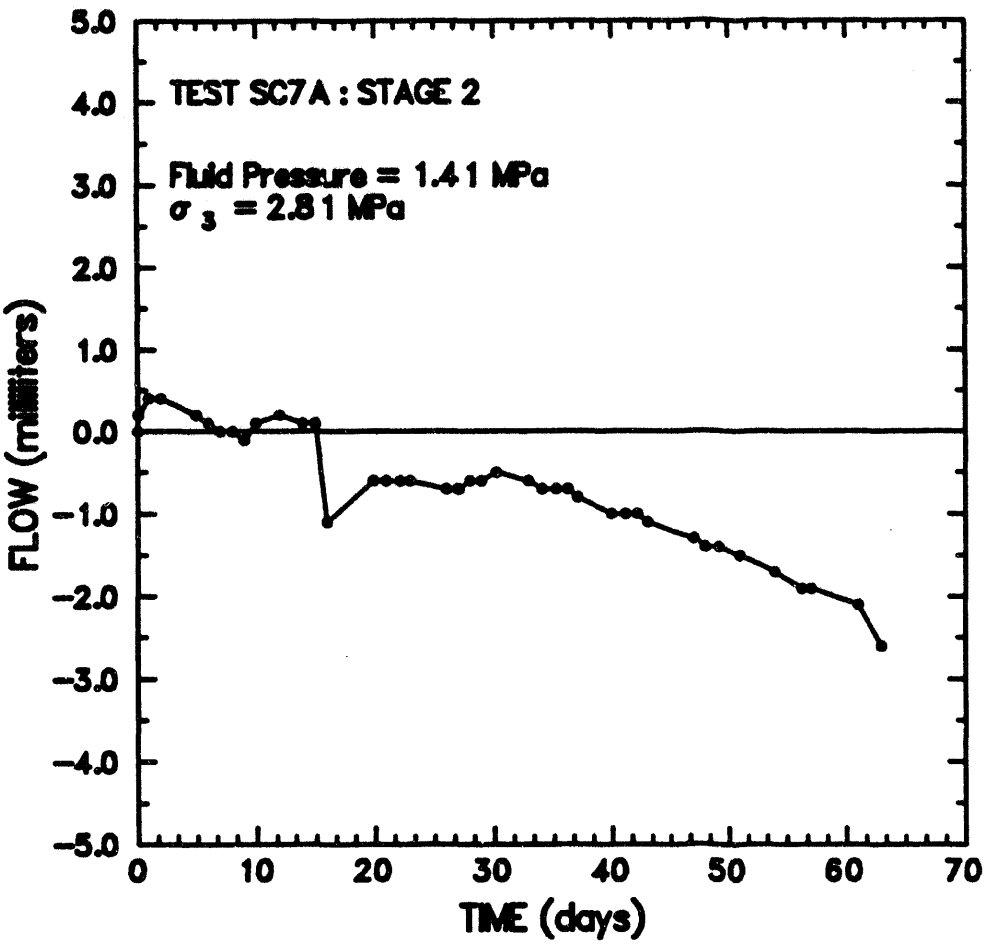

RSI-197-92-174

Figure F-13. Change in brine volume in downstream reservoir as a function of time during permeability stage for Test SC7A.

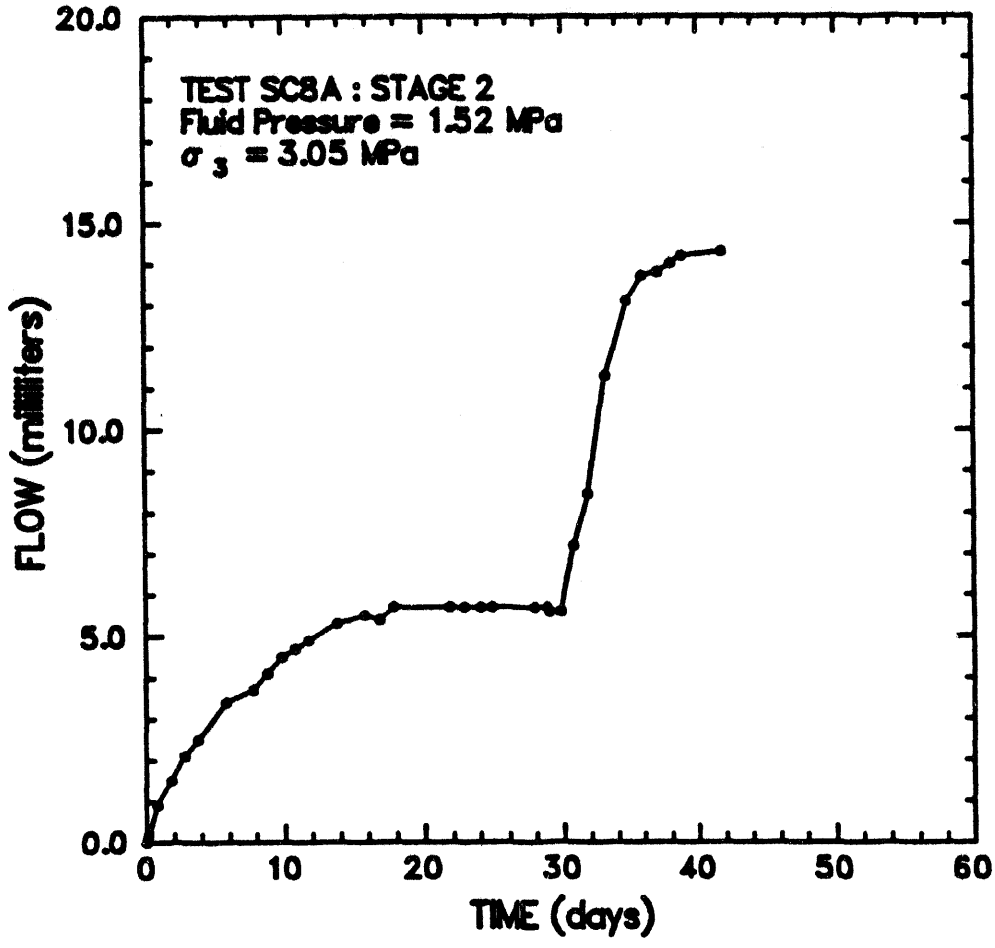

RSI-197-92-175

Figure F-14. Change in brine volume in downstream reservoir as a function of time during permeability stage for Test SC8A. The sudden increase in flow rate at 30 days is due to the release of an obstruction of salt precipitate.

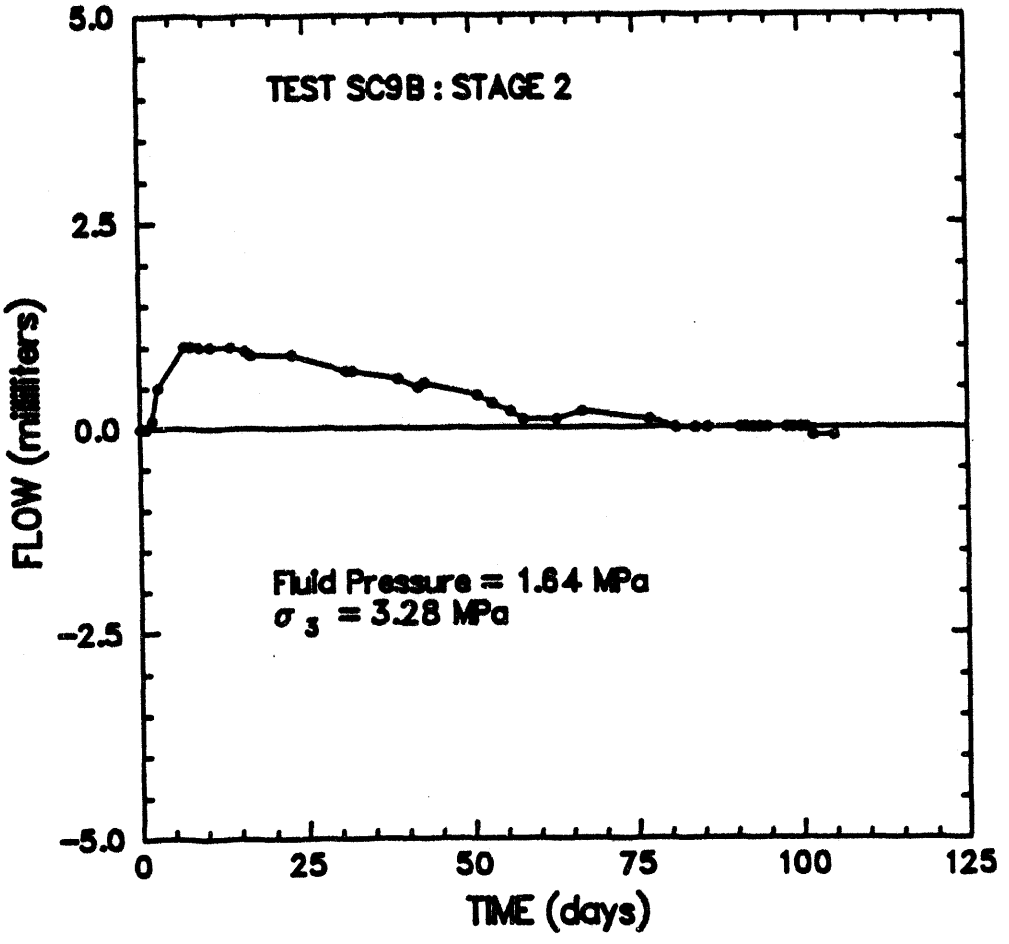

Figure F-15. Change in brine volume in downstream reservoir as a function of time during permeability stage for Test SC9B.

APPENDIX G. AXIAL STRESS STABILITY FOR STAGE 1 OF ALL SHEAR CONSOLIDATION TESTS

Figures

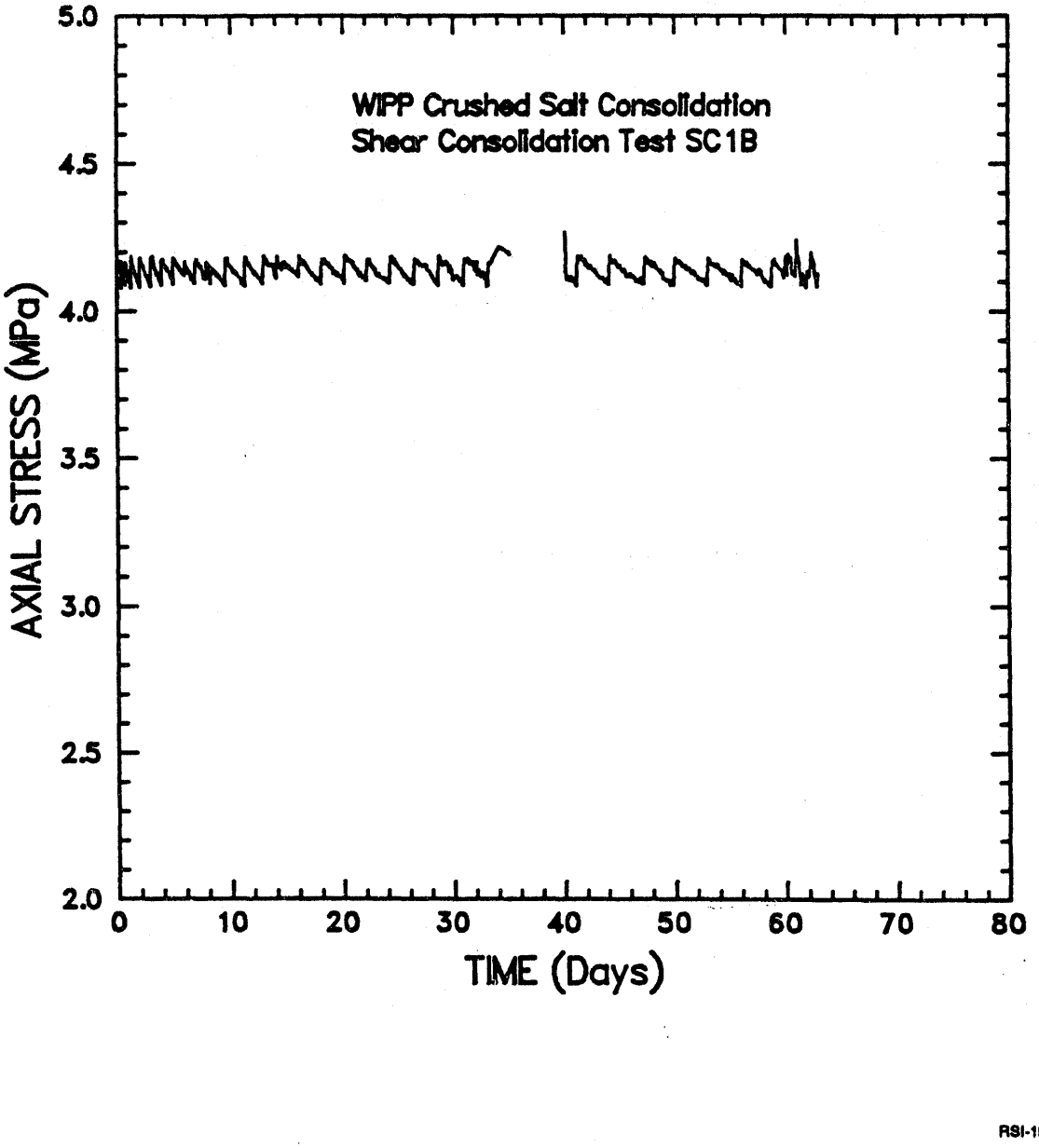

Figure G-1. Axial stress-versus-time for Test SC1B.

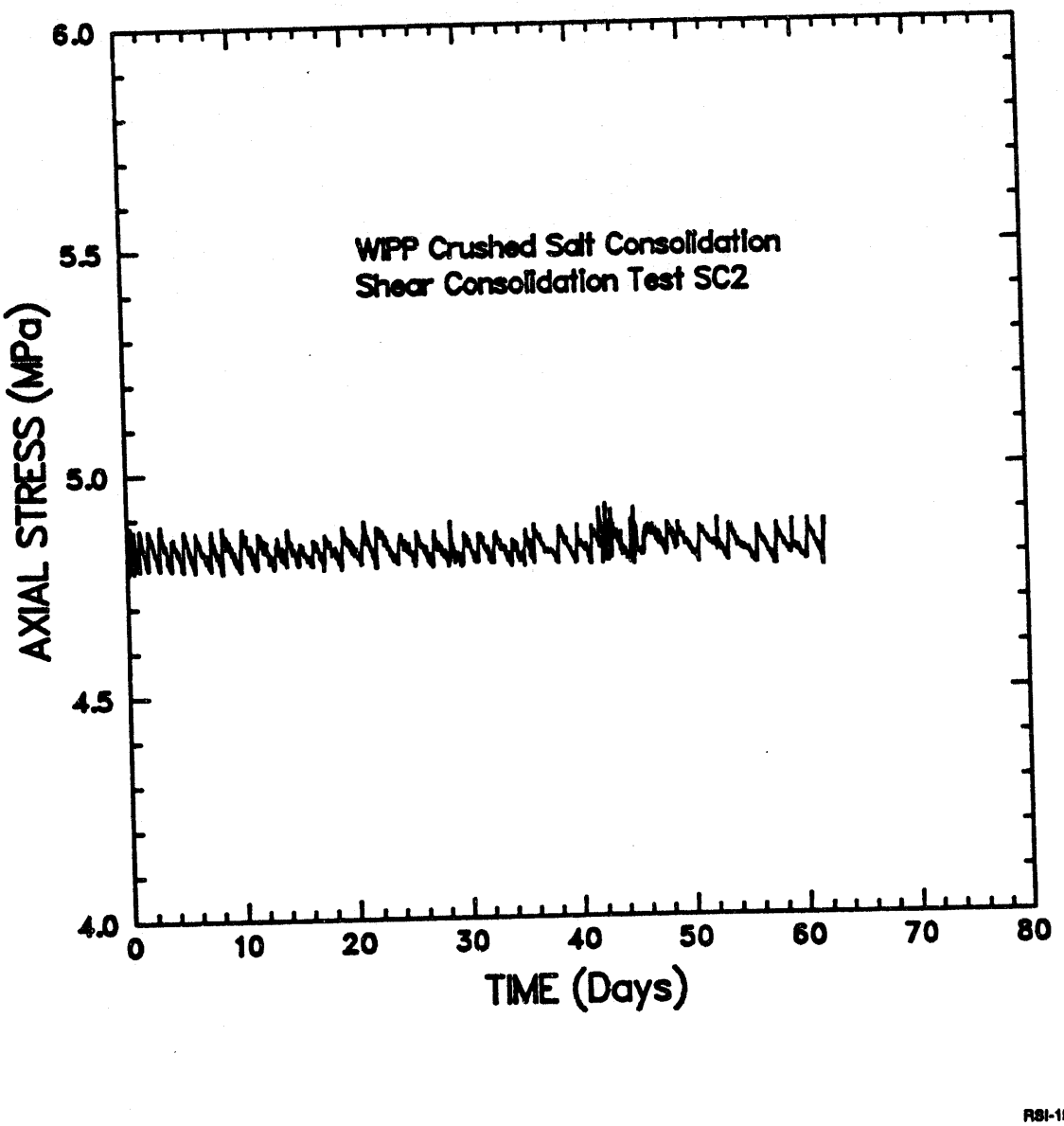

Figure G-2. Axial stress-versus-time for Test SC2A.

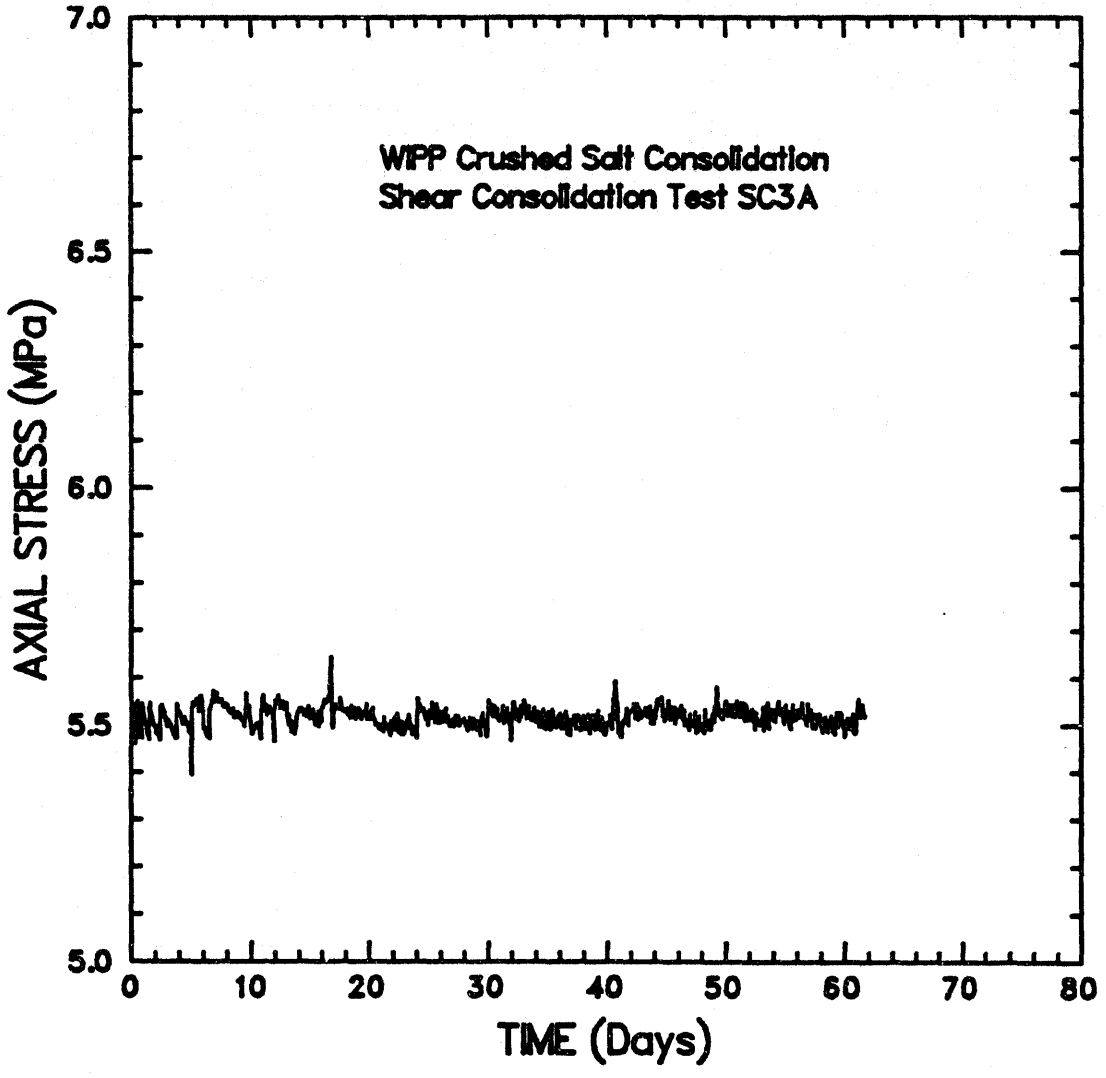

Figure G-3. Axial stress-versus-time for Test SC3A.

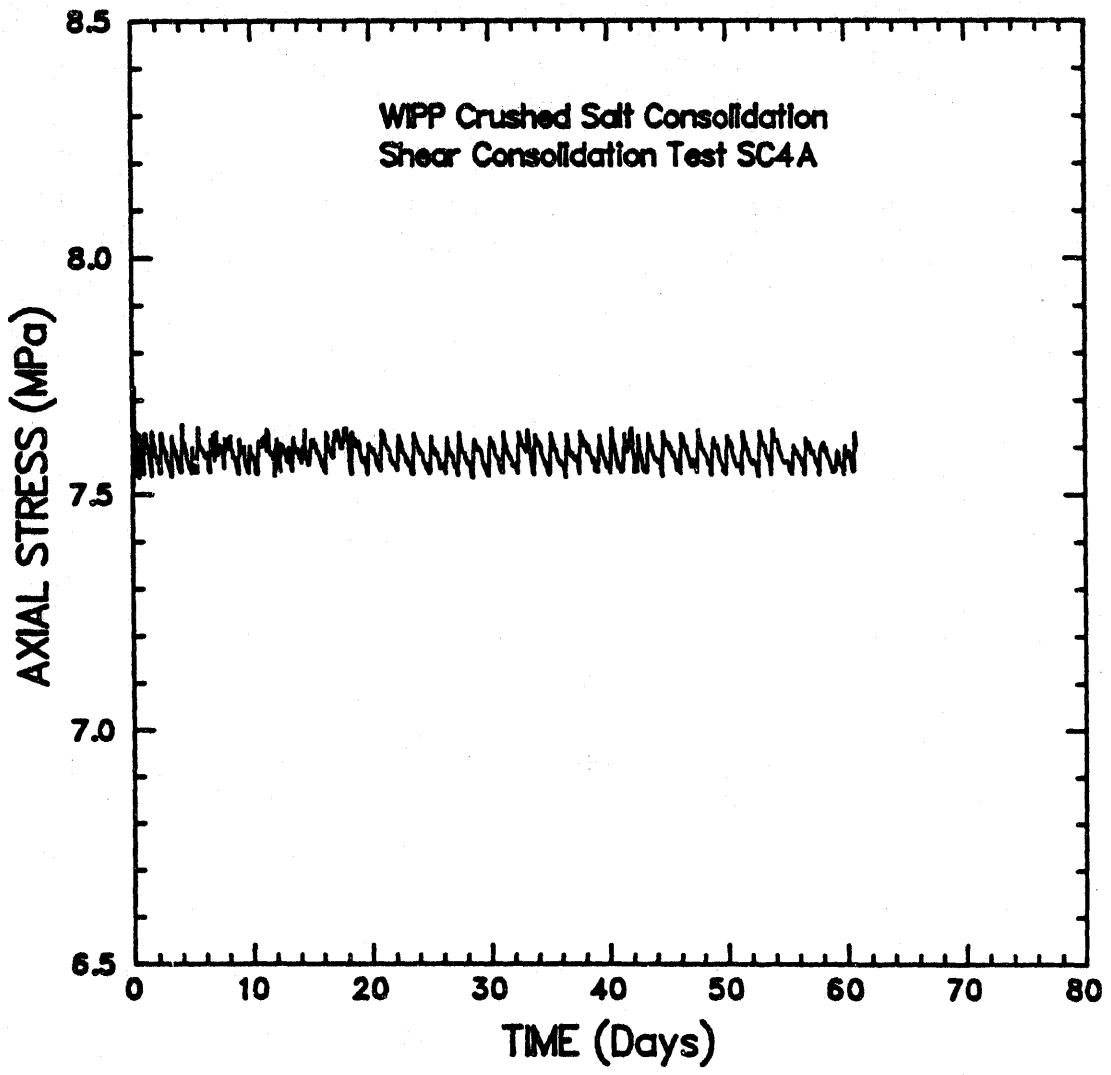

Figure G-4. Axial stress-versus-time for Test SC4A.

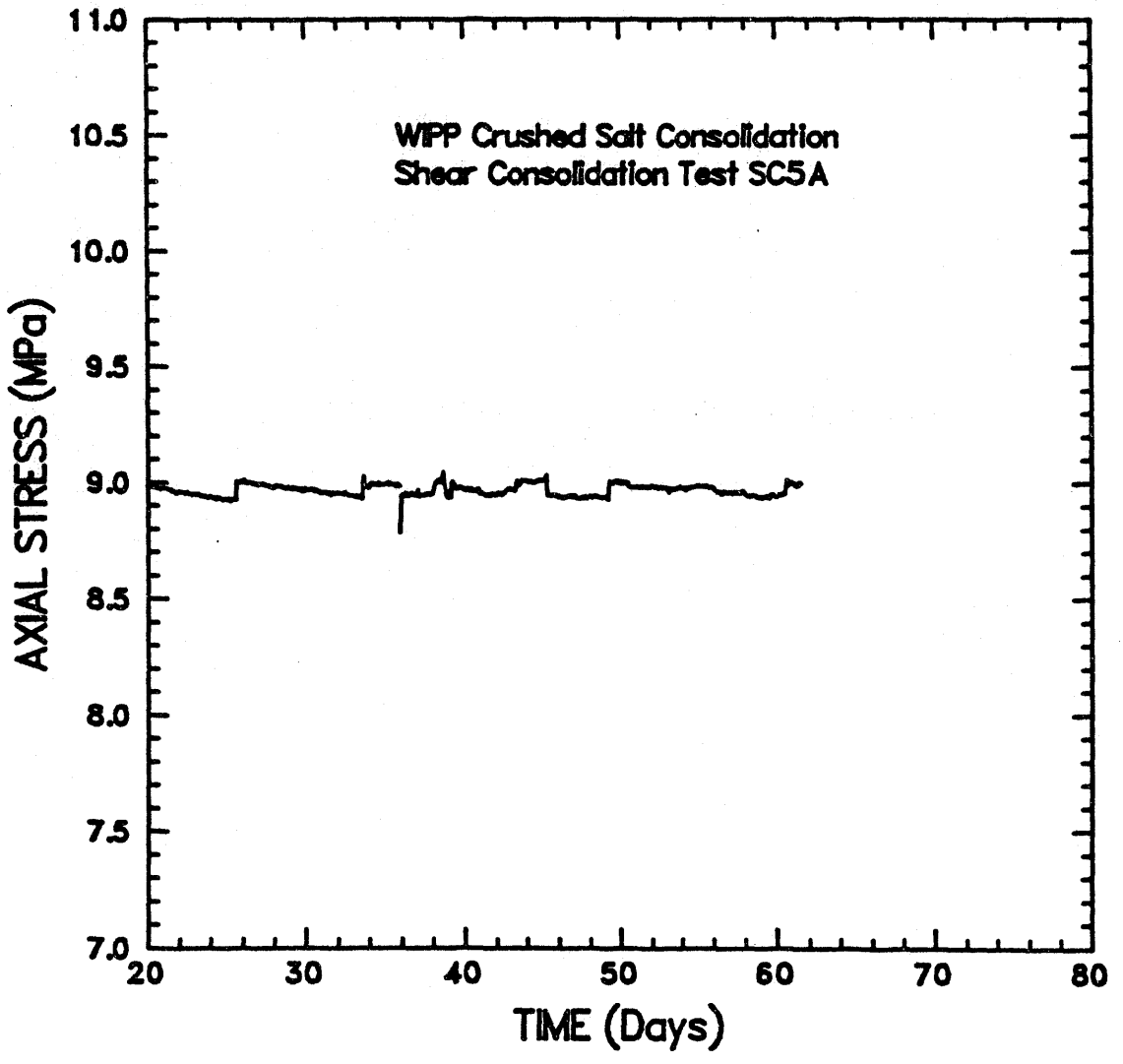

Figure G-5. Axial stress-versus-time for Test SC5A.

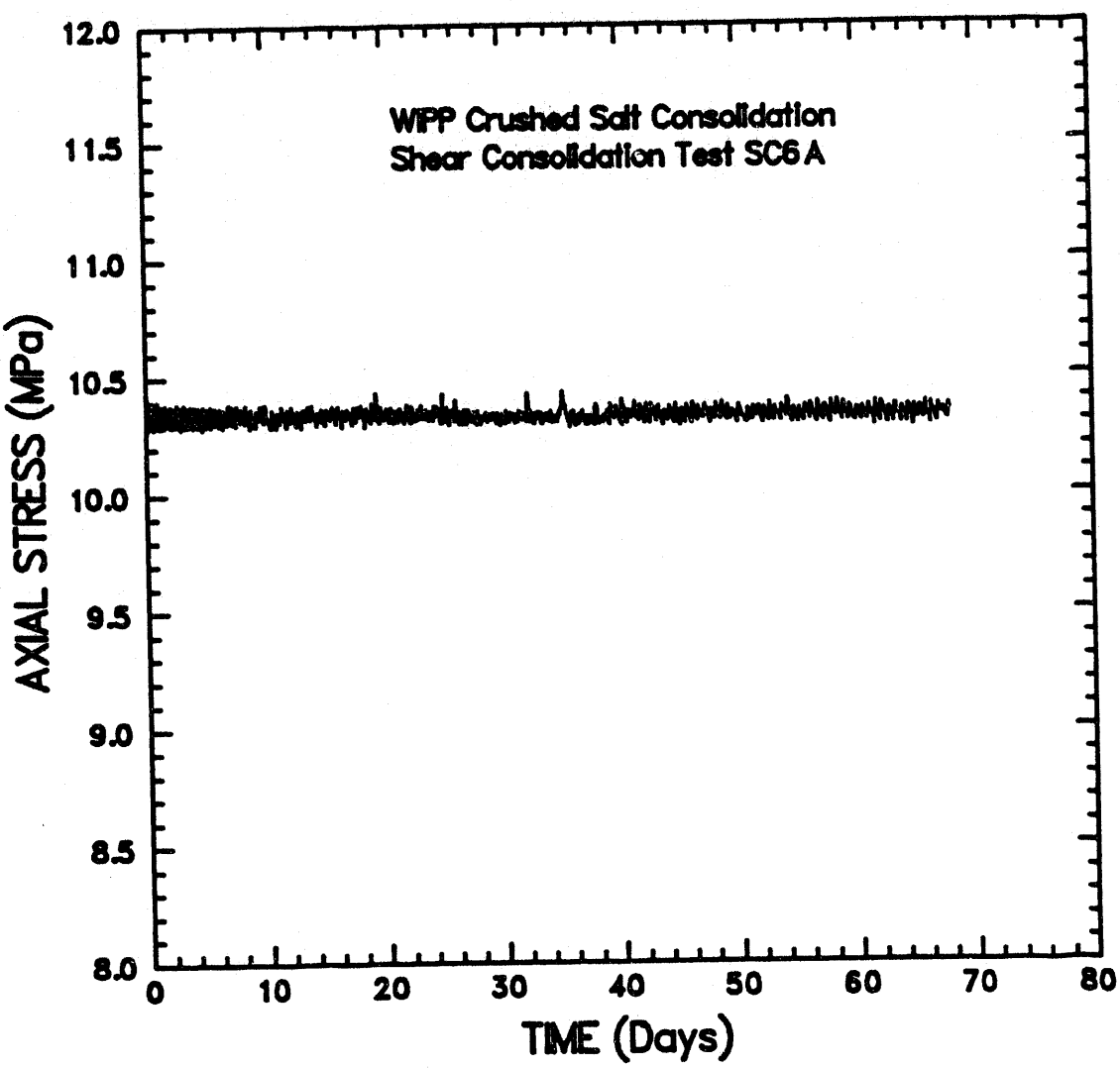

Figure G-6. Axial stress-versus-time for Test SC6A.

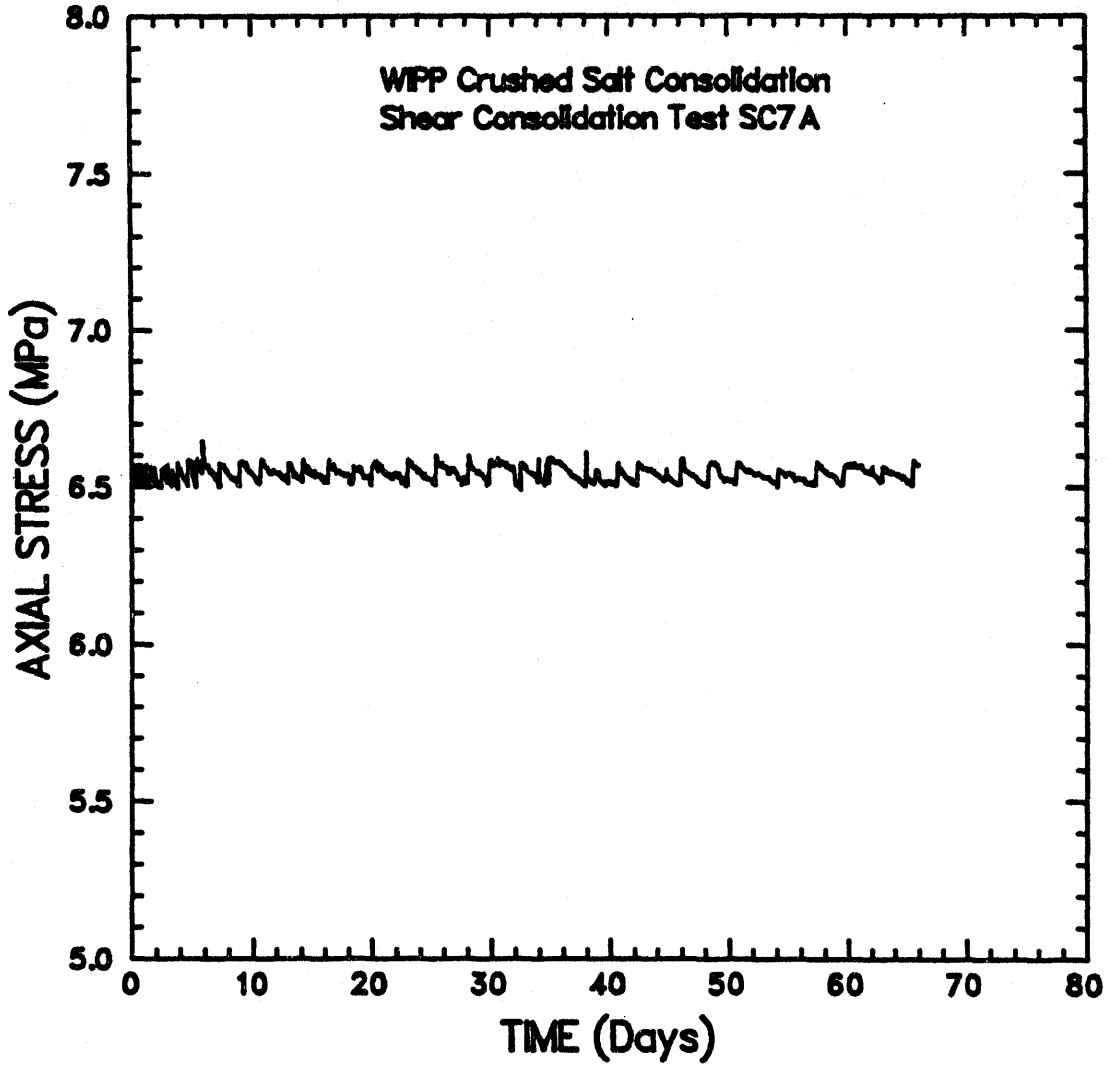

Figure G-7. Axial stress-versus-time for Test SC7A.

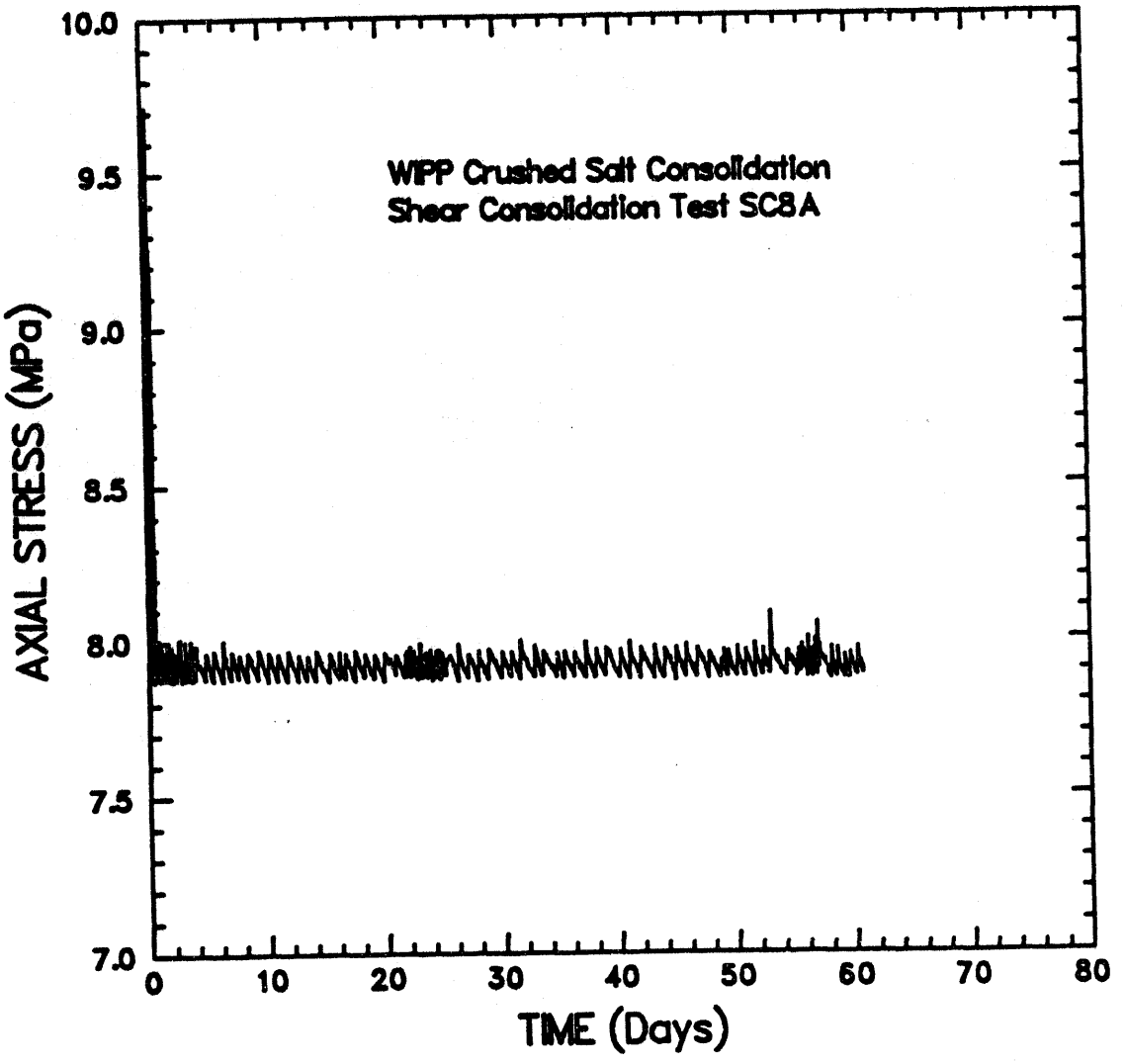

Figure G-8. Axial stress-versus-time for Test SC8A.

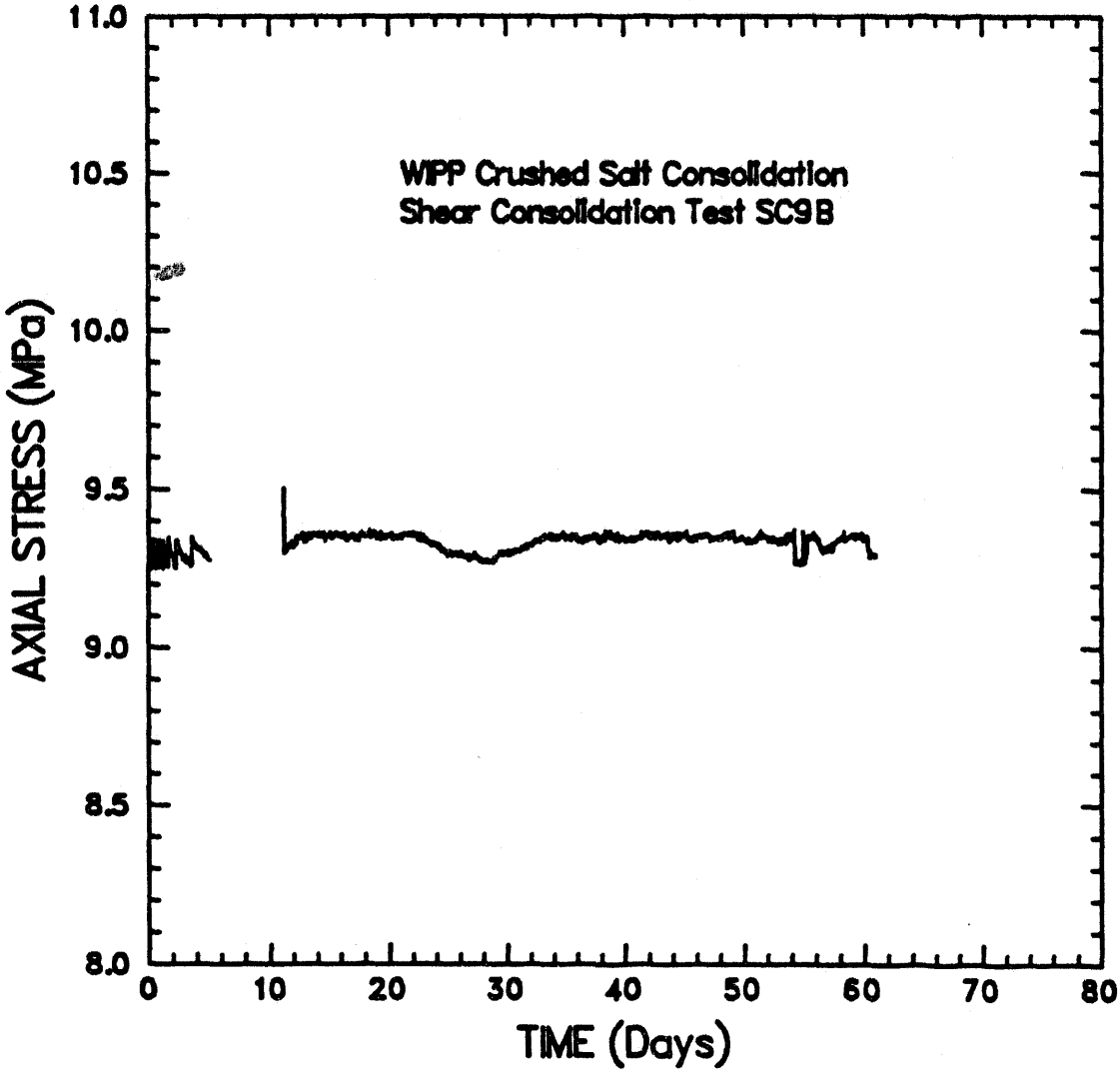

Figure G-9. Axial stress-versus-time for Test SC9B.

APPENDIX H. CONFINING PRESSURE STABILITY FOR ALL HYDROSTATIC AND SHEAR CONSOLIDATION TESTS

Figures

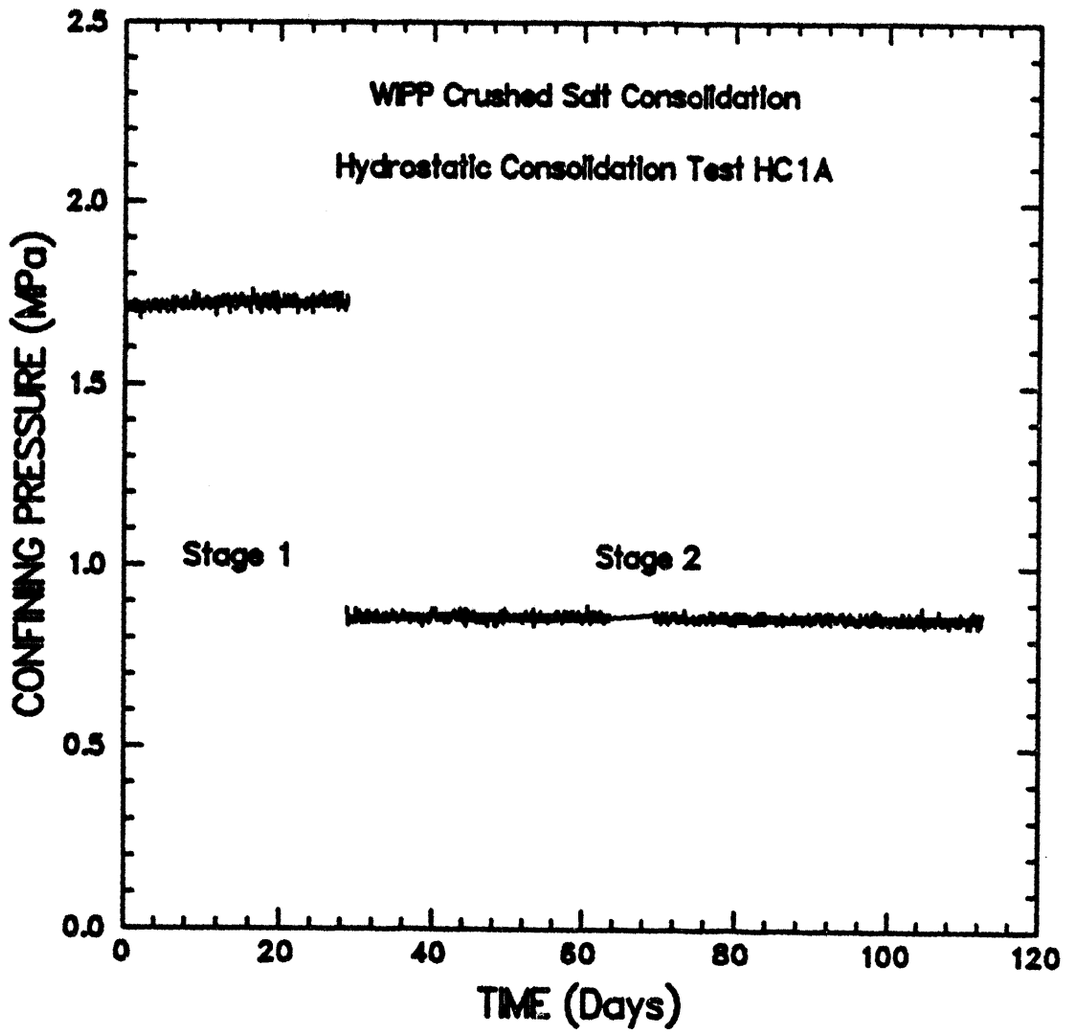

Figure H-1. Confining pressure-versus-time for Test HC1A.

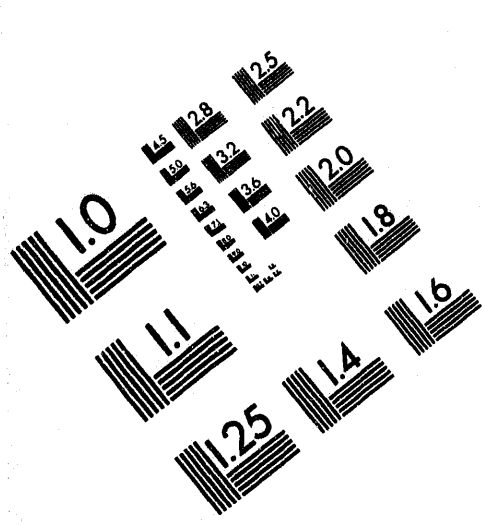

Association for Information and Image Management
1100 Wayne Avenue, Suite 1100
Silver Spring, Maryland 20910
301/587-8202

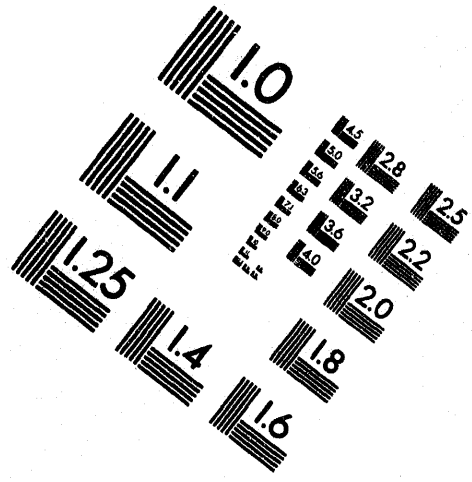

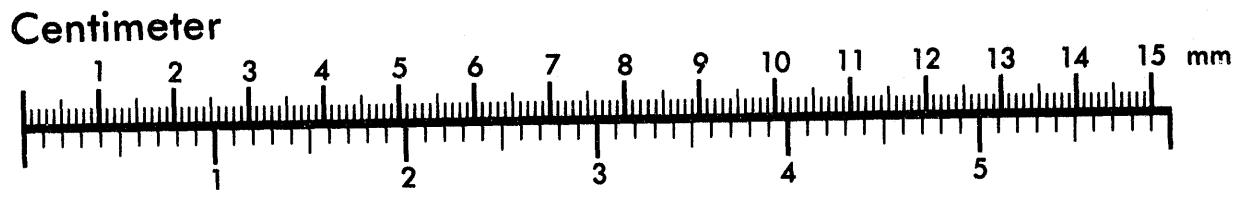

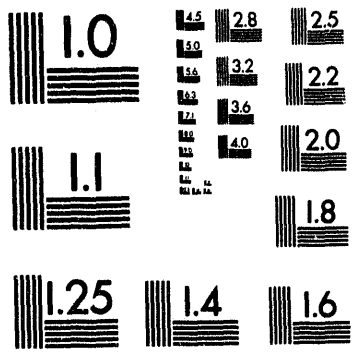

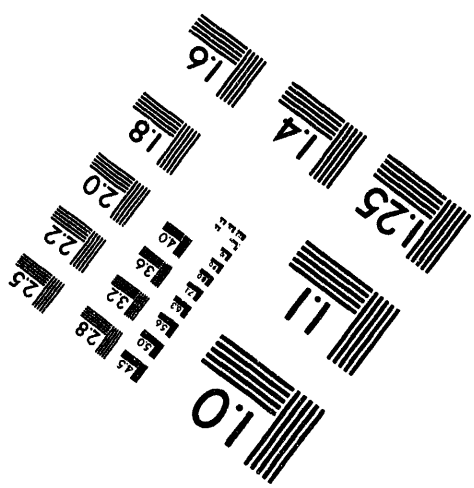

MANUFACTURED TO AIIM STANDARDS
BY APPLIED IMAGE, INC.

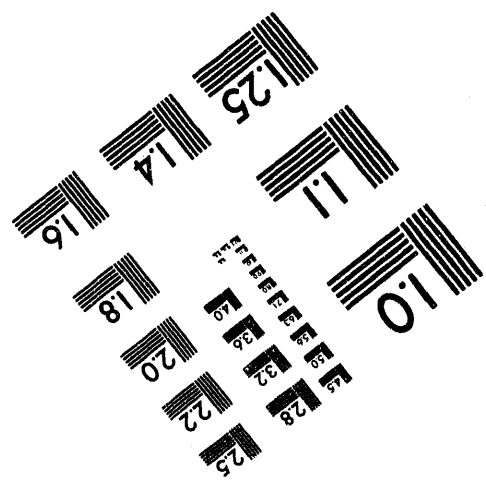

3 of 3

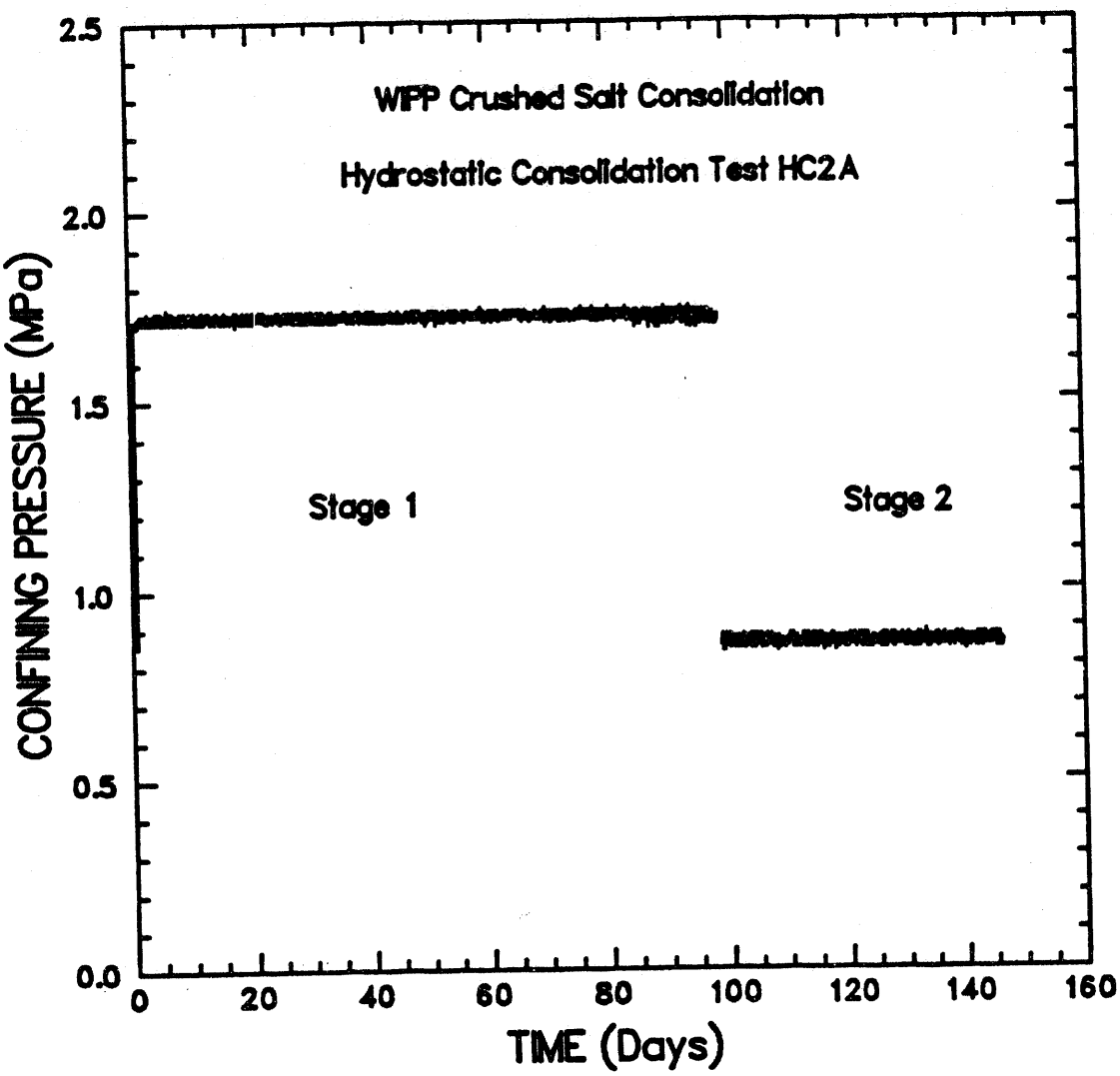

Figure H-2. Confining pressure-versus-time for Test HC2A.

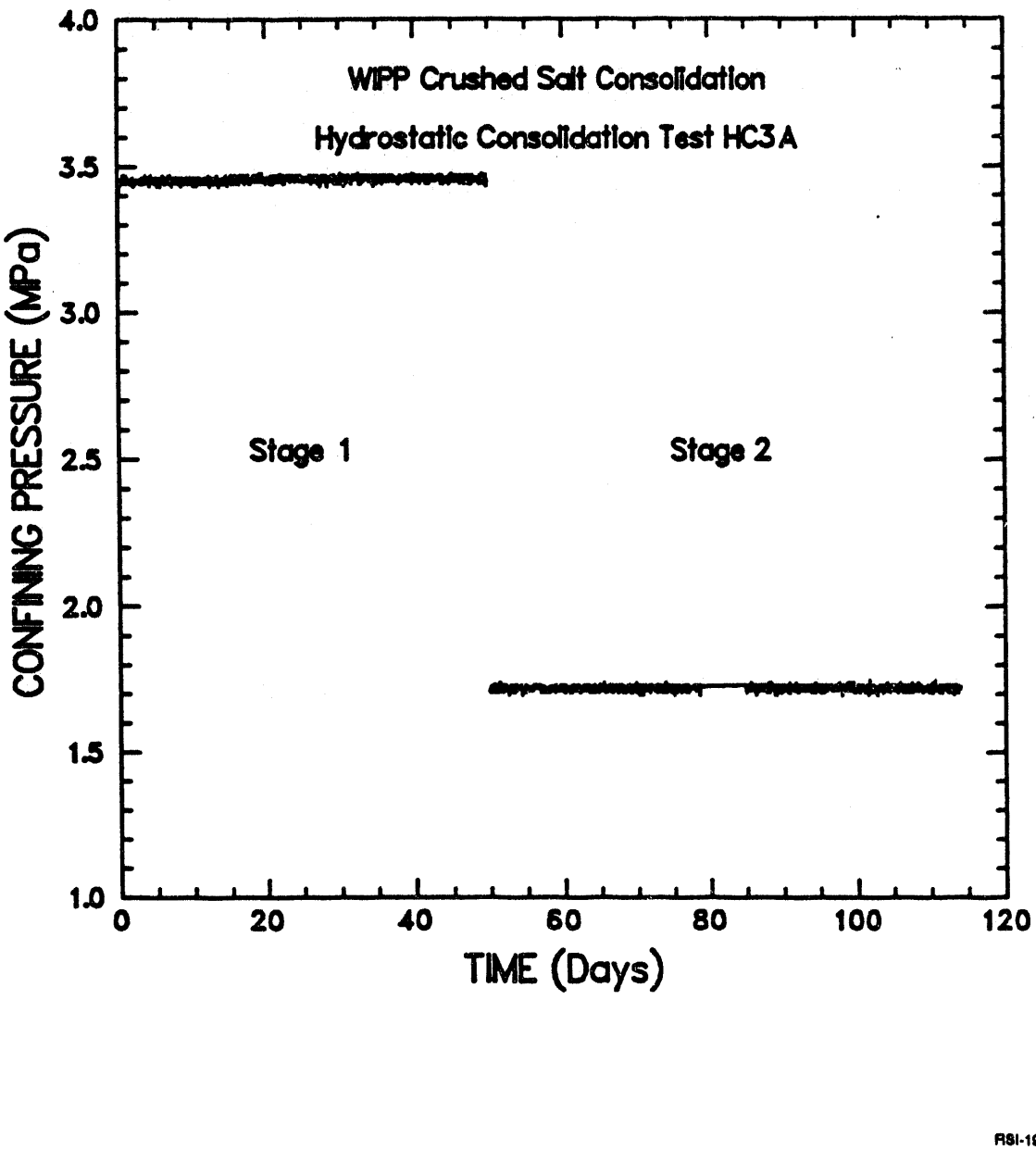

Figure H-3. Confining pressure-versus-time for Test HC3A.

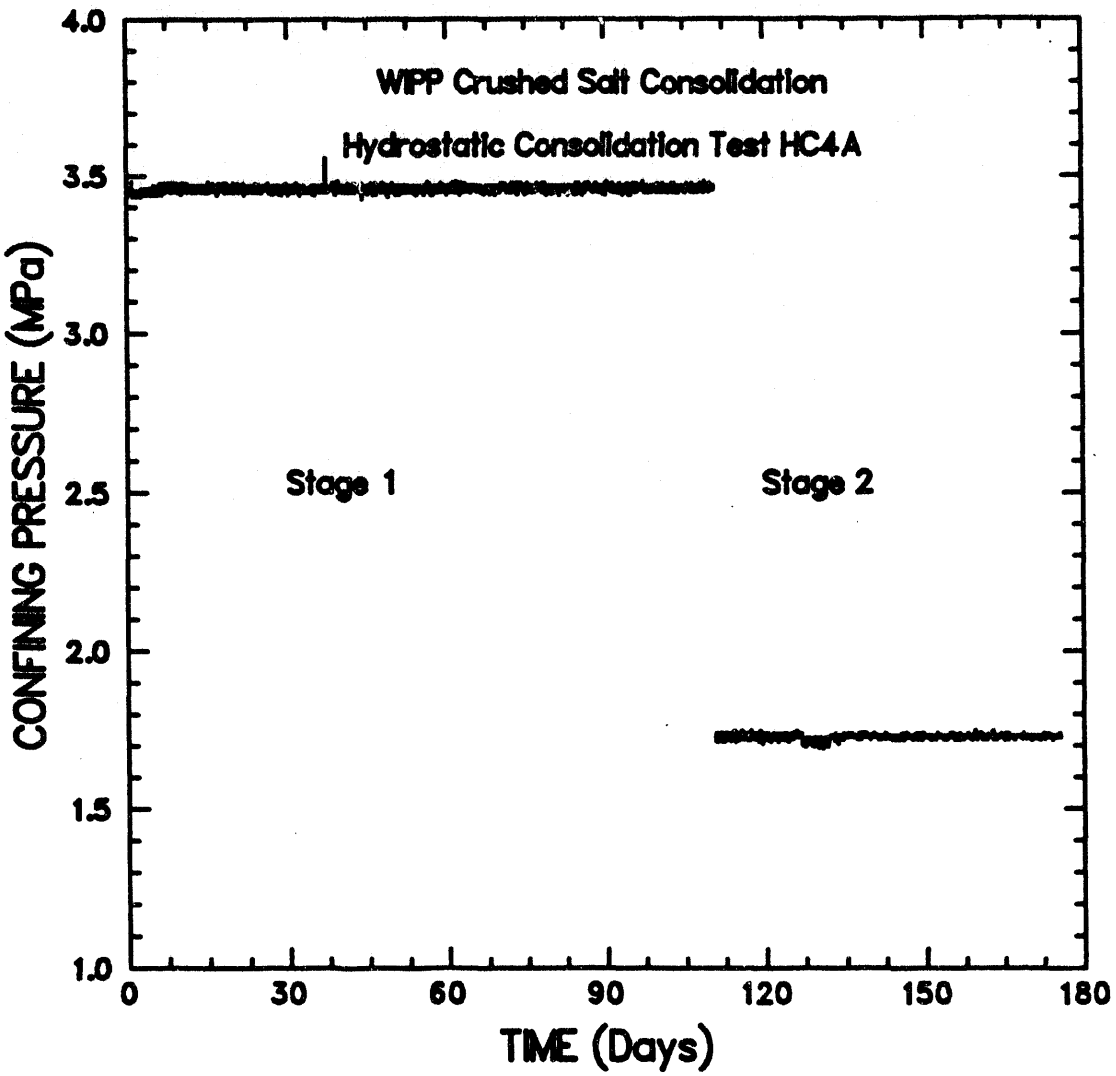

Figure H-4. Confining pressure-versus-time for Test HC4A.

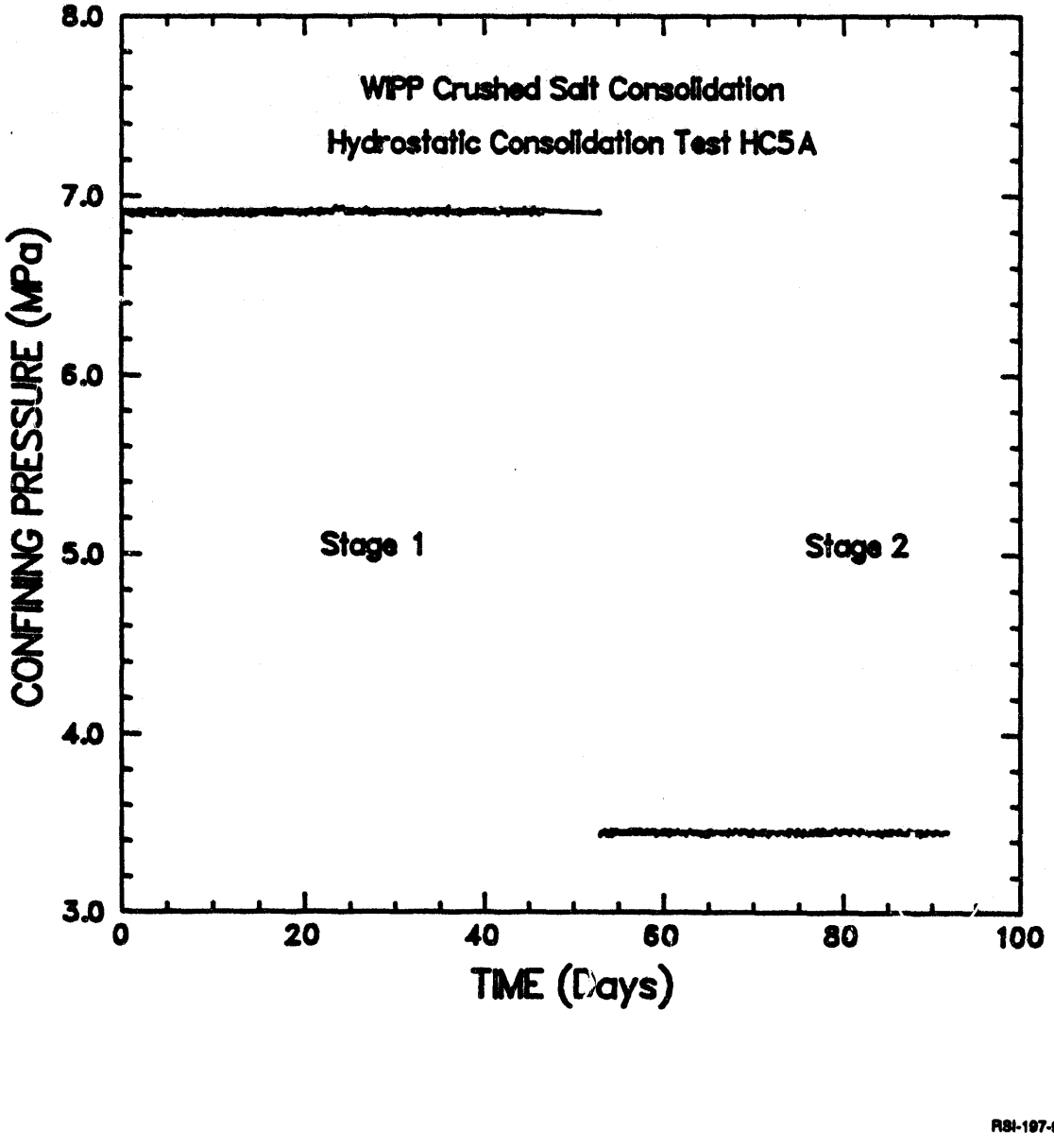

Figure H-5. Confining pressure-versus-time for Test HC5A.

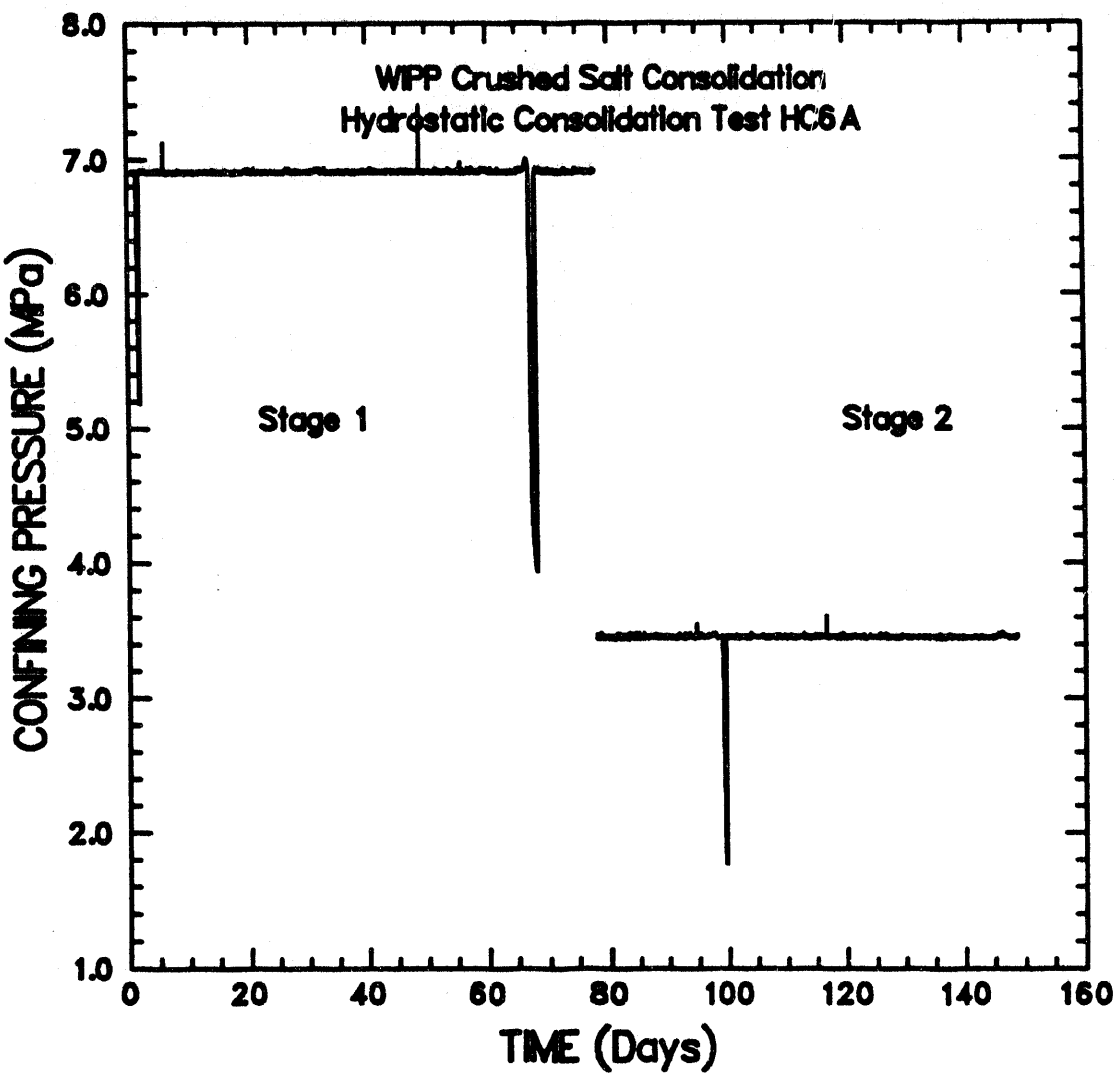

Figure H-6. Confining pressure-versus-time for Test HC6A.

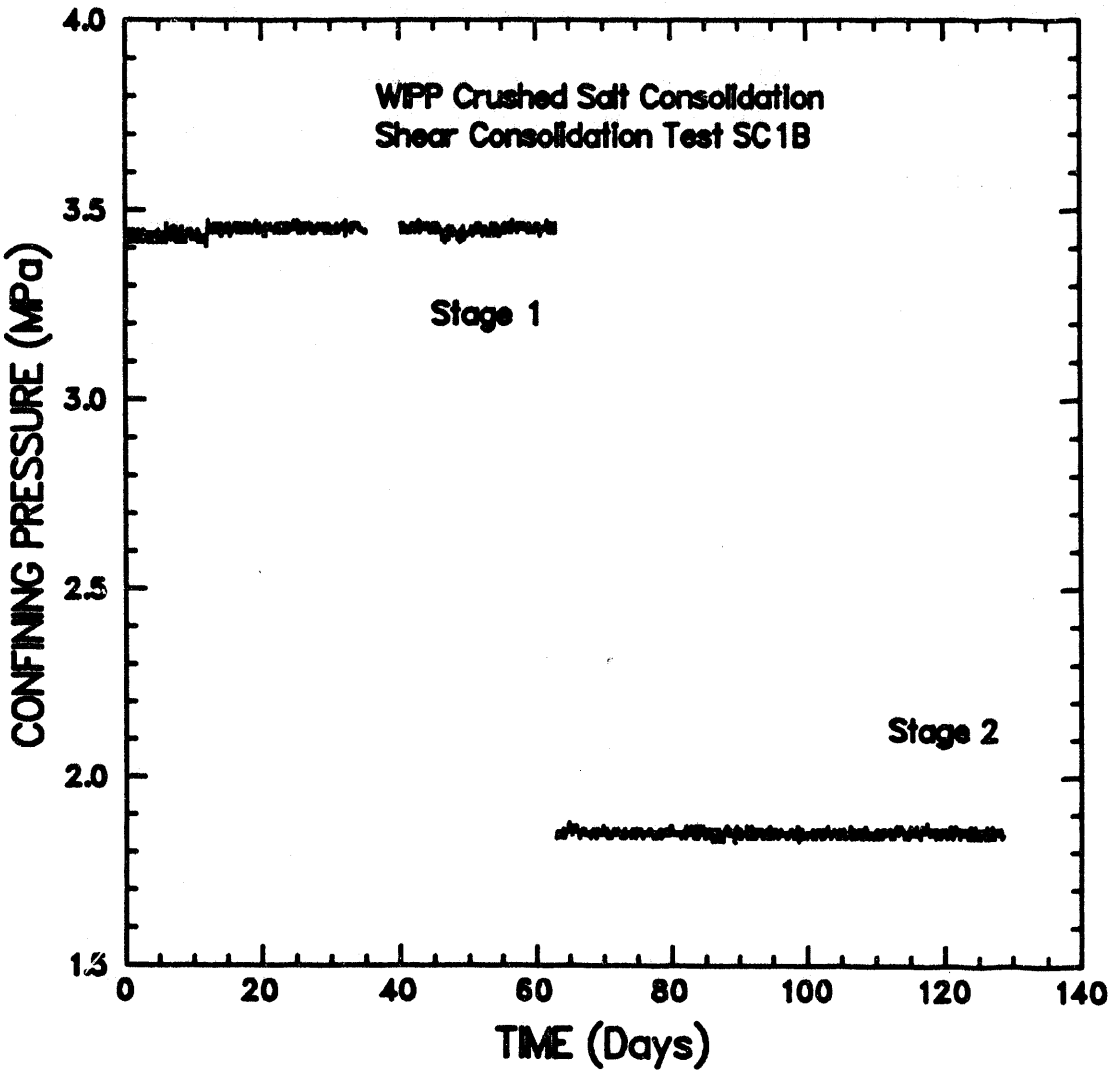

Figure H-7. Confining pressure-versus-time for Test SC1B.

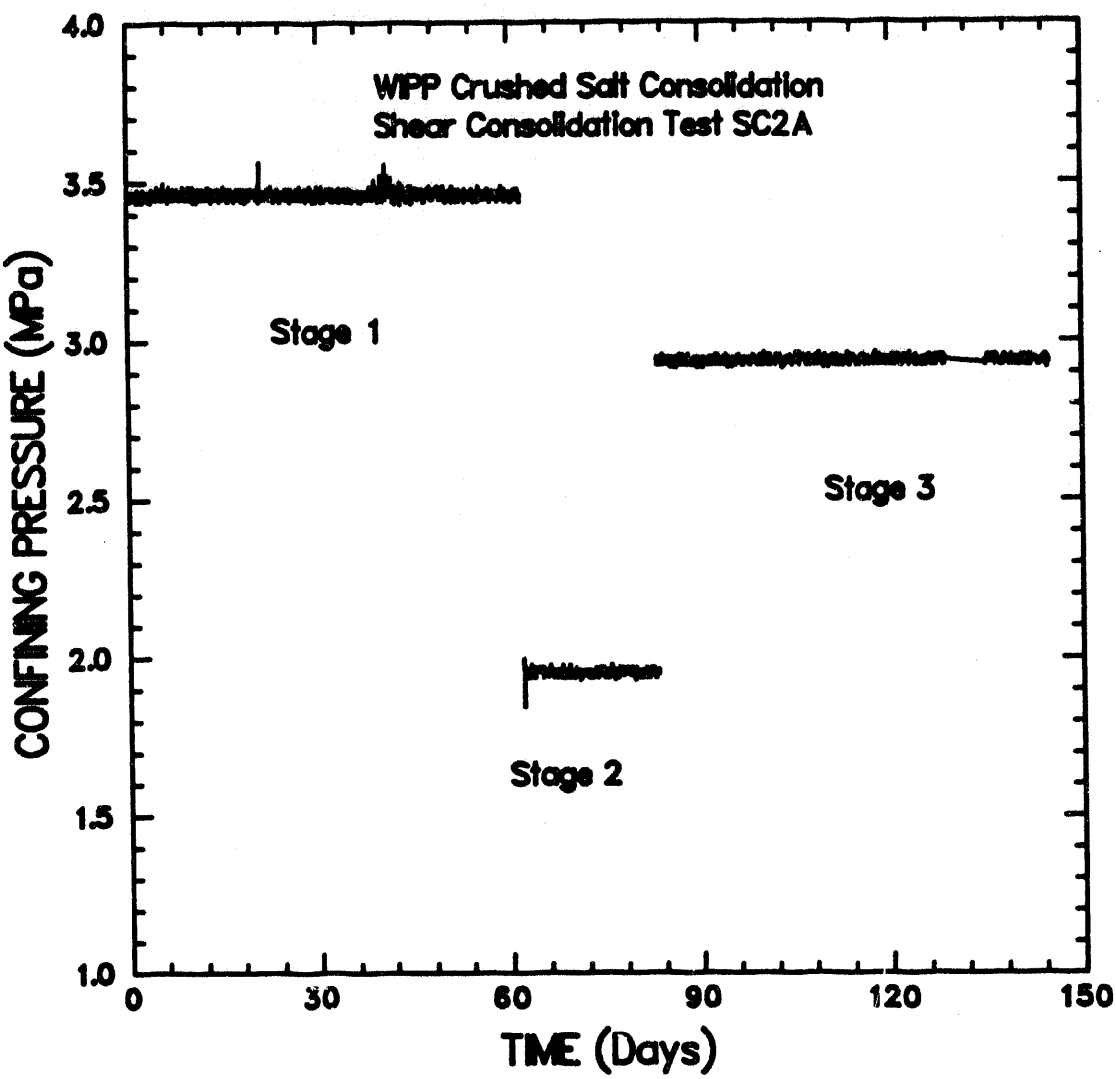

Figure H-8. Confining pressure-versus-time for Test SC2A.

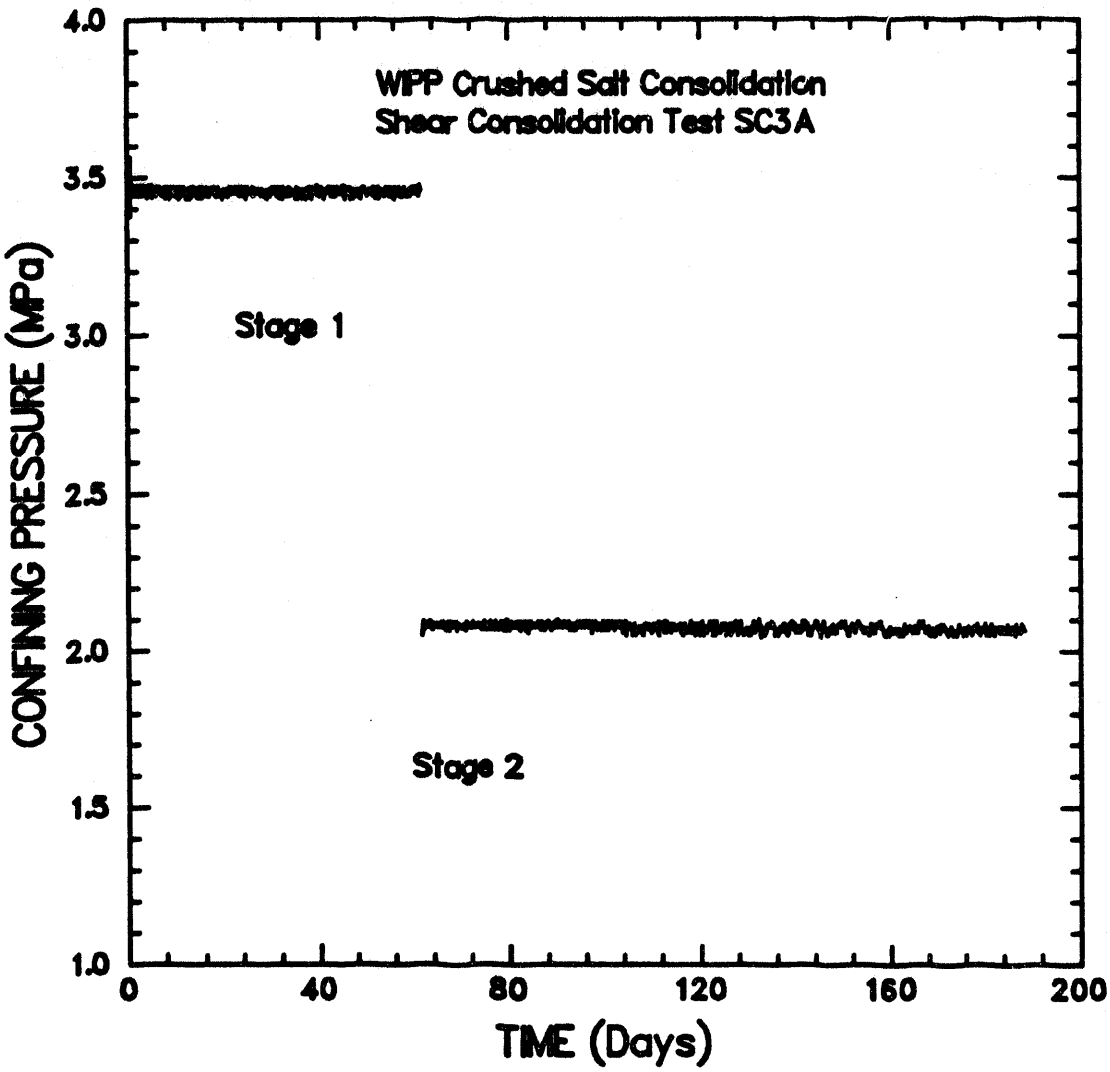

Figure H-9. Confining pressure-versus-time for Test SC3A.

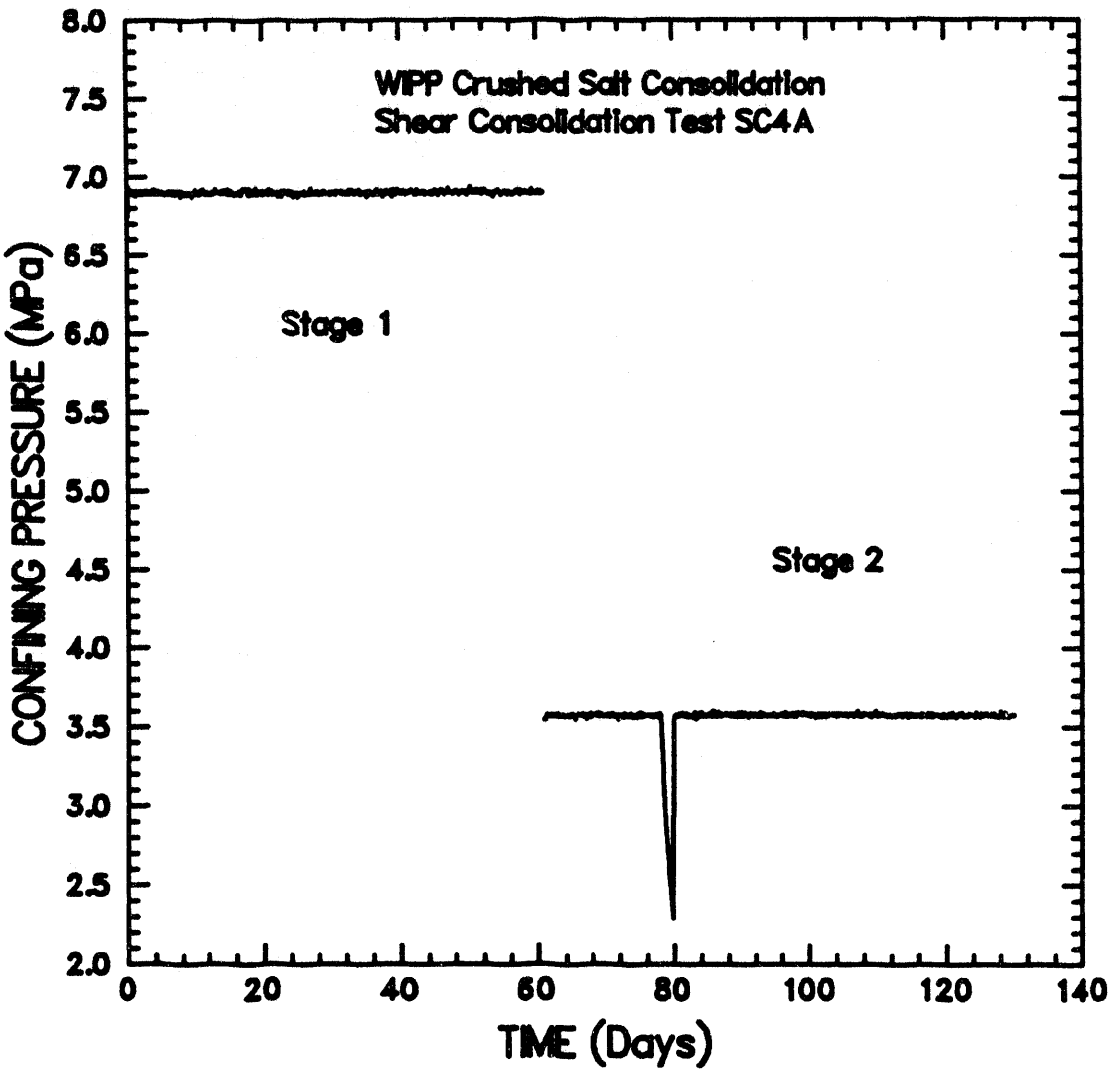

Figure H-10. Confining pressure-versus-time for Test SC4A.

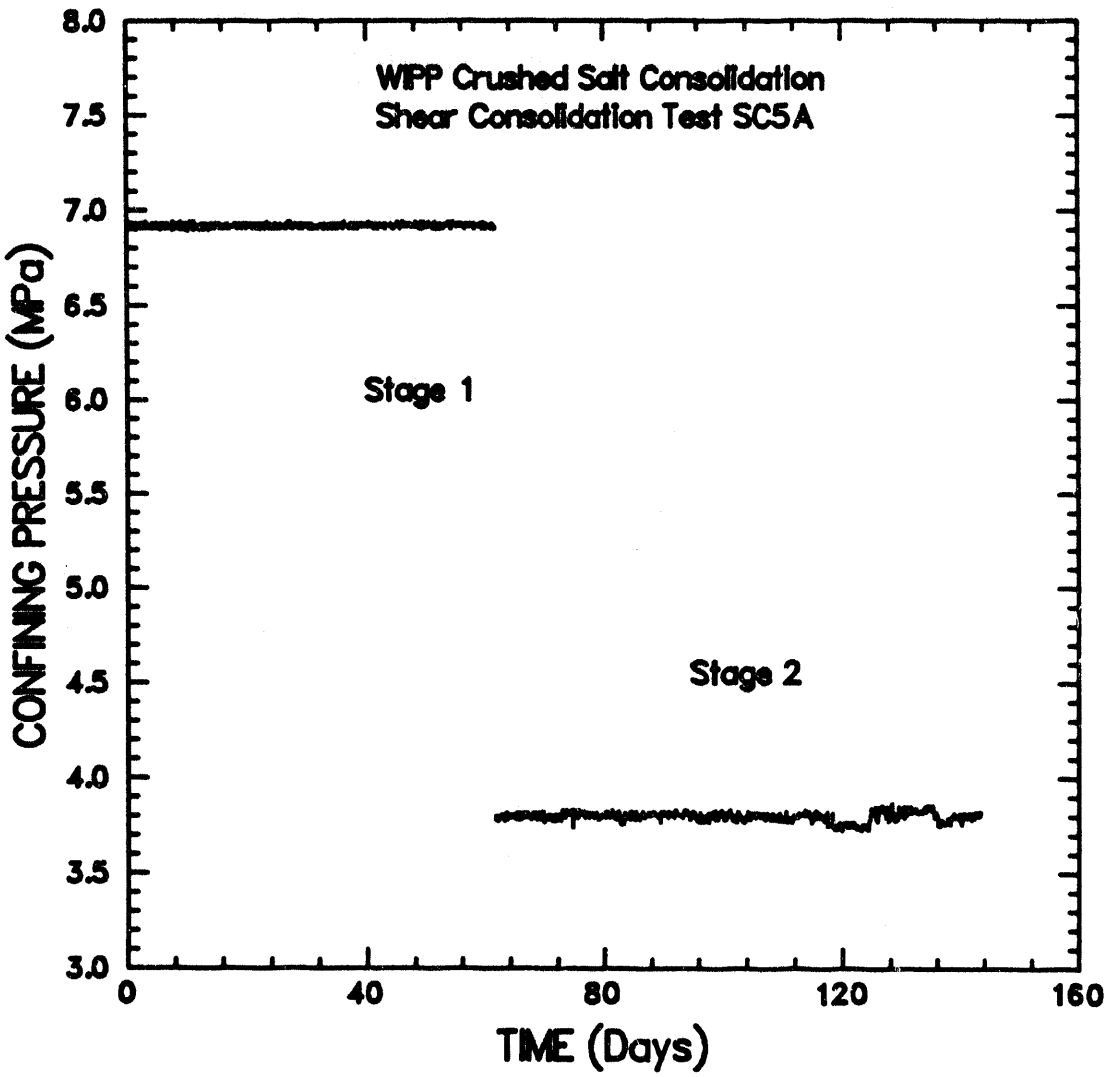

Figure H-11. Confining pressure-versus-time for Test SC5A.

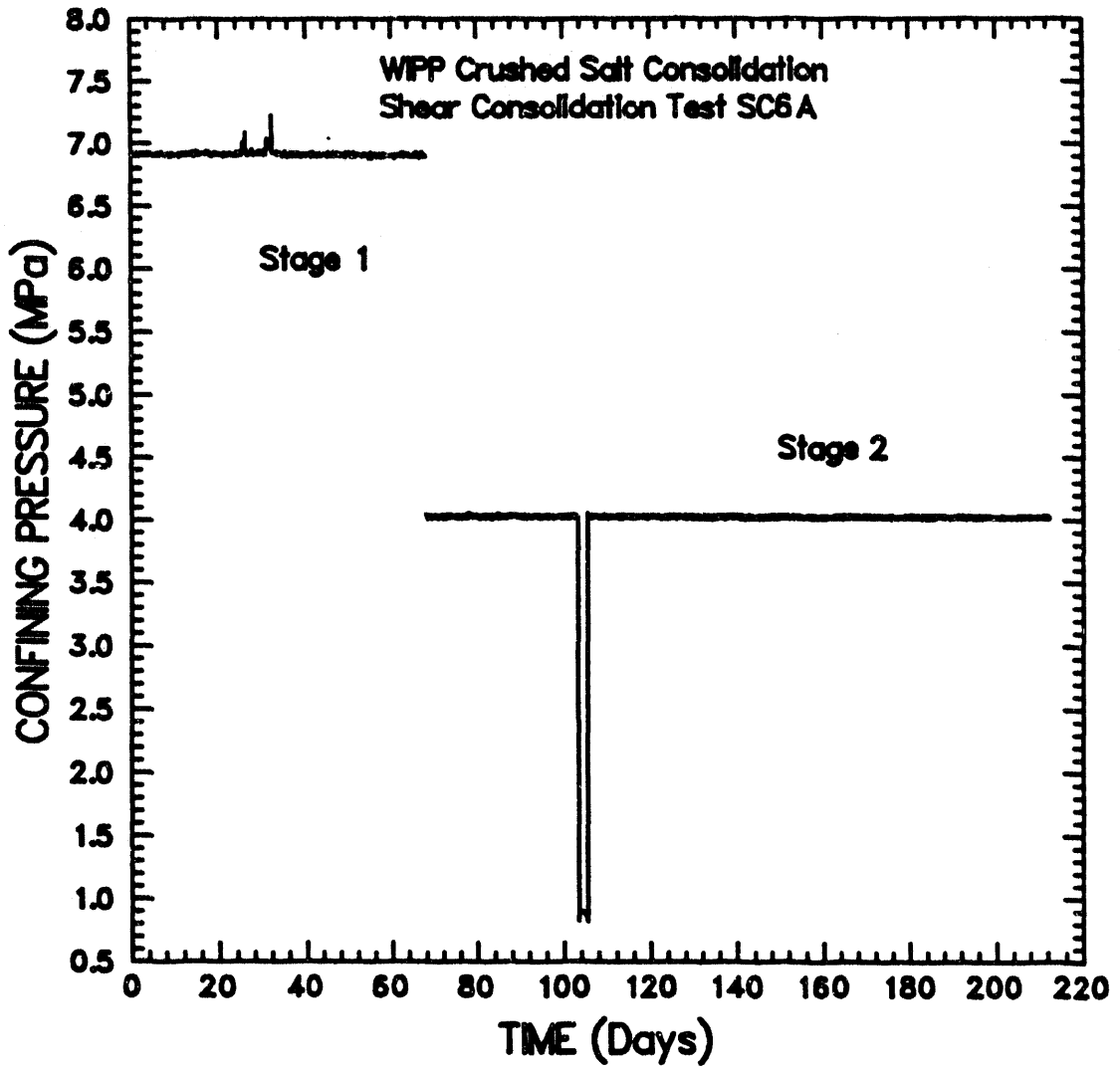

Figure H-12. Confining pressure-versus-time for Test SC6A.

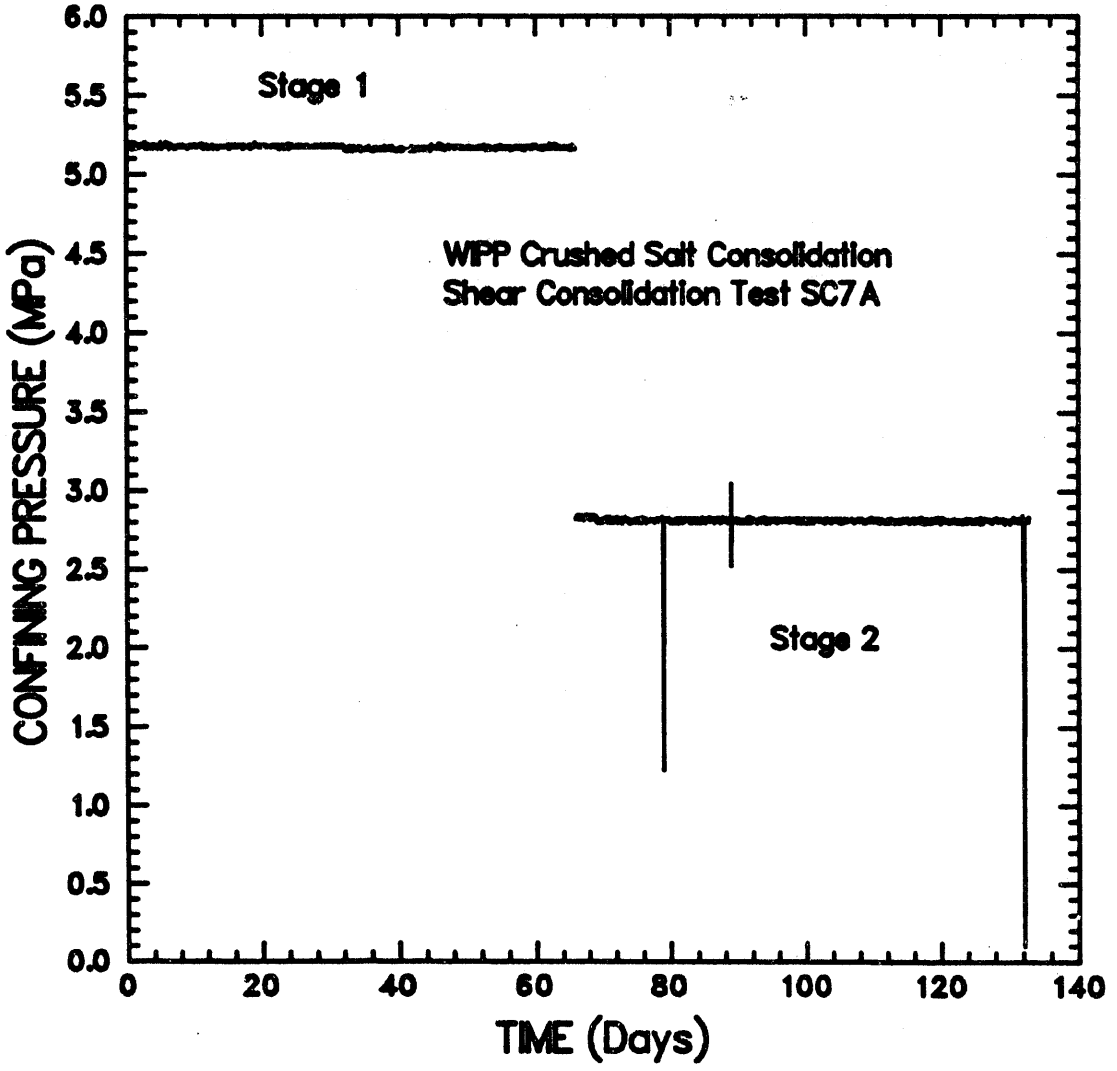

Figure H-13. Confining pressure-versus-time for Test SC7A.

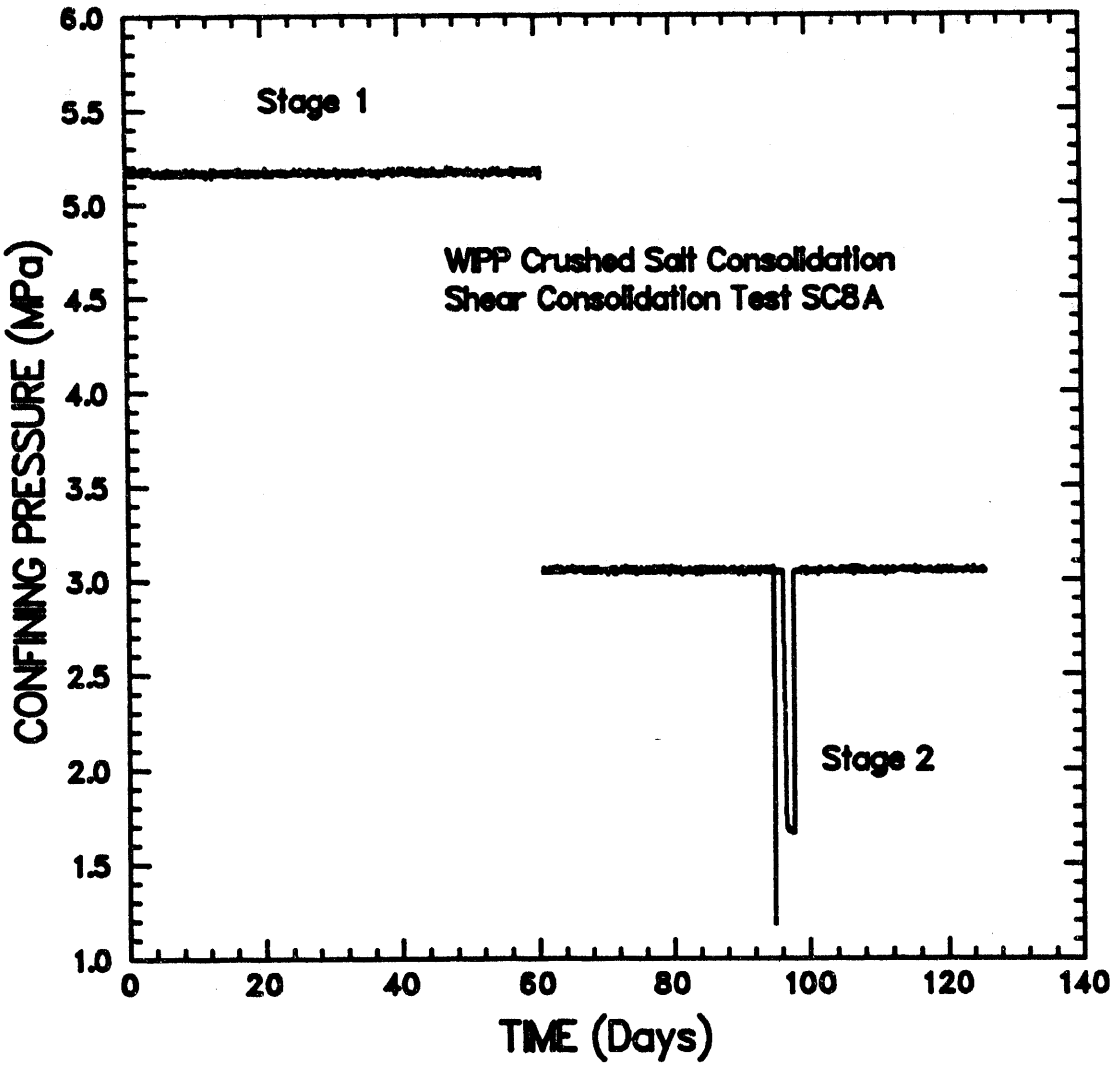

Figure H-14. Confining pressure-versus-time for Test SC8A.

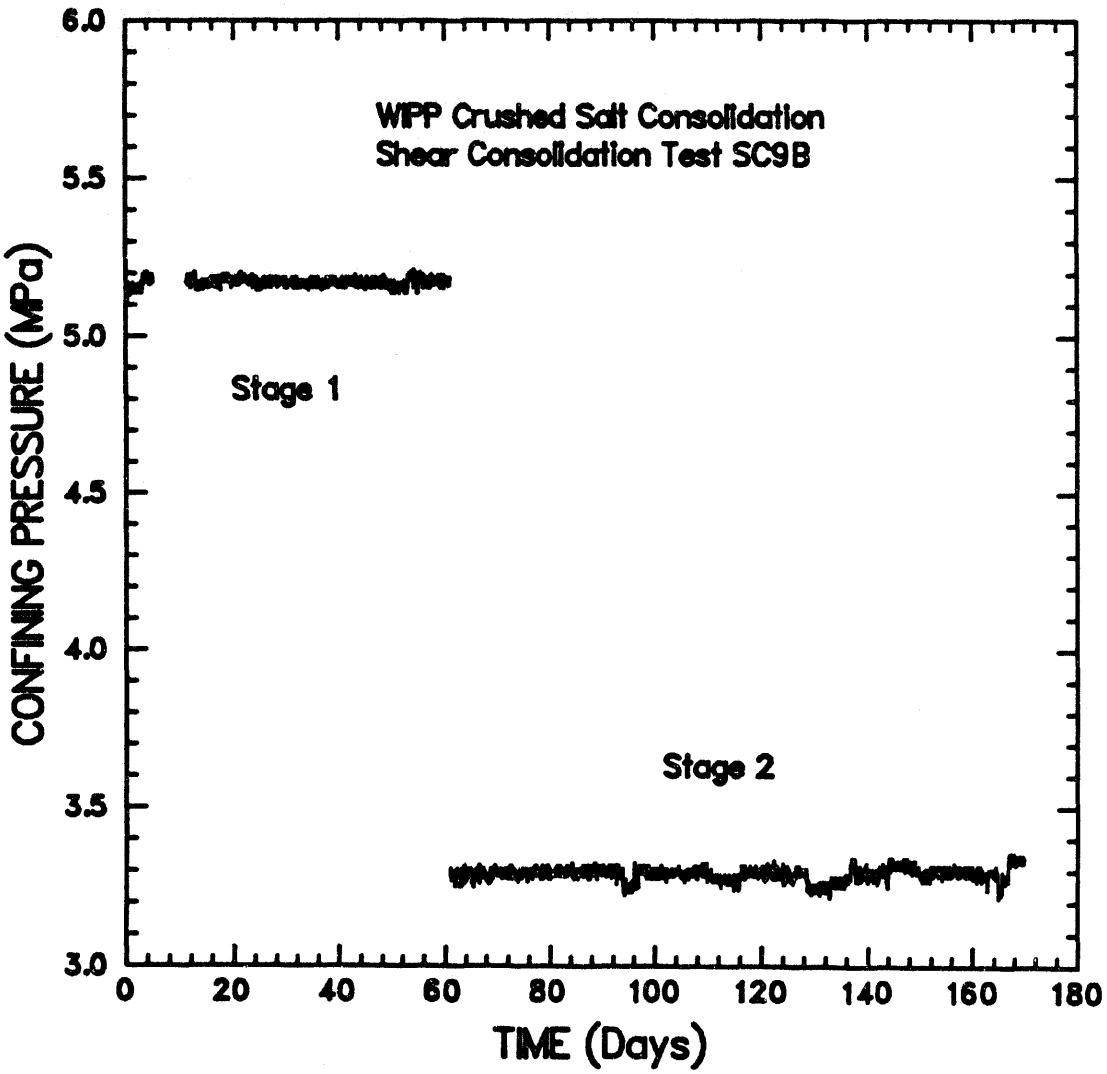

Figure H-15. Confining pressure-versus-time for Test SC9B.

APPENDIX I. TEMPERATURE STABILITY FOR ALL HYDROSTATIC AND SHEAR CONSOLIDATION TESTS

Figures

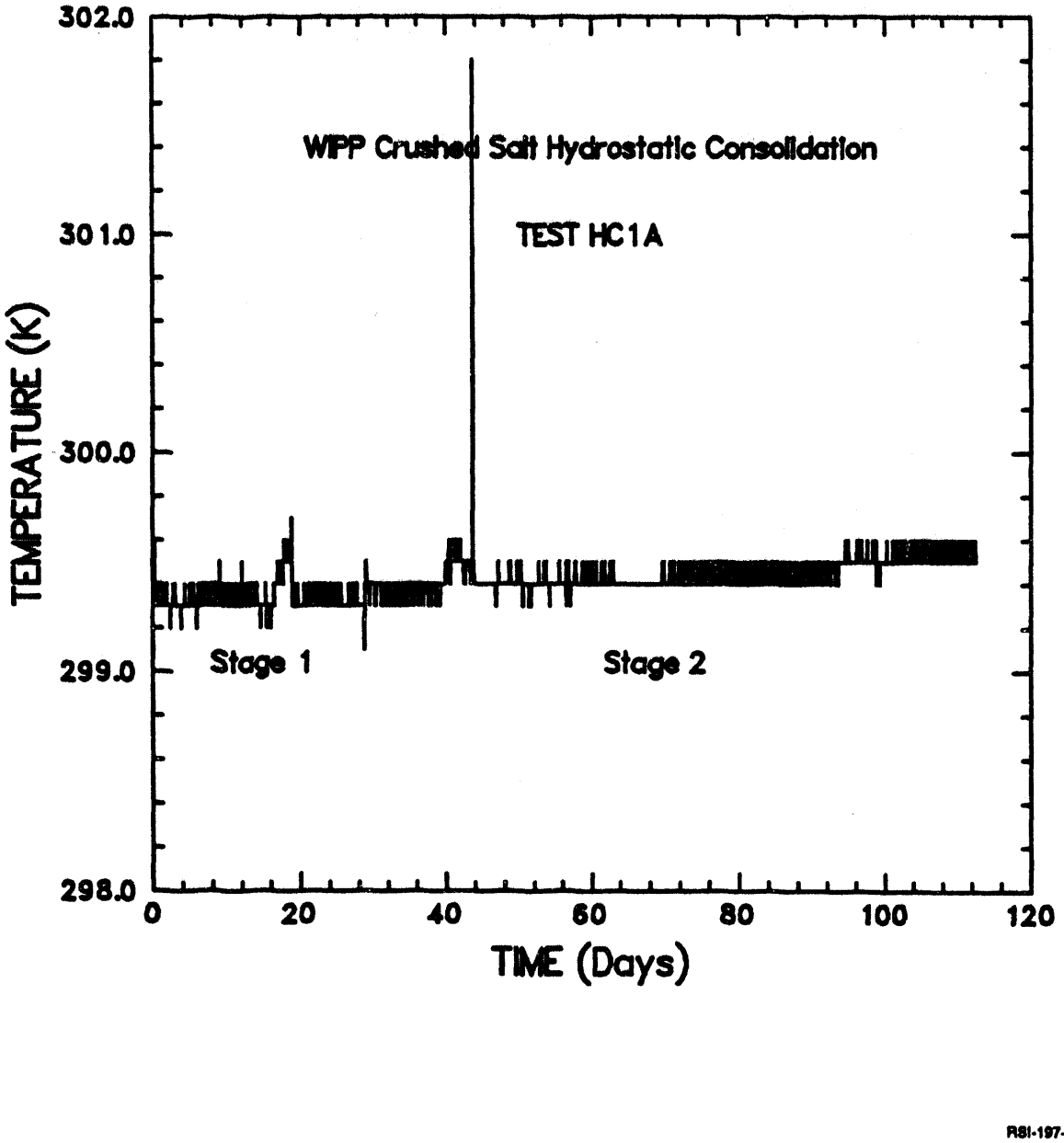

Figure I-1. Temperature-versus-time for Test HC1A.

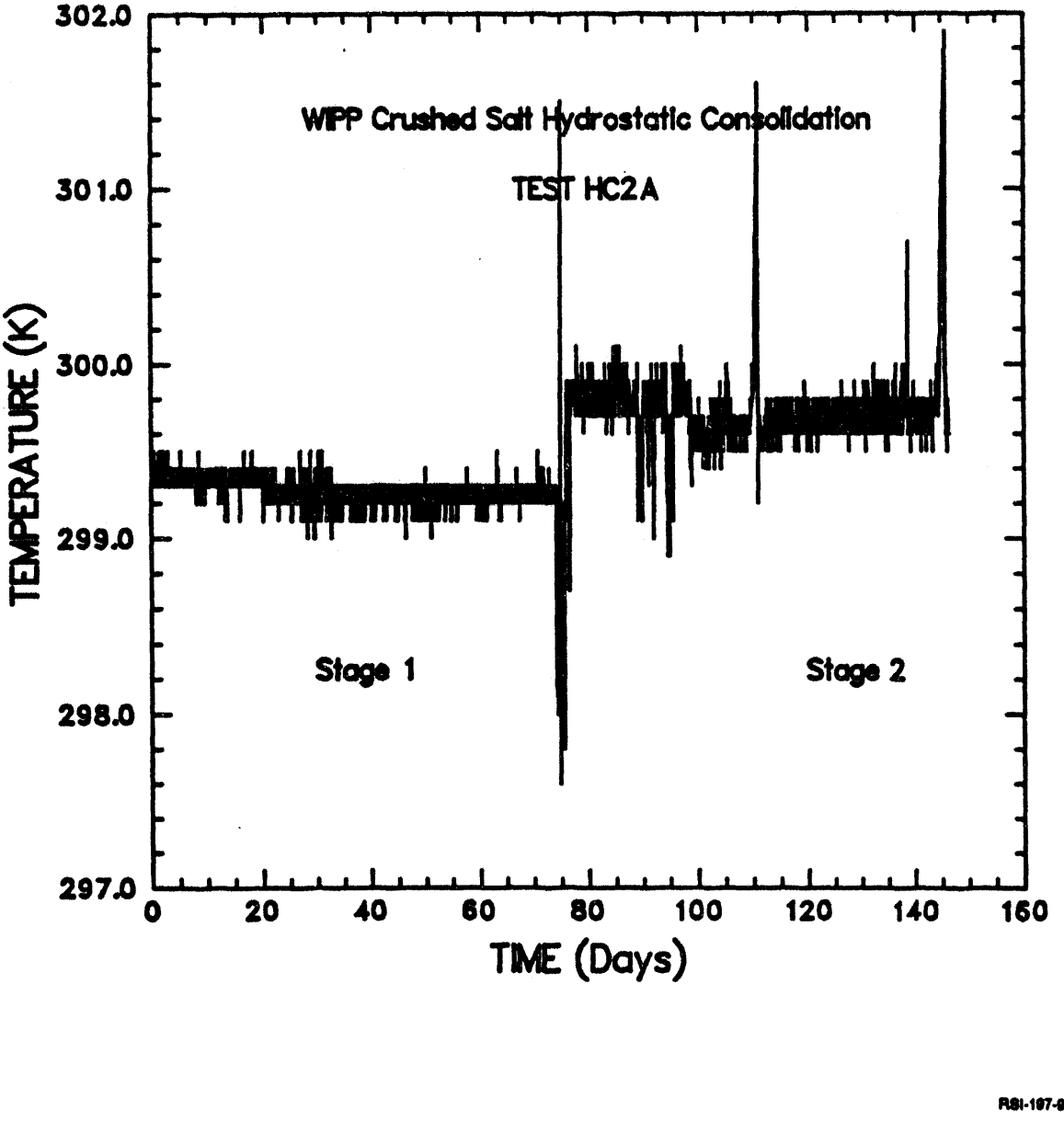

Figure I-2. Temperature-versus-time for Test HC2A.

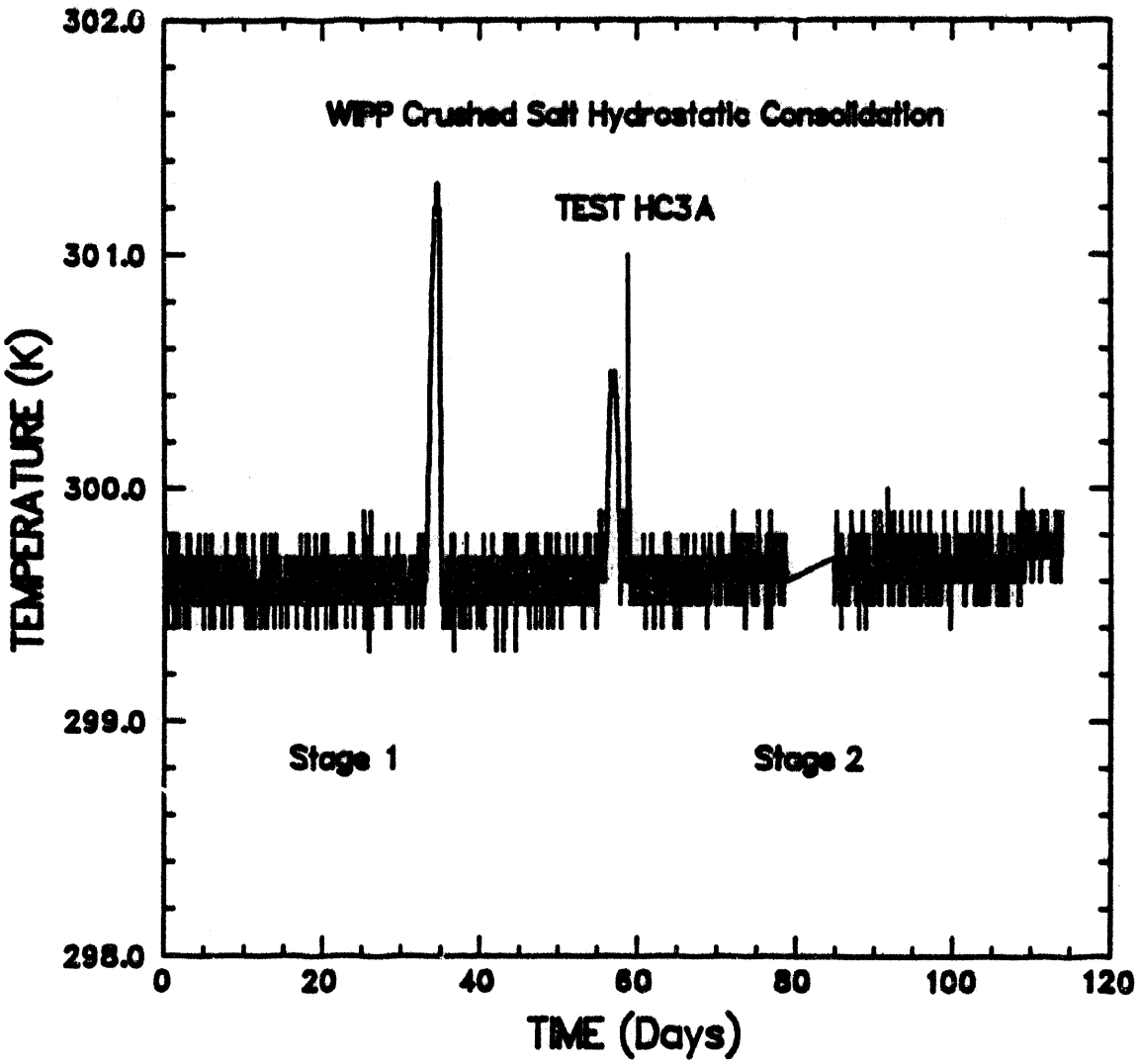

Figure I-3. Temperature-versus-time for Test HC3A.

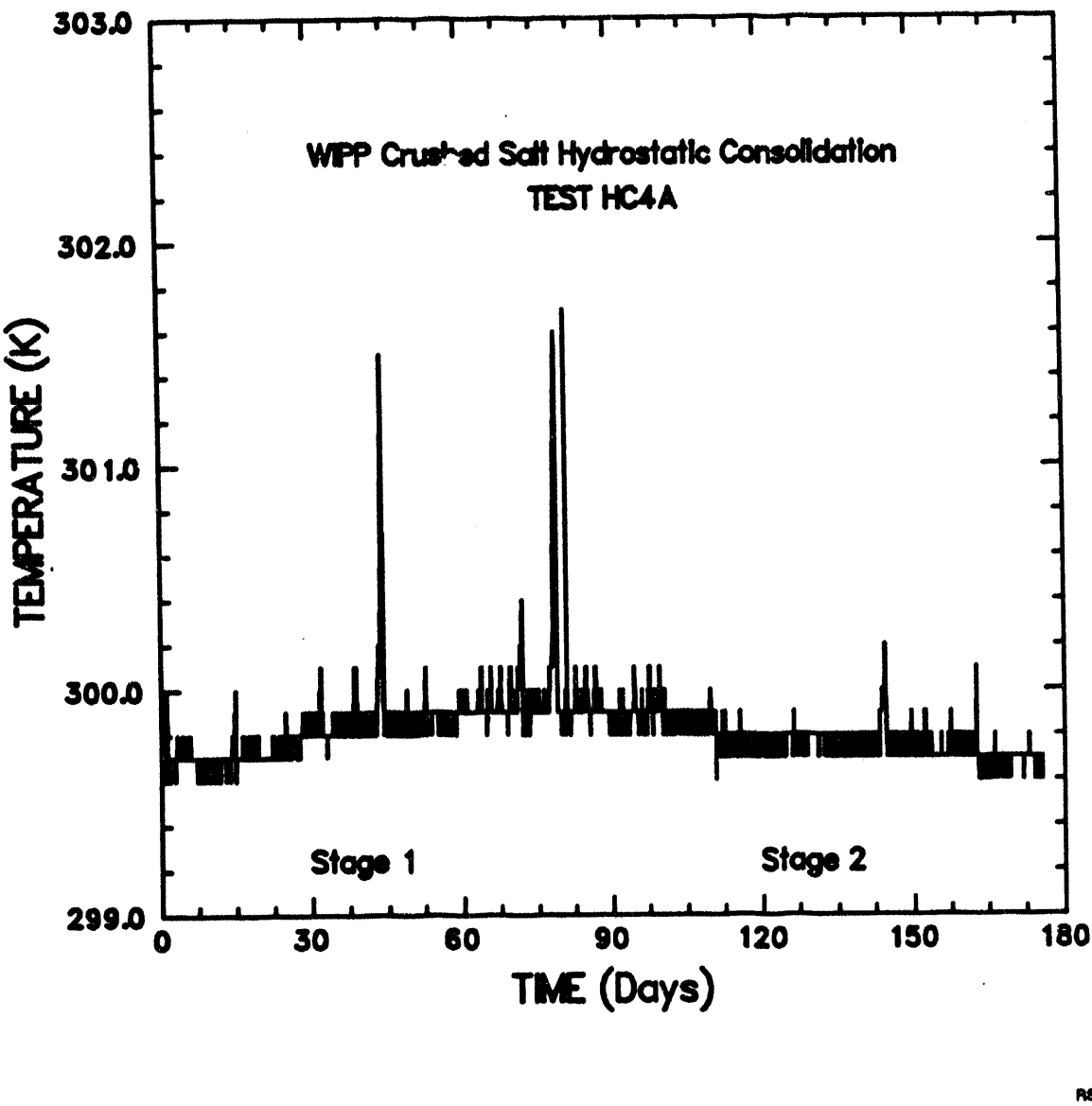

Figure I-4. Temperature-versus-time for Test HC4A.

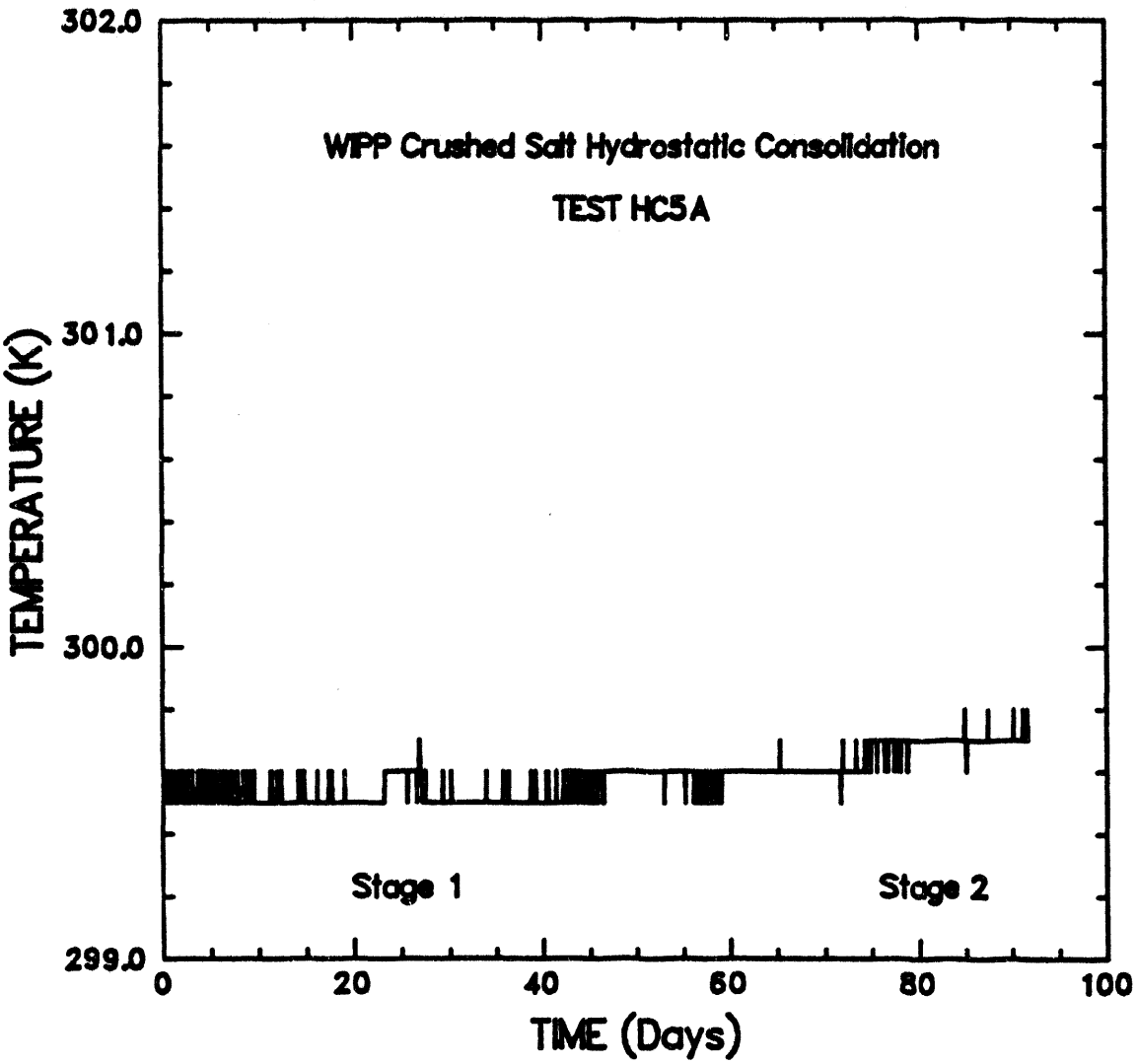

Figure I-5. Temperature-versus-time for Test HC5A.

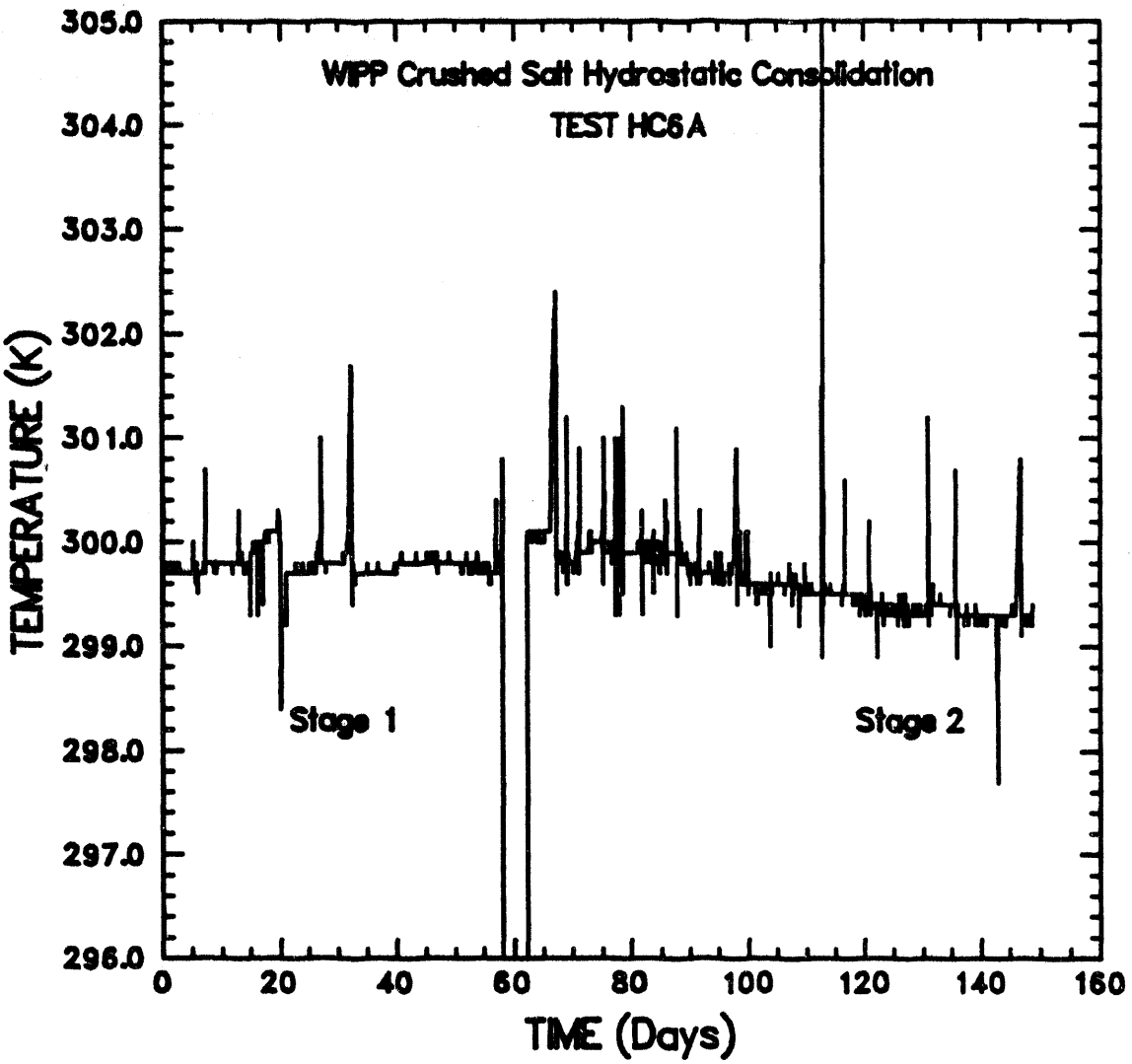

Figure I-6. Temperature-versus-time for Test HC6A.

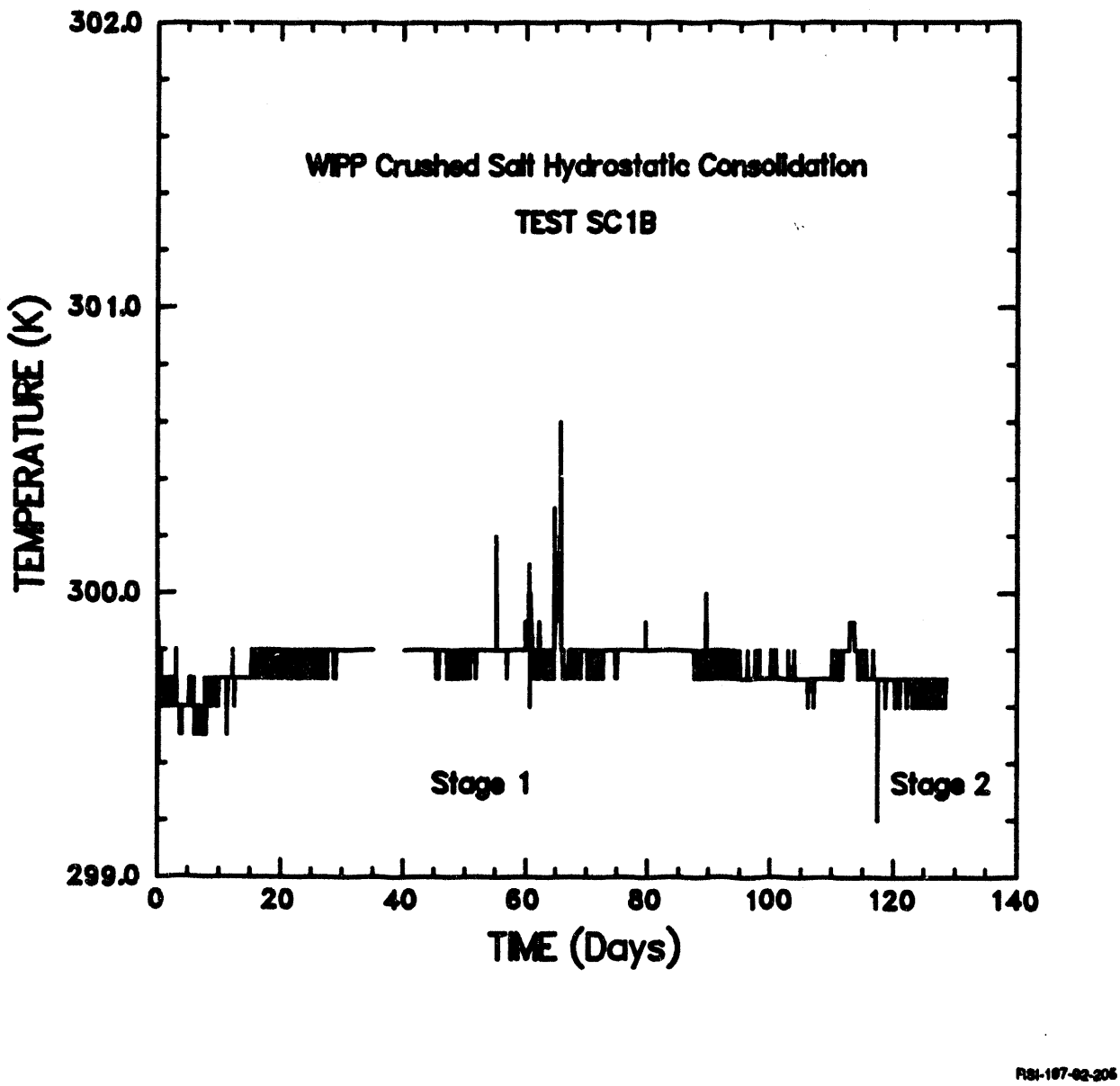

Figure I-7. Temperature-versus-time for Test SC1B.

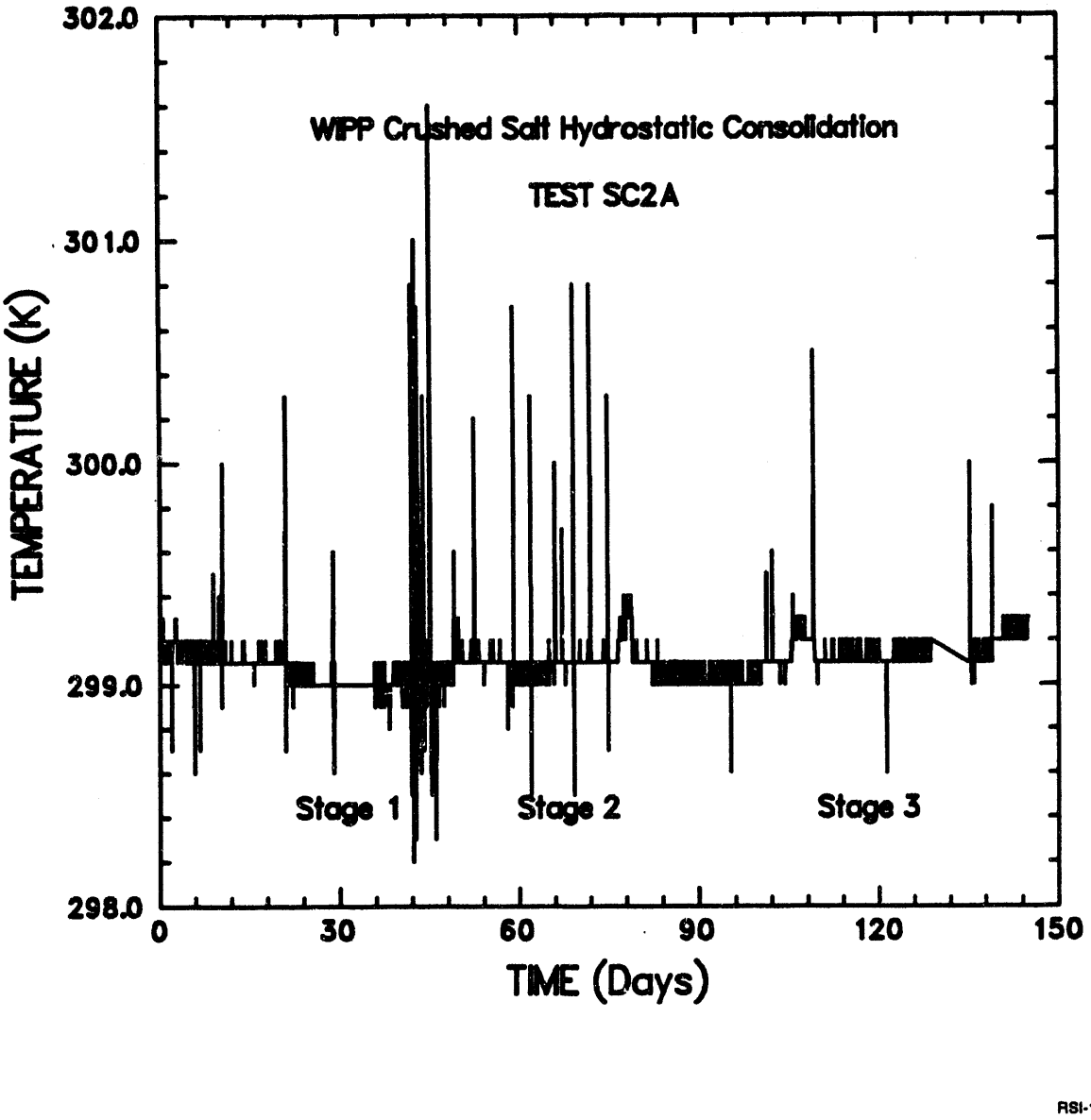

Figure I-8. Temperature-versus-time for Test SC2A.

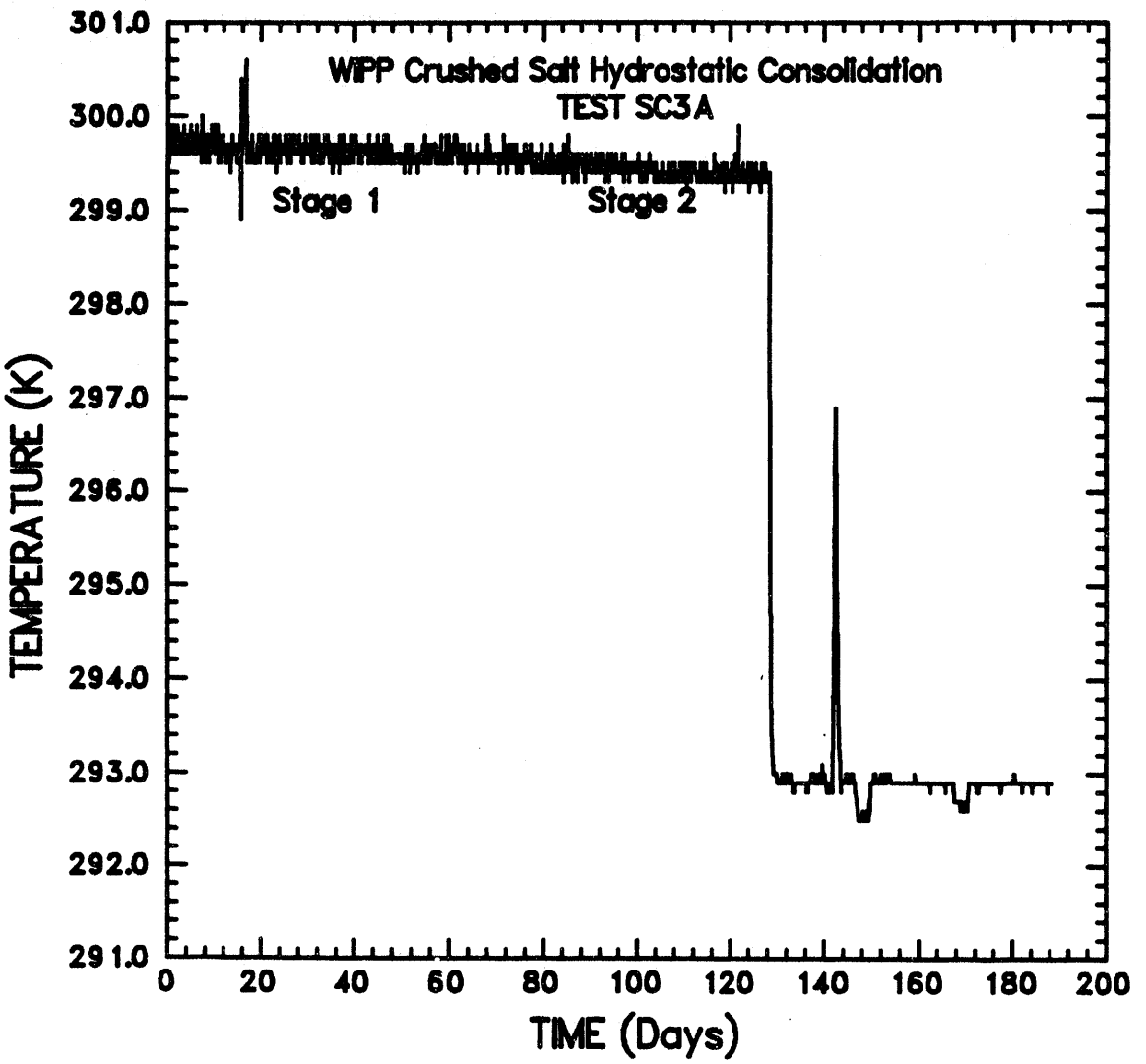

Figure I-9. Temperature-versus-time for Test SC3A. The temperature decrease at 124 days is due to an intentional shut-down of the pressure vessel heaters.

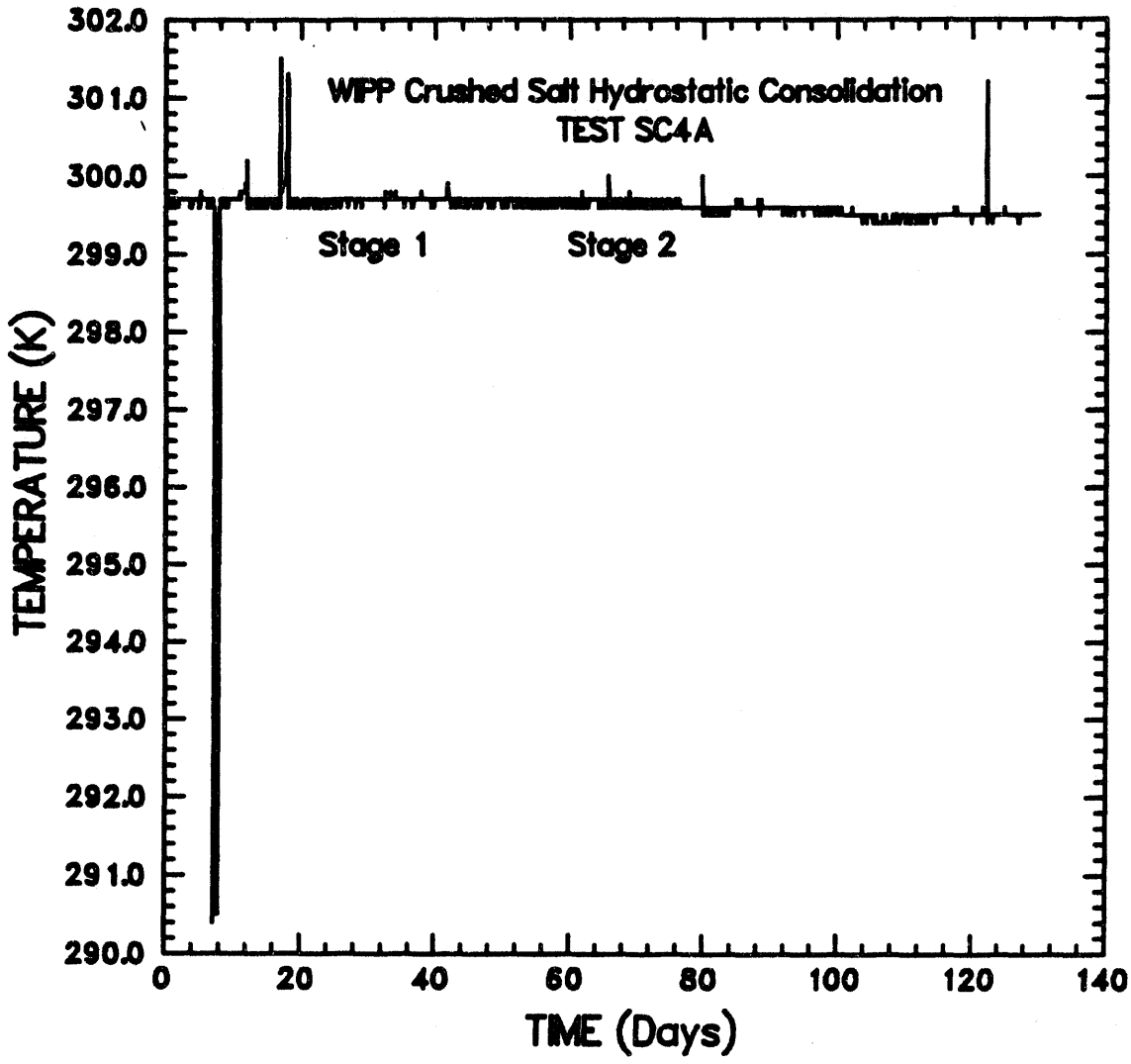

Figure I-10. Temperature-versus-time for Test SC4A.

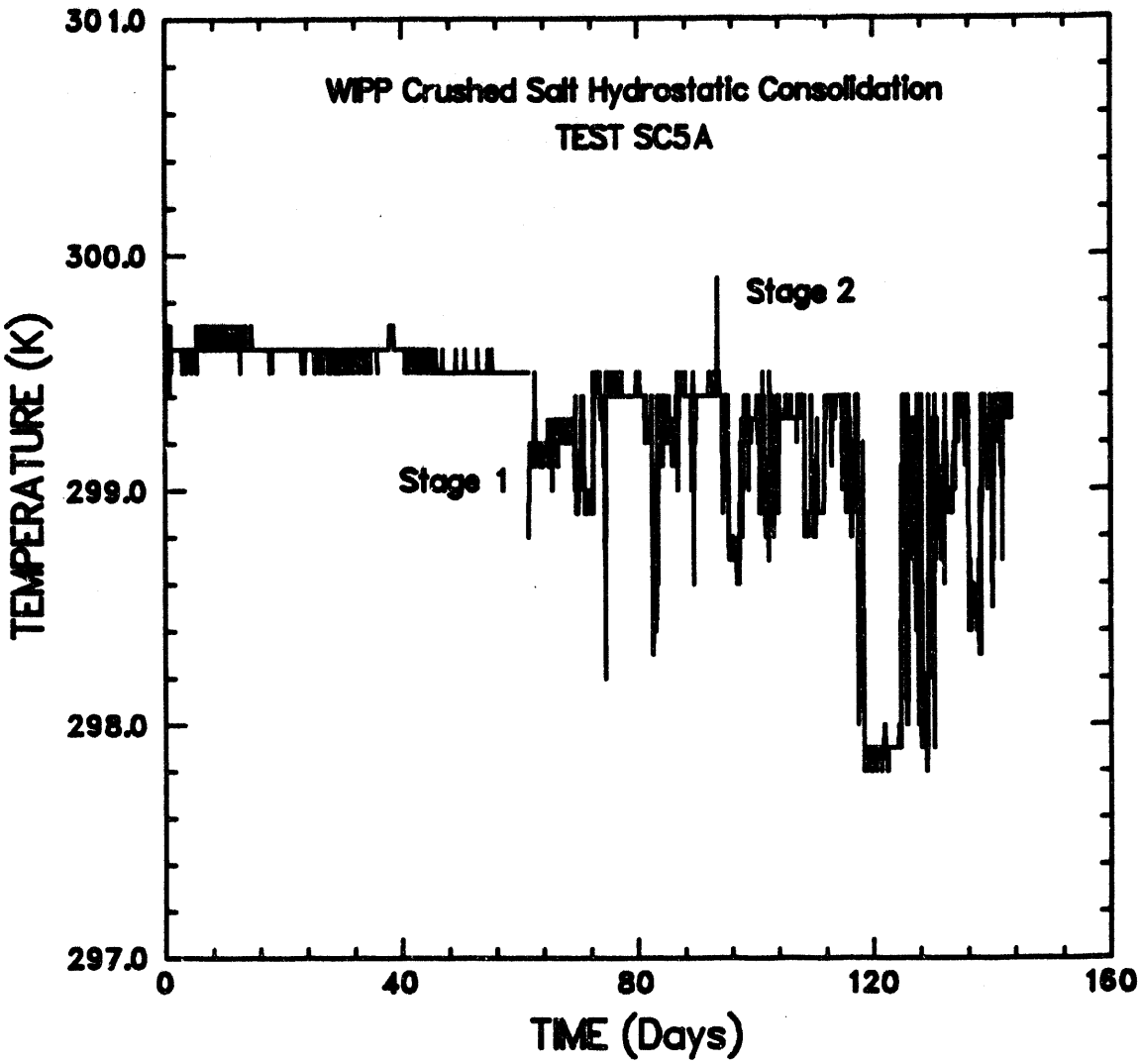

Figure I-11. Temperature-versus-time for Test SC5A.

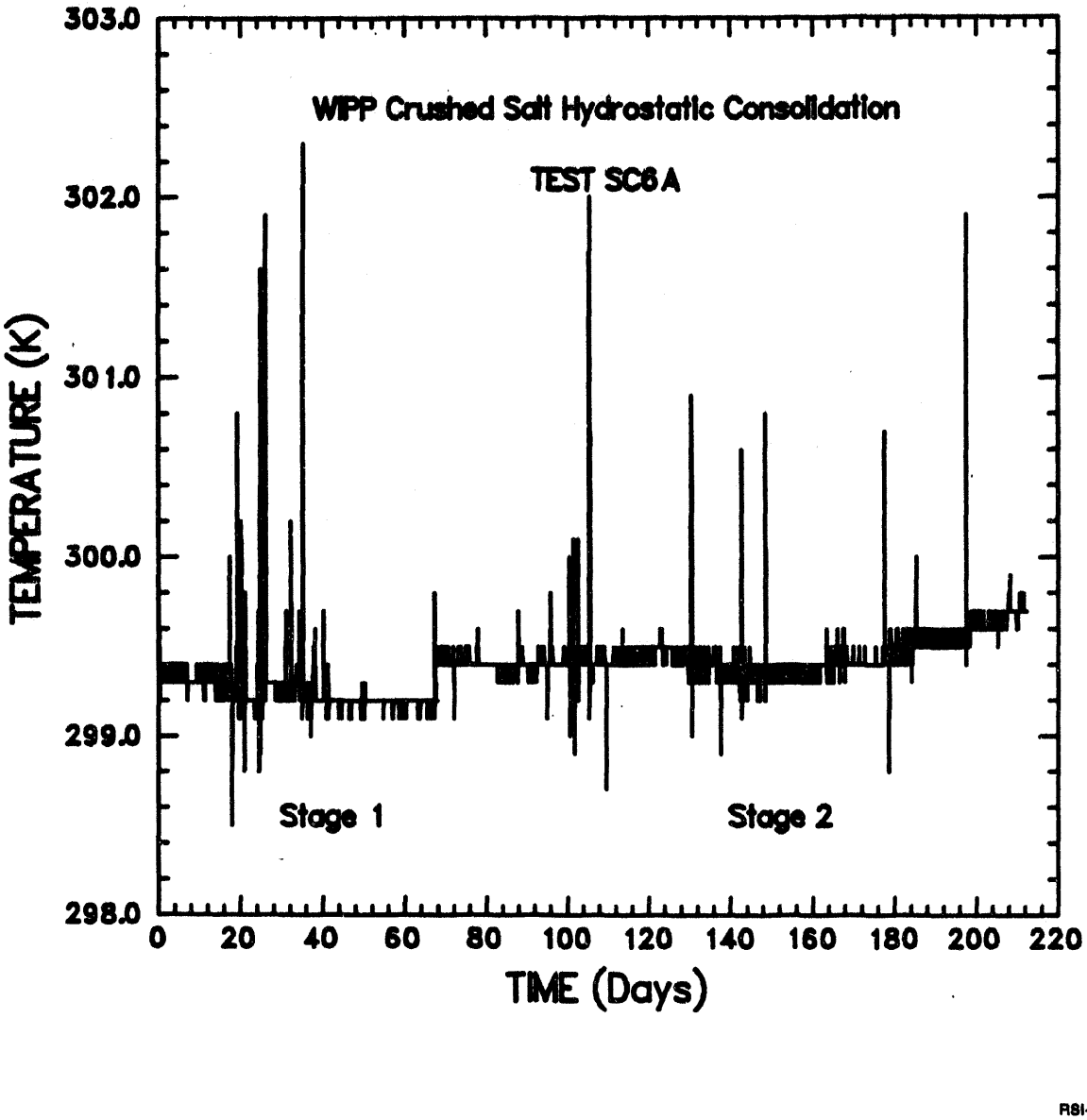

Figure I-12. Temperature-versus-time for Test SC6A.

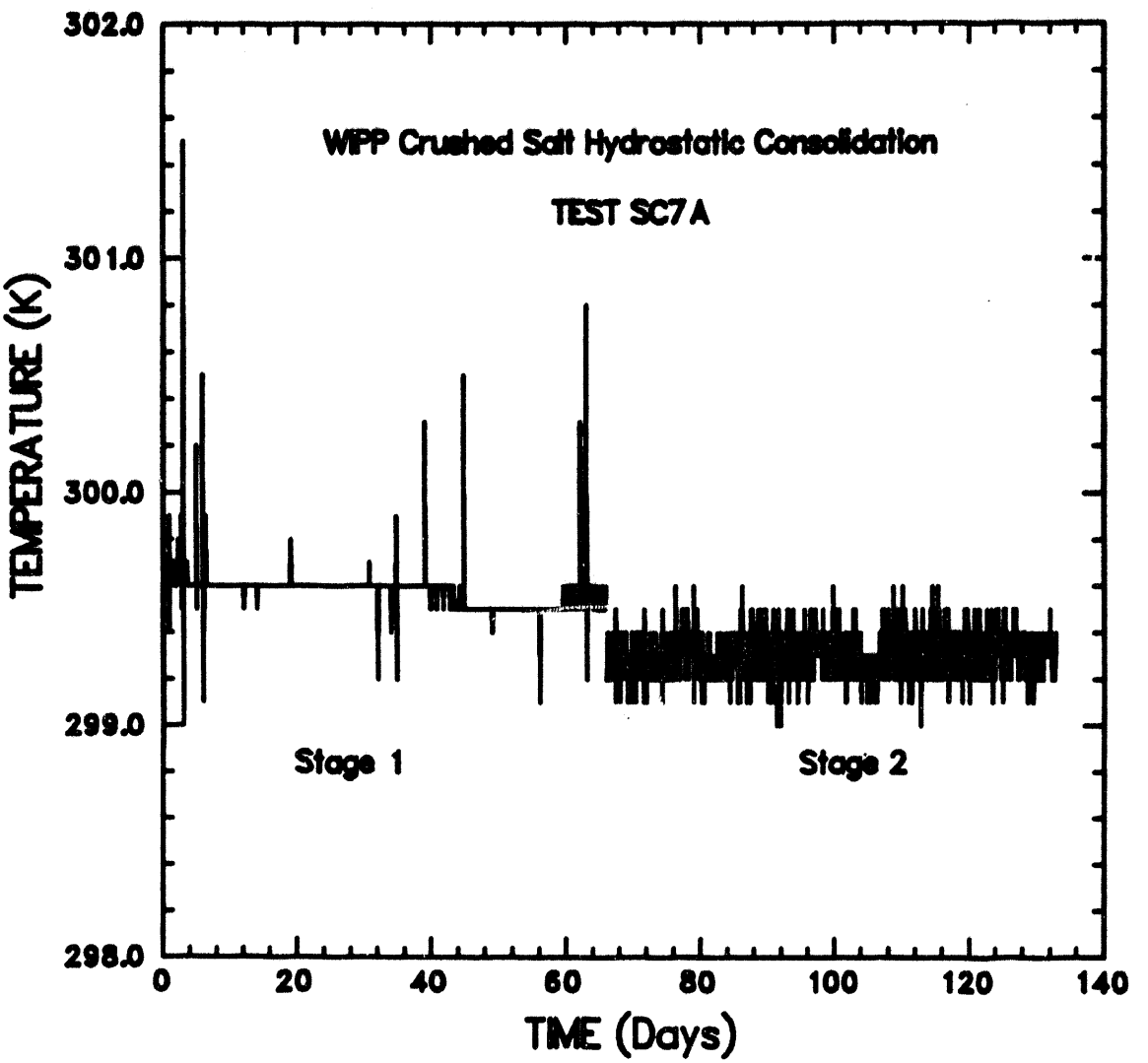

Figure I-13. Temperature-versus-time for Test SC7A.

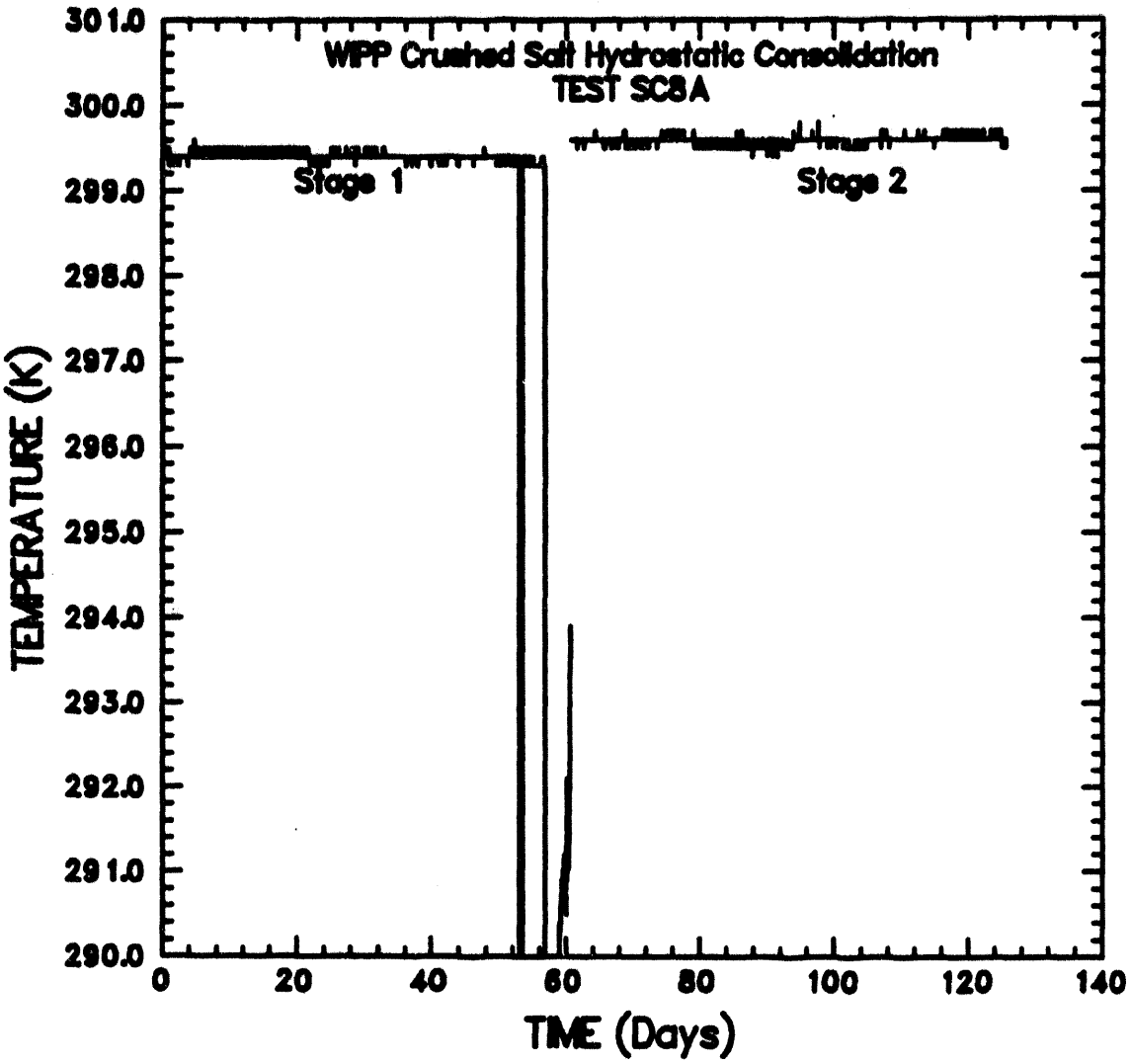

Figure I-14. Temperature-versus-time for Test SC8A.

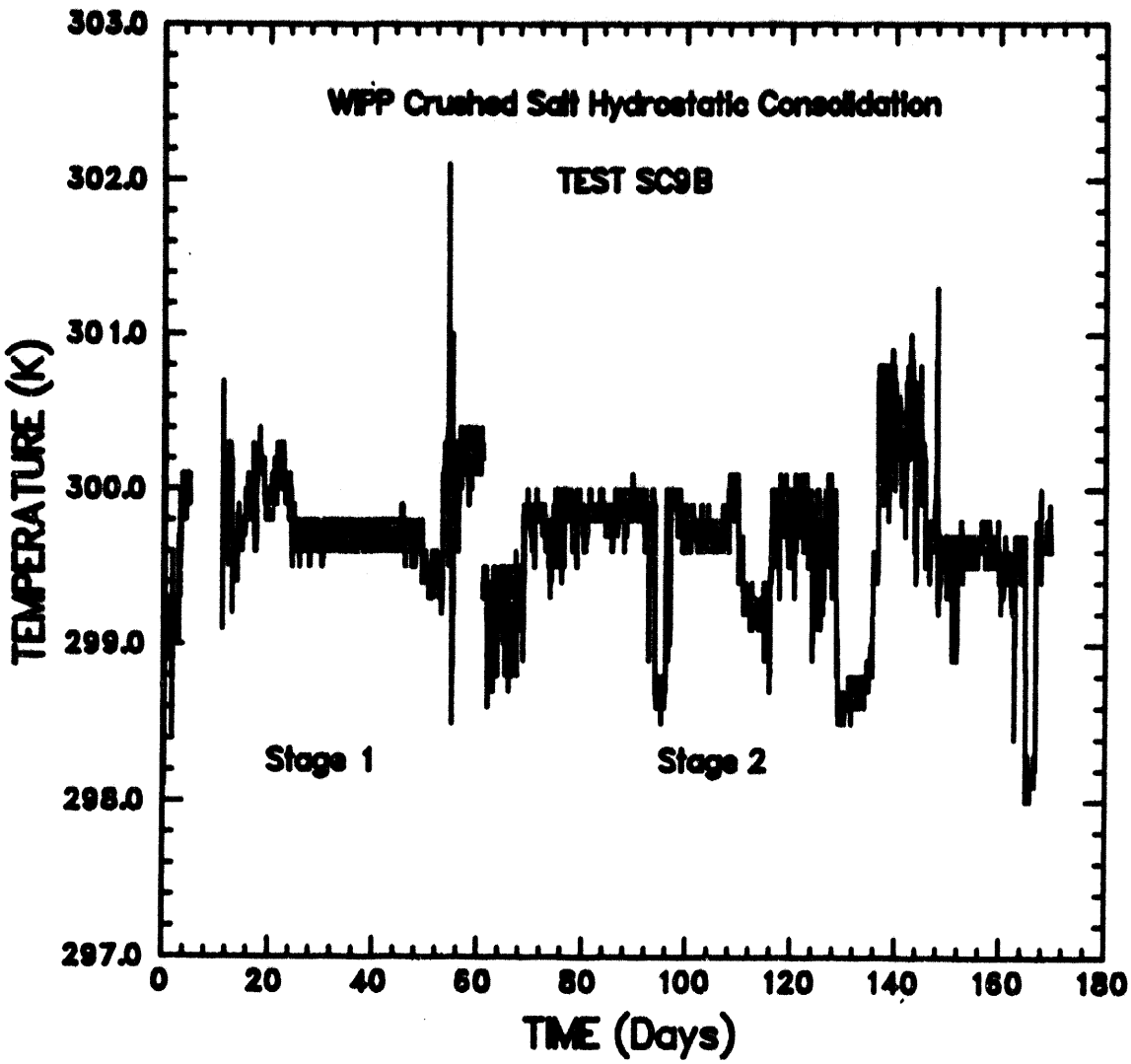

RSI-197-62-213

Figure I-15. Temperature-versus-time for Test SC9B.

DISTRIBUTION

Federal Agencies

US Department of Energy (6)
Office of Civilian Radioactive Waste Management
Attn: Deputy Director, RW-2
Associate Director, RW-10/50
Office of Program and Resources Management
Office of Contract Business Management
Director, RW-22
Analysis and Verification Division
Associate Director, RW-30
Office of Systems and Compliance
Associate Director, RW-40
Office of Storage and Transportation
Director, RW-4/5
Office of Strategic Planning and International Programs
Office of External Relations
Forrestal Building
Washington, DC 20585

US Department of Energy
Albuquerque Operations Office
Attn: National Atomic Museum Library
PO Box 5400
Albuquerque, NM 87185-5400

US Department of Energy (4)
WIPP Project Integration Office
Attn: W.J. Arthur III
L.W. Gage
P.J. Higgins
D.A. Olona
PO Box 5400
Albuquerque, NM 87115-5400

US Department of Energy (2)
WIPP Project Integration Satellite Office
Attn: R. Batra
R. Becker
PO Box 3090, Mail Stop 525
Carlsbad, NM 88221-3090

US Department of Energy
Research & Waste Management Division
Attn: Director
PO Box E
Oak Ridge, TN 37831

US Department of Energy (3)
WIPP Project Site Office (Carlsbad)
Attn: V. Daub
J. Lippis
J.A. Mewhinney
PO Box 3090
Carlsbad, NM 88221-3090

US Department of Energy
Attn: E. Young
Room E-178
GAO/RCED/GTN
Washington, DC 20545

US Department of Energy
Office of Environmental Restoration and Waste Management
Attn: J. Lytle, EM-30,
Trevion II
Washington, DC 20585-0002

US Department of Energy (3)
Office of Environmental Restoration and Waste Management
Attn: M. Frei, EM-34,
Trevion II
Washington, DC 20585-0002

US Department of Energy
Office of Environmental Restoration and Waste Management
Attn: S. Schneider, EM-342,
Trevion II
Washington, DC 20585-0002

US Department of Energy (2)
Office of Environment, Safety and Health
Attn: C. Borgstrom, EH-25
R. Pelletier, EH-231
Washington, DC 20585

US Department of Energy (2)
Idaho Operations Office
Fuel Processing and Waste Management Division
785 DOE Place
Idaho Falls, ID 83402

US Environmental Protection Agency (2)
Radiation Protection Programs
Attn: M. Oge
ANR-460
Washington, DC 20460

US Geological Survey (2)
Water Resources Division
Attn: R. Livingston
4501 Indian School NE
Suite 200
Albuquerque, NM 87110

US Nuclear Regulatory Commission
Division of Waste Management
Attn: H. Marson
Mail Stop 4-H-3
Washington, DC 20555

Boards

Defense Nuclear Facilities Safety Board
Attn: D. Winters
625 Indiana Ave. NW, Suite 700
Washington, DC 20004

Nuclear Waste Technical Review Board (2)
Attn: Chairman
S.J.S. Parry
1100 Wilson Blvd., Suite 910
Arlington, VA 22209-2297

Advisory Committee on Nuclear Waste
Nuclear Regulatory Commission
Attn: R. Major
7920 Norfolk Ave.
Bethesda, MD 20814

State Agencies

Environmental Evaluation Group (3)
Attn: Library
7007 Wyoming NE
Suite F-2
Albuquerque, NM 87109

NM Bureau of Mines and Mineral Resources
Socorro, NM 87801

NM Energy, Minerals, and Natural Resources Department
Attn: Library
2040 S. Pacheco
Santa Fe, NM 87505

NM Environment Department (3)
Secretary of the Environment
Attn: J. Espinosa
1190 St. Francis Drive
Santa Fe, NM 87503-0968

NM Environment Department
WIPP Project Site
Attn: P. McCasland
PO Box 3090
Carlsbad, NM 88221

Laboratories/Corporations

Battelle Pacific Northwest Laboratories
Attn: R.E. Westerman
MSIN P8-44
Battelle Blvd.
Richland, WA 99352

INTERA Inc.
Attn: J.F. Pickens
6850 Austin Center Blvd.
Suite 300
Austin, TX 78731

INTERA Inc.
Attn: W. Stensrud
PO Box 2123
Carlsbad, NM 88221

IT Corporation
Attn: R.F. McKinney
Regional Office
5301 Central NE
Suite 700
Albuquerque, NM 87108

Los Alamos National Laboratory
Attn: B. Erdal, INC-12
PO Box 1663
Los Alamos, NM 87544

RE/SPEC, Inc.
Attn: W. Coons
4775 Indian School NE
Suite 300
Albuquerque, NM 87110-3927

RE/SPEC, Inc.
Attn: J.L. Ratigan
PO Box 725
Rapid City, SD 57709

Southwest Research Institute (2)
Center for Nuclear Waste Regulatory Analysis
Attn: P.K. Nair
6220 Culebra Road
San Antonio, TX 78228-0510

SAIC
Attn: H.R. Pratt
10260 Campus Point Dr.
San Diego, CA 92121

SAIC (2)
Attn: M. Davis
J. Tollison
2109 Air Park Rd. SE
Albuquerque, NM 87106

Tech Reps Inc. (3)
Attn: J. Chapman
C. Crawford
T. Peterson
5000 Marble NE, Suite 222
Albuquerque, NM 87110

TRW Environmental Safety Systems
Attn: L. Wildman
2650 Park Tower Dr., Suite 1300
Vienna, VA 22180-7306

Westinghouse Electric Corporation (5)
Attn: Library
C. Cox
L. Fitch
B.A. Howard
R. Kehrman
PO Box 2078
Carlsbad, NM 88221

Westinghouse-Savannah River
Technology Center (4)
Attn: N. Bibler
J.R. Harbour
M.J. Plodinec
G.G. Wicks
Aiken, SC 29802

National Academy of Sciences, WIPP Panel

Howard Adler
Oak Ridge Associated Universities
Medical Sciences Division
PO Box 117
Oak Ridge, TN 37831-0117

Ina Alterman
Board on Radioactive Waste
Management, GF456
2101 Constitution Ave.
Washington, DC 20418

Fred M. Ernsberger
250 Old Mill Road
Pittsburgh, PA 15238

John D. Bredehoeft
Western Region Hydrologist
Water Resources Division
US Geological Survey (M/S 439)
345 Middlefield Road
Menlo Park, CA 94025

Rodney C. Ewing
Department of Geology
University of New Mexico
Albuquerque, NM 87131

Charles Fairhurst, Chairman
Department of Civil and Mineral
Engineering
University of Minnesota
500 Pillsbury Dr. SE
Minneapolis, MN 55455-0220

B. John Garrick
PLG Incorporated
4590 MacArthur Blvd., Suite 400
Newport Beach, CA 92660-2027

Leonard F. Konikow
US Geological Survey
431 National Center
Reston, VA 22092

Carl A. Anderson, Director
Board on Radioactive Waste Management
National Research Council
HA 456
2101 Constitution Ave. NW
Washington, DC 20418

Jeremiah O'Driscoll
Jody Incorporated
505 Valley Hill Drive
Atlanta, GA 30350

Christopher G. Whipple
Clement International
160 Spear St., Suite 1380
San Francisco, CA 94105

Individuals

P. Drez
8816 Cherry Hills Rd. NE
Albuquerque, NM 87111

D.W. Powers
Star Route Box 87
Anthony, TX 79821

Universities

University of New Mexico
Geology Department
Attn: Library
Albuquerque, NM 87131

University of Washington
College of Ocean and
Fishery Sciences
Attn: G.R. Heath
583 Henderson Hall
Seattle, WA 98195

Libraries

Thomas Brannigan Library
Attn: D. Dresp
106 W. Hadley St.
Las Cruces, NM 88001

Government Publications Department
Zimmerman Library
University of New Mexico
Albuquerque, NM 87131

New Mexico Junior College
Pannell Library
Attn: R. Hill
Lovington Highway
Hobbs, NM 88240

New Mexico State Library
Attn: N. McCallan
325 Don Gaspar
Santa Fe, NM 87503

New Mexico Tech
Martin Speere Memorial Library
Campus Street
Socorro, NM 87810

WIPP Public Reading Room
Carlsbad Public Library
Attn: Director
101 S. Halagueno St.
Carlsbad, NM 88220

Foreign Addresses

Studiecentrum Voor Kernenergie
Centre d'Énergie Nucléaire
Attn: A. Bonne
SCK/CEN Boeretang 200
B-2400 Mol, BELGIUM

Atomic Energy of Canada, Ltd. (3)
Whiteshell Laboratories
Attn: B. Goodwin
M. Stevens
D. Wushke
Pinewa, Manitoba, CANADA ROE 1LO

Francois Chenevier (2)
ANDRA
Route du Panorama Robert Schumann
B.P. 38
92266 Fontenay-aux-Roses, Cedex
FRANCE

Jean-Pierre Olivier
OECD Nuclear Energy Agency
Division of Radiation Protection and
Waste Management
38, Boulevard Suchet
75016 Paris, FRANCE

Claude Sombret
Centre d'Études Nucléaires de la
Vallee Rhone CEN/VALRHO
S.D.H.A. B.P. 171
30205 Bagnols-Sur-Ceze, FRANCE

Gesellschaft fur Reaktorsicherheit
(GRS) (2)
Attn: B. Baltes
W. Muller
Schwertnergasse 1
D-5000 Cologne, GERMANY

Bundesanstalt fur Geowissenschaften
und Rohstoffe
Attn: M. Langer
Postfach 510 153
3000 Hanover 51, GERMANY

Bundesministerium fur Forschung und
Technologie
Postfach 200 706
5300 Bonn 2, GERMANY

Institut fur Tieflagerung (2)
Attn: K. Kuhn
Theodor-Heuss-Strasse 4
D-3300 Braunschweig, GERMANY

Physikalisch-Technische Bundesanstalt
Attn: P. Brenneke
Postfach 3345
D-3300 Braunschweig, GERMANY

Shingo Tashiro
Japan Atomic Energy Research Inst.
Tokai-Mura, Ibaraki-Ken, 319-11
JAPAN

Netherlands Energy Research
Foundation ECN
Attn: L.H. Vons
3 Westerduinweg
PO Box 1
1755 ZG Petten
THE NETHERLANDS

Svensk Kärnbränsleforsorjning AB
Attn: F. Karlsson
Project KBS (Kärnbränslesakerhet)
Box 5864
S-102 48 Stockholm
SWEDEN

Nationale Genossenschaft für die
Lagerung radioaktiver Abfälle (2)
Attn: S. Vomvoris
P. Zuidema
Hardstrasse 73
CH-5430 Wettingen
SWITZERLAND

AEA Technology
Attn: J.H. Rees
D5W/29 Culham Laboratory
Abington, Oxfordshire OX14 3DB
UNITED KINGDOM

AEA Technology
Attn: W.R. Rodwell
044/A31 Winfrith Technical Centre
Dorchester, Dorset DT2 8DH
UNITED KINGDOM

AEA Technology
Attn: J.E. Tinson
B4244 Harwell Laboratory
Didcot, Oxfordshire OX11 ORA
UNITED KINGDOM

D.R. Knowles
British Nuclear Fuels, plc
Risley, Warrington, Cheshire WA3 6AS
1002607 UNITED KINGDOM

Internal

1502	J.C. Cummings
4511	D.P. Garber
6000	D.L. Hartley
6115	P.B. Davies
6115	Staff (15)
6119	F. Gelbard
6119	Staff (7)
6121	J.R. Tillerson
6121	Staff (7)
6300	D.E. Ellis
6302	L.E. Shephard
6303	S.Y. Pickering
6303	W.D. Weart
6305	S.A. Goldstein
6305	A.R. Lappin
6306	A.L. Stevens
6342	D.R. Anderson
6342	Staff (20)
6343	V. Harper-Slaboszewicz
6343	Staff (2)
6345	R.C. Lincoln
6345	Staff (9)
6347	D.R. Schafer
6348	J.T. Holmes
6348	Staff (4)
6351	R.E. Thompson
6352	S.E. Sharpton
6352	WIPP Central Files (10)
7141	Technical Library (5)
7151	Technical Publications
7613-2	Document Processing for DOE/OSTI (10)
8523-2	Central Technical Files
6117	D.H. Zeuch (5)
6352	G.M. Gerstner-Miller (2)

RE/SPEC Inc (5)
Attn: N.S. Brodsky
P.O. Box 724
Rapid City, SD 57709

Prof. J. Daemen
Mackay School of Mines
MS-173
University of Nevada
Reno, NV 89557

*U.S. GOVERNMENT PRINTING OFFICE 1994-0-573-026/80023

DATE
FILMED
8/4/94

END